Technische Universität München
TUM School of Engineering and Design

Potentialbewertung von synthetischen, sauerstoffhaltigen C1-Kraftstoffen im direkteinspritzenden Ottomotor

Sebastian Blochum

Vollständiger Abdruck von der TUM School of Engineering and Design der Technischen Universität München zur Erlangung eines

Doktors der Ingenieurwissenschaften (Dr.-Ing.)

genehmigten Dissertation.

Vorsitz:		Prof. Ph.D. Malte Jaensch
Prüfende/-r der Dissertation:	1.	Prof. Dr.-Ing. Georg Wachtmeister
	2.	Assoc. Prof. Dr. Thomas Lauer

Die Dissertation wurde am 12.10.2022 bei der Technischen Universität München eingereicht und durch die TUM School of Engineering and Design am 14.12.2022 angenommen.

Inhaltsverzeichnis

Verzeichnisse

Abbildungen

Tabellen

Nomenklatur

Akronyme

AGR	Abgasrückführung
BEV	Battery Electric Vehicle
Cxx	xx Vol.-% DMC im Kraftstoff
C1	Molekül ohne C-C Bindung
C_3H_8	Propan
CFD	Computational Fluid Dynamics
CH_2O	Formaldehyd
CLD	Chemilumineszenzdetektor
CMOS	Complementary Metal-Oxide Semiconductor
CNG	Compressed Natural Gas
CO	Kohlenstoffmonoxid
CO_2	Kohlenstoffdioxid
CPC	Condensation Particle Counter
CVS	Constant Volume Sampling
DMC	Dimethylcarbonat
DoE	Design of Experiments
DOHC	Double Overhead Camshaft
DSU	Direkt Sampling Unit
DVPE	Dry Vapour Pressure Equivalent
Exx	xx Vol.-% Ethanol im Kraftstoff
ECU	Electronic Control Unit
EFM	Einzylinderforschungsmotor
ETBE	Ethyl-tertiär-butylether
EU2%	Energieumsatzpunkt 2 %
EU5%	Energieumsatzpunkt 5 %
EU50%	Energieumsatzpunkt 50 % (Verbrennungsschwerpunkt)
EU95%	Energieumsatzpunkt 95 %
EU98%	Energieumsatzpunkt 98 %
Fxx	xx Vol.-% MeFo im Kraftstoff
FFKM	Perfluorkautschuk
FID	Flammenionisationsdetektor
Gxx	xx Vol.-% Referenzkraftstoffanteil
GUI	Graphical User Interface
HC	Kohlenwasserstoff
HCCI	Homogeneous Charge Compression Ignition
HCR	High Compression Ratio

HDP	Kraftstoffhochdruckpumpe
HGK	Hochgeschwindigkeitskamera
LNG	Liquefied Natural Gas
LPG	Liquefied Petroleum Gas
LSPI	Low Speed Pre-Ignition
Mxx	xx Vol.-% MeOH im Kraftstoff
MDE	Messdatenerfassung
MeFo	Methylformiat
MeOH	Methanol
MOZ	Motor-Oktanzahl
n. ZOT	nach Zünd-OT
NDIR	Nichtdispersiver Infrarotsensor
NH_3	Ammoniak
NO	Stickstoffmonoxid
NO_2	Stickstoffdioxid
NO_X	Stickoxide
OH	Hydroxylradikal
OME1	Oxymethylenether
OT	oberen Totpunkt
PHEV	Plug-in-Hybrid Electric Vehicle
PKW	Personenkraftwagen
PM	Partikelmasse
PMD	paramagnetischer Detektor
PN	Partikelanzahl
PN10	Partikelanzahl > 10 nm
PN23	Partikelanzahl > 23 nm
PTFE	Polytetrafluorethylen
RDE	Real Driving Emissions
ROZ	Research-Oktanzahl
SOI	Start of Injection
STP	Standard Temperature and Pressure
SUV	Sport Utility Vehicle
TFSI	Turbocharged Fuel Stratified Injection
TKE	turbulente kinetische Energie
UV	ultraviolett
VOC	Volatile Organic Compounds
WLTP	Worldwide Harmonized Light-Duty Vehicles Test Procedure
ZZP	Zündzeitpunkt
° KW	Grad Kurbelwinkel

Symbole

COV	Coefficient of Variation
$dQ_H/d\varphi$	Heizverlauf
$K_{P,Lader}$	Korrekturfaktor
$\dot{m}_L$	Luftmassenstrom
M_{max}	maximales Drehmoment
n_{motor}	Motordrehzahl
p	Druck
φ	Kurbelwinkel
P_i	indizierte Leistung
$P_{i,rev}$	revidierte indizierte Leistung
P_{max}	maximale Leistung
p_{max}	maximaler gemittelter Zylinderdruck
p_{me}	effektiver Mitteldruck
p_{mi}	indizierter Mitteldruck
p_{mr}	Reibmitteldruck
T	Temperatur
v	spezifisches Volumen
V	Volumen
V_H	Hubvolumen
ε	Verdichtungsverhältnis
η_i	indizierter Wirkungsgrad
η_{R-G}	Wirkungsgrad Roots-Gebläse
κ	Isentropenexponent
λ	Verbrennungsluftverhältnis
σ	Standardabweichung

1 Einleitung

Die Europäische Kommission hat mit dem „European Green Deal“ ein Konzept erarbeitet, welches vorsieht, Europa bis zum Jahr 2050 in den ersten klimaneutralen Kontinent zu transformieren [1]. Das Konzept sieht eine effizientere Ressourcennutzung vor, welche mit einer umweltfreundlichen und kreislauforientierten Wirtschaft erreicht wird. Denn nur mit einem verstärkten Umweltschutz ist das Übereinkommen von Paris, mit dem Ziel, die Erderwärmung auf 1,5 °C zu begrenzen [2], erreichbar. Folglich ist eine Dekarbonisierung und somit eine Abkehr von fossilen Energieträgern im Verkehrs- und Energiesektor unumgänglich. Mit dem vom Europäischen Rat angenommenen Gesetzesvorschlag in Form des „European Climate Law“ [3] wird das Ziel verfolgt, den „European Green Deal“ im Recht zu verankern. In diesem Zuge wurde das Klimaziel für 2030 nochmals verschärft, hier sieht das Gesetz nun eine Nettoreduktion der Treibhausgasemissionen von mindestens 55 % gegenüber 1990 vor [3]. Dies steht im Einklang mit dem in der EU seit 2021 vorgeschriebenen Flottengrenzwert von 95 CO_2/km für Personenkraftwagen (PKW), welcher bis 2030 nochmals um weitere 37,5 % reduziert wird [4]. Diese Verordnung erhöht den Druck auf die Automobilindustrie, wodurch sich diese verstärkt auf klimafreundliche Antriebstechniken fokussieren muss. Hierbei planen bereits mehrere Hersteller den Verbrennungsmotor-Ausstieg [5] und konzentrieren sich verstärkt auf elektromotorische Antriebe, hauptsächlich in Form von Plug-in-Hybrid (PHEV) und batterieelektrischen Fahrzeugen (engl. Battery Electric Vehicle, BEV). Gründe hierfür sind staatliche Förderungen, die Tank-to-Wheel Betrachtung und die Supercredit-Regelung, welche eine Mehrfachwertung für leichte Nutzfahrzeuge mit einem CO_2-Ausstoß von < 50 g/km bis 2023 vorsieht [4]. Durch diese Betrachtung und Regelung werden die CO_2-Flottenverbräuche der Hersteller durch PHEVs/BEVs stark reduziert und Strafzahlungen vermieden. Um die globale CO_2-Bilanz für verschiedene Antriebsarten zu bewerten, muss entgegen der Gesetzeslage eine Cradle-to-Grave Betrachtungsweise herangezogen werden [6]. Diese inkludiert auch vorgelagerte Prozesse wie die Energieerzeugung bzw. Kraftstoffgewinnung, die Fahrzeugproduktion, -wartung und -entsorgung. Bezüglich des CO_2-Ausstoßes von BEVs ist hier neben dem erhöhten energetischen Aufwand der Batteriezellenproduktion auch der jeweilige Anteil an erneuerbaren Energien im jeweiligen Strommix entscheidend. Die Lebenszyklusanalyse von Zheng et al. [7] aus 2021 zeigt, dass aus dem Einsatz eines BEV mit dem globalen Strommix keine nennenswerte Reduktion der globalen CO_2-Emissionen folgt. Wird ein BEV in Norwegen betrieben, ist abhängig von der jeweiligen Antriebskonfiguration eine Reduktion des CO_2-Ausstoßes von bis zu 75 %, verglichen mit einem mit fossilem Kraftstoff betriebenen Verbrennungsmotor, möglich. Dies begründet sich in dem hohen Anteil von 98 % an erneuerbaren Energien im norwegischen Strommix. Gegensätzlich zeigt sich der Betrieb eines BEV in China, hier führt der hohe Kohlestromanteil von > 60 % meist zu einer Erhöhung des CO_2-Ausstoßes. Letztlich schlussfolgert Zheng et. al [7], dass nur, wenn der CO_2-Ausstoß vom jeweiligen Strommix unter 320 g/kWh liegt, eine signifikante Reduktion des CO_2-Ausstoßes über die

gesamte Fahrzeugnutzungsdauer mittels BEVs erreicht wird. Der Vergleich mit den prognostizierten spezifischen CO_2-Emissionen aus dem deutschen Strommix für 2020 mit 366 g CO_2/kWh zeigt, dass trotz des relativ hohen Anteils an erneuerbaren Energien von 44 % [8], kurzfristig keine nennenswerte Reduktion der globalen CO_2-Emissionen durch BEVs zu erwarten ist. Hierfür muss grundsätzlich der Anteil an fluktuierenden erneuerbaren Energien im Strommix weiter erhöht werden, wodurch aber die Volatilität der Energieerzeugung und somit die Anforderungen an das Energiemanagement steigen. Beispielsweise fand in Deutschland im Juni 2021, bezogen auf die Stromnetzlast, zeitpunktabhängig sowohl eine Stromüberproduktion von bis zu 39 % als auch eine Stromunterproduktion von bis zu 20 % statt [9]. Um die Stromversorgung sicherzustellen, dienten die Stromnetze der umliegenden Länder zeitweise als „Energiespeicher“. Somit werden zukünftig Energiespeicher benötigt, welche eine zeit- und ortsunabhängige Speicherung der erneuerbaren Energien bei einem Energieüberschuss sicherstellen.

Eine Möglichkeit der Energiespeicherung ist die Nutzung von gasförmigen oder flüssigen synthetischen Kraftstoffen, welche aus CO_2, Wasser und erneuerbarer Energie hergestellt werden [10]. Der hergestellte Kraftstoff ermöglicht eine langfristige Speicherung der erneuerbaren Energie und für dessen Transport kann die bereits vorhandene Infrastruktur eingesetzt werden. Der synthetische Kraftstoff ist dann je nach Anwendung zur zentralen oder dezentralen stationären Energieerzeugung, sowie zum mobilen Einsatz bspw. in Fahrzeugantrieben mit Verbrennungsmotor oder Brennstoffzelle nutzbar. Der synthetische Kraftstoff wird entsprechend der Anwendung und den damit verbundenen Eigenschaftsanforderungen, aus einer Gruppe an Stoffen ausgewählt oder aufgemischt. Für die verbrennungsmotorische Anwendung wurden C1-Oxygenatkraftstoffe als eine vielversprechende Stoffgruppe identifiziert [11–14], womit ein CO_2-neutraler Betrieb des Verbrennungsmotors möglich wird. Diese Kraftstoffe sind synthetisch herstellbar und verbrennen aufgrund ihres hohen Sauerstoffanteils und den fehlenden C-C Bindungen rußarm.

In der vorliegenden Arbeit werden C1-Oxygenatkraftstoffe in Reinform oder als Blendkomponente im direkteinspritzenden Ottomotor bezüglich ihres Emissions- und Wirkungsgradpotentials untersucht. Der Fokus liegt hierbei auf den derzeit reglementierten festen und gasförmigen Abgasemissionen, sowie dem indizierten Wirkungsgrad. Neben der rußarmen Verbrennung bietet die erhöhte Verdampfungskühlung in Verbindung mit der hohen Klopffestigkeit der C1-Oxygenatkraftstoffe Potential zur Wirkungsgradsteigerung und Emissionsreduzierung. Die Motorversuche wurden sowohl an einem Einzylinderforschungsmotor (EFM), als auch an einem Serien-Vierzylinderaggregat, welches bei Personenkraftwagen im Mittel- bis Oberklassesegment eingesetzt wird, untersucht. Am EFM wurden neben den grundlegenden thermodynamischen und optischen Untersuchungen auch weitere Detailuntersuchungen durchgeführt. Diese Arbeit dient zum erweiterten Verständnis von C1-Oxygenatkraftstoffen im direkteinspritzenden Ottomotor, um neben der Reduktion von CO_2-Emissionen zusätzlich Potentiale des jeweiligen Kraftstoffes zu identifizieren.

2 Ottokraftstoffe

Konventioneller flüssiger Kraftstoff für den Einsatz in Verbrennungsmotoren wird mittels Raffinerieverfahren aus fossilem Erdöl gewonnen und entsprechend der motorischen Anwendung gemischt. Gemischtes Motorenbenzin ist bei Raumtemperatur flüssig und besteht aus circa 200 Kohlenwasserstoffverbindungen, welche zwischen 30 °C und 210 °C sieden. Dieser Ottokraftstoff auf fossiler Basis gewährleistet seit über 100 Jahren einen Großteil der Energieversorgung des Straßenverkehrs, insbesondere aber des motorisierten Individualverkehrs. Entscheidend für diesen Erfolg sind die hohe Energiedichte, der flüssige Aggregatzustand bei Raumtemperatur und die gute Wirtschaftlichkeit. Im Laufe der Zeit wurde das Motorenbenzin stetig an die Anforderungen der Motorenentwicklung und Gesetzgebung angepasst. Hierzu zählt die heutzutage übliche Beimischung von sauerstoffhaltigen Verbindungen, wie bspw. von bis zu 10 Vol.-% Ethanol, und diversen Raffinerieadditiven wie Leitfähigkeitsverbesserer und Oxidationsinhibitoren. Diese sauerstoffhaltigen Verbindungen dienen sowohl zur Erhöhung der Klopffestigkeit als auch zur Reduzierung des fossilen Energieanteils im Kraftstoff. Weitere wesentliche Anpassungen im 21. Jahrhundert waren die schrittweise Reduzierung des maximalen Schwefelgehalts, sowie des Volumenanteils von Aromaten und Olefinen. Für Europa sind diese und weitere Qualitätsanforderungen an den Ottokraftstoff in der DIN EN 228 geregelt. [15]

Im letzten Jahrhundert wurden diverse alternative Kraftstoffe für Ottomotoren eingeführt, welche sich abhängig von Anwendung, Region, Land und vorliegender Gesetzgebung teils etabliert haben. Einen nennenswerten Marktanteil haben die fossilen gasförmigen Ottokraftstoffe CNG (Compressed Natural Gas), LNG (Liquefied Natural Gas) und LPG (Liquefied Petroleum Gas), sowie der flüssige biogene Ottokraftstoff Ethanol in der Beimischung zu Motorenbenzin von 85 Vol.-% (E85). Der gemittelte Marktanteil von alternativen Ottokraftstoffen (exkl. E5 und E10) an der bestehenden Personenkraftwagenflotte in der Europäischen Union lag 2019 letztlich aber nur bei 3,2 % [16].

Als zukünftige Kraftstoffe werden zur Umsetzung der Energiewende im Verkehrssektor feste, flüssige oder gasförmige erneuerbare Energieträger benötigt, welche eine längerfristige bzw. saisonale Speicherung großer Energiemengen ermöglichen. Diese Energieträger werden dort zum Einsatz gebracht, wo eine direkte Elektrifizierung technisch schwer umsetzbar ist oder ökonomisch keinen Mehrwert bringt [17]. Mögliche Ottokraftstoffe sind hierbei die bereits teilweise felderprobten oder intensiv untersuchten Kraftstoffe Wasserstoff [18], Methan [19], Ethanol [20] und MeOH [21]. Zudem werden weitere synthetische Kraftstoffe erforscht, welche ebenso aus Biomasse oder erneuerbarem Strom herstellbar sind, um den CO_2-Kreislauf zu schließen [10]. Hiermit wird ein CO_2-armer, oder im Optimalfall ein CO_2-neutraler Betrieb eines Verbrennungsmotors unter Berücksichtigung einer Well-to-Wheel Betrachtung möglich.

2.1 Referenzkraftstoff Motorenbenzin

Der fossile Zertifizierungskraftstoff CEC RF-02-08 E5 wird im Folgenden als Referenzkraftstoff bezeichnet. Der Referenzkraftstoff erfüllt die Anforderungen an das Motorenbenzin ROZ95 E5 der EN 228:2014. Zudem sind schmalere Toleranzen für die jeweiligen Kraftstoffeigenschaften festgelegt, wie z.B. der Ethanolanteil, welcher zwischen 4,7 – 5,3 Vol.-% liegen muss oder das DVPE@37,8°C, welches auf den Bereich zwischen 56,0 und 60,0 kPa festgesetzt ist. Mit diesen schmal gesetzten Grenzwerten für die Kraftstoffeigenschaften wird eine höhere Reproduzier- und Vergleichbarkeit bei motorischen Versuchsergebnissen, vor allem bezüglich Gemischaufbereitung, Verkokungsverhalten und Abgasemissionen, erreicht. Die jeweiligen Toleranzgrenzen für die Kraftstoffeigenschaften des Zertifizierungskraftstoff sind im Anhang aufgeführt.

2.2 C1-Ottokraftstoffe

C1-Kraftstoffe sind sogenannte Oxygenate, welche für die Nutzung als synthetischer Kraftstoff in Frage kommen. Die Abkürzung „C1“ ist aus der fehlenden C-C Bindung in den jeweiligen Stoffmolekülen abgeleitet. Durch drei herausragende Eigenschaften ist die Stoffklasse im 21. Jahrhundert in den Fokus der Verbrennungsmotorenforschung gerückt. Die wichtigste dieser Eigenschaften ist die Möglichkeit, die Oxygenate nachhaltig aus den Oxiden des Kohlenstoffs herzustellen. Weiter hat die Stoffgruppe eine gute Verträglichkeit gegenüber der Umwelt, was sich wiederrum neben dem möglichen CO_2-neutralen Betrieb positiv auf die Umweltbilanz auswirkt. Zudem ergeben sich hierdurch Vorteile beim Kraftstoffhandling und -transport. Die letzte der drei Eigenschaften bezieht sich auf das teils positive Verbrennungsverhalten. Mit den hohen Sauerstoffanteilen von > 40 Gew.-% und den fehlenden C-C Bindungen wird die Rußbildung unterdrückt, was einen weiteren Freiheitsgrad in der Verbrennungsmotorenapplikation generiert. Die Oxygenate finden, basierend auf ihrer charakteristischen Molekülstruktur, ihre Anwendung sowohl in dieselmotorischen als auch in ottomotorischen Brennverfahren. Entscheidend hierfür ist die Stellung des O-Atoms im Molekül. Während Sauerstoffbrücken zwischen C-Atomen die Molekülstruktur der Dieselkraftstoffe auszeichnet, ist der endständige Sauerstoff das charakteristische Merkmal der Ottokraftstoffe. Für die Anwendung im Ottomotor zeigen die C1-Ester Dimethylcarbonat (DMC) und Methylformiat (MeFo) herausragende Eigenschaften. Das ist begründet in ihrem sehr geringen Gesundheitsrisiko verglichen mit dem Referenzkraftstoff, den hohen Zündtemperaturen von > 400 °C und deren hohen Klopffestigkeiten mit Oktanzahlen > 100. Diese Eigenschaften, kombiniert mit der möglichen großtechnischen Herstellung aus MeOH, sind erfolgsversprechende Voraussetzungen für den ottomotorischen Einsatz. Ungeachtet dessen, besitzt der bereits im 20. Jahrhundert intensiv untersuchte C1-Alkohol MeOH ähnliche Verbrennungseigenschaften, verglichen mit den C1-Estern. Ein schwerwiegender Nachteil bei der Verwendung von MeOH als Ottokraftstoff ist die hohe Toxizität. Dies erhöht den Aufwand bei der Kraftstoffspeicherung und dem Kraftstoffhandling. Dieser Nachteil wird durch den verkürzten Weg der

nachhaltigen Herstellung teils kompensiert. Die in der vorliegenden Arbeit verwendeten reinen C1-Ottokraftsotffe DMC, MeFo und MeOH sind in Tabelle 1 im Vergleich zum Referenzkraftstoff gelistet. Für die Ermittlung des unteren Heizwertes wurde für alle in dieser Arbeit verwendeten Kraftstoffe die modifizierte Dunlong'sche Verbandsformel von Gumz [22] verwendet. Diese hat sich vor allem für die relative Vergleichbarkeit von Oxygenatkraftstoffen mit konventionellem Kraftstoff im Verbrennungsmotor bewährt [13]. Neben der Verwendung von reinen C1-Oxygenaten ist auch eine Verwendung als Beimischung zum Motorenbenzin möglich. Hierzu sind aber diverse Eigenschaften der Oxygenate zu beachten, wie bspw. die Hydrolysestabilität [23]. Im den folgenden Unterkapiteln werden die C1-Oxygenate näher beschrieben. Wobei nicht näher auf die Beobachtungen bezüglich VOC- bzw. HC-Emissionen eingegangen wird, da hier meist ein Flammenionisationsdetektor (FID) verwendet wird, welcher bei einem steigenden Sauerstoffgehalt einen verringerten Responsefaktor gegenüber VOCs aufweist [24, 25]. Dies verhindert einen sinnvollen relativen Vergleich von VOC-Emissionen bei der motorischen Untersuchung von Kraftstoffen mit unterschiedlichem Sauerstoffgehalten.

Tabelle 1: Eigenschaften der C1-Oxygenate und dem Referenzkraftstoff modifiziert nach [26]

	Einheit	**Referenz-kraftstoff**	**DMC**	**MeFo**	**MeOH**
Unterer Heizwert	MJ/kg	42,14	15,2		19,8
Dichte bei 15 °C	kg/m³	750	1079	957	790
Referenzkraftstoffäquivalent	m³/m³	1,0	1,93	2,17	2,02
ROZ	-	95,9	109	115	109
MOZ		85,8	102	114	92
Sauerstoffanteil	Gew.-%	1,86	53,29		49,93
Wasserstoffanteil		13,25	6,71		12,58
Kohlenstoffanteil		84,89	40		37,48
Luftbedarf stöchiometrisch	kg/kg	14,28	4,64		6,47
Siedebereich bzw. -punkt	° C	31,3 – 192,2	90	31,5	65
DVPE bei 37,8 °C	kPa	59,8	10,8	> 100	30,7
Verdampfungsenthalpie	kJ/kg	~ 420	418	464	1100
Oberflächenspannung	mN/m	~ 24	28,5	25	22,1
Selbstzündtemperatur	° C	~ 220	458	450	465
Zündgrenzen in Luft	Vol.-%	1,3 – 7,6	4,2 – 12,9	5 – 20	6,7 – 36
Min. Zündenergie	mJ	0,25	-	0,5	0,14
Laminare Flammengeschw. unter NTP-Bedingungen	m/s	0,4	0,3	0,33	0,68

2.2.1 Dimethylcarbonat

DMC (auch Kohlensäuredimethylester) ist ein klarer, farbloser, bei Raumtemperatur flüssiger Kohlensäureester, welcher nicht toxisch und biologisch abbaubar ist. Die chemische Verbindung findet unter anderem als Methylierungs- und Lösungsmittel Verwendung. DMC wurde im Bereich der Verbrennungsmotorenforschung bereits als Blendkomponente für ottomotorische Brennverfahren [27, 28] und als Kraftstoffadditiv für dieselmotorische Brennverfahren [29, 30] eingesetzt. Grund hierfür ist vor allem die hohe Klopffestigkeit von ROZ 109 und MOZ 102 (vgl. Tabelle 1). Als weiteren signifikanten Unterschied zum Referenzkraftstoff ist der niedrigere untere Heizwert von 15,2 MJ/kg zu nennen, welcher in dem hohen Anteil von 53,29 Gew.-% gebundenem Sauerstoff in DMC gegründet ist. Bezogen auf das Kraftstoffvolumen wird dieser von der um ~ 44 % höheren Dichte zum Teil kompensiert. Aber letztlich ist im Vergleich zum Referenzkraftstoff eine theoretische Erhöhung des eingespritzten Kraftstoffvolumens um das 1,93-fache erforderlich, um die zugeführte Energiemenge in den Brennraum konstant zu halten. Als regenerativer Ottokraftstoff in Reinform ist DMC nicht geeignet, da DMC einen niedrigen Dampfdruck von DVPE@37,8 °C = 10,8 kPa besitzt und der Gefrierpunkt bereits bei 4 °C liegt. Der hohe Gefrierpunkt macht einen Einsatz als Winterkraftstoff unmöglich und der geringe Dampfdruck erschwert im Allgemeinen die Gemischaufbereitung. Jedoch wurden trotzdem Vorversuche am EFM von Härtl et al. [11, 12] durchgeführt, um die grundlegenden Eigenschaften von DMC im Motorbetrieb zu analysieren. Hierbei wurden über eine λ-Variation zwischen 0,8 – 1,1 um den Faktor 10 geringere PN-Emissionen beobachtet. Zudem wurde eine deutliche Reduktion der NO_x-Emissionen festgestellt, was auf die erhöhte Verdampfungskühlung, aufgrund der um 177 % zusätzlich eingespritzten Kraftstoffmasse bei nahezu identischer Verdampfungsenthalpie, zurückzuführen ist. Nachteilig zeigte sich DMC in der Brenndauer und dem Stabilitätsverhalten vor allem im mageren Motorbetrieb. Hierfür ist die geringere laminare Flammengeschwindigkeit mit der verminderten Verdampfungsneigung verantwortlich.

2.2.2 Methylformiat

MeFo (auch Ameisensäuremethylester) ist ein klarer, farbloser, bei Raumtemperatur flüssiger Ameisensäureester. Dieser einfachste Methylester [31] wird üblicherweise als Bindemittel in der Gießereiindustrie [32], Treibmittel für diverse Polymere [33], Kälte- oder Lösungsmittel [34] eingesetzt. Im Kontext mit Verbrennungskraftmaschinen ist MeFo bis zu der Publikation der Versuche am EFM von Härtl et al. [12] im Jahre 2017 nahezu nicht präsent. Eine Ausnahme ist bspw. eine Patenschrift [35], in welcher MeFo als Blendkomponente mit 3,5 – 10 Vol.-% dem Normalbenzin zugemischt wurde, um die Klopffestigkeit zu erhöhen. Zudem wurden von Dooley et al. [31] die grundlegenden Verbrennungsparameter ermittelt. Diese Parameter sind von Interesse, da MeFo ein Zwischenprodukt bei der Oxidation von Oxymethylenether (OME1) ist und dieses C1-Oxygenat seit den 1990er-Jahren in diversen Veröffentlichungen als alternativer Dieselkraftstoff untersucht wurde [14]. MeFo besitz die

identische Elementarzusammensetzung wie DMC, dies bedeutet, dass MeFo und DMC denselben unteren Heizwert, Mindestluftbedarf und Stoffgehalt (C, H, O) in Gew.-% besitzen. Die wesentlichen Unterschiede zu DMC sind der um den Faktor 10 größere Dampfdruck, der um 100 °C niedrigere Schmelzpunkt und der um 58,5 °C niedrigere Siedepunkt. Aus diesen Eigenschaftsunterschieden wird deutlich, dass MeFo im Gegensatz zu DMC leicht flüchtig ist und eine sehr hohe Verdampfungsneigung besitzt, was sich positiv auf die Gemischbildung auswirkt. Aber aufgrund des sehr hohen Dampfdruckes ist reines MeFo vor allem im Sommer als Ottokraftstoff nur bedingt einsetzbar. Wie bei DMC wird der geringere untere Heizwert durch eine erhöhte Dichte teils abgefedert. Letztlich ergibt sich ein volumetrisches Referenzkraftstoffäquivalent von 2,17 bezogen auf den Energieinhalt. MeFo weist ebenfalls eine sehr hohe Klopffestigkeit auf, was ein Resultat der hohen Selbstzündtemperatur von 450 °C und der relativ hohen minimalen Zündenergie von 0,5 mJ ist. Gleich wie bei DMC wurde bei einer λ-Variation am EFM [11, 12] eine starke Reduktion der PN-Emissionen beobachtet, welche die Partikelreduktion mittels DMC nochmals um eine Zehnerpotenz übersteigt. Der Vorteil in der PN-Konzentration gegenüber DMC wird durch die verbesserte Gemischaufbereitung von MeFo erreicht. Diese gemessenen Konzentrationen liegen, bis auf wenige Ausnahmen, im Bereich von einem typischen Umgebungsniveau in Deutschland und sind die bis dato niedrigsten gemessenen PN-Emissionen aller bekannten Flüssigkraftstoffe [12]. Auch beim Einsatz von MeFo steigt die Zylinderinnenkühlung aufgrund der größeren eingespritzten Kraftstoffmasse und der höheren massebezogenen Verdampfungsenthalpie um theoretisch 206 %. Somit ist auch mit MeFo eine Reduktion der NO_x-Emissionen zu beobachten. Zudem zeigt sich, verglichen mit dem Referenzkraftstoff, ein stabileres Verbrennungsverhalten und eine etwas kürzere Brenndauer. Dies ist begründet in der guten Gemischaufbereitung von MeFo, aufgrund der niedrigen Siedetemperatur von 31,5 °C und des hohen Dampfdruckes von DVPE@37,8°C > 100 kPa.

2.2.3 Methanol

MeOH (auch Methylalkohol) ist ein klarer, farbloser, bei Raumtemperatur flüssiger Alkohol und ist zugleich das einfachste flüssige kohlenstoffhaltige Molekül unter Normbedingungen (STP) [21]. Der schwerwiegendste Nachteil von MeOH, gegenüber DMC und MeFo, ist dessen Toxizität und Organschädigung. Aber im Gegensatz zum Motorenbenzin, welches gleichermaßen toxisch ist, wird MeOH schnell biologisch abgebaut und ist zudem wasserlöslich. MeOH wurde bereits im 20. Jahrhundert intensiv motorisch untersucht und ist weiterhin ein wichtiges verbrennungsmotorisches Forschungsthema [36, 37], eine umfangreiche Zusammenfassung darüber wurde 2019 von Verhelst et al. [21] publiziert. Zudem wurden bereits Feldstudien in Form von Flottenversuchen [38, 39] durchgeführt. Wie bei DMC und MeFo senkt der gebundene Sauerstoff im Molekül den unteren Heizwert. MeOH besitzt einen höheren unteren Heizwert als DMC bzw. MeFo, hat aber zugleich eine geringe Dichte, welche nur ~ 5 % über der des Referenzkraftstoffs liegt. Woraus sich ein theoretisches Referenzkraftstoffäquivalent, bezogen auf den Energieinhalt, von 2,02 ergibt. Der Dampfdruck von

MeOH ist relativ gering und ist mit DVPE@37,8 = 30,7 kPa zwar um den Faktor ~ 2,8 höher als DMC, aber letztlich immer noch halb so hoch wie der des Referenzkraftstoffs. Der relativ niedrige Dampfdruck, verbunden mit dem Siedepunkt bei 65 °C, erschwert ein Verdampfen des Kraftstoffes während der Gemischaufbereitung. Demgegenüber ist ein herausragendes Merkmal von MeOH die sehr hohe massebezogene Verdampfungsenthalpie von 1100 kJ/kg. Wird zudem der Anstieg der Kraftstoffmasse aufgrund des geringeren unteren Heizwertes berücksichtigt, wird eine theoretische Erhöhung der energiebezogenen Verdampfungsenthalpie von 457 % gegenüber dem Referenzkraftstoff erreicht. Eine weitere positive Eigenschaft von MeOH ist eine um 70 % höhere laminare Flammengeschwindigkeit gegenüber dem Referenzkraftstoff, was zu einer kürzeren Brenndauer und letztlich zu einer Erhöhung des Wirkungsgrades führt [21]. Mit der erhöhten laminaren Flammengeschwindigkeit und der hohen Verdampfungsenthalpie, kombiniert mit einer hohen Selbstzündtemperatur von 465 °C, erreicht MeOH ebenfalls eine sehr hohe Klopffestigkeit von ROZ 102 und MOZ 92. Entgegen der hohen Klopffestigkeit liegt die minimale Zündenergie von MeOH 44 % unter der vom Referenzkraftstoff und die Zündgrenzen in Luft von 6,7 – 36 Vol.-% erstrecken sich über einen signifikant größeren Bereich. Dadurch werden, in Kombination mit der hohen laminaren Flammengeschwindigkeit, grundsätzlich Frühzündungen an heißen Oberflächen im Brennraum begünstigt [21, 40]. Die hohe Klopffestigkeit wurde von Vancoillie et al. [41] genutzt, um einen modifizierten VW 1.9L TDI Vierzylinder-Diesel-Reihen-Viertaktmotor mit einem Verdichtungsverhältnis von 19,5:1 auf ein ottomotorisches Brennverfahren mit Saugrohreinspritzung und Funkenzündung umzurüsten. Um Frühzündungen zu vermeiden, wurde der Wärmewert einer „kalten“ Zündkerze gewählt. Dabei wurde mit einem stöchiometrischen Motorbetrieb (p_{me} = 10 bar und n_{Motor} = 2500 1/min) ein maximaler effektiver Wirkungsgrad von 42 % erreicht. Dabei lagen die Abgasemissionen nach Drei-Wege-Katalysator, verglichen mit Motorenbenzin RON95, auf gleichem oder niedrigerem Niveau. Zudem berichtet Vancoillie et al. [41, 42] von einer Reduktion der NO_x-Emissionen im Bereich von 5 -10 g/kWh. Bei den Partikelemissionen berichtet Zuo et al. [43] von einer Reduktion der PN- und PM-Emissionen um den Faktor 68 bzw. 49. Wie bereits erwähnt verbrennt MeOH, gleich zu DMC und MeFo, rußarm aufgrund der C1-Molekülstruktur.

2.3 Kraftstoffmischungen

Die vorgestellten alternativen C1-Oxygenate bringen als Reinstoffe viele positive Eigenschaften für einen Einsatz im direkteinspritzenden Ottomotor mit. Trotzdem ist eine Verwendung der Reinstoffe aufgrund von Defiziten bei der Gemischaufbereitung nicht oder nur bedingt möglich. Hauptursächlich ist hierfür der Dampfdruck, sowie der Siede- und Gefrierpunkt. Mit niedrigem Dampfdruck und einem hohen Siedepunkt wird das Verdampfen des Kraftstoffes stark gehemmt, was Probleme bei einem Motorkaltstart hervorruft. Zudem verhindert ein niedriger Dampfdruck die Bildung einer Fettdampfglocke im Kraftstofftank, welche als Explosionsschutz dient. Im umgekehrten Fall, bei zu hohem Dampfdruck und einem niedrigen Siedepunkt, steigen die Verdunstungsemissionen und der

Kraftstoffverlust aus dem Kraftstoffsystem. Hinzukommt die Gefahr der verstärkten Dampfblasenbildung in den Kraftstoffleitungen. [44]

Zunächst sind zwei Kraftstoffgruppen zu definieren, welche bezogen auf ihre mögliche Markteinführungsstrategie unterschiedliche Ziele verfolgen. Eine Gruppe besteht aus Ottokraftstoffmischungen die ausschließlich aus flüssigen C1-Oxygenaten gemischt werden. Diese Gruppe ist als langfristige Lösung für zukünftige neuentwickelte Ottomotoren angedacht, welche die Potentiale des erneuerbaren synthetischen Kraftstoffs bestmöglich nutzen. Die zweite Gruppe befasst sich mit Kraftstoffmischungen, welche als Basis konventionelles Motorenbenzin nutzen und mit flüssigen C1-Oxygenaten geblendet werden. Deren Potential besteht darin, Abgasemissionen von bestehenden Ottomotoren zu reduzieren und deren Effizienz zu steigern. Dabei sind keine oder nur sehr geringfügige Anpassungen am Antriebsaggregat nötig. Erste Kraftstoffmischungen aus C1-Oxygenaten für ottomotorische Anwendungen wurden von Härtl et al. [44] aus DMC und MeFo entwickelt. Diese erfüllen die wichtigsten Ottokraftstoffanforderungen aus der EN228:2014.

Für die Gruppe der C1-Kraftstoffblends wurde DMC, unter anderem aufgrund der vollständigen Mischbarkeit mit Motorenbenzin, als Blendkomponente gewählt [27]. Zudem liegen für MeOH-Blends bereits eine Vielzahl an publizierten Motorversuchsergebnissen mit unterschiedlichsten Blendraten vor [21]. Im Gegensatz dazu ist MeFo als Blendkomponente bei einer Basis aus Motorenbenzin, aufgrund seiner hydrolytischen Instabilität, nicht ohne weiteres geeignet. Es wurde von Forbes et al. [45] gezeigt, dass in einem C1-Kraftstoffblend aus Motorenbenzin und MeFo, nach Zugabe einer geringen Menge Wasser, innerhalb von kurzer Zeit eine hydrolytische Zersetzung stattfand. Für einen Ottokraftstoff muss aber eine gewisse hydrolytische Stabilität vorliegen, da während des Transports und der Lagerung eine Kontamination durch Wasser nicht ausgeschlossen ist. Somit müssen bei der Verwendung von MeFo als Blendkomponente Stabilisatoren in Form von bspw. Additiven zugemischt werden, welche zum Zeitpunkt der Motorenversuche noch nicht bestimmt waren.

In Tabelle 2 werden die Eigenschaften der untersuchten C1-Kraftstoffmischungen und -blends gezeigt. Zur Verbesserung des Leseflusses und zur Vereinfachung der Kraftstoffbezeichnungen wird eine Namenskonvention eingeführt. Jeder Reinstoff und auch der Referenzkraftstoff werden mit einem Buchstaben abgekürzt. Diese heißen für den Referenzkraftstoff G, Dimethylcarbonat C, Methylformiat F und für Methanol M. Zudem wird der volumetrische Anteil des Kraftstoffes in Prozent dem Buchstaben nachgestellt. Somit wird bspw. eine Kraftstoffmischung aus 85 Vol.-% MeOH und 15 Vol.- % MeFo mit M85F15 abgekürzt. In den folgenden Unterkapiteln werden die jeweiligen Kraftstoffmischungen vorgestellt.

Tabelle 2: Eigenschaften der Kraftstoffmischungen modifiziert nach [26]

	Einheit	G100	C65F35	G85C15	G70C30	M85F15	M70F30
Referenzkraftstoff	Vol.-%	100	-	85	70	-	-
Dimethylcarbonat		-	65	15	30	-	-
Methylformiat		-	35	-	-	15	30
Methanol		-	-	-	-	85	70
Unterer Heizwert	MJ/kg	42,14	15,2	36,67	31,85	19,68	18,78
Dichte bei 15 °C	kg/m^3	750	1041	~ 799	~ 848	~ 817	~ 842
Referenzkraftstoff-äquivalent	m^3/m^3	1,0	2,0	1,08	1,17	1,97	2,0
ROZ	-	95,9	117	> 95,9	> 95,9	-	-
MOZ		85,8	> 120	> 85,8	> 85,8	-	-
Sauerstoffanteil	Gew.-%	1,86	53,29	12,35	21,54	50,52	51,08
Wasserstoffanteil		13,25	6,71	11,94	10,77	11,55	10,58
Kohlenstoffanteil		84,89	40	75,71	67,69	37,93	38,34
Luftbedarf stöchiom.	kg/kg	14,28	4,64	12,31	10,58	6,16	5,85
Siedebereich	° C	31,3-192,2	37,5-94	31,3-192,2	31,3-192,2	31,5-65	31,5-65
DVPE bei 37,8 °C	kPa	59,8	57	-	-	60,1	80,0
Verdampfungsenthalpie	kJ/kg	~ 420	433	~ 420	~ 419	1005	911
Oberflächenspannung	mN/m	~ 24	27,7	-	-	-	-

2.3.1 Dimethylcarbonat / Methylformiat

Es wurde die C1-Kraftstoffmischung aus DMC und MeFo gewählt, da hier bereits von Härtl et al. [44] Entwicklungsarbeit, mittels Kraftstoffanalysen und motorischen Untersuchungen am EFM, geleistet wurde. Dabei wurde die Kältebeständigkeit der Mischungen getestet, wobei der Test als bestanden gilt, wenn die Kraftstoffmischung bei – 25 °C noch flüssig vorliegt. Zudem wurden die Kraftstoffe entsprechend ihrem Dampfdruck DVPE@37,8 °C in Sommer- (45 - 60 kPa) und Winterkraftstoff (> 60 – 100 kPa) eingeteilt. Mischungen, deren Dampfdruck nicht im Bereich zwischen 45 – 100 kPa liegt, wurden als ungeeignet eingestuft. Zuletzt wurde die Hydrolysebeständigkeit durch die Zugabe von 2 Vol.-% Wasser mit einer anschließenden mindestens 1-monatigen Lagerung bei 50 °C, überprüft. Letztlich wurden dabei acht Oxygenatkraftstoffmischungen identifiziert, welche alle drei Prüfkriterien erfüllen, wobei nur die Mischung C65F35 eine C1-Charakteristik aufweist. Für diese und zwei weitere Mischungen wurden am EFM der Technischen Universität München bereits erste Untersuchungen durchgeführt [11]. C65F35 zeigte über eine λ Variation wie erwartet die niedrigsten PN-Emissionen und, gleich aller untersuchten Oxygenatmischungen, eine deutliche Reduktion der NO_x-Emissionen gegenüber dem Referenzkraftstoff. Aufbauend auf diesen Ergebnissen wurden 0D/1D-Simulationen von Wagner et al. [46, 47] mit Hilfe eines validierten Motormodells durchgeführt, um das Potential der

Oxygenatmischung C60F35E5 bezüglich des effektiven Wirkungsgrades zu untersuchen. Für das Motormodell wurde der direkteinspritzende Vierzylinder-Otto-Reihen-Viertaktmotor VW EA211 TSI evo (V_H = 1500 cm^3 / ε = 12,5 / P_{max}= 96 kW / M_{max}= 200 Nm) verwendet. Ausschließlich durch Ersetzen des Motorenbenzins RON95 E10 durch C60F35E5 wurde eine maximale effektive Wirkungsgradsteigerung von über 14 % an der Volllastlinie unterhalb von n_{motor} = 2000 1/min erreicht. Diese Steigerung wird durch die hohe Klopffestigkeit von C60F35E5 erzielt. Entgegen Motorenbenzin RON95 E10 wird dadurch der Verbrennungsschwerpunkt (EU50%) in allen Motorbetriebspunkten nah dem thermodynamischen Optimum gehalten. Dagegen zeigt C60F35E5 in der Simulation effektive Wirkungsgradverluste durch unvollständige Verbrennung bei hohen Drehzahlen und niedrigen Lasten von bis zu 4,6 %. Hierfür ist die langsame Brenngeschwindigkeit von C60F35E5 hauptverantwortlich, welche die Brenndauer erhöht und somit eine vollständige Verbrennung aufgrund der verkürzten Zyklusdauer verhindert. Bei der Simulation des RDE (Real Driving Emissions) Zyklus wurde für C60F35E5 eine gemittelte effektive Wirkungsgradsteigerung von 1,0 % ermittelt. Weiter wurde eine Adaption des Motormodells vorgenommen, um die Potentiale von C60F35E5 zu nutzen. Hierbei wurden das Hubvolumen, Verdichtungsverhältnis und die Aufladung mittels einer statistischen Versuchsplanung (engl. Design of Experiments, DoE) angepasst. Diese DoE-Studie ermittelte ein Verdichtungsverhältnis von 19:1 und ein Hubvolumen von 900 cm^3 als optimalen Kompromiss der beiden voneinander abhängigen Parameter. Das um 52 % höhere Verdichtungsverhältnis nutzt die Klopffestigkeit und das 40 % kleinere Hubvolumen den geringeren Luftbedarf von C60F35E5. Abschließend wurde mit diesen Anpassungen eine simulierte Steigerung des effektiven Wirkungsgrades im RDE-Zyklus von 11,1 % erreicht. Zudem wurde angemerkt, dass mit weiteren Anpassungen indizierte Wirkungsgrade > 50 % möglich sind. Mit den Untersuchungen von Härtl et al. [44] und Wagner et al. [47] wurde ein erweiterter Forschungsbedarf ermittelt. Dazu zählt, das Brennverfahren grundsätzlich weiterzuentwickeln, Magerbrennverfahren zu untersuchen, ölinduzierte Partikelemissionen zu identifizieren, die Klopffestigkeit zu bestimmen und Daten zur Validierung von Simulationsmodellen zu generieren.

2.3.2 Methanol / Methylformiat

Basierend auf der Tatsache, dass MeOH diverse theoretische Eigenschaftsvorteile aufweist, wurde bei diesen Kraftstoffmischungen DMC als C1-Basiskraftstoff durch MeOH ersetzt. Ein maßgebliches Argument für den Einsatz von MeOH als Basiskraftstoff ist die kürzere Prozesskette bei der Herstellung von erneuerbarem MeOH. Grundlegend haben DMC und MeOH, verglichen mit Motorenbenzin, einen relativ niedrigen Dampfdruck. Darum wird auch MeOH zur Anhebung des Dampfdrucks mit MeFo gemischt, um die Gemischaufbereitung im direkteinspritzenden Ottomotor gegenüber reinem MeOH in gewissen Betriebsmodi zu optimieren. Beispiele für die Betriebsmodi wären hier Kaltstart und Schichtladebrennverfahren. Mit der Mischung M85F15 wird ein DVPE@37,8°C von ~ 60 kPa erreicht, was einen Einsatz als Ganzjahreskraftstoff ermöglicht. Bei einer weiteren Erhöhung des MeFo Anteils

zu M70F30 liegt der Dampfdruck aufgrund der leichten Flüchtigkeit von MeFo bereits bei ~ 80 kPa, somit ist diese Kraftstoffmischung auf Grundlage der EN228:2014 nur als Winterkraftstoff zulässig. Schlussendlich sind dem Autor keine Publikationen anderer Forscher mit Motorenversuchen bekannt, welche die C1-Kraftstoffmischung aus MeOH und MeFo thematisieren.

2.3.3 Motorenbenzin / Dimethylcarbonat

Wird Motorenbenzin mit DMC geblendet, sinkt der untere Heizwert und die auf den unteren Heizwert bezogene Verdampfungsenthaplie steigt. Zudem steigt der Gefrierpunkt stark an, aufgrund des relativen hohen Gefrierpunktes von DMC, der bei 4 °C liegt. Mit einem volumetrischen DMC-Anteil von 30 % gefriert der C1-Blend zwischen – 15 °C und – 20 °C [48]. Daher wurde die maximale Blendrate von 30 Vol.-% DMC für die vorliegende Untersuchung gewählt. Mit der Ausnahme, dass für die Untersuchung des Verkokungsverhaltens des Injektors der DMC-Anteil zwischen 0 - 100 % variiert wurde, um den Einfluss mit steigendem DMC-Anteil zu verdeutlichen. Mit steigendem DMC-Anteil sinkt sowohl der Dampfdruck als auch der prozentuale Anteil an Hochsiedern aus dem Referenzkraftstoff. Beides beeinflusst die Gemischaufbereitung abhängig vom Betriebspunkt und Brennverfahren. In der Literatur finden sich eine Vielzahl an Publikationen, die sich mit dem Einsatz von mit DMC geblendeten Flüssigkraftstoffen beschäftigen, aber meist für dieselmotorische Anwendungen. Eine Zusammenfassung der Publikationen bis einschließlich 2018 wurde von Abdalla et al. [49] publiziert. Hierbei erstrecken sich die verwendeten Blendraten mit Motorenbenzin von 3,52 – 29,2 Vol.-%. Für die Untersuchung von Wen et al. [50] im Jahre 2010 wurde ein luftgekühlter Einzylinder-Otto-Viertaktmotor (V_H = 124,6 cm^3 / ε = 11,3 / P_{max}= 7,5 kW / M_{max}= 9,71 Nm) von einem Leichtkraftrad der Firma Sanyang eingesetzt. Während einer konstanten Last von 3 Nm wurde eine Drehzahlvariation zwischen 1660 1/min und 8000 1/min durchgeführt, ohne die Motorregelung zu adaptieren. Dabei wurden die volumetrischen Blendraten 5 %, 10 % und 15 % mit DMC und Ethanol untersucht. Der Vergleich zum Motorenbenzin ohne Oxygenate zeigt, dass mit steigendem Oxygenatanteil das Verbrennungsluftverhältnis, aufgrund des verringerten Luftbedarfs der Oxygenate, um bis zu $\Delta\lambda = 0{,}3$ sinkt. Trotzdem wurde für G95C5 und G90C10 eine CO-Reduktion von über 60 % beobachtet, wohingegen bei G85C15 nur eine Verringerung um 2 % erreicht wurde. Zudem wurden mit steigendem DMC-Anteil sinkende Abgastemperaturen beobachtet, welche im Großteil der untersuchten Betriebspunkte eine NO_x-Reduktion zur Folge hatten. Bedingt durch den geringeren unteren Heizwert und die Molekülstruktur von DMC wurde ein Anstieg des Kraftstoffverbrauchs und der CO_2-Emissionen beobachtet. Eine weitere experimentelle Untersuchung wurde von Gopinath et al. [51] 2012 veröffentlicht. Hierbei wurde ein wassergekühlter Vierzylinder-Otto-Reihen-Viertaktmotor (V_H = 1500 cm^3 / ε = 7,2 / P_{max}= 36,8 kW / M_{max}= 76 Nm) von Hindustan Motors mit Vergaser verwendet. Untersucht wurden die volumetrischen Blendraten 5 %, 10 %, 15 % und 20 %, welche mit Motorenbenzin verglichen wurden. Ein Anstieg des effektiven Wirkungsgrades wurde durchwegs für alle Blends beobachtet. Die maximale absolute Steigerung von 3 % wurde mit G80C20 erreicht. Zudem wurde mit steigendem DMC-Anteil eine Verringerung der CO-Emissionen über die Drehzahlvariation beobachtet. Wie zu erwarten, wurde mit steigender Blendrate ein Anstieg der CO_2-Emissionen

gemessen, was dem höheren C-Anteil der molekularen Struktur von DMC zugrunde liegt. Bei den NO_x-Emissionen wurde entgegen Wen et al. [50] mit steigender Blendrate ein Anstieg der NO_x-Emissionen ermittelt. Ein möglicher Grund dafür ist die sehr niedrige Verdichtung von 7,2:1 des Versuchsträgers und die moderate Hubraumleistung von 24,53 W/cm^3. Daraus ergeben sich grundsätzlich über die Drehzahlvariation niedrige Verbrennungsspitzentemperaturen, woraus sich wiederum sehr niedrige NO_x-Emissionen für alle untersuchten Betriebspunkte von unter 80 ppm ergeben. Mit dem Anstieg des effektiven Wirkungsgrades durch DMC, verbunden mit der intensiveren Verbrennung, ergeben sich die höheren Spitzentemperaturen während der Verbrennung. Dadurch steigen die NO_x-Emissionen um maximal 25 ppm mit dem C1-Blend G80C20. Von Schifter et al. [27, 52] wurde Normalbenzin mit DMC, Ethanol, MeOH und Ethyl-tertiär-butylether (ETBE) geblendet. Die experimentellen Untersuchungen wurden an einem AVL 5401 Einzylinder-Otto-Viertaktmotor (V_H = 500 cm^3 / ε = 10,5 / P_{max}= 25 kW) mit Saugrohreinspritzung durchgeführt. Da der Sauerstoffanteil im Ottokraftstoff diverse Eigenschaften (bspw. die Klopffestigkeit) stark beeinflusst, wurde hier der Ansatz gewählt, Blends mit gleichem massebezogenen Sauerstoffanteil zu untersuchen. Demzufolge wurden zwei DMC-Blends mit 3,52 Vol.-% und 29,2 Vol.-% untersucht. Dabei zeigen die DMC-Blends die größte Reduktion bei den NO_x-Emissionen aller Kraftstoffmischungen, aber wie auch in bereits vorgestellten Publikationen den größten Anstieg in den CO_2-Emissionen. Weiter zeigen die DMC-Blends die längste Brenndauer für Betriebspunkte mit λ = 1,0 und λ = 0,8, was sich negativ auf den thermischen Wirkungsgrad auswirkt. Wohingegen Ethanol- und MeOH-Blends mit gleichem massebezogenen Sauerstoffanteil kürzere Brenndauern als Normalbenzin zeigen. Bei einem leicht überstöchiometrischen Betrieb von λ = 1,1 ist die Brenndauer des DMC-Blends die kürzeste. Veröffentlichungen, welche zeitlich nach dem Review-Artikel von Abdalla et al. [49] erschienen sind, beschäftigen sich auch mit den ottomotorischen Partikelemissionen von DMC-Blends. Der Konferenzbeitrag von Scharrer et al. [48] behandelt sowohl die Ermittlung der Eigenschaften und Materialverträglichkeiten, als auch die motorische Testung von DMC-Blends. Als Versuchsträger dient ein Porsche EA9A2 Sechszylinder-Otto-Boxer-Viertaktmotor mit Direkteinspritzung in GTS-Serienkonfiguration und ohne Hardwaremodifikationen. Durch die Bestimmung der Blendeigenschaften und der Materialverträglichkeiten wurde eine theoretische Komptabilität des Serienantriebsaggregats von bis zu 20 Vol.-% DMC abgeschätzt. Folglich wurden die volumetrischen Blendraten 5 %, 10 % und 20 % von DMC in Motorenbenzin ROZ98 E5 motorisch untersucht. Bei Verwendung der Seriensoftware des Motorsteuergerätes erreichen alle untersuchten C1-Blends die Nennleistung des Serienmotors bei nahezu identischem effektivem Wirkungsgrad. Auch zeigt ein G80C20 unter Volllast (p_{me} ~ 23 bar) bei 2250 1/min keinen Einfluss auf abnormale Verbrennungsphänomene. Bei den Partikelrohemissionen wird über große Bereiche des Motorkennfeldes eine Reduktion von PM und PN erreicht. Hingegen zeigt G80C20 mehr Partikelrohemissionen als das Motorenbenzin ROZ98 E5 in Bereichen von niedriger Last und Drehzahl, sowie im Low-End Torque. Bei der Variation des Einspritzzeitpunkts (p_{me} = 10 bar und n_{motor} = 2000 1/min) verzeichnet G80C20 bei frühen Einspritzzeitpunkten bereits 10 °KW früher einen Anstieg der PN-Emissionen, womit sich das mögliche Zeitfenster für die Direkteinspritzung im Saughub

verkürzt. Bezüglich der NO_x-Emissionen ist die Reduktion mit G80C20 umso höher je höher die Drehzahl und je niedriger die Last. Dabei wird eine maximale Reduktion der NO_x-Emissionen von 4 g/kWh erzielt. Im oberen Lastbereich sind die NO_x-Emissionen, verglichen mit Motorenbenzin ROZ98 E5, gleich oder leicht erhöht. Letztlich wurde eine Optimierung vom ZZP aufgrund der erhöhten Klopffestigkeit von G80C20 vorgenommen. Hierdurch wurde der EU50% bei niedrigen Drehzahlen und Volllast um bis zu 5 °KW in Richtung früh verschoben. Durch die optimale EU50%-Lage wurde bei Nennleistung eine effektive absolute Wirkungsgradsteigerung von 2,3 % erreicht. Folglich steigt dabei der maximale Spitzendruck im Zylinder um bis zu 20 bar, wodurch für einen möglichen Serieneinsatz Anpassungen zur Steigerung der Bauteilfestigkeit nötig sind. Im Fahrzyklus WLTP (engl. Worldwide Harmonized Light-Duty Vehicles Test Procedure) zeigt G80C20 für die NO_x-Emissionen eine signifikante Reduktion von ~ 10 %. Zudem steigen die PN-Emissionen über den Zyklus um 15 %. Dieser Anstieg ist allein den ersten 100 Sekunden der Kaltstartphase geschuldet, in welchen G80C20 70 % mehr PN emittiert. Nach der Warmlaufphase zeigt sich G80C20 auch im dynamischen Betrieb vorteilig bezüglich der PN-Emissionen. Bei der Publikation von Chan et al. [28] wird G92C8 an einem turboaufgeladenen Vierzylinder-Otto-Reihen-Viertaktmotor (V_H = 2000 cm^3 / ε = 10 / P_{max}= 149 kW / M_{max}= 300 Nm) mit seitlicher Direkteinspritzung untersucht. Am untersuchten Betriebspunkt (n_{Motor} = 2200 1/min / λ = 1.0 / M_{Motor} = 90 Nm) zeigt G92C8 keine signifikante Veränderung im Brennverhalten gegenüber dem Motorenbenzin ROZ95 E10. Bei den gasförmigen Emissionen steigt durch den DMC-Anteil, wie bereits mehrfach erwähnt, der Anteil an Kohlenstoffmonoxid (CO) um 7 % und CO_2 um 4 % im Abgas. Konsistent zu den bisherigen Untersuchungen wurde eine Reduktion der PN10 Konzentration um 60 %, sowie eine Reduzierung des mittleren Partikeldurchmessers von 46 nm auf 41 nm beobachtet. Bei der vorliegenden Literatur wurde erst ab dem Jahr 2019 das Augenmerk auch auf die Partikelemissionen gelegt und ein möglicher Effekt auf das Verkokungsverhalten des direkteinspritzenden Injektors nicht betrachtet. Zudem wurden nur grundlegende Betriebsparameter in einem state-of-the-art direkteinspritzenden Ottomotor variiert und bspw. keine Kühlwassertemperaturvariation untersucht.

3 Zielsetzung der Arbeit

In der vorliegenden Arbeit wird das Potential von flüssigen, sauerstoffhaltigen C1-Kraftstoffen untersucht. Ziel ist es, neben dem möglichen CO_2-freien Motorbetrieb weitere Potentiale der untersuchten Kraftstoffe zu identifizieren. Im Rahmen dieser Arbeit liegt der Fokus vorwiegend auf dem indizierten Wirkungsgrad und den derzeit reglementierten Abgasemissionen.

Die größten Potentiale der ausgewählten synthetischen Kraftstoffe liegen in der rußarmen Verbrennung, der auf den unteren Heizwert bezogenen höheren Verdampfungsenthalpie und der höheren Klopffestigkeit gegenüber Motorenbenzin. Zur Untersuchung dieser Potentiale werden experimentelle Versuche an einem thermodynamischen direkteinspritzenden Ein- und Vierzylinder-Otto-Viertaktmotor durchgeführt. Zudem wird die volloptische Konfiguration des EFM genutzt, um den Verbrennungsprozess auch optisch zu diagnostizieren.

Zunächst wird die Oxygenatkraftstoffmischung C65F35, welche von Härtl et al. [44] entwickelt wurde, thermodynamisch und optisch untersucht und mit Referenzkraftstoff verglichen. Neben der Variation verschiedenster Parameter und Kenngrößen wird auch das Verdichtungsverhältnis erhöht, um das Potential der erhöhten Klopffestigkeit verstärkt zu nutzen. Aufbauend auf den gewonnenen Erkenntnissen wird C65F35 mit dem C1-Kraftstoff MeOH und einer C1-Kraftstoffmischung aus MeOH und MeFo verglichen, um die jeweiligen Vor- und Nachteile der Kraftstoffe zu bestimmen. In diesem Zuge wird auch die Widerstandsfähigkeit der Kraftstoffe gegenüber abnormalen Verbrennungsphänomenen im Low-End Torque untersucht. Hierfür wird zusätzlich das Verdichtungsverhältnis angehoben und die Ansauglufttemperatur schrittweise erhöht bis abnormale Verbrennungsphänomene auftreten. Weiter wird der Effekt von DMC als Blendkomponente im Motorenbenzin untersucht, wobei auch das Verkokungsverhalten der Injektorspitze des direkteinspritzenden Injektors mit steigendem DMC-Blendanteil bewertet wird. Darüber hinaus werden erste Voruntersuchungen mit C65F35 als C1-Kraftstoff im gespülten Vorkammerzündsystem von Stadler et al. [53] durchgeführt. Hierbei soll das Potential der rußarmen Verbrennung genutzt werden, um im aktiven Vorkammerbetrieb die Partikelemissionen zu reduzieren. Zuletzt wird erneut die rußarme Verbrennung von C65F35 als Entwicklungswerkzeug am EFM genutzt, um die ölinduzierten von den kraftstoffinduzierten Partikelemissionen zu separieren.

Die vorliegende Arbeit knüpft nahtlos an die publizierten Untersuchungen von Härtl et al. [11, 12, 44] und Wagner et al. [46, 47] an, wobei der ermittelte Forschungsbedarf aus den Publikationen aufgegriffen und untersucht wird. Letztlich dient die Arbeit zur Erweiterung der motorischen Kenntnisse der C1-Kraftstoffe DMC und MeFo, welche in Relation zum bereits intensiv untersuchten Kraftstoff MeOH bewertet wurden. Die vorliegende Arbeit soll zusätzlich dazu dienen, Maßnahmen abzuleiten, welche in seriennahen Antriebsaggregaten eingesetzt werden, um zukünftig die Potentiale der C1-Kraftstoffe zu nutzen.

4 Experimenteller Aufbau und Versuchsmethodik

Im Zuge dieser Arbeit wurden Versuche an einem EFM durchgeführt, welcher je nach Untersuchung in den verschiedenen Motorkonfigurationen thermodynamisch oder optisch betrieben wird. Der Versuchsbetrieb erfolgte stationär an einem Motorenprüfstand gegen eine Leistungsbremse (Asynchronmaschine) mit entsprechender Prüfstandsteuerung und Messdatenerfassung. Für die vorliegende Arbeit wurde eine grundlegende Versuchsmethodik festgelegt, welche für die jeweiligen Versuchskampagnen entsprechend angepasst wurde. Anschließend sind die generierten Ergebnisse über MATLAB-Routinen nachbereitet und ausgewertet worden.

4.1 Einzylinder-Forschungsmotor

EFM eignen sich im Allgemeinen sehr gut zur stationären optischen und thermodynamischen Grundlagenuntersuchung von Brennverfahren mit diversen Vorteilen gegenüber Mehrzylinder-Forschungsmotoren [54, 55]. Ein Vorteil ist der vibrationsarme Motorlauf, welcher durch eine große Schwungmasse und einen Massenausgleich von I. und II. Ordnung erreicht wird. Zudem wird für die Konditionierung gegenüber Serienanwendungen meist ein Vielfaches der Menge des jeweiligen Mediums vorgehalten. Verbunden mit den oftmals nicht gewichtsoptimierten Hardwarekomponenten ergibt sich eine große thermische Trägheit. Damit werden stationäre Betriebsbedingungen geschaffen, womit die Messgüte und Reproduzierbarkeit des Versuchsträgers steigen. Bei der Entwicklung und Konstruktion von EFM wird im Normalfall auf eine gute Zugänglichkeit und Montierbarkeit geachtet, was Komponentenuntersuchungen erleichtert. Im Gegensatz dazu wirkt sich die mechanische und thermische Trägheit negativ auf einen transienten Motorbetrieb aus, welcher sich nicht oder nur bedingt auf einen Mehrzylindermotor übertragen lässt. Gleich dem ist eine exakte Nachbildung von akustischen Effekten zwischen benachbarten Zylindern eines Vollmotors während des Ladungswechsels nicht möglich. Der in dieser Arbeit eingesetzte EFM basiert auf dem AUDI EA888 [56, 57] Vierzylinder-Otto-Reihen-Viertaktmotor mit Lanchester-Ausgleich [58] der I. und II. Ordnung und wurde von Schauer [59] entwickelt bzw. aufgebaut. Mittels darauf aufbauender Arbeiten [60, 61] wurde der Versuchsträger weiterentwickelt und modifiziert. Mit der vorliegenden Arbeit sind Kühlmittelkonditionierung, Ventiltrieb und mobile Kraftstoffeinheit überarbeitet worden. Durch die Überarbeitung sind niedrige Kühlmitteltemperaturen von bis zu – 7 °C, ein schneller Wechsel der Kolbengruppe, sowie ein Betrieb des Kraftstoffsystems mit nahezu jeglicher Art von Flüssigkraftstoff möglich.

4.1.1 Thermodynamische Konfiguration mit Peripherie

Zur Untersuchung der Abgasemissionen und der Thermodynamik der unterschiedlichen Flüssigkraftstoffe wird der EFM in der thermodynamischen Konfiguration betrieben. Mit Verwendung der Serienkolbengruppe des 1.8 TFSI und einer leicht modifizierten Brennraumgeometrie ergibt sich ein

Verdichtungsverhältnis von ε = 10,92. Durch die in-house entwickelte Kurbelwelle und die Serienzylinderbohrung wird ein Hubvolumen von 463 cm^3 erzielt, welches um 3 % über dem des 1.8 TFSI Serienmotors liegt. Aufgrund von vorangegangenen HCCI-Untersuchungen [62, 63], bei welchen hohe Zylinderspitzendrücke erreicht wurden, ist ein Pleuel aus einem Dieselmotor im Einsatz. Der Forschungsmotor wurde in der thermodynamischen Konfiguration mit einer maximalen Last von p_{mi} = 17 bar und einer maximalen Drehzahl von n_{Motor} = 3500 1/min betrieben. In Tabelle 3 sind die wichtigsten technischen Daten des thermodynamischen EFMs gelistet.

Tabelle 3: Spezifikationen des thermodynamischen EFMs

Motorbasis	AUDI EA 888	
Bohrung	82.51 mm	
Hub	86.6 mm	
Pleuellänge	144 mm	
Hubvolumen	463 cm^3	
Verdichtungsverhältnis	mit Serienkolben 1.8 TFSI	10.92:1
	mit HCR-Kolben	14.91:1
Anzahl Einlassventile	2	
Anzahl Auslassventile	2	
Ventilhub Auslass	7 mm bei 250 °KW n. ZOT	
Auslassventil offen	132 °KW n. ZOT	
Auslassventil geschlossen	368 °KW n. ZOT	
Ventilhub Einlass	6 mm bei 460 °KW n. ZOT	
Einlassventil offen	348 °KW n. ZOT	
Einlassventil geschlossen	572 °KW n. ZOT	
Maximale Motorlast in p_{mi}	17 bar	
Maximale Motordrehzahl	3500 1/min	
Schmieröltemperatur	25 - 80° C	
Kühlwassertemperatur	-7 - 80° C	

Mit der Neukonstruktion des Ventiltriebs mit DOHC (engl. Double Overhead Camshaft) Steuerung wurden die Referenzsteuerzeiten und Ventilhübe des vorangegangenen vollvariablen Ventiltriebs übernommen. Die in Abbildung 1 dargestellten Ventilhübe sind gemäßigt und die Steuerzeiten weisen eine Ventilüberschneidung von 20 °KW auf.

Mit Hilfe eines modifizierten Kolbens (HCR-Kolben) [53] besteht die Möglichkeit, das Verdichtungsverhältnis zu erhöhen. Der Vergleich des Serienkolbens mit dem HCR-Kolben ist in Abbildung 2 dargestellt. Der Kolben besitzt, bis auf die aufgefüllte Kolbenmulde, die identische Kolbengeometrie des Serienkolbens. Durch die aufgefüllte Kolbenmulde wird das Verdichtungsverhältnis von 10,92:1 auf 14,91:1 angehoben. Als Zündsystem dient eine konventionelle

Funkenzündung mittels Transistorspulenzündung, wobei die Zündenergie mittels einer Zündkerze in den Brennraum eingebracht wird.

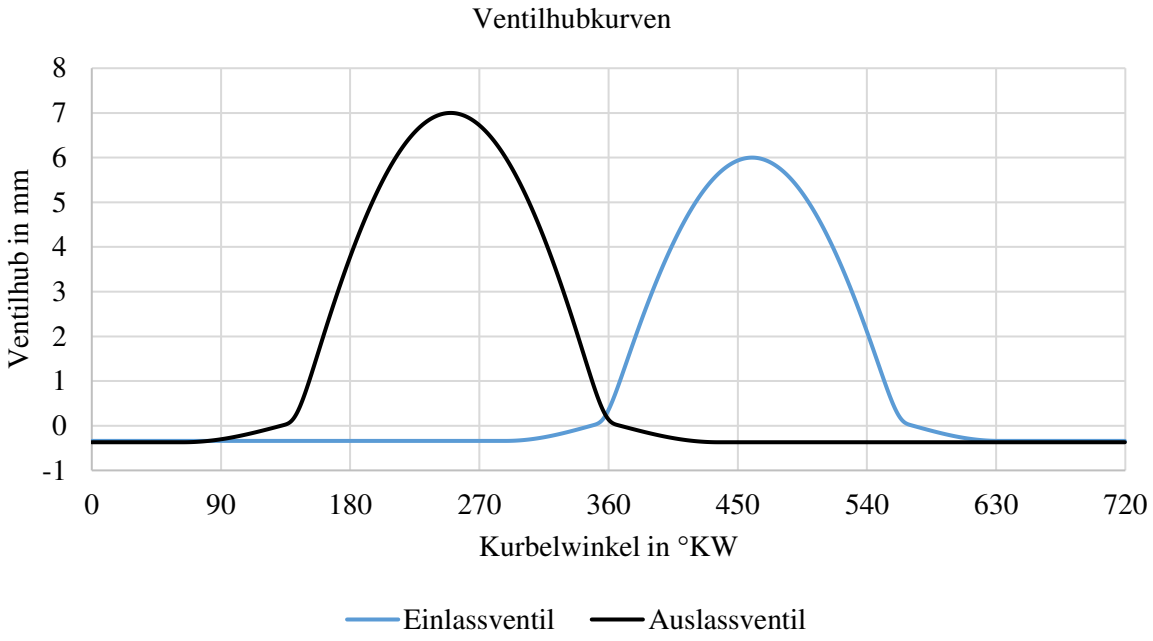

Abbildung 1: Ventilhubkurven EFM

Des Weiteren wurde für einen Stichversuch das Vorkammerzündsystem von Stadler et al. [53] aus Abbildung 3 verwendet, um das Potential von Oxygenatkraftstoffen unter Verwendung eines Magerbrennverfahrens mit Vorkammerzündung abzuschätzen.

Serienkolben	**modifizierter Kolben (HCR)**
	
ε = 10.92 →	ε = 14.91

Abbildung 2: Vergleich Serienkolben und modifizierter Kolben (HCR) des EFM

Bei dem Vorkammerzündsystem handelt es sich um eine gespülte Vorkammer, welche aus einem Vorkammerinjektor, Vorkammerzündkerze, Hauptkörper, Drucksensor, Temperatursensor und Düsenkappe besteht. Das schachtförmige Vorkammervolumen beträgt 2,1 cm^3, das entspricht 4 % des Kompressionsvolumens des Forschungsmotors. Durch das somit um 3 % vergrößerte Kompressionsvolumen verringert sich das Verdichtungsverhältnis von 10,92:1 auf 10,54:1 mit Standardkolben bzw. von 14,91:1 auf 14,18:1 bei Verwendung des HCR-Kolbens. Durch die Integration des Hochdrucksensors ist eine Auswertung des Vorkammerdrucks möglich und mittels des Temperatursensors wird die Temperatur des Vorkammerkörpers überwacht. Die Zündung des Vorkammervolumens erfolgt gleich dem der konventionellen Zündung mit einer Transistorspulenzündung mittels einer M10 Serienzündkerze. Mit einem speziell für die Vorkammeranwendung konzipierten direkteinspritzenden Injektor wird die gewünschte Energiemenge in das Vorkammervolumen eingebracht.

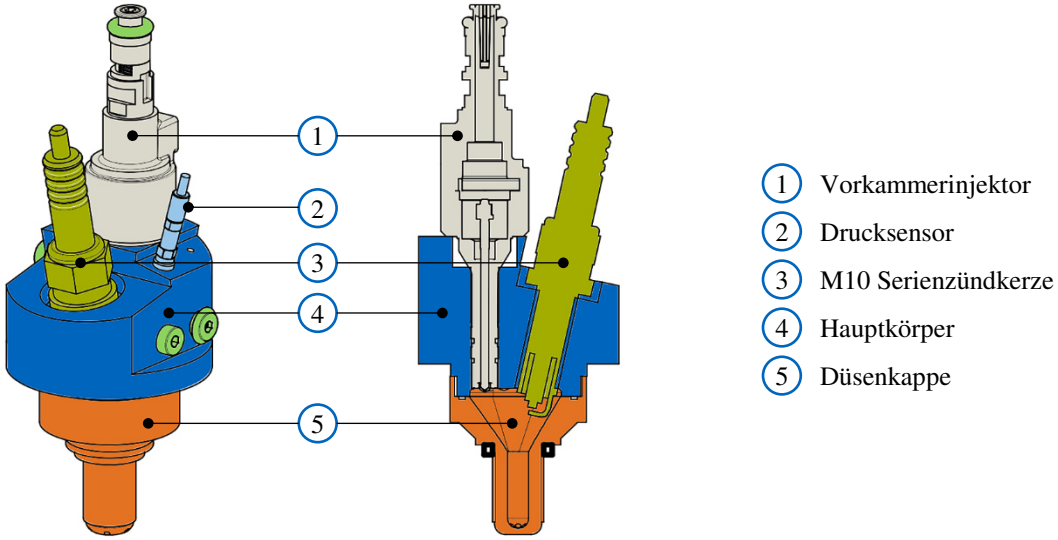

Abbildung 3: Vorkammerzündsystem von Stadler et al. modifiziert nach [53]

Zur grundsätzlichen Kraftstoffzufuhr wird ein seitlich eingebauter direkteinspritzender Magnetventilinjektor verwendet, welcher mit einem maximalen Kraftstoffdruck von 35 MPa betrieben wird. Das Spray-targeting ist passend zur Injektoreinbaulage und den geometrischen Abmessungen des Brennraums gewählt. Der verwendete Injektor wurde aus einer Reihe von Magnetventilinjektoren mit gleichem Spray-targeting aber unterschiedlichen Düsenlochgeometrien ausgewählt, da dieser die beste Performance bezüglich der PN-Emissionen aufweist. Die wichtigsten technischen Daten der eingesetzten direkteinspritzenden Injektoren zeigt Tabelle 4.

Abbildung 4 zeigt das Schema des Motorenprüfstands in thermodynamischer Standardkonfiguration, welches einen Überblick über die wichtigsten Komponenten in den jeweiligen Subsystemen liefert. Im Ladeluftsystem wird Umgebungsluft über ein Filtersystem angesaugt und in einem stationär betriebenen Schraubenkompressor verdichtet. Anschließend wird die verdichtete Luft in einem Kältetrockner Mark

MDX5200 getrocknet und die auskondensierte Flüssigkeit abgeschieden. Nachfolgend wird die verdichtete und getrocknete Luft in einem 150 Liter Drucktank gespeichert. Wird ein Absolutdruck von 8 bar erreicht, schaltet der Schraubenkompressor ab. Dem Tank sind direkt ein Ölabscheider und ein Feinfilter nachgeschaltet. Anschließend ist mittels eines manuellen Druckminderers ein Absolutdruck von ca. 2,1 bar eingestellt, worauf wiederrum ein Ladeluftkühler folgt. Als direkter Pufferspeicher vor Drosselklappe dient ein zweiter 150 Liter Drucktank, welcher mittels eines Überdruckventils auf einen Absolutdruck von 2 bar regelt. Nach Drucktank misst eine Aerzen Luftuhr den Luftvolumenstrom, wobei zeitgleich Druck und Temperatur der Luft zur Bestimmung des Luftmassenstroms gemessen werden. Anschließend wird mit der Drosselklappe der gewünschte Ladedruck eingeregelt und mittels Luftheizer wird die Luft auf die gewünschte Einlasstemperatur erhitzt. Zuletzt folgt ein Plenum, welches zur Aufgabe hat, turbulente Strömungen zu beruhigen und Druckschwingungen zu dämpfen. Das Plenum ist über einen Ansaugstutzen, in welchem ein Saugrohrinjektor integriert ist, mit dem Zylinderkopf verbunden.

Tabelle 4: Technische Daten der direkteinspritzenden Injektoren

Bezeichnung	**DI Injektor**	**DI-preCh Injektor**
Injektor	Multi-hole DI	Single-hole DI
Art der Einspritzung	Haupteinspritzung	Vorkammereinspritzung
Aktuierung	magnetisch	
Spitzen-Durchmesser	6 mm	
O-Ring Durchmesser	9,4 mm	
Spritzlochbohrung	konvergent	zylindrisch
Spraytarget	Serie	Prototyp
Injektoreinbaulage	Hauptbrennraum seitlich	Vorkammer senkrecht
Anzahl Spritzlöcher	6	1
Verwendeter Einspritzdruck	25 MPa und 35 MPa	35 MPa
Statischer Durchfluss @ 10 MPa	13,8 cm^3/s	0,99 cm^3/s

Das mobile Kraftstoffsystem wurde zur Durchführung dieser Arbeit für den Einsatz mit synthetischen Kraftstoffen modifiziert. Hierfür wurden alle starren Kraftstoffleitungen in Edelstahl und alle flexiblen Leitungen in PTFE (Polytetrafluorethylen) ausgeführt. Als Dichtungsmaterialen wurden FFKM (Perfluorkautschuk) und PTFE eingesetzt. Für die Verbindung des Kraftstoffsystems mit dem Rail wird eine flexible Hochdruckschlauchleitung mit POM-Seele verwendet. Hauptgründe für den bevorzugten Einsatz des mobilen Kraftstoffsystems gegenüber dem ortsfesten Kraftstoffsystem des Prüfstands ist die deutlich geringere Kraftstoffmenge zur Systemfüllung und der einfache Spülvorgang bei einem Kraftstoffwechsel. Nachteilig ist der auf 25 MPa begrenzte Kraftstoffdruck, der im Laufe der Untersuchung durch Implementierung einer neue Kraftstoffhochdruckpumpe (HDP) auf 35 MPa angehoben wurde. Bei Betrieb wird mittels Niederdruckpumpe und Überdruckventil die HDP mit einem

Kraftstoffdruck von 6 bar versorgt. Die mit einem elektrischen Antrieb bei konstanter Drehzahl betriebene Nockenwelle, treibt den Kolben der HDP an. Der Kraftstoffhochdruck wird über das Druckregelventil in der HDP mit Hilfe einer NI CompactRIO Steuerung geregelt. Zudem wird die für die Regelung benötigte Nockenlage über einen magnetischen Inkrementalencoder an der Nockenwelle erfasst. Der Kraftstoffmassenfluss wird mit einer Coriolis-Massendurchflussmessung niederdruckseitig vor HDP gemessen. Um Störeinflüsse aus Druckschwingungen zu minimieren, wurde der Massendurchflussmessung je ein Membranausdehnungsgefäß vor- und nachgeschalten. Aufgrund der bedarfsgerechten Regelung der HDP ist bei dieser keine Möglichkeit zum Druckabbau bei Außerbetriebnahme vorgesehen. Um diesen Druckabbau, bspw. bei einer Komponentenvariation, zu ermöglichen, wird im Hochdruckteil ein elektromechanisch aktuiertes 2/1-Wege Ventil mit Rücklauf zum Tank eingesetzt.

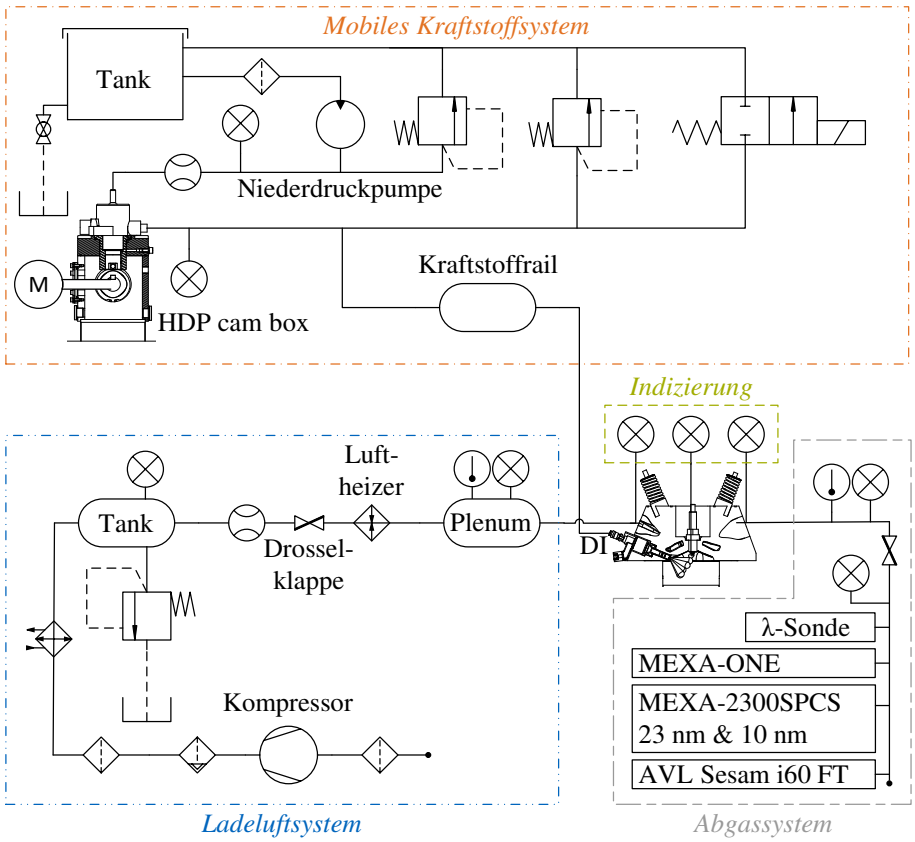

Abbildung 4: Schema des Prüfstands in thermodynamischer Konfiguration modifiziert nach [64]

Das Abgassystem beinhaltet mehrere Abgasanalysegeräte sowie eine Breitbandlambdasonde und eine Abgasdrossel. Die Breitbandlambdasonde Bosch LSU 4.9 wird mit dem ETAS LA4 Lambda Meter verwendet und ist nach Abgasdrosselklappe ins Abgasrohr eingeschraubt. Für jedes Abgasanalysegerät ist eine separate Probenentnahmestelle vorgesehen. Als Gasentnahmesonde wird ein im 45° Winkel abgeschnittenes Rohr verwendet, wobei die Öffnung des Rohrs in Richtung des Abgasstroms orientiert ist. Für die Messung der gasförmigen Emissionen wird eine HORIBA MEXA-ONE-D1 und ein AVL

SESAM i60 FT SII genutzt. Die HORIBA MEXA-ONE-D1 nutzt sechs Analysatoren mit vier verschiedenen Messprinzipien. Mit nichtdispersiven Infrarotsensoren (NDIR) wird der Anteil an CO und CO_2 im Abgas ermittelt, wobei für CO zwei Analysatoren verwendet werden, um den Messbereich zu vergrößern bei zugleich hoher Messgenauigkeit bei niedrigen Konzentrationen von unter 5000 ppm. Mit einem paramagnetischen Detektor (PMD) wird der O_2-Anteil im Abgas bestimmt Für eine exakte Bestimmung der NO_x-Emissionen wird ein Chemilumineszenz Detektor (CLD) verwendet. Zur gesetzeskonformen Messung der Kohlenwasserstoffe (HC) verwendet die HORIBA MEXA-ONE-D1 einen FID, welcher mit Propan (C_3H_8) kalibriert ist. In der vorliegenden Arbeit werden Kraftstoffmischungen mit meist hohen Sauerstoffgehalten untersucht, daher werden die unverbrannten Kraftstoff- bzw. Schmierölanteile als VOC zusammengefasst. Mit steigendem Sauerstoffanteil in der organischen Verbindung sinkt der Response-Faktor des FIDs [25], womit ein absoluter Vergleich der Kraftstoffmischungen mit unterschiedlichen Sauerstoffanteilen nur bedingt möglich ist. Deswegen wird zusätzlich ein AVL SESAM i60 FT SII verwendet, welches ein Fourier-Transformations-Infrarotspektrometer nutzt, um eine Vielzahl an Abgaskomponenten zu bestimmen. Das ist notwendig, um auch derzeit nicht reglementierte gesundheits- oder umweltschädliche Abgasemissionen, wie bspw. Formaldehyd (CH_2O) oder Ammoniak (NH_3) zu überwachen. Um eine hohe Messgenauigkeit zu erreichen, ist eine Abstimmung der softwareseitigen Auswertemethode auf die zu erwartende Abgaszusammensetzung vorzunehmen. Im Zuge dieser Arbeit standen zwei Methoden für die Messung von Motorenbenzin und C65F35 zur Verfügung. Daher wurden nur für ausgewählte Untersuchungen Messergebnisse des AVL SESAM i60 FT SII herangezogen und bewertet. Derzeit werden am Motorenlabor der TUM mit Unterstützung eines Messgeräteherstellers Anstrengungen unternommen, adäquate Messmethoden für die jeweiligen Kraftstoffmischungen zu entwickeln. Dies ermöglicht bei zukünftigen Motorenversuchen eine präzise Messung der unverbrannten Kraftstoffanteile mit deren Zwischenprodukten. Denn damit erhöht sich die Genauigkeit einer Druckverlaufsanalyse und zudem wird ein absoluter Vergleich der VOC-Emissionen unterschiedlicher Kraftstoffmischungen möglich. Die Messung der Festkörperpartikelemissionen übernimmt eine HORIBA MEXA-2300SPCS, welche um einen zweiten Kondensationspartikelzähler (engl. Condensation Particle Counter, CPC) erweitert wurde. Die CPCs besitzen je eine Zähleffizienz von 50 % (D_{50}) bei unterschiedlichen Partikelgrößen von 23 nm (PN23) und 10 nm (PN10), womit eine zusätzliche Differenzierung von Sub-23nm Partikeln ermöglicht wird. Der Partikelzähler wird nicht mit einem Konstantvolumen-Probenentnahmesystem (engl. Constant Volume Sampling, CVS), sondern mit einer Direktentnahmeeinheit (engl. Direkt Sampling Unit, DSU) betrieben. Mehrere Publikationen [65–67] bestätigen die Vergleichbarkeit von Partikelkonzentrationsmessungen aus dem Rohabgas mit DSU, gegenüber einer Messungen mit CVS.

Die Indizierung nutzt für Einlass-, Brennraum- und Auslassdruck je einen Drucksensor. Für Ein- und Auslass wird ein piezo-resistiver Drucksensor verwendet, wobei ein wassergekühlter Kistler 4075A10 abgasseitig mit Umschaltadapter betrieben wird und ein Kistler 4045A10 einlassseitig verbaut ist. Der

Zylinderdruck wird mit einem wassergekühlten piezo-elektrischen Drucksensor Kistler 6056A-3-2 gemessen. Die zur Indizierung benötigte Kurbelwinkelposition wird mittels eines magnetischen Inkrementalencoders bestimmt, wobei die Abtastrate 0,1 °KW beträgt.

Zur Steuerung und Regelung des Motorenprüfstandes werden zwei voneinander getrennte Systeme verwendet, welche über eine CAN-Schnittstelle kommunizieren. Hierbei dient ein dSpace-System als Motorsteuergerät (engl. Electronic Control Unit, ECU) und ein NI PXI-System zur Prüfstandautomatisierung und Messdatenerfassung (MDE). Mit dem dSpace-System werden die Drosselklappenstellungen, der ZZP, die Stellung des AGR-Ventils, die Injektorbestromungsdauern und -zeitpunkte geregelt. Um die Injektorbestromungsprofile an den jeweiligen Injektor anzupassen, wird ein NI-cRio basiertes Subsystem verwendet, wobei mit Hilfe einer grafischen Benutzeroberfläche (engl. Graphical User Interface, GUI) das zeitbasierte Bestromungsprofil abschnittsweise festgelegt wird. Für alle in dieser Arbeit vorgestellten Motorversuche wurden zwei Regler in der ECU verwendet. Der Regler für die Motorlast regelt den benötigten Luftmassenstrom über die Drosselklappenstellung anhand der Regeldifferenz des p_{mi}. Ein zweiter Regler für das Verbrennungsluftverhältnis regelt die benötigte Kraftstoffmenge über die Bestromungsdauer des Injektors anhand der Regeldifferenz von λ, wobei der geregelte Luftmassenstrom als Störgröße eingeht. Weiter wird die Lage vom ZZP durch die manuelle Vorgabe des Prüfstandfahrers bestimmt. Das NI PXI-System übernimmt bei der Prüfstandautomatisierung die Regelung der Motordrehzahl über die Motorbremse, sowie die Regelung der Temperaturen von Ansaugluft, Kühlmittel und Schmieröl. Zudem werden die Regelgrößen inklusive deren übergeordnetem System überwacht und freigegeben. Die Überwachung beinhaltet sowohl optische Warnmeldungen auf der Benutzeroberfläche, sowie diverse Notabschaltungen bei hochpriorisierten Warnmeldungen, um Schäden an Motor und Peripherie zu minimieren. Zudem beinhaltet das NI PXI-System die MDE, was die Online-Darstellung der Druckverläufe aus der Brennraumindizierung zur Überwachung ermöglicht.

4.1.2 Optische Konfiguration und Messtechnik

Die optische Zugänglichkeit des EFMs ist mittels eines Bowditch-Design [68] Kolbens realisiert, welcher in Abbildung 5 in der isometrischen Ansicht mit Viertelschnitt dargestellt ist. Dafür wird der Forschungsmotor um eine zusätzliche Laufbuchse erweitert, in welcher die oberen PTFE-Kolbenringe des Optikkolbens ohne Schmieröl trocken laufen. Die Laufbuchse aus dem thermodynamischen Betrieb bleibt dabei unverändert. Hier wird mit dem Serienölabstreifring auf dem Optikkolben das Kurbelgehäuse gegenüber der Umgebung abgedichtet. Durch den ortsfesten Spiegel, welcher inmitten der Längsnut im Optikkolben im 45°-Winkel zur Zylinderachse platziert ist, wird der Brennraum in Richtung der Zylinderachse für Lichtemissionen optisch zugänglich. Abhängig von der Kolbenposition liegt der Sichtdurchmesser des Brennraums durch den Glaskolbeneinsatz zwischen 53,2 mm und 78 mm. Die Kolbenkrone ist flach ausgeführt, um optische Verzerrungen zu vermeiden. Dadurch weicht

die Brennraumgeometrie zwischen thermodynamischer und optischer Konfiguration voneinander ab, womit sich zudem das Verdichtungsverhältnis auf 9,36:1 verringert. In Abbildung 5 ist auch der schematische Aufbau der beiden verwendeten Messaufbauten #1 und #2 am Optikmotor dargestellt. Mit einem Glasring zwischen Zylinderkopf und Laufbuchse ist ein weiterer optischer Zugang zum Brennraum im rechten Winkel zur Zylinderachse gegeben. Aufgrund des für Ottomotoren üblichen Dachbrennraums ist steuertriebseitig ein dritter Zugang über ein dreieckiges Quarzglasfenster im Zylinderkopf vorhanden. Dieser ermöglicht den optischen Zugang zu Zündkerze und dem seitlichen direkteinspritzenden Injektor quer zur Zylinderachse.

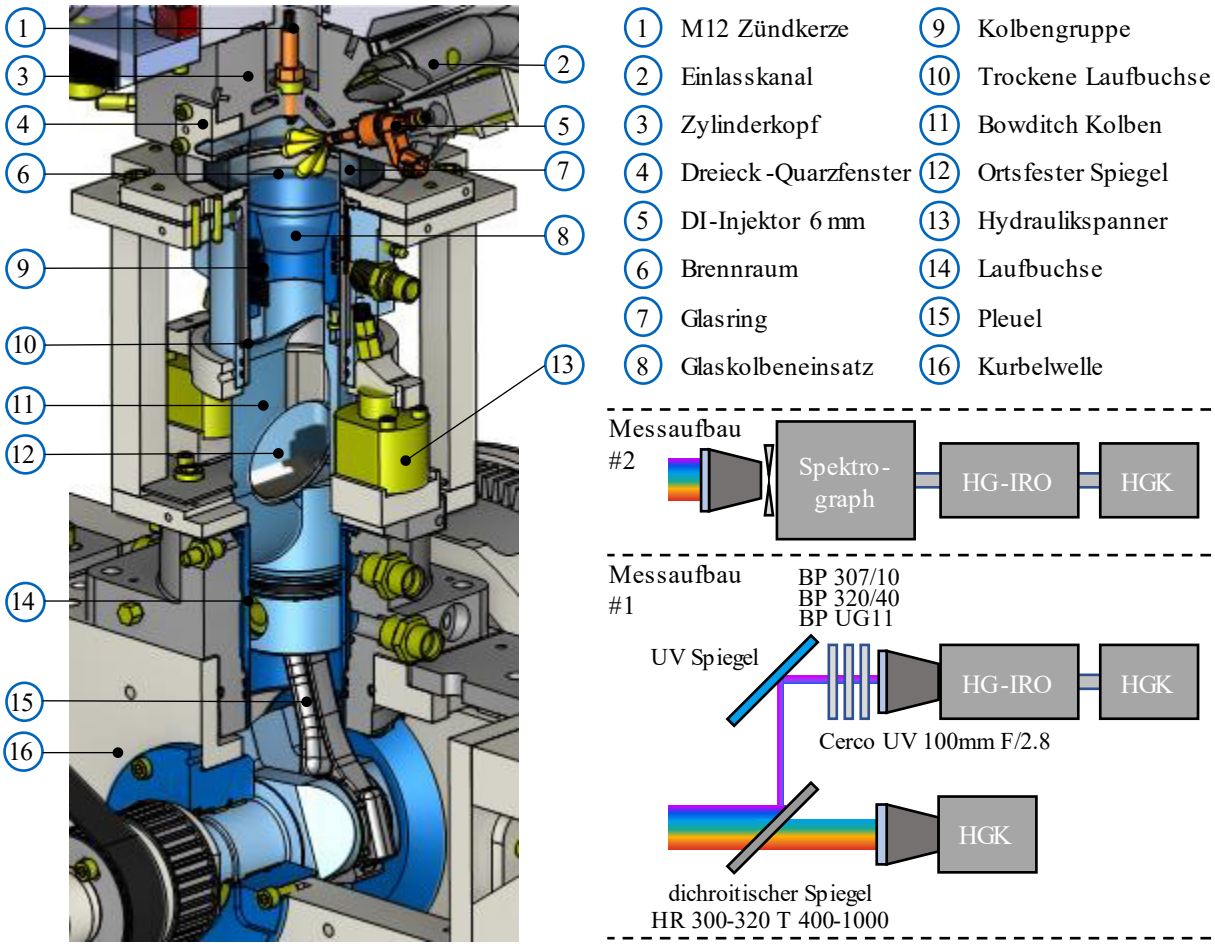

Abbildung 5: Viertelschnitt Optikmotor und optische Messaufbauten modifiziert nach [69]

Neben dem geänderten Kolben und der zusätzlichen Laufbuchse sind noch zwei weitere Modifikationen am Prüfstandsaufbau nötig. Durch die höhere Kolbenmasse ist die Unwucht der Massenausgleichswellen zu erhöhen. Zudem wird die Riemenführung des Steuertriebs geändert. Mit den moderaten Unterschieden zwischen thermodynamischer und optischer Konfiguration ist eine grundlegende Vergleichbarkeit der jeweiligen Ergebnisse gegeben. Durch Verwendung der trockenlaufenden und geschlitzten PTFE-Kolbenringe erhöht sich bei gleichem indiziertem Mitteldruck der Blow-By Massenstrom aufgrund von verminderter Abdichtung, wodurch der Luftbedarf steigt. Durch die begrenzte thermische und mechanische Belastbarkeit der Glaskomponenten ist die

Motordrehzahl auf 2000 1/min, die Motorlast auf einen indizierten Mitteldruck von 6 bar und der gefeuerte Motorbetrieb auf 60 Sekunden begrenzt. Begründet in dem auf 60 Sekunden limitierten nur quasi-stationären gefeuerten Motorbetrieb, werden beim optischen Motorbetrieb keine Abgasanalysatoren für gasförmige oder feste Abgasemissionen eingesetzt. Zur schnellen Reinigung des Kolbenglases ist die trockene Laufbuchse durch zwei Hydraulikspanner fixiert, welche nach Absteuern des Hydraulikdrucks ein Ablassen der Laufbuchse und ein Reinigen der Kolbenkrone ermöglichen. Für den Messaufbau #1 wurde der optische Pfad mit seinem elektromagnetischen Spektrum mit einem dichroitischen Spiegel in einen Pfad mit ultraviolettem (UV) Licht und in einen Pfad mit dem für den Menschen sichtbaren Licht aufgespalten. Somit ist ein paralleler Einsatz von zwei CMOS-Hochgeschwindigkeitskameras (HGK) möglich. Das sichtbare Licht wurde ungefiltert mit Hilfe einer Hochgeschwindigkeitsfarbkamera Phantom v2012 aufgenommen. Die Farbaufnahmen des sichtbaren Lichts werden zu Identifizierung und Bewertung der Flammenausbreitung, also auch zur Detektion von Rußpartikelquellen herangezogen. Der UV-Pfad wurde nochmals mit Bandpassfiltern aufbereitet, um ein möglichst störungsfreies Signal der Lichtemission des Hydroxyl-Radikals (OH*-Chemilumineszenz) zu erhalten, welches einen Peak im UV-Bereich bei einer Wellenlänge von 308 nm verzeichnet. Daher müssen alle optischen Komponenten zur Aufnahme UV-fähig sein. Das OH*-Radikal zu detektieren ist von großem Interesse, da es ein gut detektierbares Zwischenprodukt bei Verbrennungsprozessen von wasserstoffhaltigen Kraftstoffen ist. Es wird zur Charakterisierung und Lokalisierung der Wärmefreisetzung herangezogen. Durch die in Relation schwache Lichtemission des OH*-Radikals wurde der monochromen HGK Phantom v2011 der Hochgeschwindigkeitsbildverstärker (HG IRO) LaVision HS IRO vorgeschalten.

Mit dem Messaufbau #2 wurde das elektromagnetische Emissionsspektrum eindimensional mittels des bildgebenden Spektrometers Princeton Instruments IsoPlane SCT320 aufgezeichnet. Dazu wurde dem Spektrometer der auch im Messaufbau #1 verwendete HG IRO nachgeschaltet, auf welchen wiederrum die monochrome HGK Phantom v2011 folgt. Gleich dem UV-Pfad des Messaufbau #1 sind alle verwendeten optischen Komponenten UV-fähig. Bei der Konfiguration und Kalibrierung wurde darauf geachtet, das gesamte, relevante Radikalspektrum im Bereich von ~ 300 – 600 nm aufzulösen. Das ermöglicht die zeitgleiche Bewertung der relevanten Radikale OH (308 nm), CN (359 nm / 388 nm), HCHO (370 – 480 nm), CH (431 nm), C_2 (473 nm, 516 nm & 563 nm) und Na (589 nm). Der Aufnahmebereich mit örtlich eindimensionaler Auflösung des Spektrometers in Form einer Linie wurde quer zur Kurbelwellenachse mittig in den Brennraum gelegt. Somit erstreckt sich diese beginnend vom seitlichen direkteinspritzenden Injektor zwischen den Einlassventilen über die Zündkerze hin zur Quetschkante des Zylinderkopfs zwischen den Auslassventilen. Letztlich ermöglichen die 1D-Spektrometer Ergebnisse eine vertiefte Analyse der 2D-Ergebnisse und Verbrennungsphänomene aus dem Messaufbau #1.

4.2 Versuchs- und Auswertemethodik

4.2.1 Versuchsdurchführung und Messdatenerfassung

Wie bereits erwähnt, wird ein NI PXI-System zur MDE genutzt. Diese besitzt eine Online-GUI zur Visualisierung und Überwachung aller zur Verfügung stehenden Messwerte aus Sensoren, Detektoren, der Indizierung, sowie der Motorregelungsparameter aus der ECU. Zudem kalkuliert die MDE für die Regelung und Überwachung wichtige Indizierungsgrößen online. Eine dieser Kenngrößen ist der Heizverlauf, welcher sich nach [70] errechnet:

$$\frac{dQ_H}{d\varphi} = \frac{\kappa}{\kappa - 1} p \frac{dV}{d\varphi} + \frac{1}{\kappa - 1} V \frac{dp}{d\varphi} \tag{1}$$

Mit: φ = Kurbelwinkel; κ = Isentropenexponent; p = Druck; V = Volumen

Aus dem Heizverlauf wird bei der Versuchsdurchführung Online der EU50% bestimmt. Des Weiteren wird der indizierte Mitteldruck p_{mi} nach [71] kalkuliert:

$$p_{mi} = \frac{\oint p \, dV}{V_H} \tag{2}$$

Mit: p = Druck; V = Volumen, V_H = Hubvolumen

Der indizierte Mitteldruck repräsentiert die auf das Hubvolumen normierte Motorlast und dient als wichtiger Regelparameter beim Motorversuch. Zudem wird zur Bewertung der Regelmäßigkeit bzw. Stabilität der Verbrennung die Varianz des indizierten Mitteldrucks (engl. Coefficient of Variation, COV_{pmi}) der letzten 200 Arbeitsspiele herangezogen. Diese Varianz wird wie folgt berechnet [71]:

$$COV_{pmi} = \frac{\sigma_{p_{mi}}}{\bar{p}_{mi}} \tag{3}$$

$$\sigma_{p_{mi}} = \sqrt{\frac{1}{n-1} \sum_{i=1}^{n} (p_{mi_i} - \bar{p}_{mi})^2} \tag{4}$$

Mit: $\sigma_{p_{mi}}$ = Standardabweichung des p_{mi}; $\bar{p}_{mi}$ = Mittelwert des p_{mi}

Steigt der COV_{pmi} aufgrund von Zündaussetzern oder unvollständigen Verbrennungszyklen, sinkt die Stabilität des jeweiligen Betriebspunktes. In der vorliegenden Arbeit ist die Stabilitätsgrenze mit einem COV_{pmi} = 3 % definiert, somit werden Betriebspunkte mit größeren Varianzen als nicht realisierbar bewertet. Neben den genannten wird eine Vielzahl an weiteren Kenngrößen berechnet wie bspw. Wirkungsgrade, Leistungen, Kraftstoffverbräuche, max. Umsatzraten oder max. Drücke.

Wird ein Snapshot in der GUI der MDE ausgelöst, werden die indizierten Drücke von Einlass, Abgas, Brennraum und ggf. Vorkammer der letzten 200 Arbeitsspiele kurbelwinkelbasiert in einer Messdatei

gespeichert. Zudem werden die gemittelten Indizierkenngrößen, Berechnungskenngrößen und die mit reduzierter Frequenz abgetasteten Größen, wie Volumen- und Massenströme, Temperaturen, Drücke, Emissionswert, in einer separaten Messdatei gespeichert. Unabhängig vom Auslösen eines Snapshots, werden alle Größen, mit Ausnahme der Druck- und Heizverläufe, kontinuierlich mit 1 Hz im Logging mit aufgenommen. Hiermit ist die Auswertung von Größen über einen weiteren Zeitbereich möglich. Beim Betrieb des Optikmotors wird eine weitere von der MDE des NI PXI-Systems unabhängige optische MDE eingesetzt, welche die Imaging Software DaVis von LaVision verwendet. Die optische MDE erhält von der ECU sowohl die Motordrehzahl als auch das Auslösesignal zum gewünschten ° KW. Wird die Aufnahme ausgelöst, werden die folgenden 50 Arbeitszyklen mit dem entsprechend eingesetzten Messsystem #1 oder #2 aufgenommen und in einem softwarespezifischen Rohdatenformat abgelegt. Die Aufnahme erfolgt mit einer Frequenz von 0,5 °KW über einen Bereich von 100 °KW, woraus sich eine Bildanzahl von 200 Bildern pro Arbeitsspiel ergibt. Die Auslösung der optischen MDE wird so abgestimmt, dass die 50 Arbeitszyklen in den Bereich der 200 Arbeitszyklen der MDE des NI PXI-Systems fallen. Zudem wird vom optischen Messsystem, synchron zum aufgenommenen Zyklus, ein 5V-Signal ausgegeben, welches mittels Indizierkanal aufgezeichnet wird. Das ermöglicht die Zuordnung des indizierten Druckverlaufs zur jeweiligen Bildreihe von jedem Arbeitszyklus. Nach erfolgter Aufnahme besteht zudem die Möglichkeit der visuellen Kontrolle der Aufnahmen durch die GUI von DaVis.

Bei der Versuchsdurchführung werden für die beiden Konfigurationen des EFMs unterschiedliche Referenzpunkte verwendet. Aufgrund der begrenzten thermischen und mechanischen Belastbarkeit der Optikkomponenten muss für die optische Konfiguration die Motordrehzahl auf 1500 1/min und die Motorlast auf 6 bar p_{mi} verringert werden. Die Betriebsparameter des Referenzpunktes für die beiden Motorkonfigurationen sind in Tabelle 5 gelistet. Zudem werden durch den auf 60 Sekunden eingeschränkten, gefeuerten Betrieb des Optikmotors keine stationären Betriebsbedingungen erreicht. Bei der Versuchsdurchführung wird hier, bereits 12 Sekunden nach dem ersten gefeuerten Arbeitsspiel, der Snapshot für die thermodynamischen Messdaten in der MDE ausgelöst. Abhängig von der Motordrehzahl wird dann entsprechend zeitversetzt die optische Messtechnik aktuiert. Somit werden bspw. bei einer Motordrehzahl von 1500 1/min die 50 Arbeitszyklen zwischen 18 - 20 Sekunden nach dem ersten gefeuerten Arbeitsspiel aufgezeichnet. Dementgegen wird im Normalfall bei der Versuchsdurchführung mit der thermodynamischen Konfiguration der Motorbetriebspunkt min. 120 Sekunden gehalten, bis keine kontinuierliche Veränderung ausgewählter Messgrößen mehr feststellbar ist. Grundsätzlich wurde für alle in dieser Arbeit vermessenen Betriebspunkte der EU50% mit Hilfe der Online-Heizverlaufsberechnung auf 8 °KW n. OT eingeregelt. Wenn abnormale Verbrennungsphänomene auftraten, wurde der EU50% in Richtung spät verschoben. Zur grundlegenden Untersuchung des Motorbetriebs bei Verwendung der Oxygenatkraftstoffe wurden Variationen von Last, Drehzahl, λ, ε, SOI, Kraftstoffeinspritzdruck, Kühl-/Schmieröltemperatur und Lufttemperatur mit

beiden Motorkonfigurationen durchgeführt. Im Thermodynamikmotor wurde zudem die eingebrachte Energiemenge in die gespülte Vorkammer variiert.

Tabelle 5: Betriebsparameter der Referenzpunkte des Forschungsmotors

Konfiguration	**thermodynamisch**	**optisch**
Motordrehzahl in 1/min	2000	1500
Motorlast p_{mi} in bar	7	6
Verbrennungsluftverhältnis	1,0	
EU50% in °KW n. OT	8	
SOI in °KW n. OT	430	
Anzahl an Einspritzungen	1	
Kraftstoffeinspritzdruck in MPa	35	25
Kolbenkühldüse aktiv	$p_{mi} \geq 11$ bar	nicht verfügbar
Schmieröl- & Kühlwassertemperatur in °C	80 °C	
Lufttemperatur Plenum in °C	30 °C	

Die Parametervariationen aus der vorliegenden Arbeit sind in Tabelle 6 aufgelistet. Zudem wurden weiterführende Untersuchungen mit der thermodynamischen Konfiguration vorgenommen, wie die Untersuchung des Injektorverkokungsverhaltens bei steigendem DMC-Blendanteil. Für diesen Versuch wurde der Forschungsmotor am Referenzpunkt mit einem reduzierten Kraftstoffdruck von 25 MPa für 90 min betrieben. Der Kraftstoffdruck wird reduziert, um die Verkokungsneigung zu erhöhen, da auch im Serienbetrieb der Kraftstoffdruck an den jeweiligen Betriebspunkt angepasst wird. Vor jedem Verkokungslauf wurde die Injektorkuppe gründlich gereinigt und der Zustand unter einem digitalen Mikroskop überprüft. Neben den Partikelemissionen wurde auch der zeitliche Verlauf des Verkokungsvorgangs der Injektorkuppe bewertet, indem zu definierten Zeitintervallen der Motorbetrieb gestoppt und der Injektor demontiert wurde. Der Verkokungszustand wurde dann unter einem digitalen Mikroskop begutachtet und mit einer digitalen Bildaufnahme festgehalten. Anschließend wurde die Injektorkuppe wieder gereinigt und der Verkokungslauf wurde von neuem begonnen. Somit wurde ein Störeinfluss durch den Injektor Aus- und Einbau ausgeschlossen. Weiter wurde aufgrund der hohen Klopffestigkeiten der Oxygenatkraftstoffe die Widerstandsfähigkeit dieser gegen abnormale Verbrennungsphänomene untersucht. Hierfür wurde der Versuchsmotor stationär bei einer niedrigen Drehzahl von 1500 1/min und der maximalen Motorlast von $p_{mi} = 17$ bar betrieben. Zudem wurde das Verdichtungsverhältnis auf 14,91:1 angehoben und die Temperatur der Ansaugluft beginnend mit 30 °C sukzessive gesteigert, um abnormale Verbrennungsphänomene zu provozieren. Zuletzt wurde mit C65F35 der Einfluss des Kolbenringpakets auf die teils schmierölinduzierten Abgasemissionen PN und VOC untersucht, wobei das C1-Kraftstoffgemisch als Entwicklungswerkzeug diente. Da C65F35 rußarm verbrennt, was eine Analyse der ölinduzierten Partikelemissionen isoliert von den Partikelemissionen aus dem Kraftstoff ermöglicht. Aufbauend auf PRIME 3D® Simulationen, wurde

am Kolbenringpaket das Stoßspiel des zweiten Kolbenrings variiert, um den Aerosolfluss zwischen Brennraum, Kolbengruppe und Kurbelgehäuse gezielt zu manipulieren.

Tabelle 6: Variierter Parameter für die jeweilige Motorkonfiguration

Variierter Bereich	thermodynamisch		optisch
	ohne VK	mit VK	
λ	0,8 – 1,6	1,4 – 2,4	0,8 – 1,4
Motorlast p_{mi} in bar	3 - 17	7	6
Verdichtungsverhältnis	10,94 & 14,91	14,18	9,36
SOI in °KW n. OT	390 - 670	430	430 - 630
Drehzahl in 1/min	1000 - 3000	2000	1500
Kühlwassertemperatur in °C	-5 - 80	80	
Schmieröltemperatur in °C	25 - 80	80	
Kraftstoffeinspritzdruck in MPa	25 und 35	35	25
Lufttemperatur Einlass in °C	30 - 200	30	
Kraftstoffenergieanteil VK in %	-	1,68 - 4,63	-
DMC-Anteil in G100 in %	0 - 100	0	0 - 30
MeFo-Anteil in DMC in %	35		
MeFo-Anteil in MeOH in %	0 -30	-	30

Nach jedem Ringwechsel wurde ein 225-minütiges Einlaufprogramm absolviert, um Einlaufeffekte der Kolbenringgruppe auszuschließen. Im Zuge dieser Messkampagne wurden Last, Drehzahl und Einlassdruck Variationen vermessen.

4.2.2 Messdatenaufbereitung

Die erstellten thermodynamischen Messdateien der einzelnen Betriebspunkte von der MDE werden mittels eines MATLAB-Tools umgewandelt und in Messdatenblöcken, die mehrere Snapshots beinhalten, abgelegt. Zudem werden diverse zusätzliche Kenngrößen kalkuliert bzw. auf eine andere Basis umgerechnet, wie bspw. die PN-Konzentration von der volumetrischen Basis #/cm^3 auf eine energiebezogene Basis #/kWh. In diesem Zuge wurde für aufgeladene Betriebspunkte auch die indizierte Leistung (P_i) mit einem Korrekturfaktor ($K_{P,Lader}$) multipliziert, um die benötigte Leistung zum Verdichten der Ladeluft zu berücksichtigen, gleich Stadler et al. [72]. Weiter wurden mit der revidierten indizierten Leistung ($P_{i,rev}$) die Wirkungsgrade und Verbrauchskennwerte nachberechnet. Zur Berücksichtigung der Verdichterleistung wurde eine isentrope Verdichtung gewählt, wobei der Wirkungsgrad eines Roots-Gebläse von η_{R-G} = 75 % angenommen wurde. Die Wahl des Wirkungsgrades entspricht in etwa dem durchschnittlichen Wirkungsgrad eines Roots-Gebläses, wenn

dieses bei den vorliegenden moderaten Druckdifferenzen zwischen Umgebungs- und Ladedruck betrieben wird. Demzufolge wurden die $P_{i,rev}$ und der $K_{P,Lader}$ wie folgt berechnet:

$$P_{i,rev} = P_i \cdot K_{P,Lader} \tag{5}$$

$$K_{P,Lader} = 1 - \left(\frac{c_p \cdot T_1 \cdot \left(\left(\frac{p_1}{p_2} \right)^{\frac{\kappa-1}{\kappa}} - 1 \right) \cdot \dot{m}_L}{P_i \cdot \eta_{R-G}} \right) \tag{6}$$

Mit: c_p = isobare spez. Wärmekapazität; T_1 = Lufttemperatur vor Verdichter; p_1 = Druck vor Verdichter; p_2 = Druck nach Verdichter; $\dot{m}_L$ = Luftmassenstrom

Mit den nachbereiteten Messdatenblöcken wurden im Anschluss mittels einer MATLAB-GUI Diagramme zur Visualisierung und Bewertung erstellt.

Für die Aufbereitung der optischen Aufnahmen der HGKs aus dem Messaufbau #1 werden ebenfalls MATLAB Routinen verwendet. Aufgrund der mehrfachen Spiegelung und der unterschiedlichen Länge des optischen Pfades müssen die Aufnahmen zunächst transformiert und skaliert werden, um einen sinnvollen Vergleich des OH*-Bildes mit dem des sichtbaren Lichts zu ermöglichen. Hierzu wurden zu Versuchsbeginn und Motorstillstand Kalibrierbilder für die beiden optischen Pfade erstellt, worauf die Zündkerze und die Ventile eindeutig sichtbar sind. Mit diesen Bildern wird dann die benötigte Skalierung, Drehung und Verschiebung ermittelt und im Auswerteskript verankert. Somit ist nach erfolgter Transformation der Bilder eine Vergleichbarkeit von verschiedenen Betriebspunkten und den jeweiligen optischen Pfaden gegeben. Nachfolgend wurden die Bilder über die mittleren 20 der 50 Zyklen gemittelt, um die Aufnahmen statistisch abzusichern. Wird die Anzahl der gemittelten Zyklen erhöht, gehen aufgrund der Zyklusschwankungen durch den homogenen Motorbetrieb mit Funkenzündung Detailinformationen verloren. In der weiteren Aufbereitung der Aufnahmen wurden Kollagen erstellt und die Einzelbilder mit Betriebspunkt und Kraftstoffinformationen beschriftet. Für alle Aufnahmen wurden identische Belichtungszeiten, Aufnahmefrequenzen und Bilderverstärkereinstellungen verwendet, was eine Vergleichbarkeit über alle Betriebspunkte hinweg ermöglicht. Wenn die Aufnahmen aufgrund von verringerter Lichtemission eine zu geringe Intensität in Counts aufwiesen, wurden die Intensität mit einem Faktor skaliert. Es wurden ausschließlich Aufnahmen mit demselben Skalierungsfaktor verglichen.

5 Publizierte Untersuchungen

Im Folgenden werden die publizierten Untersuchungen erläutert und diskutiert. Zunächst wurde der Forschungsbedarf von Härtl et al. [12] bezüglich C65F35 aufgegriffen, wobei thermodynamische Versuche am EFM und Vierzylinder-Serienmotor durchgeführt wurden. Aufbauend auf den Ergebnissen wurden nachfolgend Untersuchungen am volloptischen EFM durchgeführt, um die gewonnenen thermodynamischen Erkenntnisse zu ergänzen und festigen. Hierzu wurde der Verbrennungsprozess auf zwei optischen Pfaden mittels High-Speed Kameras aufgelöst und visualisiert. Neben dem für das menschliche Auge sichtbaren Lichts wurde in dieser Untersuchung auch der emittierte UV-Wellenlängenbereich erfasst, welcher die Lichtemission des Hydroxyl-Radikals beinhaltet. Im nächsten Schritt wurden die gewonnenen Erkenntnisse weiteren potenziellen C1-Oxygeanten gegenübergestellt. Dabei wurden sowohl reine C1-Kraftstoffmischungen als auch ein mit C1-Oxygenaten geblendeter Referenzkraftstoff untersucht, um die jeweiligen Vor- und Nachteile des Kraftstoffes zu identifizieren. In der letzten Untersuchung wurden die Kraftstoffeigenschaften von C65F35 genutzt, um die kraftstoffinduzierten Partikelemissionen nahezu vollständig zu eliminieren, womit eine isolierte Betrachtung der ölinduzierten Partikelemissionen möglich wird. Durch die Variation des Stoßspiels des zweiten Kompressionsrings wurden die Zwischenringdrücke der Kolbengruppe gezielt manipuliert, was in der Folge den Aerosolfluss zwischen Kurbelgehäuse und Brennraum beeinflusst. Dieser Aerosolfluss wirkt sich betriebspunktabhängig auf die Partikelemissionen aus, womit der Einfluss der Kolbenringgruppe auf die ölinduzierten Partikelemissionen bewertet wurde.

5.1 Thermodynamische Untersuchung von DMC/MeFo am Einzylinder & Vollmotor

Die thermodynamische Untersuchung wurde in der folgenden Veröffentlichung publiziert:

BLOCHUM, S., GADOMSKI, B., RETZLAFF, M., THAMM, F. et al., *"Potential Analysis of a DMC/MeFo Mixture in a DISI Single and Multi-Cylinder Light Vehicle Gasoline Engine," SAE Int. J. Adv. & Curr. Prac. in Mobility 4(1):15-31, 2022, https://doi.org/10.4271/2021-01-0561*

Bei der thermodynamischen Untersuchung von C65F35 wurden Versuche am Ein- und Vierzylindermotor durchgeführt. Die Versuche am EFM umfassten die Variation des Luft-Kraftstoffverhältnisses, SOI und Verdichtungsverhältnisses. Bei der Variation des SOI wurde ein später Einspritzzeitpunkt zu Beginn des Kompressionshubs gewählt und schrittweise in Richtung spät verschoben. Verglichen mit der saugsynchronen Direkteinspritzung wurde hierbei, entgegen G100, für C65F35 eine verbesserte Verbrennungsstabilität erreicht. Zudem war mit C65F35 auch bei einem um 60 °KW späteren SOI gegenüber G100 eine hohe Verbrennungsstabilität zu beobachten. Diese Beobachtung wird mit den weiten Zündgrenzen von DMC/MeFo in Kombination mit der erhöhten TKE

zum ZZP durch die Einspritzung begründet. Aufgrund der engeren Zündgrenzen und dem erhöhten Luftbedarf von G100 treten hier bereits bei einem SOI von 70 °KW n. UT Zündaussetzer auf, worauf die Stabilitätsgrenze des Betriebspunktes überschritten wird. Mit der Verlagerung des Einspritzzeitpunktes in den Kompressionshub wurden für C65F35 teilweise Wirkungsgradsteigerungen von bis zu $\Delta\eta_i = 1{,}4$ % erreicht. Grundsätzlich wurden bei nahezu allen Versuchen am EFM für C65F35 deutlich niedrigere NO_X- und PN23-Rohemissionen beobachtet, wobei die PN23-Konzentration immer nahe und meist auf Umgebungsniveau lag. Mit der Variation des Luft-Kraftstoffverhältnisses zeigt C65F35 verglichen mit G100 speziell im mageren eine längere Brenndauer und schlechtere Verbrennungsstabilität, was folglich in einer früher einsetzenden Magerlaufgrenze bei $\lambda = 1{,}3$, gegenüber $\lambda = 1{,}6$ für G100, endet. Wird die Direkteinspritzung in den Kompressionshub gelegt wird die Magerlaufgrenze auf $\lambda = 1{,}5$ verschoben. Auffällig zeigen sich sowohl die teils um über 50 % reduzierten NO_X-Emissionen im Magerbetrieb als auch die unverändert niedrige PN23-Konzentration bei der Variation von λ. Die niedrigen NO_X-Emissionen begründen sich mit der höheren Verdampfungskühlung von C65F35 und die niedrigen PN23-Emissionen mit der C1-Molekülstruktur in Kombination mit dem hohen Sauerstoffgehalt von C65F35. Bei der Bewertung des Wirkungsgradpotentials zeigt C65F35 bei unverändertem Verdichtungsverhältnis von $\varepsilon = 10{,}92$ am EFM erst ab einem $p_{mi} > 13$ bar einen Wirkungsgradvorteil. Denn hier muss aufgrund von klopfenden Verbrennungen der EU50% für G100, zu Ungunsten des η_i, in Richtung später verschoben werden. Wird das Verdichtungsverhältnis auf 14,91 angehoben wird mit C65F35 gegenüber G100 ($\varepsilon = 10{,}92$) in allen untersuchten Betriebspunkten eine Wirkungsgradsteigerung erzielt. Die maximale Steigerung von $\Delta\eta_i = 4{,}1$ % wird bei der maximalen Last von $p_{mi} = 17$ bar gemessen.

Bei den Untersuchungen am Vierzylinder-Serienaggregat wurden ausschließlich diverse Parameter in der ECU angepasst. Dazu zählt unter anderem die Verlängerung der Einspritzdauer aufgrund des verringerten Heizwertes sowie die Aktivierung der Tumbleklappe in großen Teilen des Betriebskennfelds. Zudem wird mit dem Einsatz von C65F35 eine Volllastanfettung aufgrund der hohen Verdampfungsenthalpie obsolet, wodurch im gesamten Betriebskennfeld für C65F35 ein stöchiometrisches Luft-Kraftstoffgemisch eingesetzt wurde. Grundsätzlich wurden die Versuchsergebnisse vom EFM, wie die Klopffestigkeit, der erhöhte Bedarf an TKE, die niedrigeren NO_X- und PN23-Rohemissionen, bestätigt. So wurden über das gesamte Motorbetriebskennfeld nur bei einem $p_{me} > 10$ bar Wirkungsgradvorteile aufgrund der konstanten EU50%-Lage von C65F35 beobachtet. Der maximale effektive Wirkungsgradgewinn gegenüber G100 von $\Delta\eta_{eff} = 16$ % wurde im Low-End Torque bei $p_{me} = 23$ bar und $n_{motor} = 1750$ 1/min erreicht. In diesem Betriebspunkt wurde mit C65F35 der maximale gemittelte Zylinderdruck gegenüber G100 mit $p_{max} = 119$ bar nahezu verdoppelt. Die PN23-Konzentration wurde über einen weiten Bereich des Betriebskennfeldes, verstärkt bei höheren Lasten und Drehzahlen, um 95 – 99 % reduziert. In für den WLTC relevanten Betriebsbereichen bei niedrigeren Lasten und Drehzahlen wurde eine geringere Reduktion der PN23-Emissionen von

0 – 60 % erreicht. Bei den NO_X-Emissionen wurde durch die erhöhte Verdampfungsenthalpie und den damit einhergehenden verringerten Verbrennungsspitzentemperaturen eine durchschnittliche Reduktion von 40 % erzielt. Hingegen stiegen in den Randbereichen des Betriebskennfelds die NO_X-Emissionen um bis zu 89 %, im Low-End Torque durch die frühere Lage des EU50%, im High-End Torque durch den stöchiometrischen Motorbetrieb. Im Gegenzug wird aber durch den stöchiometrischen Betrieb im High-End Torque eine Reduktion bei den CO-Rohemissionen erzielt, da hier mit G100 durch die Anfettung und dem damit einhergehenden Luftmangel vermehrt CO emittiert wird. Grundsätzlich zeigten aber auch die CO-Rohemissionen über weite Bereiche des Betriebskennfelds ein verringertes Niveau. Weiter wurde im Rohabgas eine erhöhte Konzentration der Abgaskomponenten MeOH + 90 %, CH_2O + 30 % und Methan + 80 % festgestellt, welche aber nach dem Drei-Wege-Katalysator unterhalb der Nachweisgrenze des Messsystems lagen. Bei den simulierten Testzyklen RDE und WLTC am Motorenprüfstand wurden ≤ 21 % des Maximalwertes der reglementierten Abgaskomponenten PN23, CO und HC der Euro 6d Norm erreicht. Für NO_X wurde der Grenzwert nur beim RDE-Testzyklus um 55 % überschritten. Ursächlich dafür ist, dass für die Lastsimulation ein SUV-PKW der Kategorie J angenommen wurde, was in Verbindung mit der höheren Lastanforderung des RDE zur Folge hatte, dass der Motor kurzzeitig in einem Betriebspunkt mit erhöhtem NO_X-Ausstoß betrieben wurde.

Individueller Beitrag an der Publikation:

Der Autor hatte nach Recherche der bestehenden Literatur die Idee zur vorliegenden Publikation und hat diese konzipiert. Der Autor hat alle Versuche am EFM geplant und durchgeführt. Anschließend hat der Autor die generierten Versuchsdaten mittels individuell erstellten Auswerteroutinen visualisiert und bewertet. Diese Versuchsergebnisse wurden darauffolgend vom Autor interpretiert und tiefgreifend diskutiert. Zudem waren zur Durchführung des Experiments diverse Modifikationen/Entwicklungen am EFM nötig, wie bspw. die Entwicklung eines für synthetische Kraftstoffe resistivem Kraftstoffsystem. Diese Entwicklungen hat der Autor federführend umgesetzt. Der Autor war sowohl Ansprechpartner/Bearbeiter während des Reviewprozesses, als auch Vortragender bei der Präsentation der Veröffentlichung.

Die Mitautoren Gadomski, Retzlaff und Thamm haben federführend die Untersuchungen am Vierzylinder-Serienaggregat durchgeführt und diese Versuchsergebnisse visualisiert, bewertet und interpretiert.

5.2 Optische Untersuchung von DMC/MeFo am Einzylinderforschungsmotor

Die optische Untersuchung wurde in der folgenden Veröffentlichung publiziert:

MÜHLTHALER, M., **BLOCHUM, S.**, STADLER, A., HÄRTL, M. ET AL., *"Optical Investigations of an Oxygenated Alternative Fuel in a Single Cylinder DISI Light Vehicle Gasoline Engine," SAE Technical Paper 2021-01-0557, 2021, https://doi.org/10.4271/2021-01-0557*

Aufbauend auf den Kenntnissen der thermodynamischen Untersuchung von C65F35 wurden Versuche mit der optischen Konfiguration des EFMs durchgeführt. Bei der Untersuchung wurden das Luft-Kraftstoff-Verhältnis und der SOI bei einer Motordrehzahl von n_{Motor} = 1500 1/min und einer Last von p_{mi} = 6 bar variiert. Im Zuge der Variation von λ wurden bei G100 für ein unterstöchiometrisches Gemisch von λ = 0,8 neben der bläulichen Flamme verstärkt Diffusionsflammen mittels High-Speed Farbaufnahmen des Flammeneigenleuchtens detektiert. Die Diffusionsflamme ist bekannt als Indikator für die Rußentstehung und bestätigt somit den starken Anstieg der PN-Konzentration in Richtung unterstöchiometrischen Motorbetrieb aus der thermodynamischen Untersuchung. Demgegenüber zeigt C65F35 beim gleichem λ eine bläuliche Flamme mit nur wenigen kleinen Diffusionsspots, welche auf vereinzelte Kraftstoff-Schmieröl-Tropfen oder abgelöste Brennraumablagerungen deuten. Im Vergleich ist die Intensität der blauen Flamme bei der C1-Oxygenatkraftstoffmischung C65F35 geringer, was auf eine geringe Brennraumtemperatur, aufgrund der in Summe höheren Verdampfungsenthalpie von C65F35, schließen lässt. Zudem zeigt C65F35 entgegen G100 bei überstöchiometrischen Motorbetrieb eine intensivere Verbrennung mit höherem Gradienten und Maximalwert im Heizverlauf. Die von C65F35 emittierte Lichtemission zeigt auch bei mageren Gemischen eine geringe Intensität verglichen mit G100, was auch hier die erwarteten geringeren Brennraumtemperaturen bestätigt. Bei der SOI-Variation wurden die Erkenntnisse aus den thermodynamischen Untersuchungen ebenfalls bestätigt. Gleich den thermodynamischen Versuchen am EFM war mit der Einspritzung im Kompressionshub bei einem SOI von 630 °KW nach Zünd-OT (n. ZOT) kein stabiler Motorbetrieb mit G100 möglich. Es wurden massive Zyklenschwankungen mit stark ausgeprägten Diffusionsflammen und Zündaussetzern detektiert. Dementsprechend sinkt sowohl der Gradient als auch der Maximalwert des Heizverlaufes und zudem verlängert sich die Brenndauer für G100 signifikant. Mit C65F35 wird grundsätzlich, wie bei den thermodynamischen Untersuchungen, ein positiver Einfluss der Direkteinspritzung im Kompressionshub auf die Verbrennungsstabilität beobachtet. Folglich steigt beim Heizverlauf der Gradient und Maximalwert durch die verbesserte Umsetzung der Brennraumladung. Bei der Analyse des OH*-Radikals über den zweiten optischen Pfad ist gemäß der Erwartung für eine Einspritzung im Kompressionshub mit geringer Gemischaufbereitungszeit eine asymmetrische Verbrennung der Brennraumladung zu beobachten. Hiermit lässt sich auf eine inhomogene und unvollständige Gemischaufbereitung schließen, welche durch diverse Kraftstoffeigenschaften von

C65F35 bei einem SOI im Kompressionshub überkompensiert wird. Zu diesen Eigenschaften zählen die für überstöchiometrische Gemische weiteren Zündgrenzen in Luft von 12,9 Vol.-% bei DMC und 20 Vol.-% bei MeFo. Dies ermöglicht gegenüber G100 die Zündung lokal fetterer Gemische bei gleichzeitiger Unterbindung der Rußentstehung durch die C1-Molekülstruktur. Der späte Einspritzzeitpunkt mit der unvollständigen Gemischaufbereitung wirkt sich bei C65F35 zudem positiv auf die Verbrennungsstabilität aus, da durch den verringerten Anteil an verdampftem Kraftstoff die Brennraumtemperatur steigt, was die Zündbedingungen verbessert. Mit der 1D-Flammenemissionsspektroskopie wurde mit C65F35 eine deutlich verringerte Intensität der Flammenemission beobachtet, was sich auf die verringerten Brennraumtemperaturen zurückführen lässt. Diese Erkenntnis deckt sich mit der ausgeprägten Intensität des CH-Radikals bei G100, da das Radikal verstärkt bei hohen Temperaturen in der Flammenfront auftritt. Ebenfalls zeigen die C_2-Radikale speziell im Bereich der C_2-Swan-Bande bei 563 nm, 516 nm und 473 nm eine hohe Intensität für G100 bei $\lambda = 0{,}8$. Dies bestätigt die erhöhten Partikelemissionen von G100, da C_2-Radikale als Rußvorläufermoleküle gelten und in der Theorie des Rußenstehungsprozesses als Polymerisationskerne dienen. Zudem deutet bei C65F35 die geringere Intensität des CN-Radikals, welches in der Flammenforschung als Zwischenprodukt bei der Bildung von Prompt-NO_X bekannt ist, in Kombination mit den geringeren Brennraumspitzentemperaturen auf geringe NO_X-Emissionen hin. Diese Ergebnisse decken sich mit den Forschungsergebnissen aus den vorangegangenen thermodynamischen Untersuchungen.

Individueller Beitrag an der Publikation:

Der Autor hatte aufbauend auf seiner vorangegangenen Untersuchung die Idee zur vorliegenden Publikation und hat diese mit dem Erstautor Mühlthaler konzipiert. Der Autor hat in Zusammenarbeit mit Mühlthaler alle Versuche am EFM geplant und durchgeführt. Anschließend hat der Autor Teile der generierten Versuchsdaten mittels individuell erstellten Auswerteroutinen visualisiert und bewertet. Die Interpretation und Diskussion der Versuchsergebnisse wurde in Zusammenarbeit mit Mühlthaler durchgeführt. Den Aufbau und die Inbetriebnahme der verschiedenen optischen Messaufbauten hat der Autor in Zusammenarbeit mit dem Erstautor durchgeführt.

5.3 Potentialvergleich von DMC/MeFo mit weiteren C1-Kraftstoffen

Die Potentialvergleich wurde in der folgenden Veröffentlichung publiziert:

BLOCHUM, S., FELLNER, F., MÜHLTHALER, M., HÄRTL, M. ET AL., *"Comparison of Promising Sustainable C1-Fuels Methanol, Dimethyl Carbonate, and Methyl Formate in a DISI Single-Cylinder Light Vehicle Gasoline Engine," SAE Technical Paper 2021-01-1204, 2021, https://doi.org/10.4271/2021-01-1204*

Mit den gewonnenen Erkenntnissen über C65F35 im direkteinspritzenden Ottomotor aus den vorangegangenen Publikationen war der nächste Schritt der Vergleich von C65F35 mit weiteren C1-Oxygenatkraftstoffen in Reinform und als Blendkomponente. Als weiteres C1-Oxygenat wurde MeOH verwendet, da dieses ähnliche Kraftstoffeigenschaften wie DMC besitzt, es ein bereits sehr intensiv erforschter Kraftstoff ist und er sich effizienter herstellen lässt. Als schwerwiegendster Nachteil ist aber die toxische Wirkung von MeOH zu nennen. Zu Beginn wurde eine Voruntersuchung mit verschiedenen Reinstoffmischungen aus MeOH und MeFo durchgeführt, um die Reinstoffmischung mit dem größten Potential in Bezug auf die Rohemissionen und den indizierten Wirkungsgrad zu identifizieren. Hier zeigte M70F30 den besten Kompromiss für die MeOH- und MeFo-Reinstoffmischungen, da es gegenüber Mischungen mit höheren MeOH-Anteilen nur geringfügige Nachteile beim indizierten Wirkungsgrad zeigt, aber deutlich weniger PN-Emissionen bei späten Einspritzzeitpunkten emittiert. Im Nachfolgenden wurde eine Variation der Motorlast, des Einspritzzeitpunkts im Kompressionshub und von λ durchgeführt, wobei bei den Versuchen am Thermodynamikmotor zudem der Einfluss einer Kühlwassertemperatur von -5° C und 40° C gegenüber 80° C untersucht wurde. Über die Variation von λ bei p_{mi} = 7 bar und 2000 1/min zeigt M70F30 gleich C65F35 keine signifikante Sensitivität gegenüber PN-Emissionen. Entgegen der Erwartung ist hin zu fetten Gemischen aber ein Trend zu sinkenden PN-Emissionen zu erkennen. Über die Lastvariation bei einer Motordrehzahl von 2000 1/min ist für M70F30 entgegen C65F35 auch bei Lasten von p_{mi} > 11 bar kein Anstieg in den PN-Emissionen zu beobachten. Eine Erklärung hierfür sind die speziell für fettere Gemische weiteren Zündgrenzen von MeOH in Luft. Denn durch die bei höheren Lasten größere Menge an eingespritztem Kraftstoff, in Verbindung mit der hohen Verdampfungsenthalpie von MeOH, steigt der Anteil an nicht vollständig aufbereitetem Kraftstoff. Die somit entstehenden lokal fetten Brennraumzonen sind aufgrund der weiteren Zündgrenzen und der geringeren Zündenergie von MeOH für M70F30 zündwilliger. Für C65F35 steigt in Relation zu M70F30 folglich der Anteil an nicht bzw. unvollständig verbranntem Kraftstoff, welcher bei der Messung der Festkörperpartikel im Rohabgas teilweise zu einer erhöhten PN führt. Grund dafür ist, dass das Verdampfungsrohr im Messsystem die hohe Menge an volatilen organischen Verbindungen nicht vollständig verdampft und folglich flüssige Kraftstofftropfen als Festkörperpartikel gezählt werden. Bei NO_X- und CO-Emissionen zeigt M70F30 ein über weite Bereiche sehr ähnliches Verhalten wie C65F35. Wird die Kühlwassertemperatur von

80° C auf 40° C gesenkt steigen für C65F35 die PN23-Emissionen über den Lastschnitt um den Faktor 2,8, zudem liegen die PN23-Emissionen über denen von G100. Bei M70F30 liegen die PN23-Emissionen hingegen auf unverändert niedrigem Niveau. Wird die Kühlwassertemperatur weiter auf - 5° C reduziert, steigen auch für M70F30 die PN-Emissionen stark an, liegen aber dennoch unter dem Niveau von C65F35. Durch die niedrige Motortemperatur und die große, benötigte Verdampfungswärmemenge beim Motorbetrieb mit den C1-Kraftstoffmischungen steigt der Anteil an nicht aufbereitetem Kraftstoff. Durch die schmaleren Zündgrenzen und die höhere benötigte minimale Zündenergie von C65F35 ist die Brennraumladung bei 3 - 5 bar p_{mi} im untersuchten Punkt nur bedingt zündfähig, wodurch kein stabiler Motorbetrieb möglich ist. Bei der Variation des SOI im Kompressionshub zeigt M70F30 ähnliche positive Verbrennungseigenschaften wie C65F35 bei den vorangegangenen Untersuchungen und erreicht um 12 % niedrigere PN23-Emissionen als C65F35. Gleich C65F35 ist ein Motorbetrieb mit einem SOI von 670 °KW n. ZOT möglich, hierbei endet die Einspritzung für M70F30 lediglich 12,5 °KW vor dem ZZP bei einem EU50% von 8 °KW n. ZOT. Diese Beobachtungen wurden bei den optischen Untersuchungen am EFM bestätigt. Verglichen mit dem SOI von 430 °KW n. ZOT zeigt der Betriebspunkt mit einer späten Einspritzung im Kompressionshub, bis auf die asymmetrische Flammenausbreitung, ein sehr ähnliches Verhalten bei den High-Speed Farbaufnahmen. Im nächsten Schritt wurde die Widerstandsfähigkeit der beiden C1-Kraftstoffmischungen gegenüber abnormaler Verbrennungsphänomene untersucht. Hierfür wurde, verglichen mit dem Referenzpunkt, das Verdichtungsverhältnis ε von 10,92 auf 14,91 mittels des HCR-Kolbens erhöht, die Motordrehzahl auf 1500 1/min reduziert und die Last auf p_{mi} = 17 bar angehoben. Zudem wurden die in der Motorenforschung bekannten Kraftstoffe MeOH und Toluol in Reinform untersucht, um einen relativen Vergleich von C65F35 und M70F30, für künftige Forschungsvorhaben wie bspw. 3D-CFD Simulationen, zu ermöglichen. Unter den genannten Motorbetriebsbedingungen sind bei keinem der Kraftstoffe abnormale Verbrennungsphänomene aufgetreten, worauf die Ansauglufttemperatur $T_{Einlass}$ beginnend von 30° C sukzessive erhöht wurde. Die ersten abnormalen Verbrennungsphänomene traten für M70F30 in Form von Frühzündungen bei $T_{Einlass}$ = 80° C auf. Die hier auftretenden Frühzündungen werden in der Literatur als Low Speed Pre-Ignition (LSPI) bezeichnet. Dieses Phänomen tritt verstärkt bei Alkoholen auf. Ausgangspunkt dafür ist das Benetzen der Laufbuchse mit Kraftstoff durch die Direkteinspritzung. Grund dafür ist beim Einsatz von M70F30, dass die doppelte Menge an Kraftstoff eingespritzt wird, MeOH eine um das 4,57-fache höhere Verdampfungsenthalpie als G100 besitzt und eine aufgrund der niedrigen Motordrehzahl geringe TKE im Brennraum vorliegt. Zusätzlich ist die maximale Sprayeindringtiefe durch seitliche Injektorlage begrenzt. Das hat zur Folge, dass ein Teil des eingespritzten Kraftstoffs in flüssiger Form auf die Laufbuchse trifft und zur Ölverdünnung führt, was die Viskosität und Oberflächenspannung des Schmieröls senkt. Damit steigt die Wahrscheinlichkeit, dass Öl-/Kraftstofftropfen durch die Kolbenbewegung von der Laufbuchsen- oder Kolbenoberfläche abgelöst werden. Diese Tropfen sind bereits bei niedrigen Temperaturen zündfähig und entzünden sich meist an

heißen Oberflächen, wie beispielsweise der Zündkerzenelektrode. Bei M100 treten die LSPI, aufgrund der höheren Verdampfungsenthalpie und den damit geringeren Brennraumtemperaturen, erst bei einer weiteren Erhöhung der Ansauglufttemperatur um 50° C auf 130° C auf. Durch die Frühzündungen wurden maximale Brennraumspitzendrücke von über 140 bar erreicht, wobei darauf nur bei einem einzigen Zyklus eine klopfende Verbrennung folgte. Für Toluol treten ebenfalls bei $T_{Einlass}$= 130° C erste abnormale Verbrennungsphänomene in Form von klopfenden Verbrennungen auf. Toluol hat eine minimal geringere Verdampfungsenthalpie und eine etwas höhere Energiedichte wie G100, wobei verglichen mit G100 eine sehr ähnliche Brennraumkühlung durch die Direkteinspritzung erzielt wird. Somit ist mit keiner verstärkten Kraftstoffbenetzung von Laufbuchse oder Kolben zu rechnen. Gegenüber M100 bzw. M70F30 liegen mit Toluol deutlich höhere Brennraumtemperaturen vor, welche in Folge der einsetzenden Verbrennung zu Klopfen mit maximalen Brennraumspitzendrücken von 130 bar führen. Die nichtsdestotrotz hohe Klopffestigkeit von Toluol begründet sich mit dessen Ringstruktur im Molekül und den daraus resultierenden Eigenschaften, wie z. B. den relativ schmalen Zündgrenzen oder der hohen Selbstzündtemperatur. Unter den genannten Versuchsbedingungen zeigte C65F35 den höchsten Widerstand gegenüber abnormalen Verbrennungsphänomenen. Für C65F35 wurden erste klopfende Verbrennungen bei $T_{Einlass}$ = 200° C mit einem maximalen Brennraumspitzendruck eines einzelnen Zyklus von 137 bar beobachtet. C65F35 benötigt rund die Hälfte der Verdampfungswärme wie M100, woraus mit einer geringeren Menge an flüssigen Kraftstofftropfen zu rechnen ist, welche die Oberflächen an Laufbuchse und Kolben benetzen. Zudem besitzt C65F35 schmalere Zündgrenzen und eine höhere minimale Zündenergie, womit die Wahrscheinlichkeit von LSPI gegenüber M100 sinkt. Die höhere Klopffestigkeit von C65F35 gegenüber Toluol begründet sich mit der höheren Verdampfungsenthalpie von C65F35, wodurch niedrigere Brennraumtemperaturen vorliegen, sowie durch die höhere Mindestzündenergie von C65F35.

Für die Untersuchung von geblendetem Referenzkraftstoff mit dem C1-Oxygenat DMC wurde ebenfalls eine Voruntersuchung mit G70C30 und G85C15 durchgeführt. Wie erwartet zeigt hier der Blend mit dem größten DMC-Anteil die höchste Klopffestigkeit, was im Lastschnitt bei 2000 1/min mit der größten Steigerung im η_i einhergeht. Bei G70C30 wurde ausschließlich bei p_{mi} = 17 bar der EU50% aufgrund klopfender Verbrennungen in Richtung spät verschoben, wohingegen bei G85C15 bereits bei p_{mi} = 13 bar Klopfen auftrat. Zudem zeigte G70C30 die niedrigsten PN10-Emissionen bei der Variation des SOI und zeigte gemittelt über die Variation gegenüber G100 eine Reduktion der PN10-Emissionen von 58 %. Aufgrund dieser Ergebnisse wurde der Blend G70C30 zunächst ausgewählt, um diesen bei weiteren Parametervariationen mit G100 zu vergleichen. Bei der λ-Variation wirkt sich der DMC-Anteil positiv auf die Partikelemissionen aus, vor allem von λ = 1,2 hin zu fetteren Gemischen. Bei der optischen Untersuchung wurden entgegen G100 auch bei λ = 0,8 keine größeren Diffusionsflammen detektiert. Zugleich verringert sich mit der Blendkomponente DMC die Magerlaufgrenze im

Referenzbetriebspunkt aufgrund der geringeren Brennraumtemperaturen und der höheren benötigten Zündenergie von DMC von $\lambda = 1{,}6$ auf $\lambda = 1{,}4$. Bei der Lastvariation mit verschiedenen Kühlwassertemperaturen von -5 °C, 40 °C und 80 °C, zeigt G70C30 geringere Partikelemissionen bei höheren Motorlasten ab $p_{mi} = 9$ bar. Bei warmem Motorbetrieb steigen die NO_X-Emissionen für G70C30 gemittelt über den Lastschnitt um 10 % an. Dies ist auf die frühere EU50%-Lage von G70C30 bei Lasten ≥ 13 bar p_{mi} als Folge der höheren Klopffestigkeit zurückzuführen. Aus der thermodynamischen Untersuchung von C65F35 ist bekannt, dass DMC als Kraftstoffmischung mit MeFo auch bei sehr später Einspritzung mit unvollständiger, inhomogener Gemischaufbereitung rußarm verbrennt. Daher wurde auch für G70C30 eine SOI-Variation im Kompressionshub durchgeführt. Für G70C30 war gegenüber G100 ein Motorbetrieb auch bei einem um 40 °KW späteren SOI = 650 °KW n. ZOT möglich. Insgesamt wurde bei dieser SOI-Variation mit G70C30 eine gemittelte PN23-Reduktion von 80 % erreicht, welche sich auch im Optikmotor durch eine signifikante Reduktion der Diffusionsflammen widerspiegelte. Zuletzt wurde bei der Untersuchung der Blendkraftstoffe der Einfluss des DMC-Anteils am Injektorverkokungsverhalten ermittelt. Begonnen mit dem Blendkraftstoff G70C30 wurde der volumetrische DMC-Anteil weiter auf 50 Vol.-% und 100 Vol.-% erhöht. Bei dem 90-minütigen Motorlauf mit G100 am Referenzbetriebspunkt und einem Kraftstoffdruck von 25 MPa startet der PN23-Drift ca. 20 Minuten nach Motorstart. Nach weiteren 20 min endet der PN-Drift mit einer um den Faktor 12 höheren PN. Wird G70C30 verwendet ist selbiges Phänomen zu beobachten, nur startet hier der PN23-Drift 20 Minuten verzögert und endet auf einem um ca. 50 % niedrigeren PN23-Niveau. Bei den Kraftstoffmischungen G50C50 und C100 ist über den 90-minütigen Motorlauf kein Partikeldrift aufgetreten. Bei der Analyse des Verkokungszustandes der Injektorkuppe unter dem Mikroskop wurde bei C100 zudem keinerlei Verkokung der Injektorkuppe beobachtet. Für G50C50 stellt sich nach 20 Minuten ein moderater Verkokungszustand ein, welcher bis zum Ende des 90-minütigen Motorlaufs nahezu unverändert bleibt. Bei G70C30 und G100 ist die Injektorkuppe nach dem PN-Drift bereits stark verkokt und der Verkokungszustand nimmt bis zum Ende des Motorlaufs weiter zu. Diese weitere Zunahme der Verkokungsschicht hat aber keine signifikante Auswirkung auf die PN-Emissionen im Rohabgas.

Zuletzt wurde in einem Stichversuch das Potential von C65F35 als Kraftstoff in einem gespülten Vorkammerzündsystem mit erhöhtem Verdichtungsverhältnis untersucht. Denn bei dem Einsatz des gespülten Vorkammerzündsystems mit G100 ist einer der Hauptnachteile die hohe PN-Emission, welche aus den teils unterstöchiometrischen Verbrennungsbedingungen in der Vorkammer resultiert. Unter diesen Bedingungen zeigen die C1-Oxygenate signifikante Vorteile gegenüber G100 durch ihre rußarme und stabile Verbrennung. Mit dem gespülten Vorkammerzündsystem wird das Verbrennungsluftverhältnis gezielt mit den jeweiligen direkteinspritzenden Injektoren für Vor- und Hauptbrennkammer manipuliert. Somit wird erreicht, dass ein sehr mageres Gemisch im Hauptbrennraum durch ein fetteres Gemisch in der Vorkammer gezündet wird. Durch die

Überströmbohrungen der Vorkammer treten nach der Zündung Verbrennungsradikale in den Hauptbrennraum ein und lösen eine Raumzündung aus. Die daraus resultierende schnelle Umsetzung des mageren Gemischs ermöglicht eine signifikante Steigerung des indizierten Wirkungsgrades. Bei der Untersuchung wurde die eingespritzte Kraftstoffmasse in die Vorkammer kontinuierlich erhöht, um die Sensitivität des Kraftstoffs auf die PN-Emissionen zu bewerten. Mit der eingespritzten Kraftstoffmasse steigen bei G100 die PN-Emissionen stark an. Bei C65F35 verbleiben die PN-Emissionen auf unverändert niedrigem Niveau, wobei die PN23-Emissionen um ca. drei Zehnerpotenzen niedriger liegen. Mit konventioneller Zündung ist die Stabilitätsgrenze von C65F35 am Referenzbetriebspunkt (p_{mi} = 7 bar, n_{Motor} = 2000 1/min) bei λ = 1,5 erreicht. Mit dem Vorkammerzündsystem wird die Stabilitätsgrenze für C65F35 bei λ = 2,0 erreicht. Werden die Betriebspunkte miteinander verglichen zeigt sich, dass mit Vorkammerzündsystem eine Reduktion der NO_X-Emissionen von 97 % auf einen Absolutwert von 27 ppm erreicht wird. Ebenso steigt der η_i relativ um 10 % auf einen Absolutwert von 41,6 %, bei CO- und PN23-Emissionen ist hingegen ein Anstieg auf 0,25 Vol.-% und 10.500 #/cm^3 zu verzeichnen. Trotzdem liegt die PN23-Konzentration nur leicht über dem gemittelten Umgebungsniveau in Deutschland und das CO-Niveau liegt deutlich unter dem Emissionsniveau bei stöchiometrischen Bedingungen.

Individueller Beitrag an der Publikation:

Der Autor hatte auf Basis seiner vorangegangenen Untersuchungen von C65F35 die Idee zur vorliegenden Publikation und hat diese konzipiert. Der Autor hat alle Versuche geplant und durchgeführt. Anschließend hat der Autor die generierten Versuchsdaten mittels individuell erstellten Auswerteroutinen visualisiert und bewertet. Diese Versuchsergebnisse wurden darauffolgend vom Autor interpretiert und tiefgreifend diskutiert. Zudem waren zur Durchführung des Experiments diverse Modifikationen am Versuchsträger nötig, welche federführend vom Autor umgesetzt wurden. Der Autor war sowohl Ansprechpartner/Bearbeiter während des Reviewprozesses, als auch Vortragender bei der Präsentation der Veröffentlichung.

Der Zweitautor Fellner hat mit dem Autor die Untersuchung am gespülten Vorkammerzündsystem mit erhöhtem Verdichtungsverhältnis durchgeführt. Die Versuchsergebnisse wurden von Fellner visualisiert und mit dem Autor bewertet, interpretiert und diskutiert.

5.4 DMC/MeFo als Entwicklungswerkzeug in der Motorenforschung

Der Einsatz von DMC/MeFo als Entwicklungswerkzeug in der Motorenforschung wurde in der folgenden Veröffentlichung publiziert:

BLOCHUM, S.; RUCH, F.; BASTUCK, T.; HÄRTL, M. ET AL., *"Identification of In-Cylinder Aerosol Flow Induced Emissions due to Piston Ring Design in a DISI Single Cylinder LV Engine Using Oxygenated Synthetic Fuels," SAE Int. J. Adv. & Curr. Prac. in Mobility 3(5):2395-2409, 2021, https://doi.org/10.4271/2021-01-0625*

Grundgedanke dieser Untersuchung war, die Eigenschaft der rußarmen Verbrennung von C65F35 zu nutzen, um die kraftstoffinduzierten von den ölinduzierten Partikelemissionen zu separieren, ohne dabei die innermotorischen Randbedingungen signifikant zu verändern. Um diese Annahme zu bestätigen, wurden der EFM in thermodynamischer Konfiguration mit C65F35 und G100 betrieben, um Betriebspunkte bei identischer Motorlast und -drehzahl, sowie EU50%-Lage zu vergleichen. Besonderes Augenmerk wurde hier auf den Druckverlauf über °KW gelegt, da die Druckverhältnisse zwischen Brennraum, Kurbelgehäuse und die daraus resultierenden Zwischenringdrücke starken Einfluss auf den Öltransport haben. Hierbei wurde ein über weite Bereiche sehr ähnlicher Druckverlauf beobachtet. Einzig im Kompressionstakt zwischen 690 – 720 °KW wurde bei einer Last von p_{mi} = 11 bar für C65F35 ein niedrigerer Brennraumdruck detektiert. Die Begründung hierfür liegt in der höheren Verdampfungsenthalpie von C65F35, woraus niedrigere Brennraumtemperaturen und -drücke folgen. Basierend auf dieser Erkenntnis wurde zunächst das Modell zur Simulation von Brennraumdruck, Zwischenringdrücken und Kurbelgehäusedruck des Serienmotors validiert. Aufbauend darauf wurden Simulationen durchgeführt, bei welchen gezielt das Stoßspiel des Nasenminutenrings manipuliert wurde. Hierbei ist ein starker Einfluss auf den Verlauf des Drucks im 1. Steg zwischen Top Ring und Nasenminutenring, sowie dem Blow-By zu beobachten. Wird das Stoßspiel des Nasenminutenrings um 20 % verringert, wenn die restlichen Komponenten des Kolbenringpakets unverändert bleiben, wird eine gesteigerte Dichtwirkung zwischen Brennraum und Kurbelgehäuse erzielt. Diese Versuchskonfiguration wird im Folgenden als V0 bezeichnet. Grundsätzlich folgt der Druck im 1. Ringsteg dem Brennraumdruck in Folge der Kompression und der einsetzenden Verbrennung zeitverzögert. Durch die erhöhte Dichtwirkung erreicht der Druck im 1. Ringsteg ein höheres Druckniveau verglichen mit der Serienkonfiguration. Entgegen dem schnellen Druckabfall im Brennraum durch die Gasexpansion im Arbeitstakt und dem anschließenden Öffnen der Auslassventile, fällt der Druck im 1. Ringsteg aufgrund der hohen Dichtwirkung von Topring und Nasenminutenring nur stark verzögert hab. Daraus folgt, dass der Druck im 1. Ringsteg zeitweise den des Brennraumdrucks übersteigt und ein Aerosolfluss aus Schmieröl, Kraftstoff und Verbrennungsprodukten vom 1. Ringsteg hin zum Brennraum stattfindet. Am simulierten Referenzpunkt tritt dieser Zustand über ein weiten Zeitbereich von 90 – 540 °KW auf. Dieser Aerosolfluss wird in der vorliegenden Arbeit als Blow-Back

bezeichnet. Mit dem verringerten Stoßspiel von V0 sinkt zugleich der Blow-By Wert über alle simulierten Betriebspunkte. Weiter wurde die Variante V1 simuliert, bei welcher das Stoßspiel des Nasenminutenrings um 50 % erhöht wurde. Hier stellte sich entgegen V0 nur kurzzeitig ein höherer Druck im 1. Ringsteg gegenüber dem Brennraumdruck mit einem sehr geringen Blow-Back für mittlere bis niedrige Motorlast bis hin zu keinem Blow-Back ab p_{mi} = 11 bar ein. Gegensätzlich dazu steigt das Blow-By mit dem größeren Stoßspiel von V1. Aufbauend auf den Simulationsergebnissen wurden Versuche mit den Kolbengruppenkonfigurationen V0 und V1 am thermodynamischen EFM durchgeführt. Für die Versuche wurde ein bereits eingelaufener Kolben verwendet, welcher nach Bestücken mit der jeweiligen Kolbenringkonfiguration V0 und V1 einem 225-minütigen Einlaufprogramm unterzogen wurde. Während des Einlaufprogramms wurden keinerlei Einlaufeffekte bei PN-Emissionen oder beim Reibmitteldruck festgestellt. Am EFM wurden die Motorlast p_{mi} = 3 – 11 bar, die Motordrehzahl n_{Motor} = 1000 – 3000 1/min und der Saugrohrdruck bei geschlepptem Motorbetrieb zwischen 0,25 – 1,0 bar variiert. Gleich dem Simulationsergebnis zeigt V1 durch das größere Ringstegspiel mit der verringerten Drosselwirkung im Mittel um ≥ 20 % höhere Blow-By Werte bei der Last und Drehzahl Variation. Mit dem verringerten Blow-Back von V1 werden die PN23-Emissionen gegenüber V0 über die Last um 39 % und über die Drehzahl um 31 % reduziert. Grundsätzlich liegt das PN23-Niveau für beide Kolbengruppenkonfigurationen aber im Bereich des durchschnittlichen Umgebungsniveaus in Deutschland, welches zwischen 1.000 – 10.000 #/cm^3 liegt. Nur bei einer Motorlast von p_{mi} = 9 – 11 bar liegen für V0 die PN23-Emissionen leicht über dem Umgebungsniveau. Weiter wurden die VOC-Emissionen, trotz des stark verringerten Responsefaktors des FID-Analysators für C65F35, für einen relativen Vergleich von V0 und V1 herangezogen. Denn mit den VOC-Emissionen lassen sich Rückschlüsse auf den relativen Anteil von Schmieröl im Rohabgas ziehen. Beim Vergleich der VOC-Emissionen beider Varianten zeigt sich, dass mit V1 und dem verringerten Blow-Back eine gemittelte Reduktion der VOC-Emissionen über alle gefeuerten Betriebspunkte von 9 % erreicht wurde. Für die NO_X-Emissionen und Abgastemperaturen waren die gemittelten Abweichungen zwischen beiden Varianten < 1 %. Zudem waren die Abweichungen bei der Brenndauer an den jeweiligen Betriebspunkten ≤ 1° KW. Was wiederrum bestätigt, dass die vorgenommene Modifikation des Ringstoßspiels keinen signifikanten Einfluss auf den Verbrennungsprozess hat. Zuletzt wurde bei geschlepptem Motor n_{Motor} = 2000 1/min der Einlassdruck variiert um den Einfluss des geänderten Ringstoßspiels auf diverse Motorbetriebsmodi wie Lastabschaltung, Segeln, etc. zu bewerten. Hier zeigt sich das vergrößerte Ringstoßspiel von V1 speziell für Einlassdrücke < 1,0 bar nachteilig. Mit der verringerten Drosselwirkung von V1 und einem Druckgefälle von Kurbelgehäuse hin zum Brennraum gelangt mehr Schmieröl ins Rohabgas. Damit steigen die VOC-Emissionen für V1 gegenüber V0 bei einem Einlassdruck von 0,25 bar um 25 % bzw. 94 ppm auf einen Absolutwert von 469 ppm an. Steigt der Einlassdruck, fallen die VOC-Emissionen exponentiell. Ab einem Einlassdruck von ≥ 1 bar liegen die VOC-Emissionen für beide Varianten unter 60 ppm. Gleich den VOC-Emissionen wurde für die PN23-Emissionen bei Einlassdrücken < 1 bar ein

signifikant höheres PN23-Niveau detektiert. Hier ist davon auszugehen, dass das Verdampfungsrohr in dem SPCS nicht alle volatilen Schmierölanteile aus dem Rohrabgas verdampft und diese nachfolgend im CPC als Festkörperpartikel gezählt werden. Hier variiert der Messwert je nach Größenverteilung und Anzahl der Öltropfen teils unabhängig von der Menge an Schmieröl. Die gemessene Anzahl an PN23 liegt hier an der oberen Grenze des Umgebungsniveaus sowie teils über den PN23-Emissionen der gefeuerten Niedrig- bis Mittellastpunkte.

Individueller Beitrag an der Publikation:

Der Autor hat in Zusammenarbeit mit den weiteren Autoren die vorliegende Publikation konzipiert. Der Autor hat alle Versuche geplant und durchgeführt. Anschließend hat der Autor die generierten Versuchsdaten mittels individuell erstellten Auswerteroutinen visualisiert und bewertet. Diese Versuchsergebnisse wurden darauffolgend vom Autor interpretiert und tiefgreifend diskutiert, sowie mit den Simulationsergebnissen abgeglichen. Zudem waren zur Durchführung des Experiments diverse Modifikationen/Entwicklungen am EFM nötig, wie bspw. die Entwicklung eines neuen Ventiltriebs, welcher ein zeiteffizientes wechseln der Kolbengruppe ermöglicht. Diese Entwicklungen hat der Autor federführend umgesetzt. Der Autor war sowohl Ansprechpartner/Bearbeiter während des Reviewprozesses, als auch Vortragender bei der Präsentation der Veröffentlichung.

Der Zweitautor Ruch hat das Simulationsmodell erstellt. Aus den Simulationsergebnissen haben Ruch und Bastuck die Konfiguration der untersuchten Kolbenringvarianten abgeleitet.

6 Diskussion

Mit den Publikationen wurden die Erkenntnisse aus vorangegangenen Publikationen [12, 44] bestätigt sowie weitere Potentiale der C1-Kraftstoffmischung C65F35 identifiziert. Hierzu zählen die hohe Widerstandsfähigkeit gegenüber abnormaler Verbrennungsphänomene, der positive Einfluss der hohen Verdampfungsenthalpie und die rußarme Verbrennung. Zudem wurde erstmals nachgewiesen und publiziert, dass der Einsatz von C65F35 in einem Serienaggregat mit einer nur geringen Applikationsanpassung in der ECU möglich ist. Für einen Dauereinsatz im Feld müssen hier aber zusätzliche Materialanpassungen bei den kraftstoffführenden Komponenten, vor allem bei Dichtungskomponenten, durchgeführt werden. Mit der Publikation der thermodynamischen Untersuchung von C65F35 wurden die Motorsimulationsergebnisse der C1-Oxygenatmischung von Wagner et al. [46, 47] bezüglich der hohen Klopffestigkeit und Wirkungsgradsteigerung bestätigt. Am EFM mit seitlicher Direkteinspritzung und konventioneller Funkenzündung sind Verdichtungsverhältnisse $\varepsilon > 15$ ohne Einschränkung aufgrund von abnormalen Verbrennungsphänomenen einsetzbar, woraus für diverse Betriebspunkte eine absolute Steigerung von $\eta_i > 10$ % folgt. Im Vergleich dazu wird beim Basismotor des EFM dem Vierzylinder-Serienaggregat EA888 bis zur Ausbaustufe Gen 3 ein ε von 9,6 eingesetzt [56, 57]. Weiter wurde durch die Variation des SOI im Kompressionshub erstmals die sehr gute Eignung von C65F35 für Schichtladebrennverfahren aufgezeigt. Die positiven Verbrennungseigenschaften von C65F35 bei unterstöchiometrischen Gemischen sind hier der Hauptvorteil gegenüber fossilem Ottokraftstoff. Hierzu zählt die rußarme Verbrennung und die weiten Zündgrenzen von C65F35 in Luft. Mit der Direkteinspritzung im Kompressionshub wurde trotz der stark verringerten Gemischaufbereitungszeit eine Steigerung des η_i erreicht. Somit wurde bewiesen, dass für C65F35 das erhöhte Turbulenzniveau zum ZZP durch die späte Direkteinspritzung die verringerte Gemischaufbereitungszeit überkompensiert, wobei keine signifikante Erhöhung der Abgasemissionen zu beobachten ist. Die inhomogene Gemischaufbereitung wurde mit den optischen EFM-Versuchen belegt, da hier die asymmetrische Flammenausbreitung bei später Direkteinspritzung beobachtet wurde. Ebenso bestätigen die Versuche am optischen EFM mit der geringen Lichtemission bei den High-Speed Farbaufnahmen und der 1D-Emissionsspektroskopie die niedrigen Brennraumspitzentemperaturen mit den folglich reduzierten NO_X-Emissionen. Die niedrigen NO_X-Emissionen wurden bereits bei den ersten publizierten Versuchen mit C65F35 von Härtl et al. [12, 44] beobachtet. Mit diesen Erkenntnissen wurde das mögliche Potential von C65F35 für den Einsatz in einem gespülten Vorkammersystem identifiziert. Wie von Stalder [73] beschrieben, ist der Betriebsbereich des Zündsystems beim Einsatz von Motorenbenzin durch die Rußemissionen stark eingeschränkt. Durch die rußarme Verbrennung von C65F35 in Verbindung mit den weiteren Zündgrenzen hin zu fetteren Gemischen wird der Betriebsbereich des Vorkammerzündsystems erweitert. Folglich ist es möglich mit C65F35, gegenüber dem Referenzkraftstoff, eine größere Energiemenge in der Vorkammer zu nutzen, um ein stark

überstöchiometrisches Gemisch in der Hauptbrennkammer zu zünden. Somit wurde für C65F35 am Referenzpunkt (2000 1/min, p_{mi} = 7 bar) mit $\lambda = 2{,}0$ ein η_i = 41,6 % bei zugleich sehr niedrigen Abgasemissionen erreicht, was eine relative Steigerung von 10 % gegenüber dem konventionellen Zündsystem an der Magerlaufgrenze bei $\lambda = 1{,}5$ mit C65F35 bedeutet. Die signifikante Steigerung des indizierten Wirkungsgrades im Teillastbereich zeigt das große Potential von C65F35 für Anwendungen im PKW, da der Ottomotor hier über weite Strecken im Teillastbereich betrieben wird. Bei der Substitution von DMC durch MeOH wurde gezeigt, dass MeOH oftmals vergleichbare Kraftstoffeigenschaften aufweist wie DMC. Gemittelt über die λ- und Lastvariation zeigt C65F35 ein um 8 % bzw. 14 % niedrigeres PN-Niveau als M70F30. Aber bei unterstöchiometrischem Motorbetrieb, unter hoher Motorlast sowie bei verringerten Kühlmitteltemperaturen zeigt sich M70F30 teils vorteilhaft bezüglich PN-Emissionen. Zudem war mit M70F30 gegenüber C65F35 ein Motorbetrieb bei einer niedrigen Motorlast p_{mi} = 3 - 5 bar und einer Kühlwassertemperatur von -5° C möglich. Weiter wurde für C65F35 eine höhere Festigkeit gegen abnormale Verbrennungsphänomene als für die aus der Literatur bekannten hochklopffesten Kraftstoffe MeOH und Toluol beobachtet. Am untersuchten Betriebspunkt traten erst bei $T_{Einlass}$ = 200° C erste klopfende Verbrennungen auf. Toluol und M100 zeigten hingegen bereits bei $T_{Einlass}$ = 130° C Frühzündungen in Form von LSPI.

Bei der Untersuchung der C1-Blends wurde nachgewiesen, dass bereits bei 30 Vol.-% DMC in der Kraftstoffmischung eine PN23-Reduktion bei verschiedenen Parametervariationen von > 50 % erreicht wird. Wobei zugleich eine absolute Steigerung des η_i von 4,9 % bei p_{mi} = 17 bar durch die höhere Klopffestigkeit von DMC erzielt wird. Bei der Untersuchung des Verkokungsverhaltens der Injektorkuppe wurde beobachtet, dass bereits mit G70C30 der PN-Drift um 20 min verzögert auftritt. Ab einem DMC Anteil von ≥ 50 Vol.-% ist innerhalb des 90 min Motorbetriebs kein PN-Drift zu beobachten. Diese Untersuchung zeigt, dass durch das Blenden von Motorenbenzin mit DMC der Partikelausstoß stark reduziert werden kann, vor allem bei Motorbetriebspunkten mit verringertem Einspritzdruck oder hoher Motorlast. Wie aus dem wissenschaftlichen Diskurs [60, 74, 75] bekannt, fördern diese Betriebspunkte die Verkokung der Injektorkuppe, worauf das Phänomen des PN-Drifts folgt. Wird der Blendkraftstoff in der Bestandsflotte eingesetzt, werden abhängig von der Blendrate umgehend der CO_2-Ausstoß und die Schadstoffemissionen signifikant reduziert. Hierfür sind aber zunächst weitere Untersuchungen bezüglich der Materialverträglichkeit für den Serieneinsatz durchzuführen, um eine sichere Verwendung des Kraftstoffs zu gewährleisten.

Bei der Untersuchung der ölinduzierten Partikelemissionen wurde erstmals die Eigenschaft der rußarmen Verbrennung von C65F35 genutzt, um kraftstoffinduzierte von ölinduzierten Partikeln zu separieren. Es wurde bewiesen, dass durch die gezielte Manipulation des Drucks im 1. Ringsteg der Aerosolfluss zwischen Kurbelgehäuse und Brennraum beeinflussbar ist. Durch die Vergrößerung des Stoßspiels des Nasenminutenrings bei V1 wurde der Blow-Back Aerosolfluss reduziert. Hiermit wurden gemittelt über die gefeuerte Last- und Drehzahlvariation die PN23-Emissionen um 36 %, die

PN10-Emissionen um 51 % und die VOC-Emissionen um 9 % reduziert. Nachteilig zeigt sich V1 bei geschlepptem Motorbetrieb und Einlassdrücken < 1 bar, wo gemittelt 20 – 26 % mehr VOCs emittiert werden. Zusätzlich steigt das Blow-By gemittelt über alle Lastpunkte um 22 %. Diese Erhöhung senkt theoretisch den indizierten Wirkungsgrad aufgrund des gestiegenen Druckverlustes im Brennraum. Dieser Verlust war für alle untersuchten Messpunkte < 0,1 %. Zudem wurde nachgewiesen, dass unter bestimmten Bedingungen bei geschlepptem Motorbetrieb mehr VOC- und PN-Emissionen emittiert werden als bei gefeuertem Motorbetrieb. Mit der Untersuchung wurde gezeigt, dass auch beim Einsatz von C1-Oxygenatkraftstoffen mit gezielten Maßnahmen an der Kolbengruppe Rohabgasemissionen weiter signifikant reduziert werden.

Zukünftig sind die synthetischen, sauerstoffhaltigen C1-Kraftstoffe tiefgreifender bezüglich ihres Emissionsverhaltens zu untersuchen. Hierzu sind speziell für die Kraftstoffmischungen entwickelte Auswertemethoden für ein Fourier-Transformations-Infrarotspektrometer zu nutzen. Somit wird die exakte Bestimmung der unverbrannten Kraftstoffanteile und die Identifikation weiterer Schadstoffe im Abgas ermöglicht. Des Weiteren sind höhere Verdichtungsverhältnisse, als in der vorliegenden Arbeit im Bereich von $\varepsilon \sim 18$ einzusetzen, welche möglicherweise tiefgreifendere konstruktive Änderungen des Versuchsträgers verursachen, aber weitere Steigerungen von η_i mit sich bringen. Weiteres Potential haben die weiteren Zündgrenzen in Luft und die teils niedrigeren min. Zündenergien. In Verbindung mit der rußarmen Verbrennung lassen sich Motorbetriebsmodi mit teils lokal fettem Gemisch realisieren. Hierzu zählen Schichtladebrennverfahren, welche mit Motorenbenzin im Betrieb im Serienmotor nur schwer kontrollierbar sind. Die untersuchten Kraftstoffe zeigen hier eine stark verbesserte Verbrennungsstabilität bei unverändert niedrigem Emissionsniveau. Gleich dem ist die Verwendung der C1-Oxygenate in einem gespülten Vorkammerzündsystem weiter zu erforschen. Durch die rußarme Verbrennung zeigt die eingespritzte Kraftstoffmasse in die Vorkammer, entgegen dem Referenzkraftstoff, keinen signifikanten Einfluss auf die PN-Emissionen. Dies generiert einen weiteren Freiheitsgrad bei der Betriebsstrategie eines gespülten Vorkammerzündsystems und ermöglicht auch für mittlere Motorlasten hohe indizierte Wirkungsgrade. Letztlich wurde mit der vorliegenden Arbeit bewiesen, dass neben dem möglichen CO_2-neutralen Betrieb des direkteinspritzenden Ottomotors, sowohl Steigerungen des η_i, als auch teilweise starke Reduktionen der reglementierten Abgasemissionen durch C1-Kraftstoffe möglich sind.

7 Zusammenfassung

Mit der vorliegenden Arbeit wurden synthetische, sauerstoffhaltige C1-Kraftstoffe bezüglich ihres Potentials im direkteinspritzenden Ottomotor untersucht. Die Untersuchungen wurden zu großen Teilen an einem EFM in thermodynamischer und optischer Konfiguration durchgeführt. Hierbei wurden sowohl reine C1-Kraftstoffmischungen, aber auch ein mit C1-Krafstoffen geblendeter Referenzkraftstoff untersucht. Ausgangspunkt der Untersuchung von synthetischen Kraftstoffen ist der, von der Herstellung des Kraftstoffs abhängige, mögliche global CO_2-neutrale Betrieb des Verbrennungsmotors. Ungeachtet dessen wurde in der vorliegenden Arbeit das Potential von C1-Oxygenatkraftstoffen bezüglich des indizierten Wirkungsgrades und der Rohabgasemissionen untersucht.

Zunächst wurde die C1-Oxygenatmischung C65F35 sowohl thermodynamisch als auch optisch untersucht und dem Referenzkraftstoff gegenübergestellt. Die Wahl der C1-Kraftstoffmischung begründet sich im Grundsatz mit den vorangegangenen Untersuchungen am EFM [11, 12, 44], welche C65F35 als potenziellen synthetischen Kraftstoff identifiziert haben. Neben der rußarmen Verbrennung aufgrund der C1-Molekularstruktur hat C65F35, bezogen auf den Heizwert, eine um den Faktor ~ 2,9 höhere Verdampfungsenthalpie. Diese beiden Eigenschaften wirken sich stark positiv auf die NO_X- und PN-Emissionen aus. Somit wurde bspw. am Vierzylinder-Serienaggregat eine Reduktion von 80 % NO_X und 78 % PN im WLTC erzielt. Am Optikmotor wurden die Ergebnisse des Thermodynamikmotors bekräftigt. Hier wurden die in weiten Betriebsbereichen verringerten Brennraumtemperaturen bei C65F35 durch die niedrigere Lichtemission bestätigt. In Kombination mit der geringeren Intensität des CN-Radikals, welches ein Zwischenprodukt bei der Bildung von Prompt-NO_X ist, werden die geringeren NO_X-Emissionen erklärt. Entgegen dem Referenzkraftstoff wurden zudem niedrige PN-Emissionen und lediglich vereinzelt auftretende, kleine Diffusionsflammen beobachtet. Weiter zeigte C65F35 bei $\lambda = 0{,}8$ gegenüber G100 für die C_2-Radikale speziell im Bereich der C_2-Swan-Bande eine geringere Intensität, was die geringeren PN-Emissionen im Rohabgas bestätigt. Weiteres Potential bietet bei C65F35 die hohe Widerstandsfähigkeit des Kraftstoffes gegenüber abnormaler Verbrennungsphänomene. Um dieses Potential zu nutzen, wurde mittels eines modifizierten HCR-Kolbens das Verdichtungsverhältnis ε am EFM von 10,91 auf 14,92 angehoben, womit eine relative maximale Steigerung des indizierten Wirkungsgrades gegenüber dem Referenzkraftstoff von 11 % bei $p_{mi} = 17$ bar und $n_{Motor} = 2000$ 1/min erreicht wurde. Im gesamten Betriebsbereich des EFM war es bei $T_{Einlass} = 30$ °C und einem EU50% = 8 °KW n.OT. nicht möglich abnormale Verbrennungsphänomene zu provozieren. In einem weiteren Schritt wurde C65F35, nach einer Voruntersuchung mit verschiedenen Mischungen aus den C1-Oxygenaten MeOH und MeFo, mit M70F30 verglichen. Dabei wurde festgestellt, dass M70F30 unter verschiedenen Betriebsbedingungen oftmals vergleichbare Messergebnisse wie C65F35 liefert. Hier ist bspw. das sehr stabile Verbrennungsverhalten bei einer späten Direkteinspritzung im Kompressionshub zu nennen. Trotzdem zeigt M70F30 gemittelt über die λ- und Lastvariation ein

höheres PN-Niveau als C65F35. Aber unter extremen Betriebsbedingungen mit unterstöchiometrischem Gemisch, hoher Motorlast oder verringerten Kühlmitteltemperaturen zeigt sich M70F30, bezogen auf PN-Emissionen, vorteilhaft. Aufgrund der niedrigen minimalen Zündenergie von MeOH war mit M70F30 auch ein Motorbetrieb bei niedrigen Motorlasten $p_{mi} \leq 5$ bar und einer Kühlwassertemperatur von -5° C möglich. Um den EFM unter diesen Betriebsbedingungen mit C65F35 zu betreiben, musste die Direkteinspritzung vom Ansaugtakt in den Kompressionstakt gelegt werden. Im nächsten Schritt wurde für einen relativen Vergleich der Widerstandsfähigkeit gegen abnormale Verbrennungsphänomene der EFM mit $\varepsilon = 14{,}91$, $n_{Motor} = 1500$ 1/min und $p_{mi} = 17$ bar betrieben, wobei die $T_{Einlass}$ von 30° C schrittweise auf bis zu 200° C erhöht wurde. Neben C65F35 und M70F30 wurden zudem M100 und Toluol untersucht. Für die MeOH-haltigen C1-Kraftstoffmischungen M70F30 und M100 traten Frühzündungen, sogenannte LSPI, bei $T_{Einlass} = 80°$ C bzw. 130° C auf. Hierbei wurden Brennraumspitzendrücke durch LSPI von bis zu 140 bar detektiert. Der hoch klopffeste Kraftstoff Toluol zeigte ebenfalls bei $T_{Einlass} = 130°$ C erste klopfende Verbrennungszyklen. Die höchste Widerstandsfähigkeit im untersuchten Betriebspunkt zeigte C65F35, bei welchem bei $T_{Einlass} = 200°$ C erste klopfende Verbrennungen bei einem maximalen Brennraumdruck von 137 bar beobachtet wurden. Weiter wurden mit ersten Stichversuchen die Eigenschaften von C65F35 bei Verwendung eines gespülten Vorkammerzündsystems untersucht. Dabei zeigte C65F35 keinerlei Sensitivität im Spannungsfeld von eingespritzter Kraftstoffmasse in die Vorkammer zu PN-Emissionen im Rohabgas, was bedeutet, dass selbst bei einer großen eingespritzten Kraftstoffmasse in die Vorkammer sehr geringe PN-Emissionen gemessen wurden. Letztlich wurde bei einer mittleren Last von $p_{mi} = 7$ bar, einer Motordrehzahl von 2000 1/min und einem λ von 2.0 ein $\eta_i = 41{,}6$ % erzielt, wobei die NO_X-Rohabgasemissionen auf 27 ppm fielen. Zuletzt wurde C65F35 aufgrund der sehr rußarmen Verbrennung als Entwicklungswerkzeug eingesetzt, um ölinduzierte Partikel von kraftstoffinduzierten Partikeln zu separieren. Bei dieser Untersuchung wurde der Aerosolfluss gezielt durch Manipulation des Stoßspiels des Nasenminutenrings beeinflusst. Die theoretischen Ergebnisse aus der 3D-CFD Simulation wurden am EFM bestätigt. So wurde mit einem vergrößerten Stoßspiel der Blow-Back Aerosolfluss verringert. Damit wurde bei gefeuertem Motorbetrieb eine relative gemittelte Reduktion der PN23- und PN10-Emissionen von 36 % bzw. 51 %, sowie eine relative gemittelte Reduktion der VOC-Emissionen von 9 %, erzielt. Nachteilig wirkt sich das vergrößerte Stoßspiel bei geschlepptem Motorbetrieb und Einlassdrücken > 1 bar aus, hier werden bis zu 26 % mehr VOCs emittiert. Verursacht werden die Emissionen durch das größere Stoßspiel, wodurch aufgrund des erhöhten reverse Blow-By mehr Schmieröl in Richtung Brennraum transportiert wird. Mit der Untersuchung wurde nachgewiesen, dass das Schmieröl einen messbaren Anteil an den Abgasemissionen verursacht und auch hier Potential zur Emissionsreduktion besteht.

Bei der Untersuchung vom geblendeten Referenzkraftstoff mit DMC, wurde im Anschluss an die Voruntersuchungen der Blend G70C30 intensiver untersucht. Durch die hohe Klopffestigkeit von DMC

werden bei einer Motordrehzahl von 2000 1/min und Motorlasten $p_{mi} \geq 13$ bar Steigerungen des η_i erzielt, welche auf die optimalere EU50%-Lage bezüglich η_i zurückzuführen sind. Mit dieser Wirkungsgradsteigerung geht zugleich eine Steigerung der NO_X-Emissionen von 10 % über den Lastschnitt aufgrund der höheren Verbrennungsspitzentemperaturen einher. Bei G70C30 wurde zudem eine Reduktion der PN-Emissionen speziell hin zu fetteren Gemischen, sowie verstärkt bei der SOI-Variation im Kompressionshub, von > 80 % erzielt. Dementsprechend wurden bei den Versuchen am Optikmotor eine deutlich reduzierte Anzahl an Diffusionsflammen beobachtet. Abschließend wurde bei einem 90-minütigen Motorlauf das Injektorverkokungsverhalten mit steigendem Blendanteil von DMC untersucht. Bei G70C30 trat der PN-Drift gegenüber G100 20 min verspätet auf und endete auf einem 50 % niedrigen PN23-Niveau. Ab einem Blendanteil von 50 % DMC trat bei der Untersuchung kein PN-Drift mehr auf und bei reinem DMC war kein Verkoken der Injektorspitze unter dem Mikroskop zu beobachten.

Literaturverweise

[1] Europäische Kommission, “MITTEILUNG DER KOMMISSION AN DAS EUROPÄISCHE PARLAMENT, DEN EUROPÄISCHEN RAT, DEN RAT, DEN EUROPÄISCHEN WIRTSCHAFTS- UND SOZIALAUSSCHUSS UND DEN AUSSCHUSS DER REGIONEN Der europäische Grüne Deal: COM(2019) 640 final,” 2019.

[2] Europäischen Union, “BESCHLUSS (EU) 2016/1841 DES RATES vom 5. Oktober 2016 über den Abschluss des im Rahmen des Rahmenübereinkommens der Vereinten Nationen über Klimaänderungen geschlossenen Übereinkommens von Paris im Namen der Europäischen Union: (EU) 2016/1841,” 2016.

[3] Press office - General Secretariat of the Council, “Rat beschließt Europäisches Klimagesetz: PRESSEMITTEILUNG 562/21,” 2021.

[4] Europäischen Union, “VERORDNUNG (EU) 2019/631 DES EUROPÄISCHEN PARLAMENTS UND DES RATES vom 17. April 2019 zur Festsetzung von CO2-Emissionsnormen für neue Personenkraftwagen und für neue leichte Nutzfahrzeuge und zur Aufhebung der Verordnungen (EG) Nr. 443/2009 und (EU) Nr. 510/2011: (EG) Nr. 443/2009 und (EU) Nr. 510/2011,” 2019.

[5] Köllner, C., “Verbrenner-Ausstieg: Die Pläne der Autohersteller: Teil 2: Wer plant wann den Verbrennungsmotor-Ausstieg?,” https://www.springerprofessional.de/antriebsstrang/verkehrswende/verbrenner-ausstieg--die-plaene-der-autohersteller/18906344.

[6] Goericke, D., Thee, R., and Tutsch, P., “Cradle-to-Grave Life-Cycle Assessment in the Mobility Sector: A Meta-Analysis of LCA Studies on Alternative Powertrain Technologies,” R595, 2020.

[7] Zheng, G. and Peng, Z., “Life Cycle Assessment (LCA) of BEV’s environmental benefits for meeting the challenge of ICExit (Internal Combustion Engine Exit),” *Energy Reports* 7:1203–1216, 2021, doi:10.1016/j.egyr.2021.02.039.

[8] Icha, P., Lauf, T., and Kuhs, G., “Entwicklung der spezifischen Kohlendioxid - Emissionen des deutschen Strommix in den Jahren 1990 - 2020,” *Climate Change*(45), 2021.

[9] Fraunhofer-Institut für Solare Energiesysteme ISE, “energy-charts: Nettostromerzeugung in Deutschland im Juni 2021,” https://energy-charts.info/charts/power/chart.htm?l=de&c=DE&interval=month&month=06.

[10] Maus, W. (ed.), “Zukünftige Kraftstoffe,” Springer Berlin Heidelberg, Berlin, Heidelberg, ISBN 978-3-662-58005-9, 2019.

[11] Härtl, M., Pélerin, D., Dworschak, P., Maier, T. et al., "Potential of the sustainable C1 fuels OME, DMC, and MeFo for particle-free combustion in SI and CI engines," in: Liebl, J., Beidl, C., and Maus, W. (eds.), *Internationaler Motorenkongress 2018*, Proceedings, Springer Fachmedien Wiesbaden, Wiesbaden, ISBN 978-3-658-21014-4:459–478, 2018.

[12] Härtl, M., Stadler, A., Backes, F., Wachtmeister, G. et al., "Potenziell CO2-neutrale Kraftstoffe für saubere Ottomotoren," *MTZ Motortech Z* 78(7-8):80–88, 2017, doi:10.1007/s35146-017-0056-5.

[13] Härtl, M., "Emissionsreduktion bei Dieselmotoren durch den Einsatz sauerstoffhaltiger Kraftstoffe," Dissertation, Technische Universität München.

[14] Härtl, M., Gaukel, K., Pélerin, D., and Wachtmeister, G., "Oxymethylenether als potenziell CO2-neutraler Kraftstoff für saubere Dieselmotoren Teil 1: Motorenuntersuchungen," *MTZ Motortech Z* 78(2):52–59, 2017, doi:10.1007/s35146-016-0170-9.

[15] Dörmer, W. and Baron, U., "Betriebsstoffe," in: van Basshuysen, R. (ed.), *Ottomotor mit Direkteinspritzung und Direkteinblasung*, Springer Fachmedien Wiesbaden, Wiesbaden, ISBN 978-3-658-12214-0:387–414, 2017.

[16] European Automobile Manufacturers Association, "ACEA Report - Vehicle in use Europe: January 2021," 2021.

[17] Stollenwerk, S., Kanacher, J., and Drake, F.-D., "Strom und erneuerbare Kraftstoffe – gemeinsame Lösung für die Verkehrswende," in: Maus, W. (ed.), *Zukünftige Kraftstoffe*, Springer Berlin Heidelberg, Berlin, Heidelberg, ISBN 978-3-662-58005-9:136–151, 2019.

[18] Yip, H.L., Srna, A., Yuen, A.C.Y., Kook, S. et al., "A Review of Hydrogen Direct Injection for Internal Combustion Engines: Towards Carbon-Free Combustion," *Applied Sciences* 9(22):4842, 2019, doi:10.3390/app9224842.

[19] Distaso, E., Amirante, R., Cassone, E., Palma, P. de et al., "Analysis of the combustion process in a lean-burning turbulent jet ignition engine fueled with methane," *Energy Conversion and Management* 223:113257, 2020, doi:10.1016/j.enconman.2020.113257.

[20] Niven, R.K., "Ethanol in gasoline: environmental impacts and sustainability review article," *Renewable and Sustainable Energy Reviews* 9(6):535–555, 2005, doi:10.1016/j.rser.2004.06.003.

[21] Verhelst, S., Turner, J.W.G., Sileghem, L., and Vancoillie, J., "Methanol as a fuel for internal combustion engines," *Progress in Energy and Combustion Science* 70:43–88, 2019, doi:10.1016/j.pecs.2018.10.001.

[22] Gumz, W., "Eine neue Heizwertformel für feste Brennstoffe.," *Feuerungstechnik* 26(10):322–323, 1938.

[23] Tschöke, H. and Marohn, R., “11. Tagung Einspritzung und Kraftstoffe 2018,” Springer Fachmedien Wiesbaden, Wiesbaden, ISBN 978-3-658-23180-4, 2019.

[24] Jorgensen, A.D., Picel, K.C., and Stamoudis, V.C., “Prediction of gas chromatography flame ionization detector response factors from molecular structures,” *Anal. Chem.* 62(7):683–689, 2012, doi:10.1021/ac00206a007.

[25] Wallner, T., “Correlation Between Speciated Hydrocarbon Emissions and Flame Ionization Detector Response for Gasoline/Alcohol Blends,” *ASME 2010 Internal Combustion Engine Division Fall Technical Conference*, ASME 2010 Internal Combustion Engine Division Fall Technical Conference, San Antonio, Texas, USA, 12.09.2010 - 15.09.2010, ASMEDC, ISBN 978-0-7918-4944-6:119–128, 2010.

[26] Blochum, S., Fellner, F., Mühlthaler, M., Härtl, M. et al., “Comparison of Promising Sustainable C1-Fuels Methanol, Dimethyl Carbonate, and Methyl Formate in a DISI Single-Cylinder Light Vehicle Gasoline Engine,” *SAE Technical Paper Series*, SAE Technical Paper Series, SAE Powertrains, Fuels & Lubricants Digital Summit, SEP. 28, 2021, SAE International400 Commonwealth Drive, Warrendale, PA, United States, 2021.

[27] Schifter, I., González, U., and González-Macías, C., “Effects of ethanol, ethyl-tert-butyl ether and dimethyl-carbonate blends with gasoline on SI engine,” *Fuel* 183:253–261, 2016, doi:10.1016/j.fuel.2016.06.051.

[28] Chan, J.H., Tsolakis, A., Herreros, J.M., Kallis, K.X. et al., “Combustion, gaseous emissions and PM characteristics of Di-Methyl Carbonate (DMC)-gasoline blend on gasoline Direct Injection (GDI) engine,” *Fuel* 263:116742, 2020, doi:10.1016/j.fuel.2019.116742.

[29] Li, M., Zhao, Y., Fang, J., Zhao, S. et al., “Effect of dimethyl carbonate on the micromorphology and structure of combustion particles from diesel engines,” *Energy Sources, Part A: Recovery, Utilization, and Environmental Effects* 42(9):1155–1165, 2020, doi:10.1080/15567036.2019.1602225.

[30] Rounce, P., Tsolakis, A., Leung, P., and York, A.P.E., “A Comparison of Diesel and Biodiesel Emissions Using Dimethyl Carbonate as an Oxygenated Additive,” *Energy Fuels* 24(9):4812–4819, 2010, doi:10.1021/ef100103z.

[31] Dooley, S., Burke, M.P., Chaos, M., Stein, Y. et al., “Methyl formate oxidation: Speciation data, laminar burning velocities, ignition delay times, and a validated chemical kinetic model,” *Int. J. Chem. Kinet.* 42(9):527–549, 2010, doi:10.1002/kin.20512.

[32] Jin, G., Wei, J., Sun, Y., Xue, M. et al., "The research on core making technology in sodium silicate cold box," in: *69th World Foundry Congress 2010: (WFC 2010) : Hangzhou, China, 16-20 October 2010*, Curran Associates, Inc, Red Hook, NY, ISBN 978-162276286-6:1000–1004, 2012, 2010.

[33] Al-Moameri, H.H., Nabhan, B.J., M., T.W., and Abdulrehman, M.A., "Impact of blowing agent-blends on polyurethane foams thermal and mechanical properties," *2ND INTERNATIONAL CONFERENCE ON MATERIALS ENGINEERING & SCIENCE (IConMEAS 2019)*, AIP Conference Proceedings, 2ND INTERNATIONAL CONFERENCE ON MATERIALS ENGINEERING & SCIENCE (IConMEAS 2019), Baghdad, Iraq, 25–29 September 2019, AIP Publishing:20177, 2020.

[34] Lee, J.S., Kim, J.C., and Kim, Y.G., "Methyl formate as a new building block in C1 chemistry," *Applied Catalysis* 57(1):1–30, 1990, doi:10.1016/S0166-9834(00)80720-4.

[35] Klezl, P., "Fuel for internal combustion engines and use of methyl formate as fuel additive," US-Patent 5232464.

[36] Divakar Shetty, A.S., Sahu, D., Arthur Davis, J., and Kumar, R., "Comparative Study on Gasoline and Methanol in a Twin Spark IC Engine," in: Pant, P., Mishra, S.K., and Mishra, P.C. (eds.), *Advances in Mechanical Processing and Design*, Lecture Notes in Mechanical Engineering, Springer Singapore, Singapore, ISBN 978-981-15-7778-9:191–201, 2021.

[37] Mishra, P.C., Gupta, A., Kumar, A., and Bose, A., "Methanol and petrol blended alternate fuel for future sustainable engine: A performance and emission analysis," *Measurement* 155:107519, 2020, doi:10.1016/j.measurement.2020.107519.

[38] Naman, T.M. and Striegler, B.C., "Engine and Field Test Evaluation of Methanol as an Automotive Fuel," *SAE Technical Paper Series*, SAE Technical Paper Series, 1983 SAE International Fall Fuels and Lubricants Meeting and Exhibition, OCT. 31, 1983, SAE International400 Commonwealth Drive, Warrendale, PA, United States, 1983.

[39] Donnelly, R.G., Heywood, J.B., Lorusso, J., Obrien, F. et al., "Methanol as an automotive fuel: A summary of research in the M.I.T. Energy Laboratory," *Final Report Massachusetts Inst. of Tech., Cambridge. Energy Lab.*, 1976.

[40] Sarathy, S.M., Oßwald, P., Hansen, N., and Kohse-Höinghaus, K., "Alcohol combustion chemistry," *Progress in Energy and Combustion Science* 44:40–102, 2014, doi:10.1016/j.pecs.2014.04.003.

[41] Vancoillie, J., Demuynck, J., Sileghem, L., van de Ginste, M. et al., "The potential of methanol as a fuel for flex-fuel and dedicated spark-ignition engines," *Applied Energy* 102:140–149, 2013, doi:10.1016/j.apenergy.2012.05.065.

[42] Vancoillie, J., Demuynck, J., Sileghem, L., van de Ginste, M. et al., "Comparison of the renewable transportation fuels, hydrogen and methanol formed from hydrogen, with gasoline – Engine efficiency study," *International Journal of Hydrogen Energy* 37(12):9914–9924, 2012, doi:10.1016/j.ijhydene.2012.03.145.

[43] Zuo, Z.-N., Zeng, D.-J., Pei, Y.-Q., Qin, J. et al., "Investigation on the effect of ignition timing on particulate emissions from a turbo charged GDI engine fueled with gasoline/methanol blends," *Neiranji Gongcheng/Chinese Internal Combustion Engine Engineering* 37:87–92, 2016, doi:10.13949/j.cnki.nrjgc.2016.06.014.

[44] Härtl, M., Stadler, A., Blochum, S., Pélerin, D. et al., "DMC+ als partikelfreier und potenziell nachhaltiger Kraftstoff für DI Ottomotoren," in: Maus, W. (ed.), *Zukünftige Kraftstoffe*, Springer Berlin Heidelberg, Berlin, Heidelberg, ISBN 978-3-662-58005-9:758–782, 2019.

[45] Forbes, A.D. and Powell, K.G., "Gasoline Composition," GB000001411947A.

[46] Wagner, C., Grill, M., Keskin, M.-T., Bargende, M. et al., "Potential Analysis and Virtual Development of SI Engines Operated with Synthetic Fuel DMC+," SAE Technical Paper Series, WCX SAE World Congress Experience, APR. 21, 2020, SAE International400 Commonwealth Drive, Warrendale, PA, United States, 2020.

[47] Wagner, C., Keskin, M.-T., Grill, M., Bargende, M. et al., "Potential analysis and virtual development of SI Engines operated with DMC+," in: Bargende, M., Reuss, H.-C., and Wagner, A. (eds.), *20. Internationales Stuttgarter Symposium*, Proceedings, Springer Fachmedien Wiesbaden, Wiesbaden, ISBN 978-3-658-30994-7:49–74, 2020.

[48] Scharrer, O., Wieske, P., Warth, M., Schwarzenthal, D. et al., "Fahrspas ohne Reue dank synthetischem Kraftstoff-Blend/Uncompromisingly Fun to Drive thanks to Synthetic Fuel Blend," in: Geringer, B. and Lenz, H.-P. (eds.), *40. Internationales Wiener Motorensymposium 15.-17. Mai 2019*, VDI Verlag, ISBN 9783186811127:II-84-II-102, 2019.

[49] Abdalla, A. and Liu, D., "Dimethyl Carbonate as a Promising Oxygenated Fuel for Combustion: A Review," *Energies* 11(6):1552, 2018, doi:10.3390/en11061552.

[50] Wen, L.-b., Xin, C.-Y., and Yang, S.-C., "The effect of adding dimethyl carbonate (DMC) and ethanol to unleaded gasoline on exhaust emission," *Applied Energy* 87(1):115–121, 2010, doi:10.1016/j.apenergy.2009.06.005.

[51] Gopinath, D. and Sundaram E., "Experimental Investigation on the Effect of Adding Di Methyl Carbonate to Gasoline in a SI Engine Performance," *International Journal of Scientific & Engineering Research*, Volume 3, 6 Juni 2012, 2012.

[52] Schifter, I., González, U., Díaz, L., Sánchez-Reyna, G. et al., "Comparison of performance and emissions for gasoline-oxygenated blends up to 20 percent oxygen and implications for combustion on a spark-ignited engine," *Fuel* 208:673–681, 2017, doi:10.1016/j.fuel.2017.07.065.

[53] Stadler, A., Sauerland, H., Härtl, M., and Wachtmeister, G., "The Potential of Gasoline Fueled Pre Chamber Ignition Combined with Elevated Compression Ratio," SAE Technical Paper Series, WCX SAE World Congress Experience, APR. 21, 2020, SAE International400 Commonwealth Drive, Warrendale, PA, United States, 2020.

[54] Koch, T., Tiemann, C., Hamm, T., Ecker, H.J. et al., "Single cylinder test engines," *ATZautotechnology* 8(11):38–42, 2008, doi:10.1007/BF03247098.

[55] Menzel, F., Seidel, T., Schmidt, W., Pape, J. et al., "Einzylindermotor als Werkzeug zur Entwicklung neuer Brennverfahren," *MTZ Motortech Z* 67(3):168–173, 2006, doi:10.1007/BF03226771.

[56] Heiduk, T., Kuhn, M., Stichlmeir, M., and Unselt, F., "Der Neue 1,8-L-TFSI-Motor von Audi Teil 2: Gemischbildung, Brennverfahren und Aufladung," *MTZ Motortech Z* 72(7-8):596–605, 2011, doi:10.1365/s35146-011-0135-y.

[57] Eiser, A., Doerr, J., Jung, M., and Adam, S., "Der neue 1,8-l-TFSI-motor von Audi," *MTZ Motortech Z* 72(6):466–475, 2011, doi:10.1365/s35146-011-0109-0.

[58] Zima, S., "Kurbeltriebe: Konstruktion, Berechnung und Erprobung von den Anfängen bis heute," ATZ-MTZ-Fachbuch, 2nd ed., Vieweg, Braunschweig, ISBN 978-3528131159, 1999.

[59] Schauer, F.X., "Untersuchung moderner ottomotorischer Brennverfahren zur Reduktion der Partikelemissionen," Zugl.: München, Techn. Univ., Diss., 2014, 1st ed., LVK Techn. Univ, München, ISBN 978-3943813098, 2014.

[60] Backes, F., "Experimentelle Untersuchungen zu Partikelanzahlemissionen beim direkteinspritzenden Ottomotor," 1st ed., LVK Lehrstuhl für Verbrennungskraftmaschinen - Technische Universität München, München, 2021.

[61] Peer, J., "Erschließung von Potenzial zur CO2- und PN-Reduzierung von Ottomotoren durch Erhöhung des Einspritzdrucks und alternative Einspritzkonzepte," 1st ed., LVK Lehrstuhl für Verbrennungskraftmaschinen - Technische Universität München, München, ISBN 978-3-943813-28-9, 2019.

[62] Yamasaki, Y., Schauer, F.X., and Wachtmeister, G., "Development of Dynamic Models for an HCCI Engine with Fully Variable Valve-Train," *SAE Technical Paper Series*, SAE Technical Paper Series, SAE 2013 World Congress & Exhibition, APR. 16, 2013, SAE International400 Commonwealth Drive, Warrendale, PA, United States, 2013.

[63] Schauer, F.X., Zimmer, T., Bachhuber, M., Scheller, M. et al., “Development of a Model-Based HCCI Control Strategy for an Engine with a Fully Variable Valve Train,” *SAE Technical Paper Series*, SAE Technical Paper Series, SAE 2013 World Congress & Exhibition, APR. 16, 2013, SAE International400 Commonwealth Drive, Warrendale, PA, United States, 2013.

[64] Blochum, S., Ruch, F.H., Bastuck, T., Härtl, M. et al., “Identification of In-Cylinder Aerosol Flow Induced Emissions due to Piston Ring Design in a DISI Single Cylinder LV Engine Using Oxygenated Synthetic Fuels,” SAE Technical Paper Series, WCX SAE World Congress Experience, APR. 13, 2021, SAE International400 Commonwealth Drive, Warrendale, PA, United States, 2021.

[65] Khan, M.Y., Sharma, S., Liew, C.M., Joshi, A. et al., “Comparison of Full Flow Dilution, Partial Flow Dilution, and Raw Exhaust Particle Number Measurements,” *Emiss. Control Sci. Technol.* 4(2):103–112, 2018, doi:10.1007/s40825-018-0086-6.

[66] Giechaskiel, B., Lähde, T., and Drossinos, Y., “Regulating particle number measurements from the tailpipe of light-duty vehicles: The next step?,” *Environmental research* 172:1–9, 2019, doi:10.1016/j.envres.2019.02.006.

[67] Giechaskiel, B., “Differences between tailpipe and dilution tunnel sub-23 nm nonvolatile (solid) particle number measurements,” *Aerosol Science and Technology* 53(9):1012–1022, 2019, doi:10.1080/02786826.2019.1623378.

[68] Bowditch, F.W., “A New Tool for Combustion Research A Quartz Piston Engine,” *Pre-1964 SAE Technical Papers*, SAE Technical Paper Series, JAN. 01, 1906, SAE International400 Commonwealth Drive, Warrendale, PA, United States, 1906.

[69] Mühlthaler, M., Blochum, S., Stadler, A., Härtl, M. et al., “Optical Investigations of Oxygenated Alternative Fuels in a Single Cylinder DISI Light Vehicle Gasoline Engine,” SAE Technical Paper Series, WCX SAE World Congress Experience, APR. 13, 2021, SAE International400 Commonwealth Drive, Warrendale, PA, United States, 2021.

[70] Bargende, M., “Ein Gleichungsansatz zur Berechnung der instationären Wandwärmeverluste im Hochdruckteil von Ottomotoren,” Fachbereich Maschinenbau - Technische Hochschule Darmstadt, Darmstadt, 1990.

[71] Spicher, U., “Kenngrößen,” in: van Basshuysen, R. and Schäfer, F. (eds.), *Handbuch Verbrennungsmotor: Grundlagen, Komponenten, Systeme, Perspektiven*, ATZ/MTZ-Fachbuch, 7th ed., Springer Vieweg, Wiesbaden, ISBN 978-3-658-04678-1:14–25, 2015.

[72] Stadler, A., Wessoly, M., Blochum, S., Härtl, M. et al., “Gasoline Fueled Pre-Chamber Ignition System for a Light-Duty Passenger Car Engine with Extended Lean Limit,” *SAE Int. J. Engines* 12(3):323–339, 2019, doi:10.4271/03-12-03-0022.

[73] Stadler, A., “Wirkungsgrad- und Emissionspotential einer gespülten Benzin-Vorkammerzündung am PKW-Ottomotor,” 1st ed., LVK Lehrstuhl f. Verbrennungskraftmaschinen, München, ISBN 978-3-943813-35-7, 2022.

[74] Frenzel, H., Achleitner, E., Krüger, G., Rösel, G. et al., “Direkteinspritzsysteme für Ottomotoren zur Erfüllung der Real Driving Emission,” in: Tschöke, H. and Marohn, R. (eds.), *10. Tagung Diesel- und Benzindirekteinspritzung 2016*, Proceedings, Springer Fachmedien Wiesbaden, Wiesbaden, ISBN 978-3-658-15326-7:281–299, 2017.

[75] Überall, A., Otte, R., Eilts, P., and Krahl, J., “A literature research about particle emissions from engines with direct gasoline injection and the potential to reduce these emissions,” *Fuel* 147:203–207, 2015, doi:10.1016/j.fuel.2015.01.012.

A Liste der Veröffentlichungen

A.1 Peer-review Veröffentlichungen

2021

Blochum, S.; Fellner, F.; Mühlthaler, M.; Yoneya, N.; Sauerland H.; Härtl, M.; Wachtmeister, G.: Comparison of Promising Sustainable C1-Fuels Methanol, Dimethyl Carbonate, and Methyl Formate in a DISI Single-Cylinder Light Vehicle Gasoline Engine. SAE Technical Paper, 2021

Kraus, C.; Fellner, F.; Härtl, M.; Blochum, S.; Wachtmeister, G.; Sauerland, H.; Miyamoto, A.: Review of Potential CO2-Neutral Fuels in Passenger Cars in Context of a Possible Future Hybrid Powertrain, SAE Technical Paper 2021-01-1229, 2021.

Blochum, S.; Gadomski, B.; Retzlaff, M.; Thamm, F.; Kraus C.; Gelhausen, R.; Hoppe, S.; Härtl, M.; Wachtmeister, G.: Potential Analysis of a DMC/MeFo Mixture in a DISI Single and Multi-Cylinder Light Vehicle Gasoline Engine. SAE International, 2021

Blochum, S.; Ruch, F.; Bastuck, T.; Thamm, F.; Härtl, M.; Mittler, R.; Wachtmeister G.: Identification of In-Cylinder Aerosol Flow Induced Emissions due to Piston Ring Design in a DISI Single Cylinder LV Engine Using Oxygenated Synthetic Fuels. SAE International, 2021

Mühlthaler, M., Blochum, S., Stadler, A., Härtl, M. et al., “Optical Investigations of Oxygena-ted Alternative Fuels in a Single Cylinder DISI Light Vehicle Gasoline Engine,” SAE Technical Paper Series, WCX SAE World Congress Experience, APR. 13, 2021, SAE International400 Commonwealth Drive, Warrendale, PA, United States, 2021.

2020

Yoneya, N.; Blochum S.; Wachtmeister G.; Yasukawa Y.; Sugiyama Y.: High Fuel Pressure and Multiple Injection of Gasoline for the Particle Emission Reduction Under Cold Conditions. FISITA Web Congress 2020, 2020

2019

Backes, F.; Blochum, S.; Härtl, M.; Wachtmeister, G.: Experimental Analysis of Gasoline Direct Injector Tip Wetting. SAE International Journal of Engines **13** (1), 2019, 77-91

Stadler, A.; Wessoly, M.; Blochum, S.; Härtl, M.; Wachtmeister, G.: Gasoline Fueled Pre-Chamber Ignition System for a Light-Duty Passenger Car Engine with Extended Lean Limit. SAE International Journal of Engines **12** (3), 2019, 323—339

A.2 Konferenzbeiträge

2021

Härtl M., Blochum S., Kraus C., Wachtmeister G.: Energy Carriers for Future Mobility. In: Liebl J., Beidl C., Maus W. (Hrsg.) Internationaler Motorenkongress 2021. Proceedings. Springer Vieweg, Wiesbaden.

2020

Wagner, C.; Keskin, M.-T.; Grill, M.; Liming, C.; Blochum, S; Bargende, M.; Pitsch, H.: Potential analysis and virtual development of SI Engines operated with DMC+. 20. Internationales Stuttgarter Symposium, Springer Vieweg, 2020

2018

Härtl, M.; Pélerin, D.; Dworschak, P.; Maier, Th.; Stadler, A.; Blochum, S.; Gaukel, K.; Jacob, E.; Wachtmeister, G.: Potential of the Sustainable C1-Fuels OME, DMC, and MeFo for Particulate Free Combustion in DI and SI Engines. 5th International Engine Congress Baden-Baden, 2018

Härtl, M.; Pélerin, D.; Dworschak, P.; Stadler, A.; Blochum, S.; Gaukel, K.; Wachtmeister, G.: Methanol Based PtL Fuels for Particulate Free Combustion in DI and SI Engines. Perspectives on Power-to-Liquids and Power-to-Chemicals 2018, 2018

Härtl, M.; Stadler, A.; Blochum, S.; Pélerin, D.; Maier, Th.; Berger, V.; Wachtmeister, G.; Seidenspinner, Ph.; Wilharm, Th.; Jacob, E.: DMC+ as Particulate Free and Potentially Sustainable Fuel for DI SI Engines. 39. Internationales Wiener Motorensymposium (Fortschritt-Berichte VDI Reihe 12, Nr. 807), 2018, 202-229

A.3 Buchkapitel

2019

Härtl, M.; Stadler, A.; Blochum, S.; Pélerin, D.; Maier, Th.; Berger, V.; Wachtmeister, G.; Seidenspinner, Ph.; Wilharm, Th.; Jacob, E.: DMC+ als partikelfreier und potenziell nachhaltiger Kraftstoff für DI Ottomotoren. In: Zukünftige Kraftstoffe. Energiewende des Transports als ein weltweites Klimaziel. Springer, 2019

B Verwendete Veröffentlichungen

B.1 Potential Analysis of a DMC/MeFo Mixture in a DISI Single and Multi-Cylinder Light Vehicle Gasoline Engine

2021-01-0561 Published 06 Apr 2021

Potential Analysis of a DMC/MeFo Mixture in a DISI Single and Multi-Cylinder Light Vehicle Gasoline Engine

Sebastian Blochum Technical University of Munich

Bartosch Gadomski, Mario Retzlaff, and Fabian Thamm Tenneco

Christoph Kraus and Martin Härtl Technical University of Munich

Ralf Gelhausen and Steffen Hoppe Tenneco

Georg Wachtmeister Technical University of Munich

Citation: Blochum, S., Gadomski, B., Retzlaff, M., Thamm, F. et al., "Potential Analysis of a DMC/MeFo Mixture in a DISI Single and Multi-Cylinder Light Vehicle Gasoline Engine," SAE Technical Paper 2021-01-0561, 2021, doi:10.4271/2021-01-0561.

Abstract

In this study a mixture of dimethyl carbonate (DMC) and methyl formate (MeFo) was used as a synthetic gasoline replacement. These synthetic fuels offer CO_2-neutral mobility if the fuels are produced in a closed CO_2-cycle and they reduce harmful emissions like particulates and NO_X. For base potential investigations, a single-cylinder research engine (SCE) was used. An in-depth analysis of real driving cycles in a series 4-cylinder engine (4CE) confirmed the high potential for emission reduction as well as efficiency benefits.

Beside the benefit of lower exhaust emissions, especially NO_X and particle number (PN) emissions, some additional potential was observed in the SCE. During a start of injection (SOI) variation it could be detected that a late SOI of DMC/MeFo has less influence on combustion stability and ignitability. With this widened range for the SOI the engine application can be improved for example by catalyst heating or stratified mode. Furthermore, until $\lambda = 0.8$ no significant PN increase was noted in contrast to gasoline. This is also a positive capability for combustion modes with local rich areas in the mixture. From the experience of previous investigations, the synthetic fuels' high knock-resistance potential enabled an increase in the compression ratio (CR) from epsilon ~ 11 to ~ 15 to enhance the indicated efficiency.

In general, in the 4CE the positive effects of DMC/MeFo on harmful emissions were confirmed. Even in the series configuration, the brake efficiency increased by 16 % at maximum low-end torque compared to gasoline. The increased in-cylinder cooling and the lower laminar flame temperature by the DMC/MeFo implies lower maximum exhaust temperatures. Therefore, a stoichiometric mixture could be used over the whole engine map. During the legislative driving cycles, for example WLTC, the PN, NO_X, CO and CH_4 emissions decreased by 50 % or more.

In summary, oxygenated fuel opens great opportunities for replacing fossil fuel in gasoline engine applications.

Keywords

DISI engines, light-duty, single-cylinder, multi-cylinder, 4-cylinder, future combustion engine, particle number emissions, PN, harmful emissions, climate emissions, CO_2, driving cycles, RDE, WLTC, gasoline, alternative fuels, E-fuels, synthetic fuels, oxygenates, DMC, MeFo, high compression

Introduction

With the EU 2050 goal of a sustainable energy economy, [1] it has become a major challenge to develop synthetic fuels on a non-fossil basis. Synthetic hydrocarbons and oxygenates can be tailored to the specific needs of internal combustion engines and yield further benefits regarding their combustion and emission behavior [2].

For use in spark-ignition engines (SI) with direct injection (DI), an ideal fuel should have high knock resistance, a defined vapor pressure, and should reduce the formation of coking deposits, particles from combustion, and other pollutants such as NO_X and HC.

The two oxygenated fuels methyl formate (MeFo) and dimethyl carbonate (DMC) have been proposed as possible

alternatives to gasoline fuel [3] and extensively tested for their particle formation properties [4]. Their molecular structure does not contain carbon-carbon bonds ("C1-fuel") which allows virtually soot-free combustion [5]. As their lower heating value is only approximately 36 % of conventional gasoline, a higher fuel mass must be injected, leading to an increased cooling effect. This reduces thermal NO_X formation by approximately 50 % and has a positive effect on knock resistance.

MeFo and DMC are both produced from methanol (MeOH), which is considered a future platform chemical of Power-to-X routes. As MeOH itself is rated toxic to the human body, a conversion to safer E-fuels like MeFo and DMC is desirable for critical applications.

DMC is a clear liquid carbonate ester mostly used as a solvent or methylating agent [6] and is non-toxic and biodegradable. Despite its high knock resistance [7], DMC has been investigated as a diesel fuel additive owing to its ultra-low particle formation tendency [8, 9, 10, 11]. As DMC has a relatively low vapor pressure (DVPE approx. 10.8 kPa), it should be blended with more volatile components (such as MeFo) to achieve fast mixture formation in DI combustion systems.

MeFo as the methyl ester of formic acid is a clear liquid used as precursor in the chemical industry, as a solvent, and as a cooling agent [12]. MeFo and DMC have no global warming potential and do not contribute to ozone depletion [13]. MeFo was suggested as a fuel component in an OMV patent [14], and it´s basic combustion properties were investigated in [15]. MeFo has a low boiling point of 31.5 °C, which makes it necessary to blend with less volatile components like DMC for practical use.

In this paper, DMC and MeFo are blended in a ratio of 65:35 and tested in engine experiments on a single-cylinder engine (SCE) and 4-cylinder engine (4CE) and compared against a conventional gasoline fuel as reference. The observed effects on efficiency, particle, and gaseous pollutant emissions are investigated.

Theoretical predictions by Wagner et al. via 0D/1D engine simulation suggest that the high octane rating of DMC/MeFo blends above 100 allows increased engine efficiency with existing engine designs. The advantage reaches up to 14 % at full load operating points. Optimized engine concepts with increased compression ratios (CR) and downsizing measures can be expected to improve efficiency by up to 20 % [16].

Fuel

As a reference, RON95 E5 validation gasoline fuel is used, henceforward called G100. The investigated oxygenated fuel mixture consists of 65 vol.-% DMC and 35 vol.-% MeFo (C65F35). In Table 1, the properties of both fuels are shown.

The significant disparity between the conventional gasoline G100 and the oxygenated fuel C65F35 is the higher oxygen (O_2) content. Derived from that, the stoichiometric air-fuel ratio (AFR) of C65F35 is 67.5 % lower compared to G100.

In previous investigations, a slight difference between the λ probe and the calculated λ based on the exhaust gas components was detected, most significantly with lean mixtures. Hence, the calculated λ using the Brettschneider/Spindt formula is usually used for G100. But the calculation with the Brettschneider/Spindt formula has not been validated for alternative fuels with such high oxygen contents. Therefore, the measured fuel and air mass flow in SCE is used to calculate the global λ during the λ variation. The accuracy of this approach is proved by a comparison with the calculated λ based on the Brettschneider/Spindt formula using G100.

TABLE 1 Fuel properties

Name	Unit	G100	C65F35
Gasoline RON95 E5	vol. %	100	-
Dimethyl **C**arbonate		-	65
Methyl **F**ormate		-	35
LHV	MJ/kg	42.2	15.2
Density @ 15 °C	kg/m³	750.8	1041.1
Gasoline equivalent	m³/m³	1.0	2.0
RON / MON	-	96.8/86.3	117/ >120
Oxygen content	wt. %	1.7	53.3
Hydrogen content	wt. %	13.2	6.7
Carbon content	wt. %	85.1	40
AFR stoich.	kg/kg	14.28	4.64
Boiling range	°C	37.5-202.5	37.5-94
DVPE @ 37,8 °C	kPa	57.8	57.4
Enthalpy of vaporization	kJ/kg	420	433
Surface tension	mN/m	24	27.7

Another consequence is the 2.8 times lower mass-based heating value (LHV) of G100, which is calculated using DULONG's formula modified by GUMZ [17]:

$$LHV = \frac{34 \cdot C_{wt.\%} + 101.6 \cdot H_{wt.\%} - 9.8 \cdot O_{wt.\%}}{100}\ MJ/kg$$

The density of C65F35 is 38.7 % higher, which partly compensates for the significantly lower energy content. Finally, the volumetric energy content compared to a gasoline-equivalent is 2.0, and to achieve the same engine load, theoretically 10 % less intake air is needed with C65F35.

Experimental Setup and Numerical Methodology

Single-Cylinder Engine

For the fundamental investigation an in-house designed gasoline 4-stroke single-cylinder research engine is used, which has been referred to in several other publications [3, 18, 19, 20, 21]. The engine design is inspired by a series light-duty vehicle engine and it is equipped with a double overhead camshaft (DOHC) with two valves each for intake and exhaust. Table 2 shows all the important specifications of the SCE. The valve train uses fixed standard valve timing with a moderate lift and a small overlap. The SCE operates with a DI spark-ignited (DISI) combustion mode. For ignition a serial M14 spark plug and ignition coil is used.

TABLE 2 SCE specifications

Engine base	EA 888 GEN2
Bore	82.51 mm
Stroke	86.6 mm
Connecting rod length	144 mm
Displacement	463 mm
Compression ratio	10.92:1
Number of valves (intake/exhaust)	2 for each
Exhaust valve lift	7 mm @ 250 °CA aTDC
Exhaust open	132 °CA aTDC
Exhaust close	368 °CA aTDC
Intake valve lift	6 mm @ 460 °CA aTDC
Intake open	348 °CA aTDC
Intake close	572 °CA aTDC
Max. IMEP	17 bar
Max. speed	3500 1/min
Oil temp.	25-80 °C
Coolant temp.	–7-80 °C

During the experiment, a CR variation is introduced to use the potential of the higher knock resistance of the oxygenates to raise the indicated thermal efficiency η_i. The CR is increased from $\varepsilon = 10.92$ to $\varepsilon = 14.91$. As shown in Figure 1, to achieve the high CR (HCR) a different in-house designed piston from a previous investigation by Stadler et al. [22] is used.

An increase in the theoretical efficiency from the Otto cycle is expected:

$$\eta_{th} = 1 - \frac{1}{\varepsilon^{\kappa-1}}$$

The second influenceable variable in the equation is the heat capacity ratio κ. This variable increases with lean mixtures, because of the higher κ of air compared to the fuel. Owing to this benefit, a λ variation is performed with the SCE, to estimate the lean combustion potential.

The DI injector is located on the side between the intake ports of the combustion chamber. It is a series multi-hole solenoid-actuated injector with a standard spray pattern and flowrate. All additional parameters are listed in Table 3.

FIGURE 1 Comparison of conventional and high compression ratio

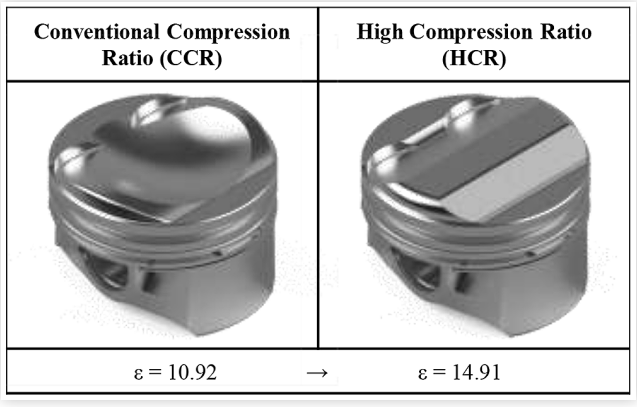

TABLE 3 DI Injector parameters

Max. pressure	35 MPa
Injector type	Multi-hole DI
Nozzle size	6 mm
Actuation	Solenoid
Number of orifices	6
Orifice shape	Convergent
Injector position	Side-mounted
Static flowrate @ 10 Mpa with n-Heptane	13.8 ccm/s

Auxiliary Units In Figure 2 the SCE auxiliary units are illustrated in a simplified structure diagram. This overview shows four system groups, called the air intake, mobile fuel, indication and exhaust system.

A stationary working screw compressor aspirates the air through an air cleaner from the environment. Afterward, the air passes an oil separator, air dryer and intercooler, before it is stored with an absolute pressure of 2 bar in a 150-liter tank. The intake throttle controls the air mass flow and the electric air heater the intake temperature. The unused air mass flow is blown off through a relief valve. The Aerzen rotary displacement meter measures the volumetric airflow. The air mass is calculated with the support of the temperature and pressure inside the flow meter. To take account of the charge air compression work, if the ambient pressure level is exceeded, a Roots-type supercharger with isentropic compression is simulated with a charger efficiency of 75 %. The calculated compression work is subtracted from the indicated engine work afterward and thus it is considered in the indicated efficiency.

The mobile fuel system is resistant to all hydrocarbon and oxygenated fuels because the pipes are made from stainless steel and the materials of the sealing parts are PTFE or FFKM. The fuel system is divided into a low- and high-pressure part.

FIGURE 2 Structure diagram

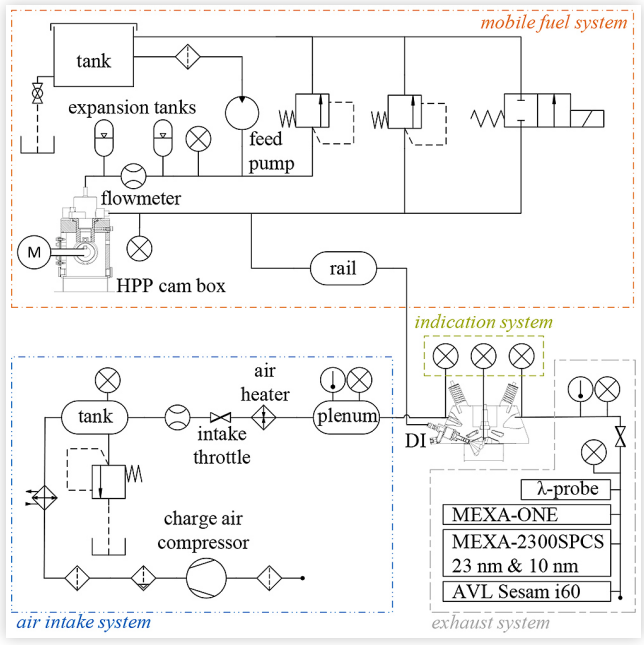

A relief valve regulates the low-pressure part to 4 bar. Between the low- and high-pressure pumps, an Endress+Hauser AG Cubemass C 100 Coriolis flowmeter measures the fuel mass flow. Before and after the flowmeter, expansion tanks damp oscillations in the fuel system. The series gasoline high-pressure pump (HPP) is driven by a camshaft, which in turn is powered by an electric motor. The HPP's control valve works quantitatively to adjust the desired fuel pressure required by the National Instruments compactRio-based electronic control unit (ECU). The HPP is a state-of-the-art DISI light vehicle fuel pump with a maximum fuel pressure of 35 MPa. The high-pressure part has two re-flow lines, one with a pressure relief valve and the other with a safety valve. An additional flexible stub line is connected to the fuel rail, which fits on the DI-Injector.

A Bosch LSU 4.9 wideband λ probe, combined with an ETAS LA4 lambda meter is mounted downstream of the exhaust manifold. The gas sample probes are connected to the exhaust gas measurement devices. The probe pipe is cut diagonally, and the orifice is oriented downstream. The gaseous emissions are monitored with a Fourier-transform infrared spectrometer (FTIR) in the form of an AVL SESAM i60 FT SII. For C65F35 an adopted evaluation method provided by AVL is used. Different additional gas analyzers are installed in a HORIBA MEXA-ONE-D1. The MEXA-ONE-D1 uses two nondispersive infrared sensor (NDIR) analyzers for high and low CO values, to cover a wide vol.-% range of CO emissions. CO_2 is measured with an NDIR analyzer under dry conditions with a range of 0 - 20 vol.-%. The magneto-pneumatic detector is applied to identify any remaining O_2 in the exhaust. A chemiluminescence detector is used to detect the NO_X emissions and a flame ionization detector (FID), calibrated with C_3H_8, detects total hydrocarbons (THC). If the engine operates with C65F35, the fuel fragments and intermediate products contain mostly oxygenates. Therefore, the definition in the appendix of the directive 1999/13/EC of the European Council declaration volatile organic compounds (VOC) is used in this paper instead of THC [23], as did Gellner et al. [24]. However, the FID response signal is highly influenced by partially oxidized carbon atoms in compounds, which are heteroatomic. If the O/C-ratio of the fuel increases the response factor is weakened. MeOH and formaldehyde (CH2O), as well as DMC and MeFo, have an O/C-ratio of 1.0. Wallner [25] showed that MeOH and CH_2O have response factors of 0.4 - 0.74 and 0. As they are intermediate or starting products of the reaction kinetics, all four components are detectable in the exhaust gas. In turn the response factor of G100 is close to 1.0, because of the extremely low O/C-ratio of 0.02 [25, 26]. Hence, the detected VOC emissions for C65F35 are, depending on the combustion conditions, at a significantly lower level.

For the detection of solid-state emissions a HORIBA MEXA-2300SPCS [27] is installed to count the non-volatile PN concentration. The SPCS is upgraded by a second condensation particle counter (CPC). The first CPC has a cutoff size of 23 nm, while the second one has a cutoff size of 10 nm particle diameter. The reference ambient PN level refers to the long-term investigations of Birmili et al. [28]. He used measurement data from 17 different locations in different region types. The averaged ambient volatile PN (30-800 nm) range was found to range between $1.12x10^3$ and $1.05x10^4$. The lowest value represents an alpine mountain, while the highest represents a roadside in a city center. The comparison of non-volatile PN from the SCE exhaust, with volatile PN from the environment, is admissible as a converting three-way catalyst (TWC) does not forward considerable volatile PN [29]. Consequently, the impact on the environment is the non-volatile PN.

Engine Control and Data Acquisition The indication system uses three piezo sensors for intake, exhaust and in-cylinder pressure. Every cycle the Kistler 6056A-3-2 relative piezo-electric pressure sensor in the cylinder is balanced with the Kistler 4045A10 absolute piezo resistive sensor at the intake manifold. The third absolute pressure absolute piezo-resistive sensor, a Kistler 4075A10, measures the exhaust gas pressure. The crank angle position is detected by an ASM posimag® rot magnetic incremental encoder, with a resolution of 0.1 °CA. With the additional information from the pressure trace, the indicated mean effective pressure (IMEP) and the apparent heat release rate (AHRR) are calculated in the data acquisition. The ECU is based on a dSPACE platform. During the experiment, an engine load and λ controller are used to adjust the desired engine operating point. The engine load controller regulates the air mass flow using the intake throttle position, while the λ controller varies the fuel mass flow by injection duration. The snapshots are triggered by the data acquisition. A snapshot includes all measured and calculated data averaged over 200 cycles, including the indicated pressure traces. Each single pressure trace of the 200 cycles is stored separately.

4-Cylinder Engine

For the demonstration of the new engine technology, a state-of-the-art DISI 4-cylinder engine (4CE) was used. The engine is based on the series engine EA888 EVO4 from Audi. The specifications are shown in Table 4. The engine is equipped with an integrated exhaust manifold that, in combination with the rotary valve module, enables faster heat up during cold start as well as lower exhaust gas temperatures under full load operation, both give a higher overall engine efficiency. In order to reach a high low-end torque and improve dynamic response while maintaining high specific peak power, a

TABLE 4 Specification 4CE

Engine Name	EA 888 EVO4
Bore	82.5 mm
Stroke	92.8 mm
Connecting rod length	144 mm
Displacement	1984 cm^3
Compression ratio	9.6:1
Nominal power	195 kW 5000-6500 1/min
Nominal torque	370 Nm @ 1750-5000 1/min
Max. speed	6800 rpm
Max. IMEP	24 bar
Fuel pressure	6.5-35 MPa

variable valve lift system is applied to the exhaust camshaft. In addition, the engine is equipped with variable camshaft phasers on both camshafts. To support charge movement during the gas exchange, the intake manifold has asymmetrical port flaps, which generate a combination of tumble and swirl of the air mass entering the cylinder. As these flaps reduce the volumetric efficiency at elevated air mass flows, the whole device can be deactivated by switching the vacuum to an actuator that rotates the shaft that carries the flaps. The DI-Injectors are side-orientated and located between the intake valves of the combustion chamber.

The engine is installed on an engine testbench with a four-quadrant dyno machine. The dyno's low moment of inertia allows the performance of realistic dynamic drive cycles like real driving emissions (RDE) or the world harmonized light-duty vehicles test procedure (WLTC). The testbench is controlled via FEV's Test Cell Manager (TCM) and Test Object Manager (TOM). While the TOM is dedicated to controlling and monitoring the engine and the dyno, the TCM handles the test bench. This includes the data acquisition of analog and digital signals, the control of auxiliary devices, the user interface, the control of an automated dyno operation and the data logging. The system is also capable of communicating with different devices through communication protocols like CAN, AK and ASAM-MCD.

Auxiliary Units As mentioned before, the auxiliary devices can be controlled by means of the TCM. Figure 2 illustrates the 4CE auxiliary units. The overview is divided into four system groups called the *fuel system*, *air intake system*, *indication system* and *exhaust system*.

The *fuel system* is a standardized system for the entire engine test house. For experimental fuels such as C65F35, a variable supply system with up to 6 IBC barrels is used. The fuel passes a fuel consumption measurement system consisting of a Coriolis measurement device, a fuel cooler and a gas separator.

The *air intake system* delivers conditioned air to the test cell. The combustion air is aspirated through a filter and routed to a Höntzsch ExactFlow II DN80 ZG1 airflow meter before entering the engine's standard inlet pipe. A water-cooled charge air cooler controls the charge air temperature using an integrated controller. The setpoint is set by the TCM and adjustable from 0 to 120 °C.

To monitor and analyze the combustion process an AVL Indimaster Advanced 671 *indication system* is used. The four Kistler 6041B water-cooled piezo pressure transducers are mounted in specially designed sleeves which are drilled into the cylinder head. The membrane of the transducers can be located at the perimeter of the combustion chamber, yielding maximum measurement accuracy and quality. A charge amplifier passes the pressure signals to the Indimaster main unit. To synchronize the cylinder pressure signals with the crank angle position, an AVL 365CC crank angle sensor with a physical resolution of 0.5 ° is used.

TDC is determined with a capacitive TDC-sensor at different engine speeds. The four pressure sensors are referenced by an absolute sensor in the intake manifold. In addition to the pressure signals, the indication system can determine injection and ignition timing based on signals from current probes which are connected to the respective actuator.

The *exhaust system* is set up according to the vehicle's exhaust system. The first lambda probe is located upstream from the turbocharger. The metered value is passed from the engine ECU to the TCM via an ASAM-MCD interface. The probes for the exhaust gas sampling are installed pre and post the three-way-catalyst (TWC). They obtain their sample gas through multi-hole-probes with five ports over the probe's length at 3 locations around its perimeter. While one port row is facing the incoming exhaust gas, the remaining two rows are arranged with 120 ° spacing. Except for the Engine Exhaust Particle Sizer (EEPS), each device has a dedicated probe at position 1 and 2 for the entire testing (compare Figure 3).

Exhaust Gas Sampling To detect the solid-state emissions an ECE-R83/R49 certified AVL APC+ is introduced. The determination of the particle size distribution is done by a TSI EEPS. Owing to the EEPS not having its own sample conditioning system, it is installed downstream from the APC+ and uses the same conditioned gas probe as the particle counter. Furthermore, to monitor the gaseous emissions, an AVL SESAM i60 FT SII is used.

The sample gas passes the tailpipe-kit and the pressure reduction unit of the APC+ to ensure constant sample conditions before entering the APC+ through the chopper-dilutor. The first dilution stage is followed by an evaporation tube that removes volatile exhaust components and prevents re-condensation or nucleation. Further downstream a variable dilution of the sample by adding filtered air at ambient temperature takes place. About 1/10 of the sample gas flow is passed through to the CPC while 9/10 are supplied to the EEPS via the exit line of the secondary dilutor. Particles with a diameter of 23 nm are detected with an efficiency of 50 % while a diameter of 41 nm is detected with an efficiency of >90 % [30].

The sample that enters the EEPS is cleaned from particles bigger than 1 µm via a cyclone separator. After passing the trap, the particles stream to the electrometer, before entering an electrometer pillar. An algorithm scales the 22 electrometers to 32 particle size classes in a range of 5.6 nm to 560 nm [31].

To detect gaseous emissions, a second probe samples gas for the AVL SESAM i60 FT SII. The device consists of two

FIGURE 3 Structure diagram (© 2020 Tenneco Inc.)

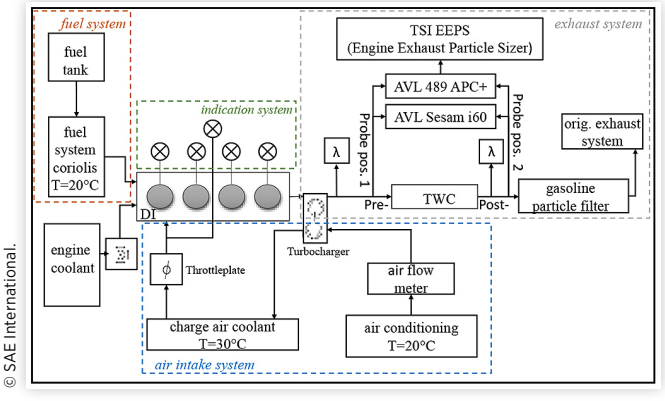

measurement units. The FTIR-spectrometer identifies the concentration of up to 32 exhaust gas components while an FID detects the total hydrocarbon content of the exhaust probe. A heated pre-filter module removes solid exhaust gas components from the sample stream and conditions the gas flow to a constant pressure and temperature. Heated lines prevent condensation of volatile emissions. Entering the actual measuring device, the sample stream is divided to feed the different units. Several evaluation methods for the FTIR-spectrum can be set for variable fuels and exhaust gas components [32]. The standard gasoline method is used for G100. For the operation with C65F35, a special method has been created in cooperation with AVL.

Results and Discussion

Single-Cylinder Engine

If not otherwise mentioned, all shown measurements on the SCE are performed with an engine speed of 2000 rpm, a medium engine load of 7 bar IMEP, and a λ = 1.0. The start of injection (SOI) is set to 430 °CA after top dead center (aTDC) to have longer for a homogeneous mixture formation without wetting the piston crown and the fuel pressure is set to 35 MPa. The intake air temperature was set to 30 °C, while the oil temperature, as well as the coolant water, are set to 80 °C. For the theoretical optimum of the indicated efficiency the center of combustion (MFB50) is adjusted to 8 °CA aTDC. In contrast to the 4CE, neither a tumble flap in the intake manifold, nor exhaust aftertreatment is used during the experiment. Owing to this, all shown SCE exhaust emissions are raw emissions.

Influence of late SOI and λ Variation In this study a global λ and SOI variation for G100 and C65F35 is performed. The λ sweep started from λ = 0.8 till the determined ignition limit of λ = 1.6 for G100 and λ = 1.5 for C65F35. For the second variation a late SOI during the compression stroke is chosen to identify the effect of less time for mixture formation on the combustion behavior. In Figure 4 the combustion parameters indicated efficiency (η_i), coefficient of variation (COV) of IMEP, and combustion duration of both sweeps are shown. At the top left side, the η_i of G100 increases over λ as suggested by the formula for the theoretical efficiency, because of the increasing κ and the decreasing throttle losses.

Above λ = 1.4 the η_i decreases owing to a longer combustion duration (Figure 4 - bottom left side) as a consequence of a less complete and unstable combustion. Because of the unstable combustion and the resulting misfires, the stability limit of COV = 3.0 %, which is marked in Figure 4 (middle left side), is exceeded. In the left column of Figure 5 an increase of the unburned G100 fuel fragments in the form of VOC and the PN for λ = 1.5 and λ = 1.6 are shown. From λ 0.8 to 1.3 the η_i curve of C65F35 has the same shape, but a lower gradient compared to G100. This is due to a longer combustion duration, especially between λ 1.0 & 1.3.

Additionally, in stoichiometric or rich engine operating points a lower conversion rate for the injected fuel amount is

FIGURE 4 Combustion parameters of λ & SOI variation @ 2000 rpm/7 bar IMEP

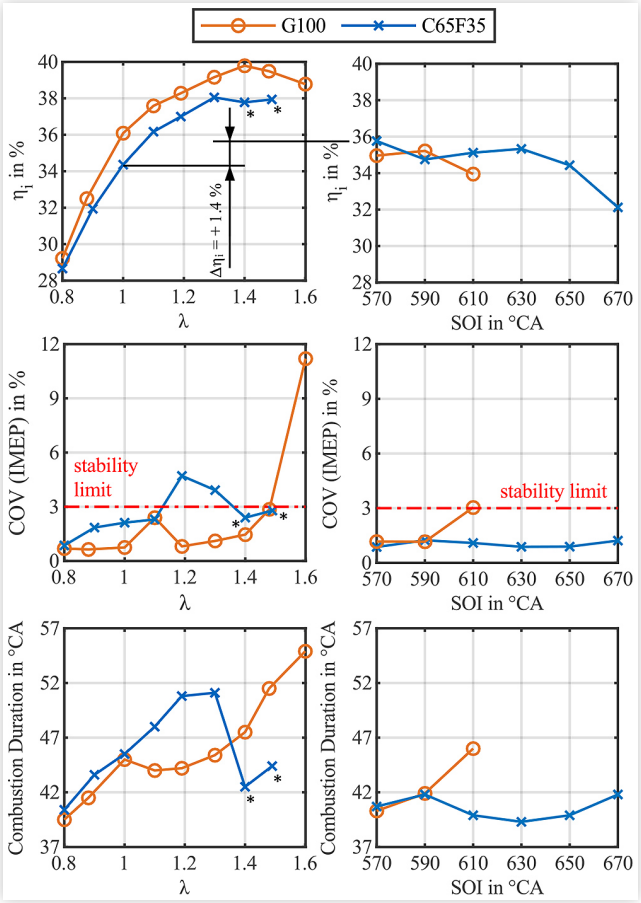

inferred from the higher CO level in Figure 5 (left column). For λ = 1.2, however, the oxygenated fuel is already exceeding the stability limit and for λ = 1.3 the ignition limit for the dedicated operating point with an SOI of 430 °CA is reached. For measurement points which are marked with an * in each diagram, the SOI was advanced from 430 °CA to 655 °CA to extend the ignition limit. Thereby, the COV falls below the stability limit again. This explains the big drop in the combustion duration and a reduction of CH_2O, as well as MeOH, shown in Figure 6 (left column). The largest differences in the λ sweep between both fuels are monitored for PN and NO_X emissions in Figure 5.

For NO_X, especially in the range of λ = 1.0 - 1.3, G100 shows an extremely high level and therefore C65F35 leads, averaged over the λ sweep, to a reduction of 53 %. This reduction is related to the higher enthalpy of vaporization and the lower laminar flame speed of C65F35. Both effects reduce the combustion peak temperatures, which prevents the Zel'dovich mechanism. The PN emissions for C65F35 are affected less over λ compared to G100, particularly for rich mixtures. On average over the λ variation, the PN23 emissions decreased by 87 %. In addition, rich mixtures improve combustion stability significantly for C65F35. Significant differences between the fuels are observed with SOI variation during the compression stroke. First, for G100 and an SOI > 610 °CA, stable combustion is not achieved. Second, for all late SOI

FIGURE 5 Raw emissions measured by MEXA-ONE-D1 and -SPCS2300 of λ & SOI variation @ 2000 rpm/7 bar IMEP

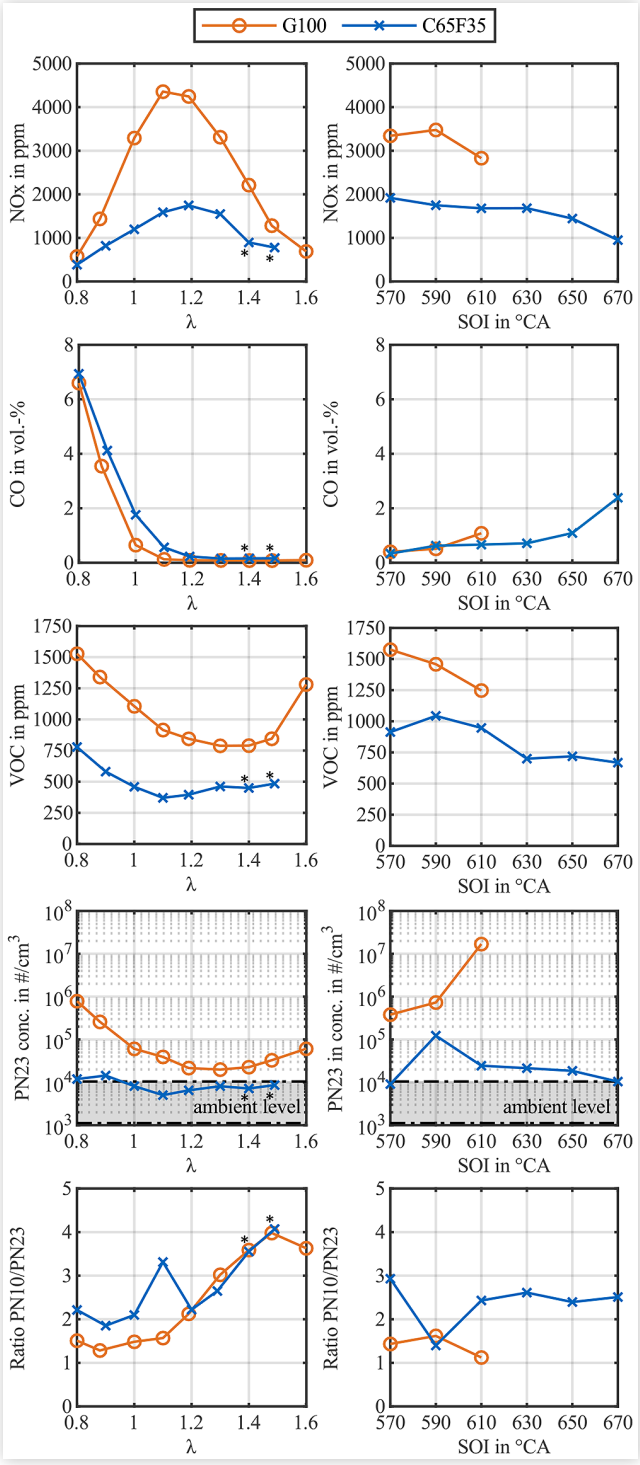

injections with G100, no benefit is observed, compared to the reference operating point with λ = 1.0 and an SOI = 430 °CA from the λ sweep. On the other hand, a clear advantage is enabled compared to the reference point for all shown combustion parameters for C65F35. Most notable is the absolute increase of $\Delta\eta_i$ of 1.4 %, which is marked at the top of Figure 4. This benefit results from a shorter combustion duration and more stable combustion with a halved COV value. This is initialized by the elevated turbulent kinetic energy due to the late injection. In Figure 7 the cylinder pressure trace and AHRR of the intake and compression stroke injections are shown.

The dotted line with the late SOI of 570 °CA has a 60 % higher max. pressure gradient and a 5 % higher max. cylinder pressure. To hold the MFB50 at 8 °CA, the ignition timing is set to 14 °CA before TDC (bTDC), which is 14.5 °CA later than the standard SOI of 430 °CA. The AHRRs maximum of SOI570 is 57 % higher and the combustion duration is 5 °CA shorter, than the standard SOI timing. This results in an indicated efficiency increase and a decrease of the exhaust manifold temperature by 11 °C. In contrast, the faster and more intensive combustion leads to higher peak temperatures during the combustion process. Therefore, the NO_X emissions rise by about 60 %, and the intermediate product CO decreases by 82 %. As a consequence of the compression stroke injection, less time for a homogeneous mixture formation is left. Thus, the ratio of unburned fuel increases. The VOC emissions in Figure 5 are doubled and the MeOH emissions increase by 34 %, shown in Figure 6. These fuel losses have a negative effect on η_i. Nevertheless, the increase of NO_X, VOC, and MeOH has no impact on the tailpipe emissions after a converting TWC, that operates at λ = 1.0 conditions, as shown by Härtl et al. [21]. In summary, the late ignition at the considered operating point is beneficial for the indicated efficiency and combustion stability, with no significant disadvantages in tailpipe exhaust emissions.

Compression Ratio Variation The oxygenated fuel's feature of high knock resistance can be used to compensate the drop in efficiency with a higher CR. The combustion parameters performed in a load sweep with a CCR and an HCR are shown in Figure 8 for C65F35.

From an IMEP of 13 bar upwards, the MFB50 has to be retarded with G100 owing to its lower knock resistance. At its maximum of 17 bar IMEP, the center of combustion is delayed for more than 13 °CA to prevent knocking. Hence, a raised CR is not recommended for G100, and in turn not investigated. Only a slight increase in the maximum cylinder pressure and a decrease in η_i is observed for G100 between 11 and 17 bar IMEP, as a result of the delayed MFB50. Owing to lower peak temperatures throughout combustion, the NO_X emissions are on a lower level than on mid-load points with a later MFB50 shown in Figure 9. With a CCR and a higher load of 15 and 17 bar IMEP, the indicated efficiency of C65F35 overcomes these of G100 by a relative maximum of 3 %. Up until 13 bar IMEP, C65F35 shows the same trend as the λ variation with an average of 1.3 % less indicated efficiency Its presumed that the lower ηi for C65F35 using CCR has its origin in the lower adiabatic laminar flame speed. Additionally, the engine design is not optimized for the oxygenated fuel. As already known from the λ and SOI variation, C65F35 has lower NO_X emissions, especially at low- to mid-load operating points, and continuously lower PN emissions. These benefits are based on the higher in-cylinder cooling and the lack of carbon-carbon bonds in the molecular structure. In spite of the HCR the NOx emissions show only slight deviations compared with the CCR. It is assumed that the pent-roof piston design of the HCR affects adversely the mixture

FIGURE 6 Raw emissions measured by SESAM i60 FT SII of λ & SOI variation @ 2000 rpm/7 bar IMEP

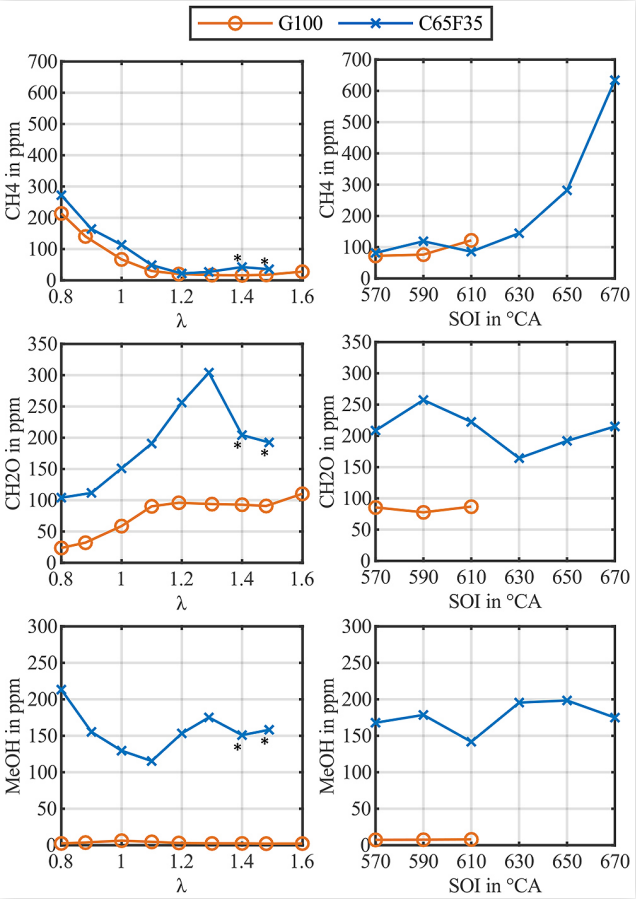

formation. Therefore, the combustion speed is deaccelerated, and the combustion peak temperatures changes only slightly. The drawback in CO emissions is significant at low- and mid-load points, because of worse combustion stability as a result of less turbulent kinetic energy. The C65F35 HCR with ε = 14.91 shows an increase in η_i for each performed point in the load sweep compared to G100. In spite of the HCR, no knocking occurred at high-load points. This results in a maximum relative η_i benefit of 11 % at 17 bar IMEP. Moreover, the average maximum cylinder pressure rises to 107 bar for C65F35, which is 46 bar higher than G100, shown in Figure 8.

In summary, the tendency with and without HCR for C65F35 emissions are equal with one exception, namely PN23. The oil jet for the piston cooling, which is enabled starting from an IMEP of 10.5 bar, causes a large increase in PN23 concentration using the HCR piston, displayed in Figure 9. With the disabled oil jet, the PN drops back to the same level as with the CCR piston. The assumption is, that the oil scraper ring functionality is limited with this in-house designed HCR piston and the series piston rings. Ultimately, the HCR confirms, that the η_i is improvable at low- and mid-load operating points when the engine is operated with C65F35.

4-Cylinder Engine

Experimental Procedure

Boundary Conditions. The different physical properties of G100 and C65F35 require a remapping of the 4CE's ECU. Initial results from the investigations on the single-cylinder engine indicate a trade-off between particulate emissions and thermal efficiency, depending on the engine's operating point. In this case, to obtain a holistic result, the engine application is carried out as a compromise. This is realized under the premise of a

FIGURE 7 Comparison of cylinder pressure & AHRR of SOI = 430 °CA and SOI = 570 °CA

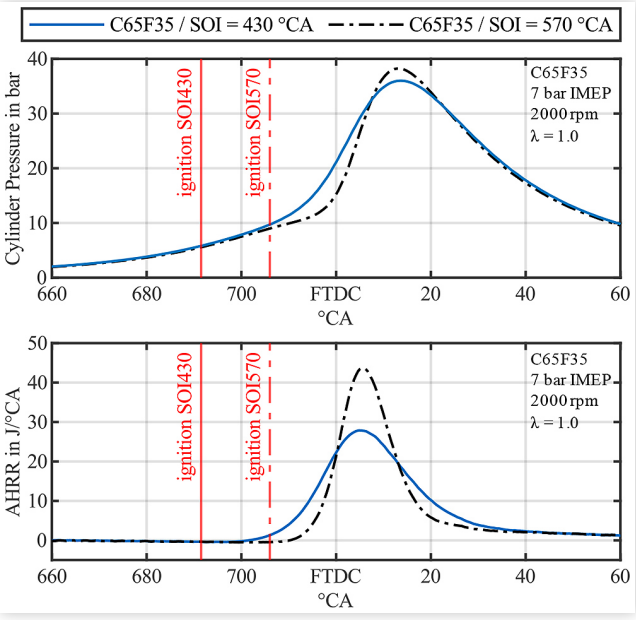

FIGURE 8 Combustion parameters of load variation @ 2000 rpm/λ = 1.0/SOI = 430 °CA

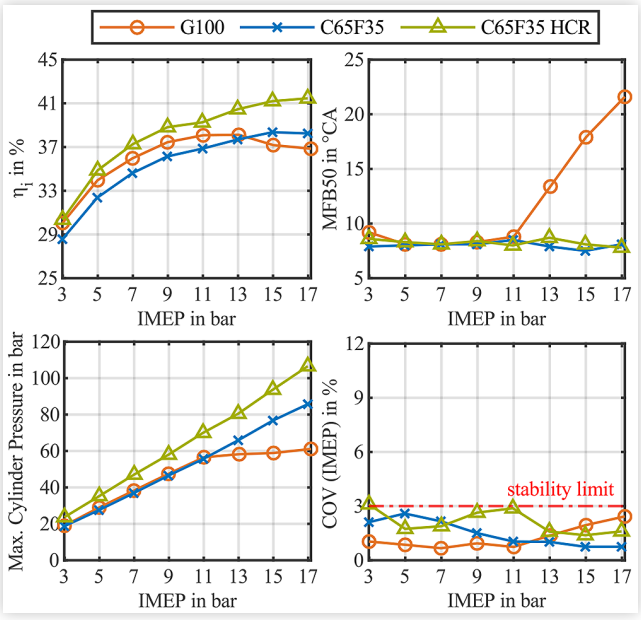

FIGURE 9 Raw emissions measured by MEXA-ONE-D1 and -SPCS2300 of load variation @ 2000 rpm/λ = 1.0/SOI = 430

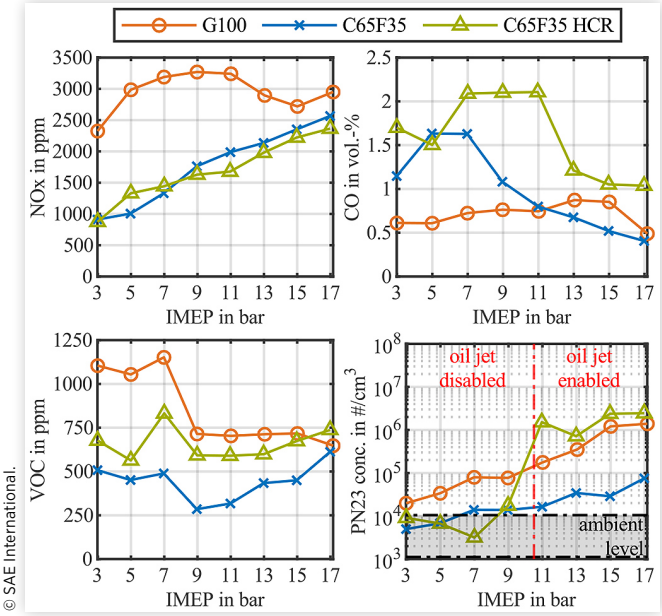

maximum firing pressure (PMAX) of 140 bar while maintaining the same power curve as G100. The target lambda in engine operation with C65F35 is lambda = 1.0. During engine operation, two different sets of environment conditions are used. In *standard condition,* ambient and charge air temperature are set to 20 °C and 30 °C. For the *hot condition* those temperatures are raised to 30 °C (ambient) and 50 °C (charge air).

Parametrization The remapping of the ECU is divided into four parts.

1. Adjustment of the base injector map to compensate the difference in the LHV to enable basic engine operation.
2. Definition of the relevant engine operating points and variation of the operating parameters to measure their effect on emissions, performance, and efficiency
3. Remapping of the entire engine map based on the findings in 2., including extrapolation and interpolation. Furthermore, the accelerator pedal position must generate the same torque output for both fuels owing to pedal and engine speed-controlled drive cycles.
4. Test dynamic response of the generated engine map using speed- and torque ramps. If necessary, tune the parametrization.

1. Compensation of the LHV. Based on the different gravimetric LHV of G100 and C65F35, the fuel mass per stroke in C65F35 operation must be extended by a factor of 2.77 compared to the standard application. As the higher density of the oxygenate fuel has a counter effect, the injection time in the base map of the ECU ultimately needs to be extended by a factor of 2. Fine adjustment of the injection timing is carried out by the Lambda-Controller of the ECU. A basic engine operation is possible with these minor changes in the engine's control unit.

2. Variation of parameters in relevant operating points. Further investigations are carried out at defined engine operating points that are relevant for driving cycles like RDE, WLTC or are significant in matters of performance and drivability. The influence of the operating conditions on performance, emissions and efficiency is investigated by sweeping the respective variable. The following variables are part of the test program: *ignition timing, start of injection, end of injection in case of multiple injections per stroke, valve timing, engine temperature, port flaps* and *fuel pressure.*

In order to maintain a constant engine operating point, the air mass flow and thereby the power output are adjusted while the *ignition timing* is altered. As the spark event has not only an impact on the progression of the combustion but also a dependency on the engine speed, MFB50 is used as an evaluation parameter. Figure 10 gives an example of an ignition timing or MFB50 sweep, respectively. The highest brake thermal efficiency (BTE) of 34.5 % can be found at an MFB50 angle of 6 °CA. For the operating point 5000rpm/23 bar BMEP the optima of PN and BTE share the same center of combustion. The mean PMAX increases with spark advance to a maximum of 127 bar. Combustion variances lead to a maximum firing pressure of 140 bar, which represents the design limit for this engine setup. Thus, any further advance of the ignition angle is not possible. With the use of C65F35 as fuel, the combustion process is restricted by the peak firing pressure rather than knocking.

Besides the high octane number, the physical properties of the oxygenate fuel help to reduce the knock-sensitivity further. The lower energy content requires an increased amount of fuel to be injected per stroke while the low boiling temperature ensures a high degree of vaporization. Table 1 shows the comparable enthalpy of vaporization for both fuels, thus a significant reduction of charge temperature under the given physical properties can be expected. In addition, C65F35 has a longer ignition delay than G100 [16]. This enables an efficient MFB50 angle even at low engine speeds, yielding high BTE values and low PN emissions throughout the whole full load curve. Another positive aspect of the advanced ignition timing is the reduction of exhaust gas temperature, as seen in

FIGURE 10 Ignition timing sweep C65F35 @ 5000 rpm and 23 bar BMEP (© 2020 Tenneco Inc.)

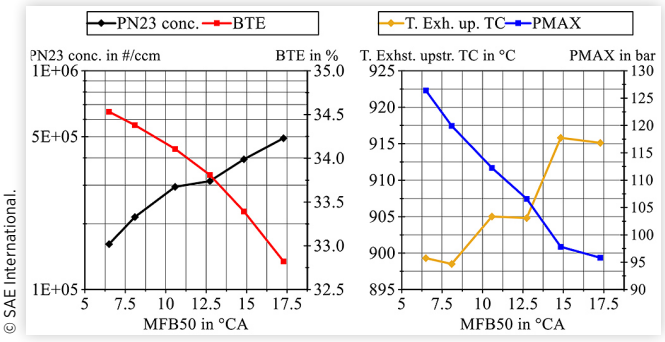

Figure 10. Fuel enrichment for protection is not required anymore.

An example of performed *start of injection* sweeps is shown in Figure 11. Power output and MFB50 angle are kept constant for this investigation.

An early start of injection leads to reduced PN emissions and increased BTE. However, starting the injection before bottom dead center (BDC) produces contrary results. This behavior is observed over the entire engine map. With a delayed SOI the ignition timing must be advanced in order to ensure an MFB50 angle of 6 °CA. Looking at the constant MFB10 angle it becomes clear that the ignition delay increases with the injection angle. It is hypothesized that the longer injection duration combined with the increased fuel mass flow harm the charge motion when the injection takes place late in the intake event. As a result, the combustion process slows down.

For some operating points, an *end of injection* (EOI) sweep revealed that the PN emissions change inversely to the BTE when the injection angle is altered. Figure 12 gives an example of a sweep with two injection events per stroke.

The split of injected fuel mass is set according to the shortest possible injection time for the second event. Approximately 10 % of the total fuel mass is injected with the second injection. A good correlation to the results from the SCE is found where late injection timing leads to lower PN but also a reduction in BTE and an increase in CO emissions. At these operating points, a compromise between the justifiable fuel consumption increase and PN reduction is applied.

Valve timing sweeps are carried out for the intake as well as the exhaust camshaft. While none of them has a major impact on PN, both affect the engine efficiency positively. The lower stoichiometric AFR of C65F35 requires more throttling in comparison to G100 for the same torque output. By closing the intake valve earlier, the compression stroke is shortened while the expansion ratio increases. The result is a reduced volumetric efficiency which can be overcome by raising the intake manifold pressure, thus de-throttling. The applied Miller valve timing typically lowers the tendencies to knock at higher loads but requires raised boost pressures to compensate the gas exchange losses. As C65F35 offers stable combustion, the advance of the intake camshaft timing is not needed for higher loads, thus increasing BTE. Further de-throttling can be achieved by an increased valve overlap when the internal exhaust gas recirculation is active. However, it is found that C65F35 is prone to combustion instability when the charge is diluted with recirculated exhaust gases.

An *engine temperature* sweep reveals the influence of the combustion chamber temperature on PN and knock tendency. The thermal management of the engine is controlled by a rotary control valve which adjusts the coolant flow to the cylinder head and engine block separately according to the temperature setpoint. As seen in Figure 13, a temperature increase leads to reduced PN. In parallel, a reduction in BTE is observed as the charge air density is lowered owing to higher component temperatures. The low boiling temperature of C65F35 and the elevated engine temperature ease the vaporization of the fuel. The fuel's resistance to knock is underlined on the right-hand side of Figure 8. It is possible to maintain an efficient MFB50 position over the entire temperature sweep.

FIGURE 11 SOI sweep C65F35 @ 1750 rpm and 20 bar BMEP (© 2020 Tenneco Inc.)

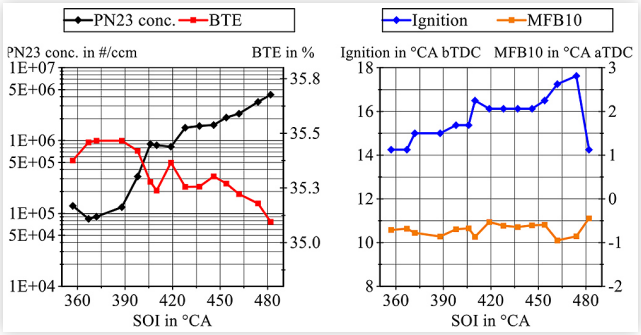

FIGURE 12 EOI sweep C65F35 @ 1750 rpm and 20 bar BMEP (© 2020 Tenneco Inc.)

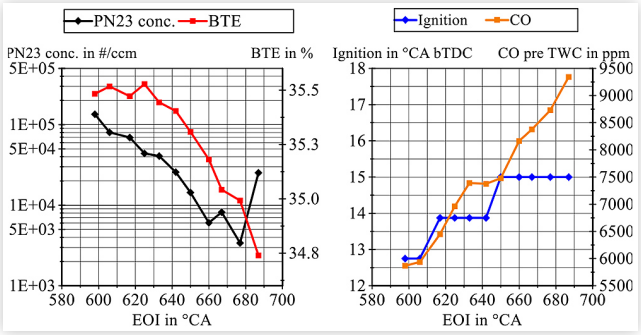

FIGURE 13 Engine temperature sweep C65F35 @ 5000 1/min and 23 bar BMEP (engine temperature sensor) (© 2020 Tenneco Inc.)

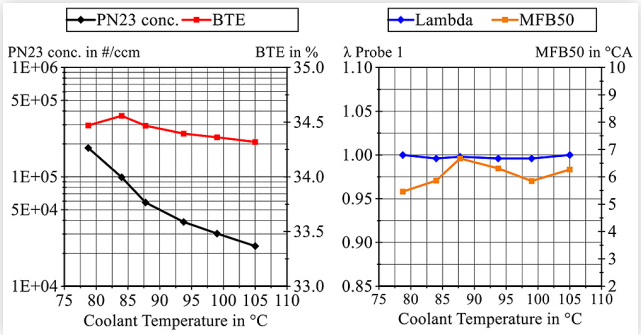

This leads to an efficient combustion process without the need for fuel enrichment as a protecting measure.

Passing through the testing program it becomes clear that the combustion of C65F35 is very sensitive to charge motion. This manifests itself during the injection sweeps as the number and timing of injection events influence the combustion process. Another way to generate charge motion is to employ port flaps. A variation over the whole engine map reveals that the activation of the flaps over a wider area, compared to the G100 application, reduce PN substantially.

The *port flap* activation is shown in Figure 14. This is related to the increased need for charge movement, homogenization and burning rate to compensate for the longer injection

FIGURE 14 Port flap control at engine operation with C65F35 and G100 (© 2020 Tenneco Inc.)

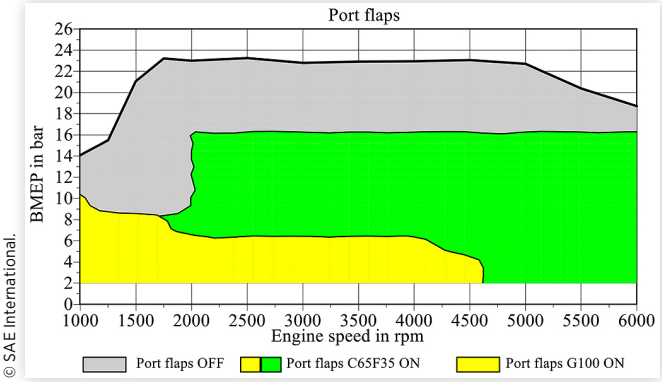

time that potentially harms these processes. At higher loads, the airflow generates sufficient charge motion so that the port flaps can be deactivated to increase the volumetric efficiency and BTE.

In order to reduce the injection duration and its negative impact on the mixture formation, a *fuel pressure* sweep is carried out. Adjustments in the direction of lower fuel pressure have, as expected, only adverse effects on PN. An adjustment in the direction of higher fuel pressure reduces the injection time only slightly. As a consequence, PN does not improve and the fuel pressure is set according the G100 set points. However, Friction Mean Effective Pressure (FMEP) increases with the higher power demand of the HPP.

Basic Research Conclusion. The described test program classifies the use of C65F35 in a state-of-the-art gasoline engine. The SCE results are confirmed with this investigation and are concluded as follows:

- The oxygenate fuel offers significant knock resistance compared to G100. During the investigation no pre-ignition or knock event could be provoked, thus enabling PN-optimized engine operation.
- C65F35 emits clearly lower PN than G100. The combination of the sweeps confirms the SCE results.
- Injection strategy becomes critical as the elevated amount of fuel may lead to interference with the charge motion.

3. Basic Research Conclusion. In order to investigate the potential of C65F35 in drive cycles, the parametrization of the entire engine map is necessary. For this, the supporting points of the map are set in 250 rpm and 2 bar BMEP steps. The engine temperature is constantly set to 105 °C while the MFB50 position is altered with regards to maximum BTE. It is necessary to adjust the engine's power output to the same accelerator pedal position for G100 and C65F35 as it represents the reference input for the drive cycle simulation. Based on the lower stoichiometric AFR of the synthetic fuel, the air mass flow has to be reduced at all operating points. The ECU's lambda controller regulates the fuel mass according to the AFR setpoint. The injection timing and pattern are adjusted to result in the lowest PN but acceptable BTE. Finally, the valve timing is altered for the best efficiency. According to this procedure, the ECU is parametrized for all operating points.

4. Dynamic response. After optimizing the static engine map, the dynamic behavior of the data set is evaluated. To investigate the torque demand response, the engine speed is held constant while the pedal position increases from 0 % to 100 % with a defined slope of 2 %/s. The resulting torque ramp follows the pedal position at a constantly rising rate while strategies for injection pattern, port flap activation, and valve timing change according to the static engine mapping. Non-uniformities require adjustments of the relevant parameters, mainly the air mass flow. An example of the performed dynamic response analysis is shown in Figure 15.

Static Operation Results

Figure 16 shows the relative changes in BTE for G100 over the entire engine map. The green and red areas represent an efficiency increase or loss. An increase in BTE is only achieved for engine loads higher than 70 % of the engine-speed-correlated full load. The highest relative increase of 16 % can be found at the low-end torque (LET) operating point. The efficiency improvements are

FIGURE 15 Pedal ramp and torque response at 1750 rpm (© 2020 Tenneco Inc.)

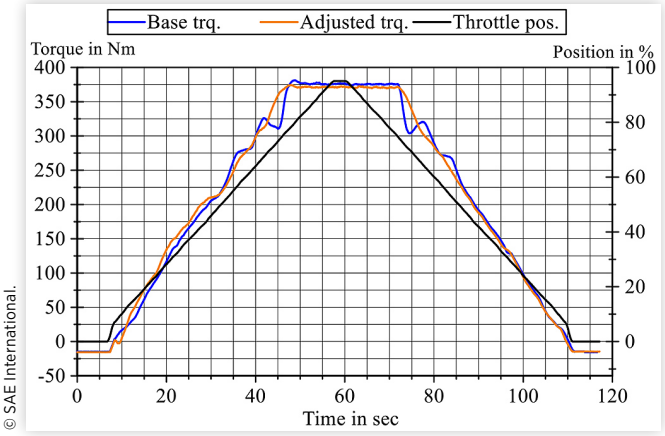

FIGURE 16 Brake thermal efficiency comparison relative C65F35 to G100 (© 2020 Tenneco Inc.)

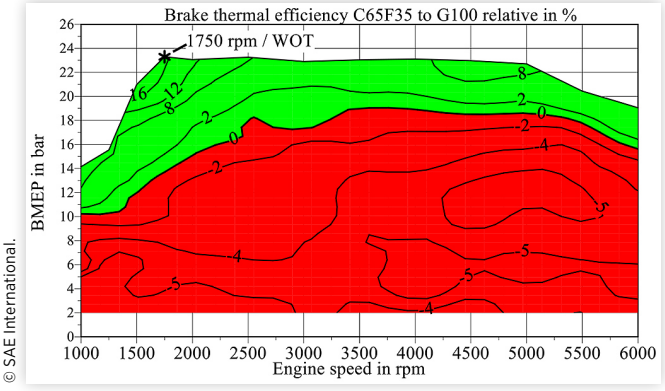

mainly based on the advanced ignition timing due to the knock resistance of C65F35.

To illustrate the thermodynamic boundary conditions, the operating point with the highest efficiency gain (1750 rpm/23 bar BMEP WOT) is shown in Figure 17. The left-hand side shows the cylinder pressure curves, while on the right-hand side the pressure-volume diagrams for G100 (red) and C65F35 (blue) are plotted. As described in paragraph *2. Variation of parameters at relevant operating points,* the ignition angle respective MFB50 was significantly advanced, thus the maximum mean PMAX is almost doubled in comparison to G100. The increased frictional losses at higher cylinder pressures are overcompensated by the more efficient combustion process. The PV-diagram reveals that the pressure during the compression stroke is lower when using C65F35. This is a result of the reduced air demand and the increased amount of fuel, which accordingly decrease the charge pressure based on a higher degree of vaporization. With the advanced MFB50 position, energy conversion becomes more efficient and less heat is transferred towards the end of the expansion stroke. As a result, the cylinder pressure and exhaust gas temperature are reduced. Figure 18 shows the relative reduction in PN emissions with C65F35 compared to the initial status with G100. A relative reduction in PN emissions of 95-99 % (green), 60-95 % (yellow) and 0-60 % (orange) is plotted over the engine map. As can be seen, significantly reduced PN emissions can be measured over large areas of the engine map. This confirms the previous results from the SCE, according to which a remarkable reduction of PN emissions can be expected when the engine is operated with oxygenates. At low speeds and medium loads, as well as for high speeds and low loads, a PN reduction of 60-95 % has been achieved.

With increased load, the PN reduction with C65F35 is more pronounced, so the PN emissions are reduced by up to 99 % along the full-load curve. However, the PN reduction with C65F35 is less pronounced at low loads and low speeds (shown in orange). This speed-load range is relevant for the certification cycle (WLTC), so the base engine's PN emission is optimized. This is confirmed in the initial measurements with G100 which are used as a reference for C65F35 operation.

The raw gaseous emissions of CO and NO_X, measured with the AVL FTIR upstream from the TWC, are shown in Figure 19. Across large parts of the engine map, less CO is emitted. At full load, the CO emissions are reduced by up to 84 %, as the engine is operated with a stoichiometric AFR. The NO_X emissions are reduced by an average of 40 % over the entire engine map. However, up to 89 % more NO_X emissions are emitted in the area of the nominal power. This relationship arises as the AFR enrichment during G100 operation leads to a CO increase and a NO_X decrease for this operating point. With C65F35 at stoichiometric operation, there are accordingly less CO but increased NO_X emissions.

As generally known, CO_2 is produced by combustion of the carbon contained in the fuel with atmospheric O_2. The CO_2 emissions, which are 27 % higher with C65F35, can be attributed to the C1 structure of the fuel. The more than 50 % reduced carbon content of the oxygenate is compensated by an additional volumetric consumption. Based on the values in Table 1, the volume and density corrected carbon mass bound in C65F35 is increased by 27%.

Consistent with previous investigations [21], the exhaust gas components MeOH, CH2O and methane are traceable in a significantly higher concentration than expected owing to the C1 structure of C65F35. Averaged over the engine map and compared to G100, MeOH emissions are increased by 90 %, CH2O emissions by 30 %, and methane emissions by 80

FIGURE 17 Cylinder pressure curve and pressure-volume diagram. Operating point: 1750 rpm/23 bar BMEP WOT (© 2020 Tenneco Inc.)

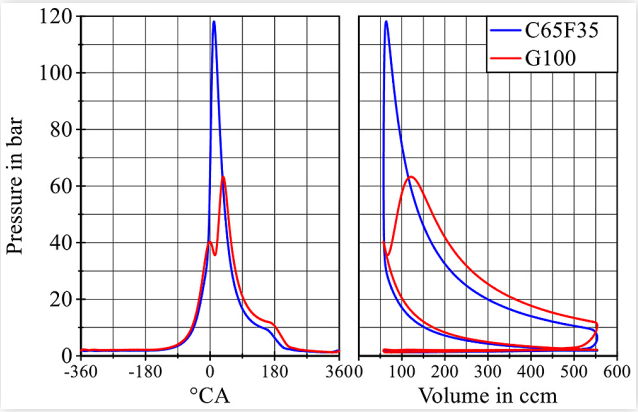

FIGURE 18 PN reduction comparison relative C65F35 to G100 (© 2020 Tenneco Inc.)

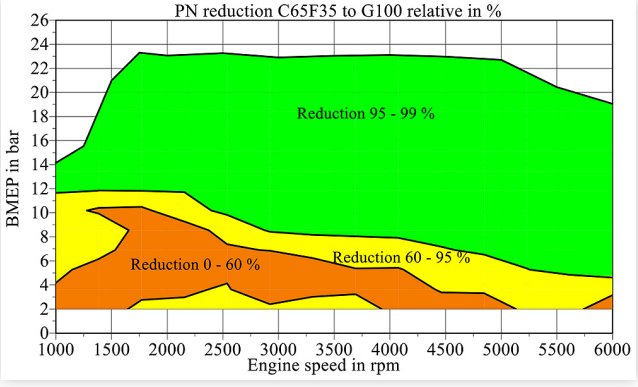

FIGURE 19 NO_X and CO raw emission trends with C65F35 (© 2020 Tenneco Inc.)

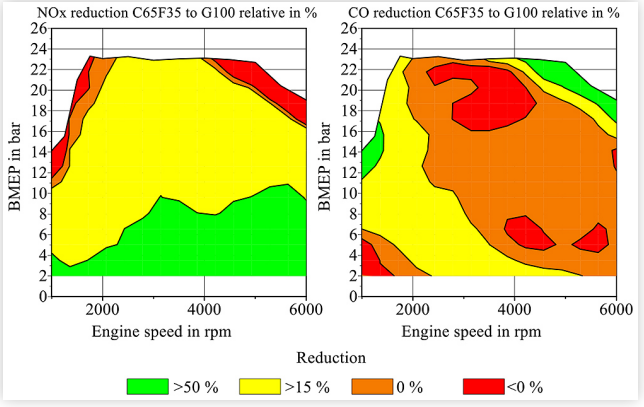

%. However, all three components are not detectable after the TWC, which confirms the results from [21]. The fuel components DMC and MeFo measured by the FTIR's special evaluation method are increased at low speeds and loads. Incomplete combustion due to insufficient mixture preparation at these operating points is assumed. The results of the raw emission measurements show, that a TWC is essential for the reduction of regulated pollutant components. Despite the stated advantage of low NO_X generation by the use of oxygenated fuel, the tailpipe nitrogen oxide emissions for both fuels are comparable (Figure 20, reduction 0 %). This confirms a high conversion rate for the catalytic converter. The averaged CO emissions after the TWC show an average reduction of 40 % in favor of C65F35. The peak CO reduction, of up to 98 %, can be found in the operating areas where the G100 operation requires enrichment of the AFR. However, in parallel to the raw emissions, an increase in CO, compared to gasoline, is found in the lower speed area until 2500 rpm and up to 12 bar BMEP.

Dynamic Operation The result that C65F35 emits significantly lower particle emissions in stationary operation does not necessarily imply a carry-over into dynamic operation. For this reason, the particle and gaseous emission behavior during homologation relevant driving cycles (WLTC and RDE) is investigated. For this, the engine is brought to its nominal operating temperature and the stop-start system is disabled. For both drive cycles a category J vehicle is simulated, which results in higher load collectives [33]. The cycle evaluation of C65F35 is based on the relative change compared to G100 and the Euro 6d limit. Gaseous emissions are represented in g/km, while particles are totaled in #/km. Fuel consumption is given in two units, volumetric (l/100km) and gravimetric (kg/100km).

The results of the higher-loaded driving cycle confirm the knowledge gained from stationary operation. For C65F35, gains in efficiency are only observed in operating points with higher loads. Table 5 compares the BTE of G100 and C65F35. For both cycles, the overall efficiency is at a comparable level. The losses in low-load operation are compensated by the gains at higher loads. The differences in fuel consumption between both fuels are based on the physical properties of the oxygenate. Considering the lower heat value and density of C65F35, the fuel consumption should increase by a factor of 2 at a constant efficiency. However, for both cycles, the consumption is only increased by 86 %. This results from the dynamic behavior of the engine. The lower exhaust gas enthalpy with C65F35 has a negative effect on the turbocharger, so the boost pressure response is delayed. This results in a lower dynamic torque output during acceleration and reduced fuel consumption compared to G100. Regarding the raw PN concentration, a reduction of 90 % in the RDE and 78 % in the WLTC cycle is achieved. The total PN emissions correspond to 13 % and 3 % of the emissions limit respectively. It is assumed that the series application of the engine is focused on reducing the PN emissions at relevant operating points of the certification cycle so that the improvement in the WLTC cycle is less distinctive.

The reduction of up to 99 %, known from the static engine operation, is not achievable in either of the cycles. The assumption is, that dynamic operation influences the formation and propagation of the charge motion and therewith the combustion. Furthermore, long idle phases and motored engine operation may lead to oil transfer into the combustion chamber, which results in higher PN emissions [34]. An analysis of the particle size distribution for the relevant operating points can provide information on the formation process. However, with the lowest possible dilution rate (1:100) of the APC+, the particle content of the sample entering the EEPS is very low during C65F35 operation. With the low concentration, the sizer requires a long averaging time which harms the dynamic response of the instrument. Further investigations are required to understand particle formation during dynamic operation.

Cycle type averaged carbon dioxide emissions per km increase by 26 % which, in contrast to the PN concentration, reflects the static measurement results.

The emissions of the regulated pollutant component THC show only a minor difference for both fuels. The absolute cycle emissions of C65F35 correspond to 17 % (RDE) and 8 %

TABLE 5 Comparison results RDE- WLTC-Cycles. Positive (+) increase, negative (–) decrease, PN pre-TWC, gaseous emissions post-TWC (© 2020 Tenneco Inc.)

		C65F35 to G100 relative in %			
	Unit	RDE	WLTC	Percent of Euro 6d emission limit	
Volume-based fuel consumption	l/100 km	+86	+86		
Mass-based fuel consumption	kg/100 km	+58	+58		
Brake thermal efficiency	-	+1	–0.4	RDE	WLTC
PN	#/km	–90	–78	13	3
NO_X	g/km	+214	–80	155	6
CO	g/km	–84	–50	16	21
THC	g/km	+3	–2	17	8
CO_2	g/km	+26	+24	-	-
CH_4	g/km	–46	–50	-	-

FIGURE 20 NO_X and CO post-TWC emission trends with C65F35 (© 2020 Tenneco Inc.)

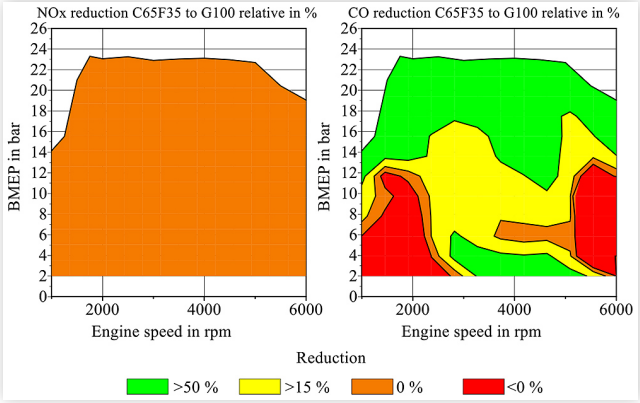

FIGURE 21 RDE cycle section with engine speed, torque, pedal position and NO_X emissions for G100 and C65F35 (© 2020 Tenneco Inc.)

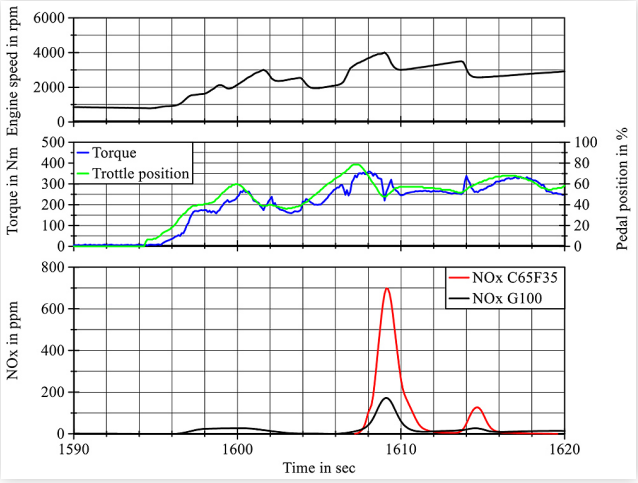

(WLTC) of the Euro 6d limit. The CO emissions of C65F35 are reduced by 50 % in comparison to G100 for the WLTC cycle. The absolute CO emissions in this low load cycle are, compared to the RDE test, increased by five percentage points based on the limit. The dominating operating points are located in the bottom left area of the engine map, where increased CO tailpipe emissions are found. The occasional full load operation in the RDE cycle causes an enriched AFR when using gasoline. As no enrichment is required by C65F35, CO emissions compared to G100 are reduced by 84 %. The total CO emissions for the RDE cycle equal 16 % of the limit.

The RDE nitrogen oxide emissions, when using C65F35, are significantly higher than with G100. A closer look at the course of the NO_X emissions during the cycle reveals, that acceleration phases followed by steep torque gradients generate peaks of NO_X. Figure 21 (time stamp 1609 sec) illustrates such a response for both fuels. It is assumed that sudden air mass flow changes, which are initiated by either engine speed or torque demand gradients, lead to incomplete mixture formation. Operation parameters such as port flap activation, valve lift, camshaft phasing and injection layout are set according to the actual air consumption and influence the combustion process significantly. This is noticeable for both fuels. However, the effect on emissions is more distinctive for C65F35. The total RDE NO_X emissions exceed the Euro 6d limit by 55 %. For the lower load operation during the WLTC cycle, C65F35 emits 81 % less nitrogen oxide than G100, which is 6 % of the absolute Euro 6d limit.

Summary and Conclusions

The benefit of C65F35 in terms of efficiency at high load, throughout the high knock resistance, is confirmed in the SCE, as well as in the 4CE. The gain in the BTE in the 4CE of 16 % at 1750 rpm and an engine load in IMEP of 23 bar confirmed the simulated growth of 14 % in efficiency by Wagner et al. [16]. The SCE with a CCR shows a maximum increase in η_i of 3 % compared to G100 and only at high loads above 13 bar IMEP. This fits very well to the results of the 4CE, where C65F35 only shows BTE benefits above 14 bar BMEP at a constant engine speed of 2000 rpm. The disadvantages in mid to low-load operation result from a long and incomplete combustion, initialized by a detrimental mixture formation. This is influenced by higher in-cylinder cooling during injection, triggered by the doubled total enthalpy of vaporization of C65F35. Combined with 10 % less needed air mass flow, which reduces the TKE in the cylinder, the vaporization of C65F35 is decelerated. The 4CE uses the option to extend the area with enabled tumble flaps in the engine map, to minimize the drawback to −5 % in BTE relatively. With the SCE an option was introduced to improve the mixture formation with a late injection in the compression stroke. It was shown that the η_i at the mid-load point of 7 bar IMEP at 2000 rpm is improved by 4.3 % compared to intake stroke injection with C65F35. Thereby the combustion stability increases and no significant drawback in exhaust emissions is observed. In general, the already known benefits in NO_X and PN emissions from previous studies are confirmed on both test beds. However, dynamic engine operation reveals an increase in NO_X emissions.

The main findings in the SCE concentrate on rich mixtures and the potential of the high knock resistance of C65F35. With the variation of λ to rich mixtures, no sensitivity for PN emissions was determined, whereas the combustion stability increased. The same phenomenon was detected with the late compression stroke injection in a stoichiometric combustion mode. Even with a short time for mixture formation and potential local rich areas, the PN emissions do not increase. These hints lead to the expectation, that C65F35 is very suitable for stratified operation modes, as well as for fueled pre-chamber ignition systems. Furthermore, the use of the HCR piston throughout a load variation resulted in a realizable CR of $\varepsilon = 14.91{:}1$. An increase in η_i for each point using C65F35, relative to G100, is confirmed. The maximum increase of 11 %, compared to G100, is reached at 17 bar IMEP. This increase also meets the simulation result of an expected increase in efficiency of 20 % with an optimized engine configuration by Wagner et al. [16]. The deviation of 9 % seems to be realistic, because of the different CR of $\Delta\varepsilon = 3$ and the significantly lower maximum load. The next steps for the SCE will be to optimize the engine configuration further with a focus on charge movement and higher CR, accompanied by improved component robustness.

A basic engine operation with the 4CE is possible with minor adaptions of the fuel amount injected per stroke, to compensate for the LHV of C65F35. The limitation of the highest possible BTE, especially at low-end torque, changes from knock events to maximum permissible firing pressure. The high RON allows the increase of coolant temperature to 105 °C, even at high load operation points, which results in significantly lower PN emissions. The BTE increases for all high load points in the engine map with adaptions in the ECU, mainly due to an earlier MFB50. To evaluate the potential for emission reduction, the engine was operated in a WLTC and RDE cycle. Both were performed with a simulation of a category J vehicle. As expected from the stationary operation results, the efficiency is reduced compared to the G100

operation. The losses are less distinctive for the higher load RDE with −13 % against the WLTC, where a drop of 15 % is observed. C65F35 fuel consumption increased for both cycles compared to gasoline. However, the more efficient operation at full load results in fewer losses in the RDE cycle. PN emissions are reduced by more than 90 % with the synthetic fuel. In comparison, the dynamic operation yields less of a reduction than predicted by the static operation results owing to the dynamic operation. With such a low particulate concentration, the sample cannot be evaluated by the EEPS with a sufficient time resolution. Further investigations with regards to the formation process of these PN emissions are necessary. Average tailpipe CO_2 increases by 26 %, while VOC shows only minor differences for both fuels. As no enriched AFR operation needs to be applied with C65F35, CO emissions are reduced for higher engine loads. However, incomplete combustion during low speeds and loads impairs the total improvement, especially for the WLTC cycle. In general, NO_X emissions are reduced with C65F35. In the case of the WLTC cycle, 81 % less nitrogen oxide or 6 % of the limit is emitted. The more dynamic speed and load changes during the RDE cycle lead to a significant increase in NO_X, which exceeds the nominal threshold by a factor of 1.55. The planned investigations concentrate on a holistic BTE increase through an increased CR while the design limit of the maximum firing pressure is extended. Additionally, lean combustion strategies are being considered to increase efficiency further and reduce NO_X and PN. With the help of modified ignition systems, the lean-burn capability is extended. The combination of both strategies paired with the knock resistance of C65F35 will lead to an efficient low-emission combustion process while maintaining the demanded peak specific power and torque output. The use of PRiME 3D will help to investigate the PN formation processes and result in an optimized piston assembly, which will be evaluated with regards to its potential for further PN reduction [35].

References

1. EUROPEAN COMMISSION, "COMMUNICATION FROM THE COMMISSION: A Clean Planet for all - A European Strategic Long-Term Vision for a Prosperous, Modern, Competitive and Climate Neutral Economy: COM(2018) 773 Final," 2018.
2. Härtl, M., Seidenspinner, P., Jacob, E., and Wachtmeister, G., "Oxygenate Screening on a Heavy-Duty Diesel Engine and Emission Characteristics of Highly Oxygenated Oxymethylene Ether Fuel OME1," *Fuel* 153:328-335, 2015, doi:10.1016/j.fuel.2015.03.012.
3. Härtl, M., Stadler, A., Backes, F., Wachtmeister, G. et al., "Potentially CO2-Neutral Fuels for Clean SI Engines," *MTZ Worldw* 78(7-8):76-83, 2017, doi:10.1007/s38313-017-0058-1.
4. Maier, T., Härtl, M., Jacob, E., and Wachtmeister, G., "Dimethyl Carbonate (DMC) and Methyl Formate (MeFo): Emission Characteristics of Novel, Clean and Potentially CO2 -Neutral Fuels Including PMP and Sub-23 nm Nanoparticle-Emission Characteristics on a Spark-Ignition DI-Engine," *Fuel* 256:115925, 2019, doi:10.1016/j.fuel.2019.115925.
5. Takahashi, F. and Glassman, I., "Sooting Correlations for Premixed Flames," *Combustion Science and Technology* 37(1-2):1-19, 2007, doi:10.1080/00102208408923743.
6. Tundo, P. and Selva, M., "The Chemistry of Dimethyl Carbonate," *Accounts of Chemical Research* 35(9):706-716, 2002, doi:10.1021/ar010076f.
7. Pacheco, M.A. and Marshall, C.L., "Review of Dimethyl Carbonate (DMC) Manufacture and Its Characteristics as a Fuel Additive," *Energy Fuels* 11(1):2-29, 1997, doi:10.1021/ef9600974.
8. Yang, J., Jiang, Y., Karavalakis, G., Johnson, K.C. et al., "Impacts of Dimethyl Carbonate Blends on Gaseous and Particulate Emissions from a Heavy-Duty Diesel Engine," *Fuel* 184:681-688, 2016, doi:10.1016/j.fuel.2016.07.053.
9. Kocis, D., Song, K., Lee, H., and Litzinger, T., "Effects of Dimethoxymethane and Dimethylcarbonate on Soot Production in an Optically-accessible DI Diesel Engine," in *SAE Technical Paper Series, International Fuels & Lubricants Meeting & Exposition*, Oct. 16, 2000, Warrendale, PA, 2000, https://doi.org/10.4271/2000-01-2795.
10. Wang, J., Wu, F., Xiao, J., and Shuai, S., "Oxygenated Blend Design and Its Effects on Reducing Diesel Particulate Emissions," *Fuel* 88(10):2037-2045, 2009, doi:10.1016/j.fuel.2009.02.045.
11. Mei, D., Wu, H., Ren, H., Hielscher, K. et al., "Combustion Cycle-by-Cycle Variations in a Common Rail Direct Injection Engine Fueled with Dimethyl Carbonate-Diesel Blend," *J. Energy Eng.* 142(1):4014059, 2016, doi:10.1061/(ASCE)EY.1943-7897.0000259.
12. Lee, J.S., Kim, J.C., and Kim, Y.G., "Methyl Formate as a New Building Block in C1 Chemistry," *Applied Catalysis* 57(1):1-30, 1990, doi:10.1016/S0166-9834(00)80720-4.
13. Dawson, B. and Spannagle, M., *The Complete Guide to Climate Change* (London: Routledge, 2009). ISBN:9781134021246.
14. Klezl, Peter, "Fuel for Internal Combustion Engines and Use of Methyl Formate as Fuel Additive," US5232464A, February 21, 1992.
15. Dooley, S., Burke, M.P., Chaos, M., Stein, Y. et al., "Methyl Formate Oxidation: Speciation Data, Laminar Burning Velocities, Ignition Delay Times, and a Validated Chemical Kinetic Model," *Int. J. Chem. Kinet.* 42(9):527-549, 2010, doi:10.1002/kin.20512.
16. Wagner, C., Grill, M., Keskin, M.-T., Bargende, M. et al., "Potential Analysis and Virtual Development of SI Engines Operated with Synthetic Fuel DMC+," in *SAE Technical Paper Series, WCX SAE World Congress Experience*, Apr. 21, 2020, Warrendale, PA, 2020.
17. Gumz, W., "Eine neue Heizwertformel für feste Brennstoffe," *Feuerungstechnik* 26(10):322-323, 1938.
18. Stadler, A., Wessoly, M., Blochum, S., Härtl, M. et al., "Gasoline Fueled Pre-Chamber Ignition System for a Light-Duty Passenger Car Engine with Extended Lean Limit," *SAE Int. J. Engines* 12(3):323-339, 2019, https://doi.org/10.4271/03-12-03-0022.
19. Peer, J., Backes, F., Sauerland, H., Härtl, M. et al., "Development of a High Turbulence, Low Particle Number, High Injection Pressure Gasoline Direct Injection Combustion System," *SAE Int. J. Engines* 9(4):2301-2311, 2016, https://doi.org/10.4271/2016-01-9046.

20. Baumgartner, L.S., Karmann, S., Backes, F., Stadler, A. et al., "Experimental Investigation of Orifice Design Effects on a Methane Fuelled Prechamber Gas Engine for Automotive Applications," in *SAE Technical Paper Series, 13th International Conference on Engines & Vehicles*, Sep. 10, 2017, Warrendale, PA, 2017.
21. Härtl, M., Stadler, A., Blochum, S., Pélerin, D. et al., "DMC+ as Particulate Free and Potentially Sustainable Fuel for DI SI Engines," in Geringer, B. and Lenz, H.P. (eds.), in *39. Internationales Wiener Motorensymposium* April 26-27, 2018, Fortschritt-Berichte VDI. Reihe 12, Verkehrstechnik, Fahrzeugtechnik, ISBN 978-3-18-380712-3, 202-229, 2018.
22. Stadler, A., Sauerland, H., Härtl, M., and Wachtmeister, G., "The Potential of Gasoline Fueled Pre Chamber Ignition Combined with Elevated Compression Ratio," in *SAE Technical Paper Series, WCX SAE World Congress Experience*, Apr. 21, 2020, Warrendale, PA, 2020.
23. The Council of the European Union, "COUNCIL DIRECTIVE 1999/13/EC of 11 March 1999 on the Limitation of Emissions of Volatile Organic Compounds Due to the Use of Organic Solvents in Certain Activities and Installations," 1999.
24. Gelner, A.D., Pastoetter, C., Beck, H.A., Härtl, M. et al., "Fuel Dosing on a Diesel Oxidation Catalyst for After-Treatment System Heating on a Heavy-Duty Engine Powered by Polyoxymethylene Dimethyl Ethers," in *SAE Technical Paper Series, SAE Powertrains, Fuels & Lubricants Meeting*, Sep. 22, 2020, Warrendale, PA, 2020.
25. Wallner, T., "Correlation Between Speciated Hydrocarbon Emissions and Flame Ionization Detector Response for Gasoline/Alcohol Blends," in *ASME 2010 Internal Combustion Engine Division Fall Technical Conference*, San Antonio, Texas, USA, Sep. 12, 2010-Sep. 15, 2010, ASMEDC, ISBN 978-0-7918-4944-6, 119-128, 2010.
26. Jorgensen, A.D., Picel, K.C., and Stamoudis, V.C., "Prediction of Gas Chromatography Flame Ionization Detector Response Factors from Molecular Structures," *Anal. Chem.* 62(7):683-689, 2012, doi:10.1021/ac00206a007.
27. Wei, Q., Oestergaard, K., Porter, S., Ichiro, A. et al., "Real-Time Measuring System for Engine Exhaust Solid Particle Number Emission - Design and Performance," in *SAE Technical Paper Series, SAE 2006 World Congress & Exhibition*, Apr. 3, 2006, Warrendale, PA, 2006.
28. Birmili, W., Heinke, K., Pitz, M., Matschullat, J. et al., "Particle Number Size Distributions in Urban Air Before and After Volatilisation," *Atmos. Chem. Phys.* 10(10):4643-4660, 2010, doi:10.5194/acp-10-4643-2010.
29. Tikkanen, J., Janka, K., Rostedt, A., Röbel, M. et al., "Dilution Artifacts. A Significant Source of Error from Absolute Concentration and Possibly Difficult to Reproduce. PMP vs. Raw Exhaust.," in *ETH-Conference on Combustion Generated Nanoparticles, 17th ETH-Conference on Combustion Generated Nanoparticles*, Zürich, Switzerland, June 23-26, 2013.
30. AVL List GmbH, "AVL Condensation Particle Counter: Product Guide," 2016.
31. TSI GmbH, "*Engine Exhaust Particle Sizer (EEPS) Spectrometer Model 3090/3090AK: Operation and Service Manual, Revision K*," 2017.
32. AVL Emission Test Systems GmbH, "AVL SESAM i60 SII: Gerätebeschreibung," 2017.
33. COMMISSION OF THE EUROPEAN COMMUNITIES, "REGULATION (EC) No 139/2004 MERGER PROCEDURE: Article 6(1)(b) NON-OPPOSITION Date: 24/07/2009: (EC) No 139/2004," 2009.
34. Gunkel, M., Frensch, M., Robota, A., and Gelhausen, R., "Innermotorische Emissionsreduzierung Zusammenhang zwischen Partikelemissionen und Ölverbrauch," *MTZ Motortech Z* 79(7-8):46-51, 2018, doi:10.1007/s35146-018-0044-4.
35. Jückstock, R., "Perspektiven zur Reibungsreduzierung im Grundmotor," *MTZ Motortech Z* 75(15):114-119, 2014, doi:10.1007/s35146-014-0421-6.

Contact Information

Sebastian Blochum
Chair of Internal Combustion Engines
Technical University of Munich
Schragenhofstraße 31, 80992 Munich, Germany
blochum@lvk.mw.tum.de

Bartosch Gadomski
Senior Test Engineer,
Federal Mogul Burscheid GmbH, Tenneco group
BGM-Schmidt-Str. 17, 51399 Burscheid, Germany
Bartosch.Gadomski@tenneco.com

Acknowledgment

The research project is financed by BMBF (Federal Ministry of Education and Research), owing to a decision of the German Bundestag. The authors would like to thank the BMBF for providing financing.

Supported by:

Federal Ministry of Education and Research

On the basis of a decision by the German Bundestag

Abbreviations

4CE - 4 Cylinder Engine
aTDC - after Top Dead Center
AFR - Air Fuel Ratio
AHRR - Apparent Heat Release Rate
BDC - Bottom Dead Center
BTE - Brake Thermal Efficiency
bTDC - before Top Dead Center
CCR - Conventional Compression Ratio

CR - Compression Ratio
C65F35 - Fuel with 65 vol.-% DMC / 35 vol.-% MeFo
CH_2O - Formaldehyde
CH_4 - Methane
CO - Carbon Monoxide
CO_2 - Carbon Dioxide
COV - Coefficient of Variation
CPC - Condensation Particle Counter
DI - Direct Injection
DISI - Direct Injection Spark Ignited
DMC - Dimethyl Carbonate
DOHC - Double Overhead Camshaft
DVPE - Dry Vapor Pressure Equivalent
ECU - Electronic Control Unit
EEPS - Engine Exhaust Particle Sizer
EOI - End Of Injection
FID - Flame Ionization Detector
FMEP - Friction Mean Effective Pressure
FTDC - Fired Top Dead Center
FTIR - Fourier-Transform InfraRed spectroscopy
G100 - Fuel with 100 vol.-% RON95 E5 Gasoline
HCR - High Compression Ratio
HPP - High-Pressure Pump
IBC - Intermediate Bulk Container
IMEP - Indicated Mean Effective Pressure
LET - Low-End Torque
LHV - Lower Heating Value
MeFo - Methyl Formate
MeOH - Methanol
MFB - Mass Fraction Burned
NDIR - NonDispersive InfraRed sensors
NO_X - Oxides of Nitrogen (NO and NO2)
O_2 - Oxygen
PMAX - Maximum firing Pressure
PN - Particle Number
PN10 - Particle Number with cut off at 10 nm
PN23 - Particle Number with cut off at 23 nm
RDE - Real Driving Emissions
RON - Research Octane Number
RPM - Revolutions Per Minute
SCE - Single-Cylinder Engine
SI - Spark Ignited
SOI - Start of Injection
SPCS - Solid Particle Counting System
TCM - Test Cell Manager
TDC - Top Dead Center
THC - Total HydroCarbons
TOM - Test Object Manager
TWC - Three-Way Catalyst
VOC - Volatile Organic Compounds
WLTC - World harmonized Light-Duty Test Procedure
WOT - Wide Open Throttle
°CA - Crank Angle Degree

Appendix

Definition of Volatile Organic Compound According to 1999/13/EC

"Volatile organic compound (VOC) shall mean any organic compound having at 293.15 K a vapor pressure of 0.01 kPa or more, or having a corresponding volatility under the particular conditions of use. For the purpose of this Directive, the fraction of creosote which exceeds this value of vapor pressure at 293.15 K shall be considered as a VOC.[A13]"

ISSN 0148-7191

B.2 Optical Investigations of Oxygenated Alternative Fuels in a Single Cylinder DISI Light-Duty Passenger Car Engine

2021-01-0557 Published 06 Apr 2021

Optical Investigations of an Oxygenated Alternative Fuel in a Single Cylinder DISI Light Vehicle Gasoline Engine

Markus Mühlthaler, Sebastian Blochum, Andreas Stadler, Martin Härtl, and Georg Wachtmeister
Technical University of Munich

Akiyasu MIYAMOTO and Henning Sauerland Hitachi Europe GmbH

Citation: Mühlthaler, M., Blochum, S., Stadler, A., Härtl, M. et al., "Optical Investigations of an Oxygenated Alternative Fuel in a Single Cylinder DISI Light Vehicle Gasoline Engine," SAE Technical Paper 2021-01-0557, 2021, doi:10.4271/2021-01-0557.

Abstract

In this study, a fully optically accessible single-cylinder research engine is the basis for the visualization and generation of extensive knowledge about the in-cylinder processes of mixture formation, ignition and combustion of oxygenated synthetic fuels. Previous measurements in an all-metal engine showed promising results by using a mixture of dimethyl carbonate and methyl formate as a fuel substitute in a DISI-engine. Lower THC and NOx emissions were observed along with a low PN-value, implying low-soot combustion. The flame luminosity transmitted via an optical piston was split in the optical path to simultaneously record the natural flame luminosity with an RGB high-speed camera. The second channel consisted of OH*-chemiluminescence recording, isolated by a bandpass filter via an intensified monochrome high-speed camera. To investigate the combustion process spectrally, spatially and temporally resolved in more detail, selected operating points were recorded again via a high-speed imaging spectrograph.

Regular gasoline fuel acts as a reference and is compared to the oxygenated mixture. Since all oxygenated fuels show a heating value lower than gasoline, the injected mass increases for constant engine load. For 65 vol-% DMC 35 vol-% MeFo, the gasoline equivalent, a product of the lower heating value and the density, results in a factor of two. Accordingly, elevated cooling effects of the mixture are expected. Because of these unfavorable conditions for mixture formation, spots of diffusion flames could be detected when using oxygenated fuels.

A lambda sweep showed that the mixture did not produce significant soot even in slightly lower than stoichiometric conditions. In addition, a very late SOI of around 90 CAD bFTDC showed reduced burning duration and lower diffusion flame intensity.

Keywords

DISI engines, Optical engine, Alternative fuels, E-fuels, Synthetic fuels, Oxygenates, Spectroscopy, Flame luminescence

Introduction

Recently, the worldwide discussion about defossilisation of the transport sector and upcoming stricter emission regulations is getting more and more public attention. In 2019, the European Parliament and the Council of the European Union agreed on a CO_2 reduction target for the new passenger car fleet of 37.5 % by 2030, based on the limit of 95 g CO_2/km in 2021 [1]. As a consequence, a significant move of internal combustion engine research in the direction of alternative e-fuels is expected. For over 100 years since Gottlieb Daimler registered his patent for the first gasoline single cylinder engine in 1885, the main distributed fuel was subject to incremental optimization. Advances in chemical processing capabilities and for example additives like lead, applied to enhance the knock resistance, changed the individual percentage of the contained hydrocarbons, but not the overall base derived from fractional distillation of petroleum.

In the future, oxygenated fuels, manufactured using renewable energies and carbon dioxide from the environment, are a promising example of a closed carbon dioxide cycle. The key in substitution of petrol with synthetic fuels is the fact, that only minor adaptations of the current vehicle technology and the existing infrastructure are necessary, [2].

This work focuses on a mixture of the oxygenates *dimethyl carbonate* (DMC) and *methyl formate* (MeFo), both of which can be classified as so called C1-oxygenates, due to the absence of C-C bonds in the molecular structure [3]. This property is one of the three main potentials of these fuels, since it enables low-soot combustion.

The second potential is the lower heating value (LHV), i.e. an increased fuel mass flow is required to maintain the same energy level as with gasoline. This seems to be a drawback at first. However, the increased in-cylinder cooling effect is advantageous, especially in the high-load area of the engine map. Reduced peak combustion temperatures have a favorable impact on NO_x-emissions. The cooling effect is further supported by an equal or higher enthalpy of vaporization of oxygenates in comparison to gasoline.

Last but not least, the given oxygenates show a higher research octane number compared to regular European gasoline (RON95) [4]. The higher knock resistance and the increased ignition delay allows setting the optimal center of combustion (MFB50) at 8 CAD aFTDC for gasoline engines [5] over a larger area of the engine map, resulting in improved efficiency [5, 6, 7, 8].

Methanol (MeOH) and *ethanol* (EtOH) are further examples of promising oxygenates, but are not investigated in this study.

Härtl et al. state DMC and MeFo as the only C1-oxygenates derived from methanol to offer an ignition temperature higher than 400 °C and octane numbers greater than 100, making them a high knock-resistant alternative to conventional gasoline fuel. Furthermore, the investigated mixture follows the applicable standard for volatility in motor fuels valid in Europe, EN228:2014, relevant in order to achieve desired cold-start performance, good mixture formation and the tank's explosion protection. In comparison to methanol or higher hydrocarbons, DMC and MeFo are the least toxic for health and the environment. Applying the UN's Global Harmonized System, they are classified neither as acute and/or toxic to specific organs, nor extremely hazardous for water. The article lists pathways of production for further reading, [3].

In this study, a blend of DMC and MeFo is compared to regular gasoline fuel (RON95). Thermodynamic and optical measurements are conducted in a single-cylinder research engine. RGB high-speed natural flame luminescence and OH*-chemiluminescence recordings allow assessment of flame propagation and visualization of combustion regimes with high temporal and spatial resolutions. Furthermore, combustion is spectrally resolved by means of high-speed imaging spectroscopy. The latter provides information about intermediate present species and their temporal evolution. The experiments include sweeps of the air-fuel equivalence ratio (λ) and the start of injection (SOI) in order to investigate the influence of these parameters on combustion characteristics.

TABLE 1 Material values of the used fuels. Data based on [3, 19]

Name	Unit	RON95	C65F35
Gasoline RON95	vol. %	100	-
Dimethyl **C**arbonate		-	65
Methyl **F**ormate		-	35
Lower heating value (LHV)	MJ/kg	42.2	15.2
Density @ 15 °C	kg/m³	750.8	1,041
Gasoline equivalent	m³/m³	1.0	2.0
RON/MON	-	96.8/86.3	> 100
Oxygen content	wt. %	1.7	53.3
A/F ratio stoich.	kg/kg	14.28	4.64
Boiling range	° C	37.5-202.5	38-94
CFPP			–30
Flash point		<-35	–9
DVPE @ 37,8 °C	kPa	57.8	57.4
Enthalpy of vaporization	kJ/kg	420	433
Surface tension	mN/m	24	27.7
Kinematic viscosity	m²/s	< 0.5 (40°C)	0.47 (20°C)

State of the Art/ Theoretical Background

Oxygenated Fuels for Gasoline Application

In recent years, a considerable amount of research has been conducted on oxygenated fuels, including ethers as well as esters and alcohols, with a focus on diesel application [9, 10]. Many publications have targeted POMDMEs of different chain lengths that have C1-structure and exhibit soot-free combustion characteristics [11, 12, 13, 14].

In contrast, investigations focusing on oxygenated fuels applicable to the gasoline combustion process mostly focus on alcohols such as MeOH and EtOH. Abdalla et al. review DMC [15] and discuss the applicability for diesel and gasoline applications. Both blends and the pure substance are considered. They found that engine-out emissions of CO and HC improved, while CO_2 emissions were negatively impacted. The results for NOx were controversial. In [16], an 8 vol-% DMC/gasoline blend decreased PM emissions by 60 % and unburned hydrocarbons by 30%. The brake thermal efficiency and combustion process remained similar to that of gasoline.

Härtl et al. identified DMC+, a mixture of DMC with MeFo and ethanol as a practically particulate-free and a potentially sustainable fuel for DI SI engines, [3], which was further studied by [17].

In Table 1, the chemical properties of fuels used in this study are listed. One batch of regular RON95 is used as the gasoline reference throughout this study. Further details on the fuel properties are provided in [18]. Gasoline equivalent is calculated by multiplying the lower heating value with the corresponding density, in relation to gasoline.

Radiative Emission in the Combustion Chamber

Natural Flame Luminescence As an exhaustive review of radiative emission from combustion phenomena lies far beyond the scope of this study, only a short introduction into the most relevant electronically excitable molecules is presented. For more detail the authors kindly refer to [20].

Hydroxyl Radical (OH) The hydroxil radical, OH*, is an important indicator in high temperature flames. Originating from the dominant reaction between oxygen and

hydrogen, it's placed in high temporal and spatial proximity to the high-temperature reaction zone of the flame. The chemical reaction involving O_2 and CH results in the products CO and OH^*, which is still the currently accepted formation path [21]. The subsequent quenching leads to radiative emission with a narrow peak of the band centered around 309 nm. In the literature, this is often regarded a marker for flame development and the initial flame kernel, [22, 23].

Radical and Molecule-Specific Radiation The emission from dominant molecules is summarized into specific flame bands or continua, [20]. The *CH band* shows its strongest peak around 4,315 Å, followed by 3,900 Å and 3,143 Å.

The *CN band* peaks around 3,883 Å, but is often masked by CH emission. A smaller peak around 3,590 Å is better distinguishable. Combined with OH radicals, CN acts as a marker for the spark discharge, [22].

The *C2 Swan band* with distinctive peaks at 4,731, 5,165 and 5,635 Å is an important soot indicator.

Vaidya's hydrocarbon flame bands, originating from HCO are strongest between 3,064 and 3,900 Å and best detectable for lean mixtures and low-temperature flames. Masking for higher temperature occurs at the borders.

Emission in *Emeléus' cool flame bands* is mainly attributed to formaldehyde, HCHO, and is spectrally spaced evenly between 3,700 and 4,800 Å [24]. The band is also visible during the auto-ignition processes in engines, but except for methyl alcohol not in a significant intensity from regular hot flames.

Even trace amounts of *sodium*, due to e.g. impurities in the fuel or the lubricating oil, show the strong D lines close to 5,893 Å.

In premixed flames, the individual band intensity varies greatly with the air fuel equivalence ratio (λ). At rich conditions, around λ = 0.65, C2 supposedly reaches its maximum intensity, while CH peaks slightly less rich at λ = 0.68. A flat peak for OH intensity is attributed to λ = 0.85. For the broader bands in general, a rising intensity from rich up to stoichiometric conditions is reported, while the best visibility is proposed there due to lower individual peak intensities in the lean regime [20].

Spectral Properties Expected for DMC/MeFo According to Gaydon [20], we expect a considerable decrease for C_2 and CH emissions for fuels containing oxygen while maintaining a strong OH emission.

Abdalla et al. [15] point out a high formaldehyde production during the oxidation process of DMC, and the formation of carbon dioxide before carbon monoxide during pyrolysis, with only a limited number of soot precursors compared to ethanol.

Spectrally resolved investigations in the literature have been performed e.g. for SI PFI [25, 26, 27] and DI [22, 23, 28, 29, 30] applications, for gasoline [10, 22, 23, 26, 28, 29, 30, 31, 32], ethanol [23], gaseous (CH_4, H_2) [25, 27] and other fuels [22, 31, 32].

To the best of the author's knowledge, no in-cylinder spectral characterization of SI DMC/MeFo has been reported.

Experimental Setup - Test Bench

Optical Single-Cylinder Engine

The optical engine, depicted in Figure 1, is fully optically accessible via two perpendicular points of view. An elongated, hollow piston according to the Bowditch principle grants access perpendicular to the liner's height axis, and a

FIGURE 1 Sectional view of the optical single-cylinder engine

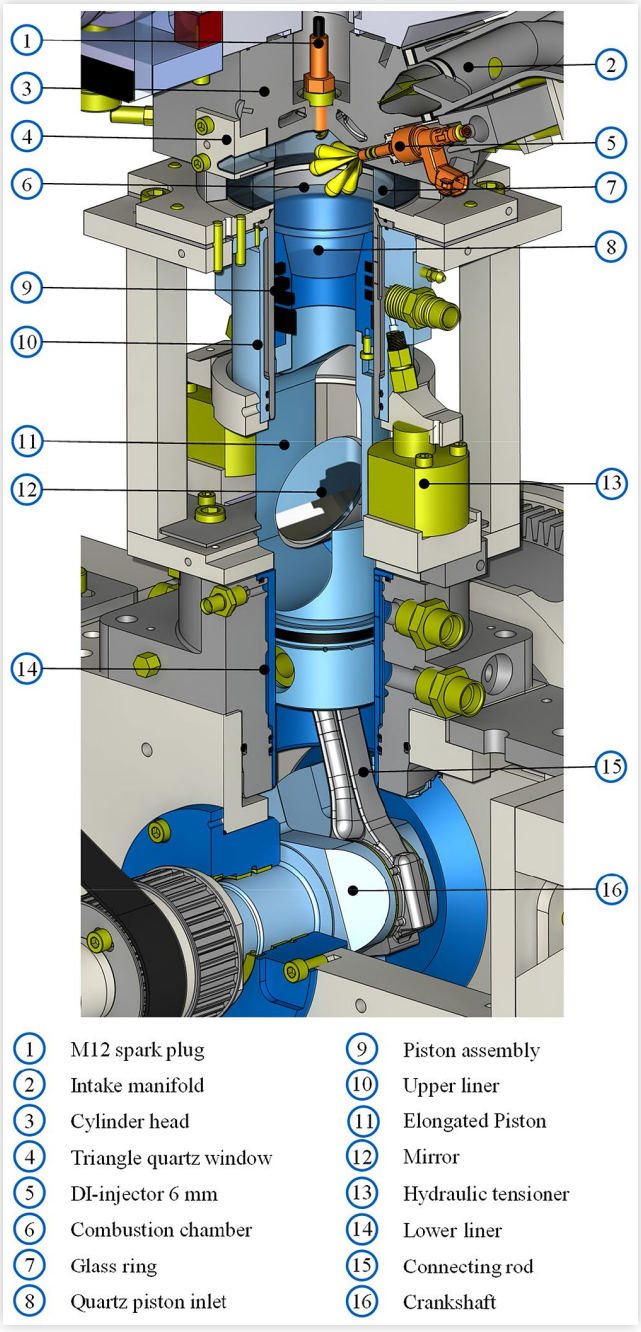

stationary mirror, angled at 45 degrees, transmits the optical signal to the detectors [33]. A glass ring with a height of 21.5 mm in combination with a triangular optical insert centered on the pent-roof chamber, resolves access along the liner height axis. The ring grants an unobstructed view of 360 degrees. Hydraulic tensioners provide the pretension necessary to seal the glass ring against the combustion pressure and enable quick accessibility for cleaning of the optical surfaces [34].

In the present study, the prismatic pent-roof access was replaced with a metal dummy, resembling the original combustion chamber contour for lower interference with the intended charge motion.

The quartz piston geometry was flat, so as not to introduce optical aberrations. A slight geometric difference compared to the metal piston and therefore also the compression ratio was present (optically 9.36 compared to 10.92).

Both the optical and metal configurations feature three piston rings. The optical piston rings, however, are slotted, dry-running and made from a PTFE and graphite compound. Further details on the metal engine are presented in [18, 35].

The non-crystalline glass ring is made from Corning 7,980 fused silica, the piston and pent-roof insert from GE 124 fused quartz.

Operation Strategy In general, the fired operation time of the optical configuration is limited, mainly due to the thermal and mechanical load on the optical components. A typical firing run consists of a few hundred working cycles. This is quite contrary to thermodynamic configuration, where continuous operation is normal and several minutes of fired operation precede an actual measurement.

In order to reach a fair and reproducible comparison basis for the recorded data in a run, the aim was to reach a quasi-steady state before the recording. To do so, the record start was set to twenty seconds after the fired operation began, with a fixed cool-down time in between individual operating points. At 1,500 rotations per minute, this equals 250 working cycles. A total of 50 working cycles are optically recorded for each set.

Engine and Test Bench

General Test Bench Arrangement Figure 2 shows the schematic arrangement of individual components and their interconnectivity on the test bench, while Table 2 contains summarized key figures.

Full monitoring and conditioning of the charge air, exhaust pressure, oil, coolant and fuel enables a reproducible operational environment.

Besides several standard sensors for torque, pressures, mass flow and temperatures, the test bench is equipped with a full pressure indication system (intake, cylinder, exhaust).

Fuel Direct-Injection System An in-house developed pressure system supplies DI-capable levels of fuel pressure as well as mass flow measurement, see Table 3. The injector is solenoid-operated and features six orifices.

FIGURE 2 Schematic arrangement of the test bench components

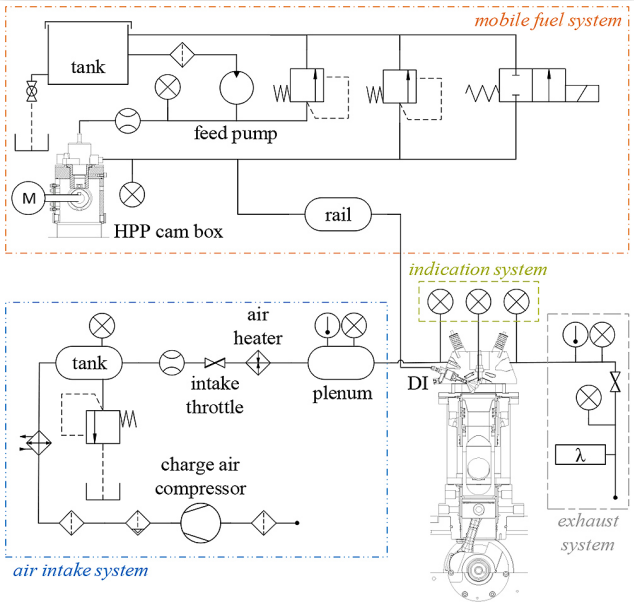

TABLE 2 Specifications of the optical engine

Engine base	AUDI EA888 GEN2 (2008)
Bore	82.51 mm
Stroke	86.6 mm
Connecting rod length	144 mm
Displacement	463 ccm
Compression ratio	9.36:1
Valve train	DOHC with VEL & VTC
Exhaust valve lift	7 mm @ 250 CAD aFTDC
Intake valve lift	6 mm @ 460 CAD aFTDC
Max. engine load	6 bar IMEP
Max. rpm	2000 1/min
Oil temperature	80° C
Coolant temperature	80° C
Ignition System	Single Coil

TABLE 3 Specification for the fuel system

Max. pressure	35 MPa
Injector type	Multi-hole DI
Nozzle size	6 mm
Actuation	Solenoid
Number of orifices	6
Orifice shape	Convergent
Injector position	Side mounted
Static flow rate @ 10 Mpa with n-Heptane	13.8 ccm/s

Data Acquisition and Engine Control System

A freely programmable ECU, implemented in a dSPACE system, controls the test bench. The engine load is fed to a

feedback controller coupled with the pressure indication system, which in turn corrects the intake pressure.

The measurements were conducted with an in-house developed rapid control prototyping system and can be categorized into two frequency domains. Slow data accounts for parameters like temperatures, torque, engine speed and pressures of subsystems and the environment; these are recorded with variable recording rates.

Fast or indicated data is recorded at a temporal resolution of 0.1 CAD. Fired top dead center (FTDC) is defined at 720 CAD.

A complete set of thermodynamic data for the optical setup consists of 50 sequentially measured cycles. Indicated values are stored in full resolution for each cycle, whereas slow data is stored as the average value calculated during the snapshot's recording time, assuming a stationary operation state.

Optical Measurement Assembly

Two optical measurement setups have been applied at the test bench. First, the flames' natural luminosity and OH*-chemiluminescence were recorded simultaneously.

Subsequently, selected operating points were investigated spectrally resolved in detail with a 1D-spatial and high temporal resolution.

Both experiments used the same optical axis, collecting the transmitted optical signal via the optical piston via the stationary mirror, as seen in Figure 1. The individual arrangement is depicted in Figure 3; the achieved field of view is summarized in Figure 7. A programmable timing unit (LaVision PTU X) was applied for synchronization and relative triggering within the devices.

A limiting factor to all applied methods in this study is their line-of-sight nature. The exact origin of the collected signal within the combustion chamber's height axis cannot be determined. From the recorded point of view, it is therefore not possible to deduce the spatial distribution along that axis.

FIGURE 3 Optical setup for 1D Flame Emission Spectroscopy and simultaneous flame luminescence/ OH* imaging

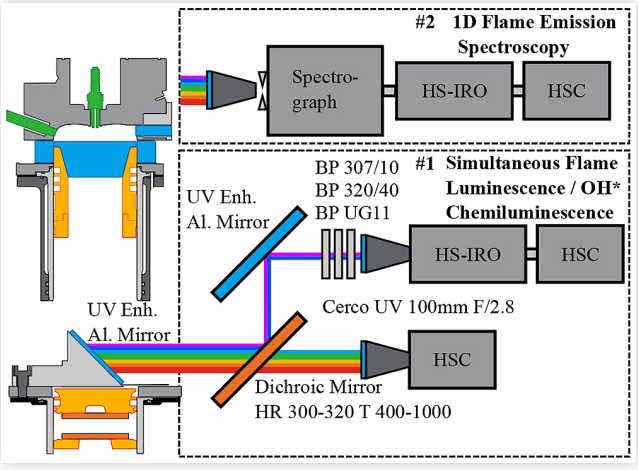

High-Speed Flame Luminescence

The optical detectors used to record the natural light emission were mounted in front of the stationary mirror, as seen in Figure 1. A custom beamsplitter case with interchangeable optical elements, situated in the optical path in front of the cameras, enabled simultaneous recording of flame luminescence and chemiluminescence, [36].

AR-coated protection windows facing the exterior of the box, hermetically shielded the beamsplitter from oil mist and contamination in general.

OH*-Chemiluminescence The wavelength range from 300-320 nm is reflected and thus separated at the splitter's first surface with an efficiency greater than 95 % and redirected via an UV-enhanced aluminum mirror, forming the chemically excited hydroxyl (OH* radicals) path. To ensure sufficiently small exposure times for the weak optical signal, a high-speed CMOS camera (Phantom v2011, monochrome) is coupled with image intensifier relay-optics (LaVision HS IRO, S20 photocathode). The intensifier gate was kept constant at a gain of 28 counts per photoelectron; the exposure time was kept at 30 µs. A frame rate of 18 kHz led to a temporal resolution of 0.5 CAD/image. A combination of optical bandpass filters, placed in front of the imaging lens (Sodern Cerco 2178 UV 100 F/2.8), enhances the signal quality by suppressing unwanted crosstalk. The central wavelength is located at 307 nm with a full width at half maximum of 10nm and an optical density OD ~ 6. The combination with two broader filters raises the optical density well beyond OD ~ 15 above 350 nm.

Natural Flame Luminescence The natural luminescence detection is oriented in the splitter's transmission path, achieving about 80 % transmission from 350 nm onwards, with a mean of 90 % up to 1,000 nm. A high-speed CMOS RGB camera (Phantom v2012, RGB) with an identical imaging lens and similar overall path-lengths is used to simplify the spatial matching of both recorded images in post-processing. The recording rate is kept constant at 18 kHz with a fixed exposure time of 50 µs. The incoming signal is recorded broadband without further optical filtering.

Figure 4 depicts the summarized transmission over wavelength for the OH* path, Figure 5 for the natural flame luminescence, including the effects of all relevant components.

High-Speed 1D Flame Emission Spectroscopy

The spectroscopic assembly omitted the beam splitter and was directly placed in front of the stationary mirror. An imaging lens (Sodern Cerco 2178 UV 100 F/2.8) projected the signal onto the entrance slit of an astigmatism-corrected imaging spectrograph (Princeton Instruments IsoPlane SCT320). Via

FIGURE 4 Individual components and resulting overall transmission efficiency "SUM" for the OH* path

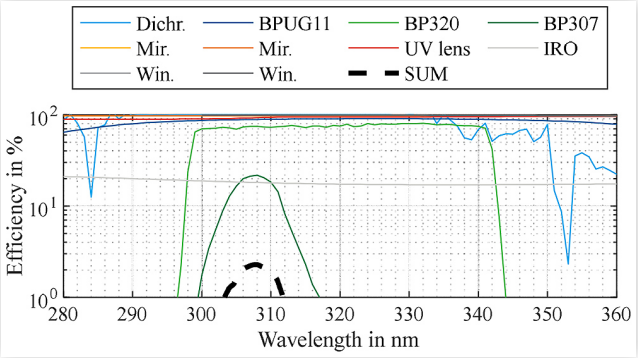

FIGURE 5 Individual components and resulting transmission efficiency "SUM" for natural flame luminescence "Blue", "Green" and "Red" depict the RGB-camera quantum efficiency

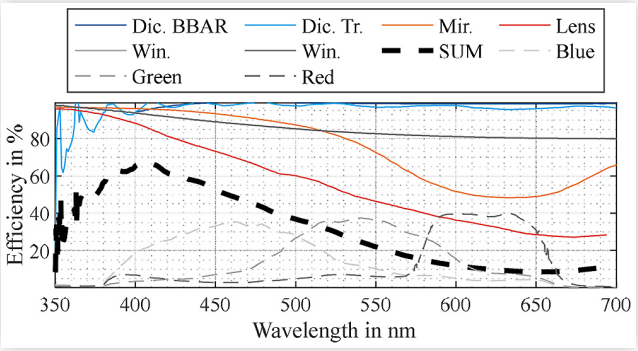

an integrated turret, multiple diffraction gratings could be applied with ease. In this study, mainly gratings with 150 groove/mm and a blaze wavelength of 500 nm to cover the overall signal, as well as 600 groove/mm with a blaze wavelength of 300 nm were applied. Along the slit, the setup enabled a 1D spatial resolution of 0.17 mm/pixels.

Care was taken to resolve the whole relevant radical spectrum in one recording. The minimum detectable wavelength with the selected central wavelength was chosen at slightly less than 300 nm, while the upper limit originates from the OH*'s second order diffraction, which is visible at around 620 nm. Longer wavelengths are hard to isolate properly due to second order diffraction; hence are not considered in this study.

A high-speed CMOS camera (Phantom v2011, monochrome) coupled to high-speed image intensifier relay-optics (LaVision HS IRO, S20 photocathode) recorded the dispersed spectral data. The frame rate of 18 kHz enabled a temporal resolution of 0.5 CAD/image. The intensifier gate remained fixed at 30 µs, while the gain was varied from 132 to 742 counts per photoelectron in order to achieve sufficient signal levels. The slit width was kept constant at 20 µm.

Calibration After the setup assembly on the test bench, an Hg(Ar) Pen-Ray line source (QuantumDesign, LSP035) placed within the combustion chamber enabled spectral calibration for each grating and desired central wavelength.

To be able to calculate the actual intensity per wavelength from the recorded raw spectrum, the influence from every involved element within the optical path needed to be accounted for. These included the quantum efficiency of the camera's CMOS chip and the intensifier's photo-cathode, the transmission of the UV lens and all relevant windows, the reflectivity of the stationary mirror, the spectrograph's grating and mirror efficiency.

With few exceptions, manufacturers' data were present and were applied for each component. In general, the transmission data's spectral range was limited, but broad enough to satisfy the desired window range from 300 to 620 nm.

The multiplication of each individual efficiency yielded the correction vector for the raw recorded spectra. Figure 6 shows the individual efficiencies of the involved elements as well as the resulting summed efficiency.

Using the spectrograph in the imaging configuration with an open slit, the absolute position of the 1D line was matched almost to the middle axis of the combustion chamber. A slight offset and angular deviation against the central axis remained, as seen in Figure 7. To ease interpretation, the area is divided into *Regions of Interest* (ROI), with ROI=1 situated in the squish region, ROI=2 between the exhaust valves, ROI=3 close

FIGURE 6 Individual components and resulting overall transmission efficiency "SUM" for 1D flame emission spectroscopy

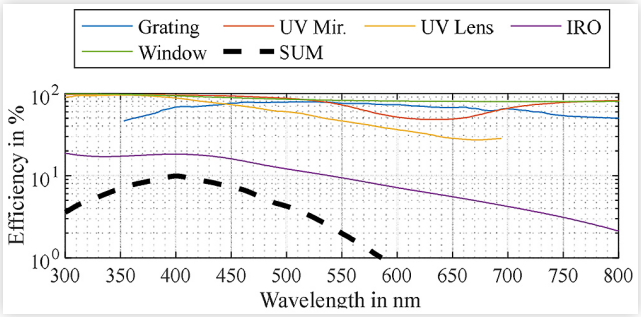

FIGURE 7 Schematic arrangement of measurement position in the combustion chamber, as seen through the quartz piston. Mapped raw image of the spectrograph with open slit and resulting middle axis in red, quartz dimensions in blue. The selected cutout for the presented OH*/RGB-images is highlighted in orange

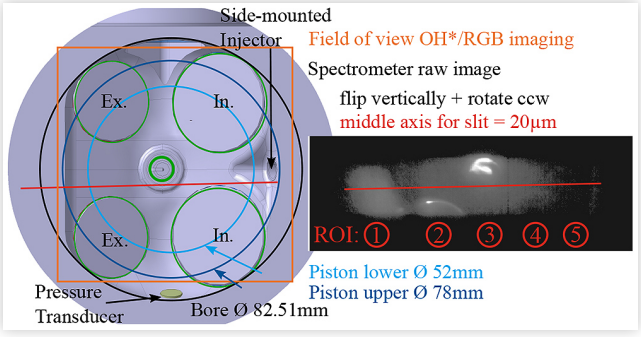

to the sparkplug, ROI=4 between the intake valves and ROI=5 close to the bore along the side-mounted injector.

Image Post-Processing

Matching - Sizing, Shifting, Rotation, Mirroring In order to evaluate spatial equivalent data and due to slightly different optical path lengths, the images are sized and locally shifted until a match in regard to calibration images is achieved. Further applied steps to ensure a proper matching include rotation and mirroring of the whole image.

Visualization Correction Over the span of the operating conditions, the recorded intensities for the RGB flame luminescence were scaled to improve visibility. The applied *scaling factor*, multiplied with the recorded counts on a pixel basis, linearly increases the pictured intensity. To improve the visibility in the OH*-recordings, the maximum intensity in counts visible at the color bar for the plot was scaled when needed, the raw values however remained untouched.

In order to ease visual impression of the flame-emission spectroscopy, the calculated efficiency correction factor is not applied in the presented figures. If the maximum intensity around 400nm, Figure 6, was fitted with a multiplication factor of one, the signal intensities close to 600 nm as a result were multiplied with double-digit numbers, thus creating a large difference in counts. However, the presented figures do not aim at absolute numbers, but at a qualitative comparison of the spatial and temporal evolution in active combustion zones.

Averaging Especially for the cycle-resolved high-speed flame luminescence and OH* recordings, the final image looks primarily less sharp and washed-out in the sharp edges when averaged over 50 cycles. Cycle-to-cycle variations inherent to an SI engine combustion process are the presumed cause. In order to enhance data visualization, the average is only calculated over the middle 20 working cycles. The same method applies to the spectroscopic data.

Results and Discussion

Operating Conditions

Table 4 contains a summary of the variable operating parameters for the conducted sweeps. Due to the chemical differences of the investigated fuels, a significant difference can be observed in their air-fuel-ratio, Table 1. For stoichiometric combustion of RON95, an AFR of about 14.28:1, in comparison to 4.64:1 for DMC and MeFo, is required. To compensate for this influence, the injected fuel mass is adapted to ensure an identical air-fuel equivalence ratio for direct comparison. Due to the lower volumetric heating value of oxygenates, higher injection pressures or adapted nozzles are needed in order to keep the injection time constant. However, in this study the nozzle remained fixed, which resulted in longer injection times for the mixture.

TABLE 4 Variable operating parameters in addition to the fixed parameters, see Table 2

Engine Speed	1500 rpm
A/F equivalence ratio λ	0.8 ... 0.2 ... 1.4
Start of Injection (SOI, CAD)	430 ... 470 ... 550 ... 630
Start of Ignition (IGN, CAD bFTDC)	Variable, to keep MFB50 @ 8 CAD aFTDC
IMEP	~ 6 bar
Fuel	RON95/C65F35

In order to reach identical IMEPs, along with the fuel mass, the air mass flow was also adapted.

The start of ignition (IGN) was varied in order to keep the 50% fuel mass burned (MFB50) at 8 CAD aFTDC. IGN is defined as the spark timing. Each sweep was performed with the fuel mixture as well as with RON95 as a fuel reference. Parameters not listed in Table 4 were kept constant as seen in Table 2.

Engine-out emissions as well as particulate numbers of the pure substances DMC and MeFO, recorded at the thermodynamic configuration, are presented by Härtl et al. [3]. Due to the response time of the present FTIR, no simultaneous recordings during the optical investigations are carried out.

Lambda Sweep - Flame Luminescence & OH*-Chemiluminescence

Figure 8 and Figure 10 contain the average recorded indicated cylinder pressures for both variations. The pressure rise for RON95 appears earlier than for the oxygenate mixture at corresponding equivalence ratios. This can be traced back to a reduced air demand for C65F35 and hence a lower intake pressure level. In addition, the achieved peak pressure is considerably higher for the reference fuel. However, for stoichiometric and even more so for the selected rich equivalence ratio of λ = 0.8, the temporal advantage is diminished and the achieved peak pressures are roughly equal.

FIGURE 8 In-cylinder pressure for λ variation, averaged data. Start of injection is kept constant at SOI = 430 CAD

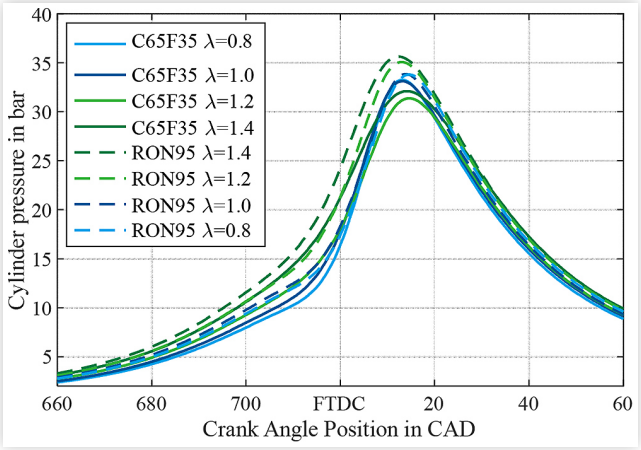

Figure 12 contains the applied Start of Ignition for both variations. Moving from stoichiometric to lean AFR, the start of ignition is forced to an earlier position, gradually increasing the advanced timing for the oxygenate mixture up to 8 CAD for λ = 1.4.

The Apparent Heat Release Rate (AHHR) presented in Figure 9 shows a continuous increase in the release rate even for lambda = 0.8 and C65F35, while the effect diminishes if RON95 is compared with lambda =0.8 and 1.0. Both fuels show peak rates for the rich mixtures, gradually decreasing towards leaner operating regimes. For the lean ratios of lambda = 1.2 and 1.4, the peak rates for RON95 exceed those of C65F35, which are prolonged overall.

Throughout the sweep, several randomly occurring bright yellow-orange spots could be identified in the natural flame luminescence even in the averaged images, overall slightly more for C65F35 than for gasoline, Figure 13. The authors assume that these spots were droplets or generally areas of insufficient mixture preparation. Since these are not visible in the OH* recordings, a lower temperature level is expected. This fits well with the assumed drop in overall temperature

FIGURE 9 Apparent heat release rate for λ variation, averaged data. Start of injection is kept constant at SOI = 430 CAD

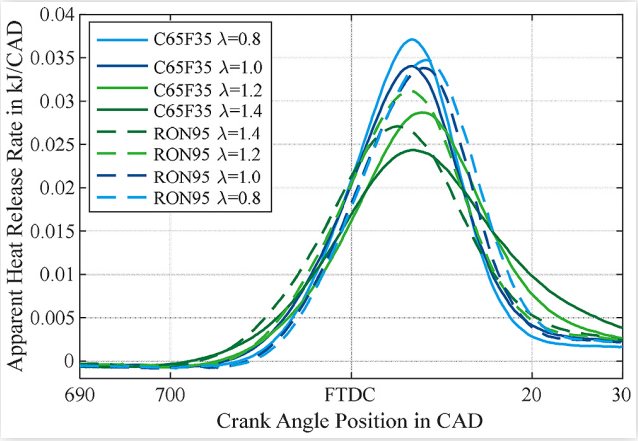

FIGURE 10 In-cylinder pressure for Start of Injection (SOI) variation, averaged data

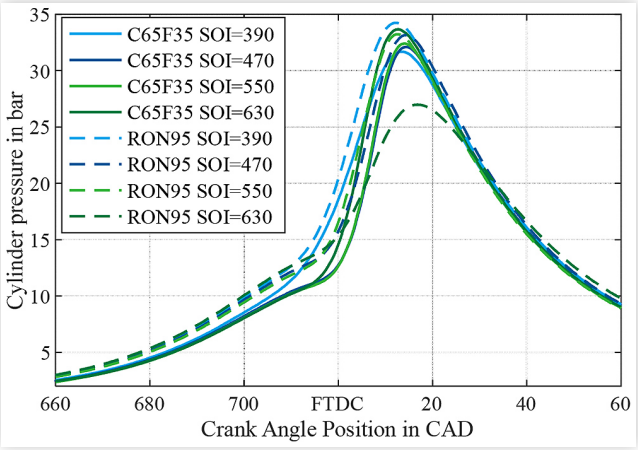

FIGURE 11 Apparent heat release rate for Start of Injection (SOI) variation, averaged data

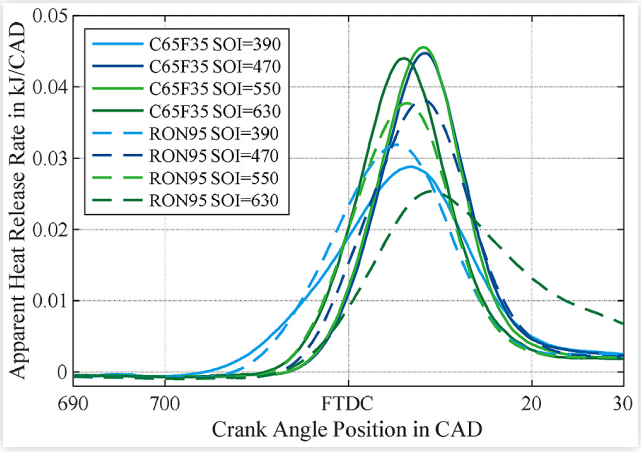

FIGURE 12 Necessary Start of Ignition (IGN) applied for the sweeps along λ and Start of Injection

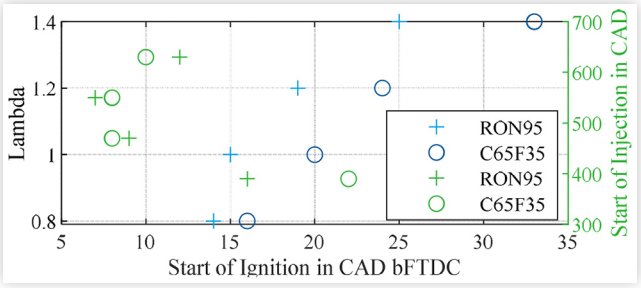

due to the increased in-cylinder cooling caused by evaporation. The specific enthalpy of vaporization for both fuels is comparable, Table 1, but considering the additional fuel mass necessary to reach an identical energy content, overall lower temperatures are explainable.

Qualitatively, the flame luminescence recordings show similar behavior for spatial distribution within the combustion chamber of the two fuels. Throughout the recordings, the absolute intensity, both for OH* and RGB flame luminescence, is significantly lower for C65F35 than for RON95. Consequently, the overall radiative emission is lower, as can be seen in the spectroscopic data as well.

The flame originates at the spark plug and a clear flame front is visible, expanding symmetrically from the center and ultimately filling the whole bore diameter.

The first part of the combustion is dominated by a bluish flame, indicative for a premixed combustion with few diffusive components. This lasts well past the fired top dead center and then changes depending on the fuel. For RON95, the switch to a more pronounced green and later orange and yellow hue is visible for earlier crank angle degrees, beginning at 21 CAD aFTDC for λ = 1.0, advancing for leaner values up to 11 CAD aFTDC for λ = 1.4. For rich mixtures, no definitive CAD-value is given, since prominent diffusion flames are visible from 4 CAD bFTDC onwards. For C65F35, the limit is protracted to about 30 CAD aFTDC for λ = 1.0 up to 17 CAD aFTDC for λ = 1.4. At λ = 1.2, the switch occurs at 21.5 CAD aFTDC.

FIGURE 13 Lambda variation, range λ = 0.8 to 1.4. Rich conditions result in diffusive combustion for gasoline, while lean conditions lead to a decreased overall intensity and shift away from the blue channel

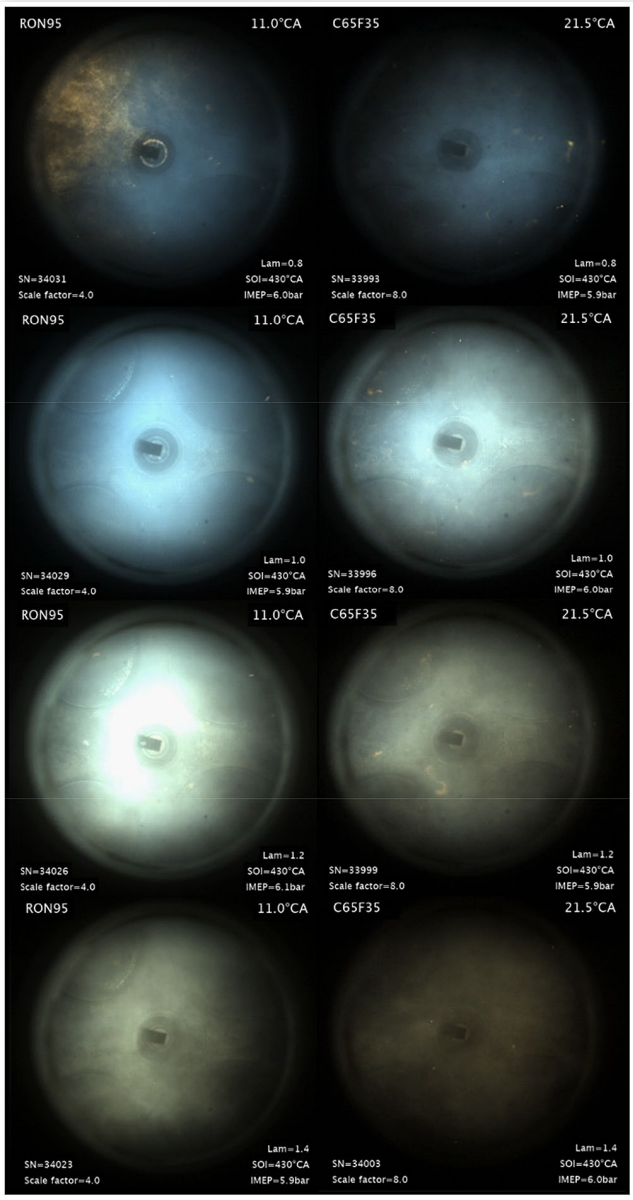

Contrary to RON95, no prominent diffusion flame is visible for λ = 0.8 and a notable change in color is only prominent after 31 CAD aFTDC.

In the later part of combustion, up to the point when no emitted radiation is detected, the dominant colors are yellow and orange hues with only a slight blue and green component. When an arbitrary yet constant threshold of 64 counts is applied to the OH* data, the emission terminates 10 CAD earlier for C65F35 than for RON95 at λ = 1.0 and 1.2. For the extreme values of lambda = 0.8, the emission ends 6 CAD earlier, while for λ = 1.4 this is only 1 CAD. The end of emission for OH* of C65F35 is at 36 CAD aFTDC both for λ = 1.2 and for 1.4; however, the end for RON95 advances only up to 37 CAD aFTDC for λ=1.4.

Figure 14 and Figure 15 visualize the lambda sweep for both fuels and summarize selected positions in crank angle degrees, both for the flame luminescence and for the OH* signal. To improve visibility despite the high dynamic range, scaling factors are adapted in between operating points. For OH*, the color map always starts at 0 counts up to the maximum depicted value; the RGB scaling factor multiplies the present counts with a factor. However, the bottom row for OH* shows a fixed color scaling matched to the selected threshold in order to visualize the hot reaction zones on a comparable level.

With the thresholded OH*, the spatial location of the hot flame zone is characterized. A change is clearly observed over the lambda sweep. Generally, the spatial extent of the OH* precedes the spatial extension of the recorded RGB-signal in agreement with the theory. At λ = 1.0, a symmetric progress of almost perfectly spherical flame propagation in the combustion chamber, originating at the sparkplug, is present. This holds especially true in the earlier stage of combustion up to 10-15 CAD aFTDC. The most intense areas show a gradual trend towards the exhaust valves away from the center axis, steadily increasing for leaner mixture ratios. In the further combustion process up towards its end, this trend intensifies towards an asymmetric behavior of the intense OH*-regions. These regions move well between the exhaust valves for λ = 1.4, away from the center, and well towards the intake valves for the rich equivalence ratio of λ = 0.8, both for RON95 and C65F35. For RON95 and the rich mixture, this agrees with the flame luminescence data, where prominent diffusion flames could be observed in the region of the exhaust valves.

FIGURE 14 Lambda variation, RON95, OH* and RGB flame luminescence. The top right corner of each image contains the crank angle position in CAD ATDC. The bottom right corner contains the scaling factor for RGB images and for OH*, the maximum visible counts in the current colormap. The signal's dynamic range required adaptations to improve visibility for presentation

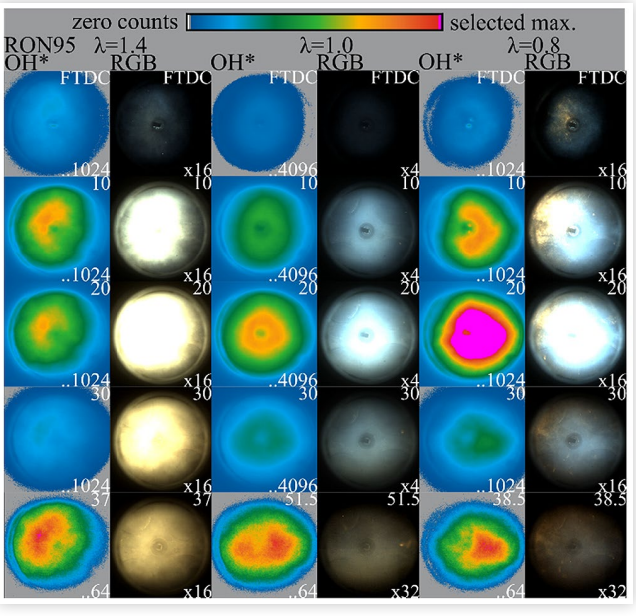

FIGURE 15 Lambda variation, C65F35, OH* and RGB flame luminescence. The top right corner of each image contains the crank angle position in CAD ATDC. The bottom right corner contains the scaling factor for RGB images and for OH*, the maximum visible counts in the current colormap. The signal's dynamic range required adaptations to improve visibility for presentation

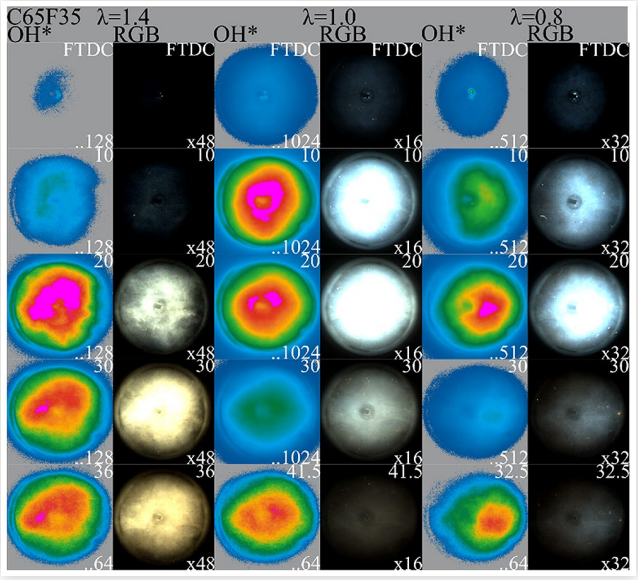

This suggests an improper mixture formation in this area, which is also the target of the side-mounted injector. Closer to the intake valves, the mixture preparation still seems to be sufficient. C65F35 exhibits no diffusion flame despite longer injection time and in theory a lower temperature level. The prolonged injection time should decrease mixture quality at the same time; however the additional oxygen inherent to the mixture seems to dominate this effect.

Flame Luminescence & OH*-Chemiluminescence–Start of Injection Sweep

The early injection timings of SOI = 390 and during the intake-stroke at SOI = 470 CAD, as depicted in Figure 10, show a similar temporal advance level of peak pressure for RON95 as for stoichiometric and lean operation. The later injection timings, beginning at SOI = 550 CAD in the compression stroke, demonstrate a delayed rise in in-cylinder pressure, only gaining momentum close to the fired top dead center (FTDC). For SOI = 550 CAD, the temporal advance for RON95 is still present, but for the late SOI = 630 CAD, a significant fall-off in the pressure gradient as well as the achieved peak pressures is detected.

Quite similar in comparison to the lean operating points, advanced ignition timing is present for the early SOI = 390 CAD, putting C65F35 ahead of gasoline by 6 CAD to keep the MFB50 constant, Figure 12. However, for SOI = 470 and 550 CAD, the difference drops to 1 CAD and is tipped around at 550 CAD. For an even closer start of injection towards FTDC at 630 CAD, gasoline ignition needs to be advanced by up to 2 CAD in relation to C65F35. Even with this shift towards earlier ignition, stable operation is barely achieved, with a rise in the coefficient of variation (CoV IMEP) for the indicated mean effective pressure up to 13.4%. In comparison, the CoV for the other operating points ranged between 1.1 and 2.1%, apart from C65F35 at λ = 1.0 and SOI=430, where it unexpectedly rose to 8.1%. A definitive reason for that could not be clearly identified even with the optical measurements. While no significant reduction in the peak in-cylinder pressure was the result for C65F35, the high CoV of 13.4 % for RON95 resulted in a notable drop of about 25 %, see Figure 10.

In the outermost operating conditions, at SOI = 550 and 630 CAD as well as λ = 0.8, the burning duration decreased by up to 2.7 CAD for C65F35. At the early SOI = 390 CAD, the burning duration for gasoline was 2.3 CAD shorter than for C65F35, while no clear trend was observable for the remaining operating points.

A comparison of the AHHR is presented in Figure 11. A temporal advance for RON95 is only found for the very early SOI = 390 CAD, where also the peak release rate is higher. All other investigated SOI = 470 - 630 CAD yield faster rise times of the release rate along with a significantly higher peak value for C65F35 than for RON95. In accordance to the prior discussed rise in CoV for the late SOI = 630 CAD, a undesired, delayed rise with considerably prolonged release rate duration is observed.

Just as for the lambda variation, the flame luminescence recordings for the Start of Injection variation generally point out slightly more, with randomly occurring bright yellow-orange spots for C65F35 compared to gasoline, see Figure 16.

Once again, the overall recorded intensities both for OH* and the flame luminescence are lower for C65F35. The largest spread of four in scaling factors is present at SOI = 550 CAD; the same spread applied to λ = 1.0 in the other sweep. For the other SOIs, the spread in flame luminescence was a factor of two.

The change in color is not as dominant as for the lambda variation. The first part of combustion up to 20 CAD aFTDC is dominated by a bluish flame, indicative of premixed combustion with few diffusive components. After that, a gradual switch towards more green up to 40 CAD aFTDC is observed, after which yellow and orange hues become stronger. This holds true for all investigated SOI, expect for SOI = 630 CAD, where a prominent diffusion flame is already present at the fired top dead center and onwards, see Figure 17. Spatially, the diffusion flame leans asymmetrically towards the exhaust valves away from the center of the combustion chamber and stays there visibly in the bottom left corner. The expected premixed flame throughout the chamber is not reached anymore for these conditions, indicating insufficient mixture preparation due to the late injection. The end of the recordable emitted radiation is dominated by yellow and orange hues and drops sharply in intensity, therefore the scaling factors for the last depicted crank angle degree are adapted, see Figure 17 and Figure 18.

To interpret the spatial location of the hot flame zone via the OH*, the same threshold as for the lambda variation is applied. For SOI = 390 CAD, C65F35 reaches this point 8.5

FIGURE 16 Start of Injection (SOI) variation, range SOI = 390 to 630 CAD. Late SOI leads to diffusive combustion for gasoline, while even for SOI = 630 CAD, C65F35 exhibits a "clean" premixed combustion

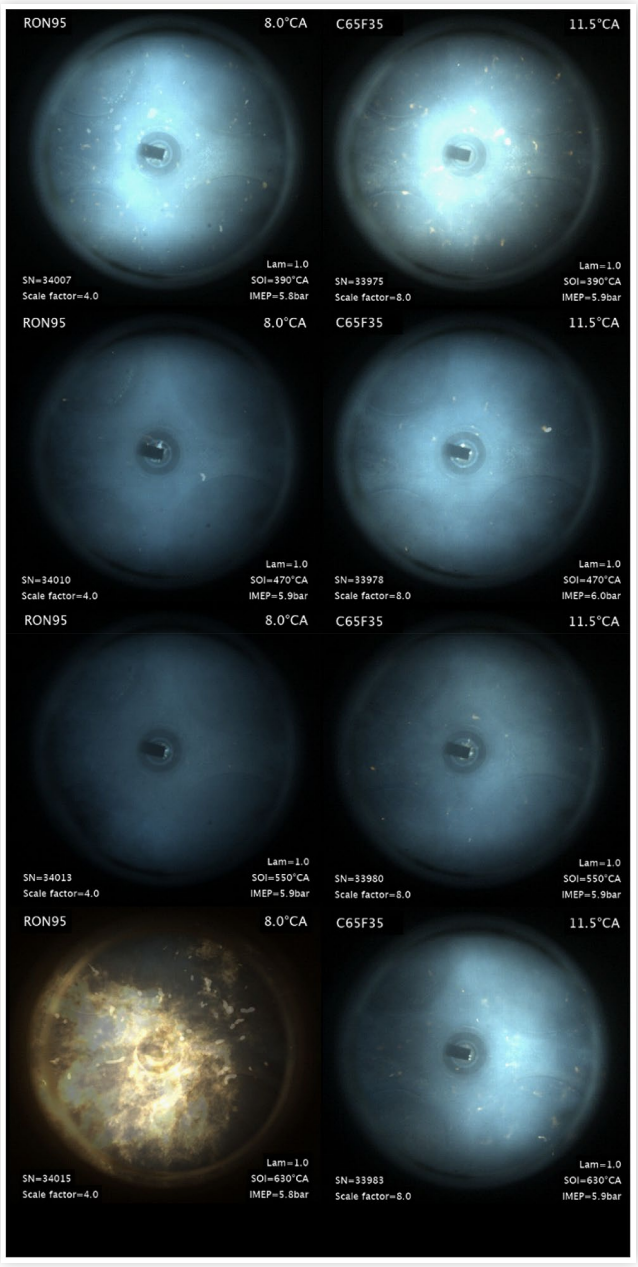

CAD earlier than RON95 at 42 CAD aFTDC. Over all SOIs, C65F35 is advanced in relation to RON95, ending at 7.5 CAD earlier at 36 CAD aFTDC, despite the advanced IGN for RON95 at SOI = 630 CAD.

On evaluation of the spatial OH* distribution of the sweep, a change for later SOI is apparent. At SOI = 390 CAD, spatial distribution behaves comparably, originates symmetrically near the spark plug and fills the whole combustion chamber, with late signal emission still centered in the chamber. For the intermediate SOI at 550 CAD, both fuels still show a similar trend, where the more intense areas for OH* and also the flame luminescence wander off-center towards the intake valves.

FIGURE 17 SOI variation, RON95, the format follows Figure 14. At late SOI = 630 CAD, diffusion flames in spatial accordance with the OH* reaction zone are visible. Intermediate SOI = 550 CAD also exhibits a one-sided trend towards the intake valves for the active OH* reaction zone

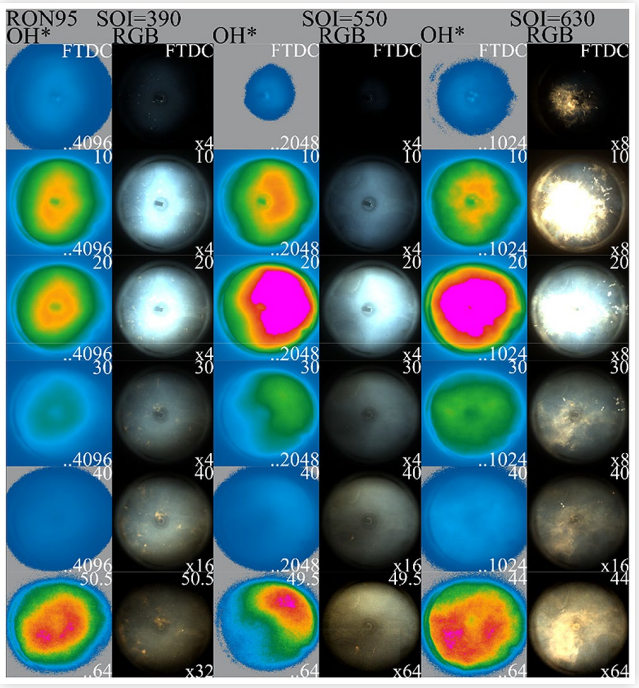

At SOI = 630 CAD, however, the fuels behave differently. The OH* signal for RON95 shows, just as in the early IGN, an almost symmetric distribution, while flame luminescence visualizes a clear diffusive flame oriented towards the exhaust valves. Interestingly, even in the late stage of combustion, the intense areas for OH* match those for the supposed diffusive flame. The high CoV IMEP of 13.4% limits the applicability of this operating point in practical application, thus narrowing the operating range for RON95. C65F35 on the other hand increases the trend that arose at the intermediate Start of Ignition and wanders further towards the intake valves, in total behaving more asymmetrically. In contrast to RON95, however, no relevant diffusion flames are identifiable. As a reason for the asymmetric behavior and the hot OH* spatial displacement towards the intake valves, the authors assume a temperature gradient due to fuel/wall interaction or wetting as a result of the late start of injection. Consequently, a less optimal spray preparation with larger droplets and more incomplete mixing with the surrounding air is expected.

Despite the less optimal spray preparation, the oxygen inherent to the oxygenated fuel attributes to a lower probability of sooting combustion in a diffusive flame, due to its local availability. However, in order to assign this effect fully to the oxygen content and to distinguish it from the effect the reduced temperature generates, an equivalence ratio-temperature plot is required.

Verhelst et al. depict a comparison of methanol and diesel. For methanol, the soot-island-boundaries are significantly shifted towards an equivalence ratio of about 3.5, while the

FIGURE 18 SOI variation, C65F35, the format follows Figure 15. For later SOI, the spatial position for the hot reaction zone in the OH* gradually moves in between the intake valves

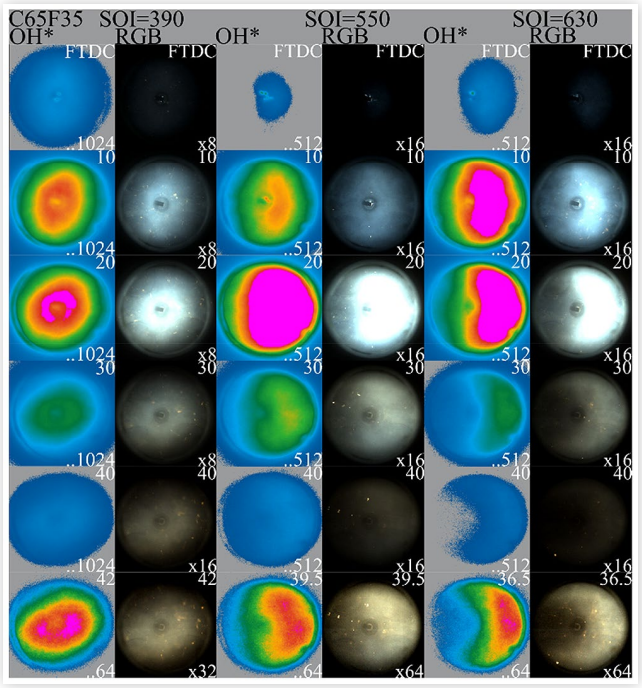

lower limit for diesel is close to 1.3, [37]. The authors expect a similar trend for the mixture of DMC and MeFo.

1D Flame Emission Spectroscopic Evaluation

The 1D flame emission spectroscopy is spatially resolved almost along the whole diameter of the bore and with a temporal resolution of 0.5 CAD per recording. Due to the scope of this paper, only selected results are presented.

Figure 19 and Figure 20 offer a surface plot for both RON95 and C65F35 for a lean operating point of λ = 1.4 and SOI = 430 CAD, evaluated at Region of Interest = 3 close to the spark-plug. The individual ROIs are referenced in Figure7; the spatial distribution within an ROI is integrated to a scalar value. All plots in this chapter show the wavelength along the x-axis and are marked at distinct wavelengths of interest - namely OH (308 nm), CN (359, 388 nm), HCHO (start at 370, end at 480 nm), CH (431 nm), C_2 (473, 516 & 563 nm) and Na (589 nm), while the y-axis contains the spatially averaged data within an ROI for a one time step, recalculated to the current crank angle position. The recording covered a range of 690 CAD up to 70 CAD aFTDC. The z-axis features the recorded counts in arbitrary units. To ease visibility, 2d contour plots are applied next to the 3d surfaces.

The selected lean operating points provide a great difference in signal evolution despite the previously shown similarities in both flame luminescence and OH*. Overall, with identical imaging parameters, RON95 leads to more counts, thus increased radiative emission is presumed. Distinct spikes matching the ignition timing are visible for OH and

FIGURE 19 ROI = 3, spark-plug, RON95, λ = 1.4 time-series surface plot

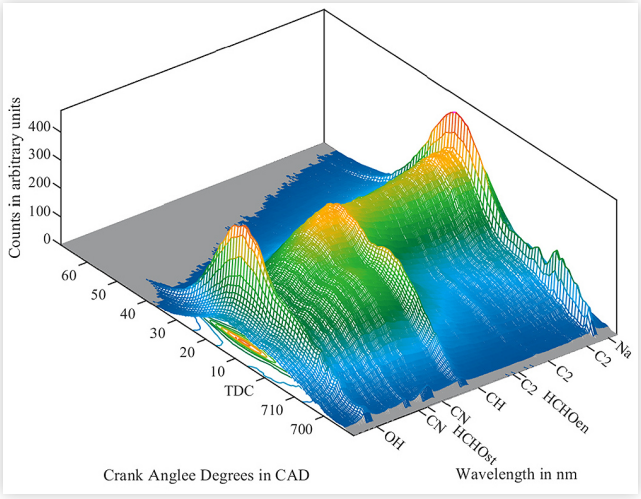

FIGURE 20 ROI 3, spark-plug, C65F35, λ = 1.4 time-series surface plot

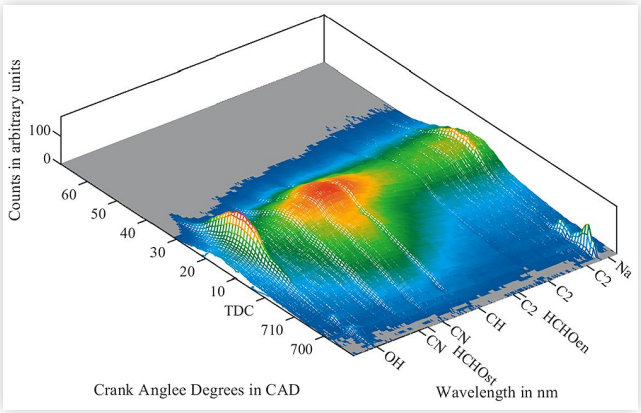

both associated CN peaks as well as CH, shortly after which they diminish in intensity. While OH and CH continue to rise strongly until the fired top dead center, the individual band for CH decreases subsequently while OH grows stronger in intensity until the peak around 18 CAD aFTDC, aligning with the association of Irimescu et al. [23] of the flame propagation phase. Meanwhile, CN emission vanishes shortly after the initial ignition phase. In the first two distinct spectral positions, a slight C_2-emission is observed. A strong signal centered at 589 nm, attributed to sodium, is present, ranging from the ignition stage towards the end of detectable emission. Of the spectrally broader bands, both emissions are observed between 300 and 480 nm with a slight peak almost matching FTDC, consisting of Vaidya's hydrocarbon and Emeleus' cool flame band, indicative of a cool flame and a weak mixture. After FTDC, OH and sodium as well as a broadband radiation spanning the Emeleus band grows in intensity, marking the transition from the flame propagation phase, along with a broadband signal ranging over the whole wavelength range, which is probably attributable to CO_2 emergence.

From 25 CAD aFTDC onwards the OH, CH and Na signals fall sharply in intensity and broadband emissions are mostly still detectable, which the authors attribute to the late oxidation stage. In comparison, C65F35, Figure 20, also shows distinct OH and CN for the ignition stage, followed by a steep decline. At 589nm, a spike in the sodium emission is detected. Up to TDC, a broadband signal spanning Vaidya's and Emeleus' bands are detectable, however, the emissions from CH and C_2 are barely detectable. The CAD positions for the maxima of OH, Na, and other visible bands almost matches the RON95 case. From TDC up to 9 CAD aFTDC, Emeleus' band is more prominent than for RON95 and is clearly distinguishable. This fits well with the proposed increased production rate of formaldehyde in the oxidation of DMC, [15].

From 9 CAD aFTDC onwards, the transition to flame propagation matches with the rise in OH and broadband intensity attributable to CO_2.

The Start of Injection sweep offered no significant change in spectral evaluation. Depending on the selected ignition time, the spectrum advanced or retreated on the time axis. A variation of the temporal expansion for the Emeleus band was observed for lean operation at SOI = 590 CAD and later, which was spatially visible for the ROI 4 and 5. A very similar behavior was noticeable for the rich mixture at λ = 0.8, as depicted in the following figures. All contour plots have a fixed scaling for the levels in steps of 20 up to 100, and after that of 100 counts; the color bar adapts to the corresponding maximum recorded intensity of the operating point.

Figure 21 and Figure 22 are located at ROI = 3 around the spark-plug. For RON95, as before at λ = 1.4, CN is barely detectable and CH emits a strong signal. Up to TDC, a distinct emission from the first two C_2 Swan bands is identified, as well as a prominent and lasting Na. C65F35 shows no detectable C_2 emission and an advanced more prominent emission in the Emeleus band, indicating increased HCHO production. The first detectable emission is about 2 CAD after that of RON95, while OH and the remaining broadband emissions fall below the detection limit almost 20 CAD earlier. Based on OH* and the flame luminescence, we expect a hotter flame and more intense reaction at ROI = 4, while at ROI = 2, a decline for C65F35 is expected, with little influence on gasoline combustion.

FIGURE 22 ROI = 3, spark-plug, C65F35, λ = 0.8

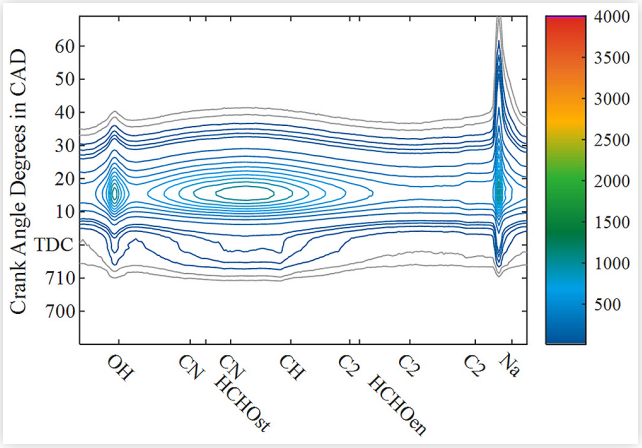

Apart from the missing CN emission that is expected due to the spatial change, a qualitative comparison of ROI = 3 and 4 yields no relevant differences. For RON95, Figure 23, CH is present up to the transition towards flame propagation, while C65F35, Figure 24, again exhibits increased intensity in the broadband HCHO region while emitting no detectable C_2 emission. If we look at ROI = 2 in more detail, a very similar pattern emerges at the exhaust valves, Figure 25 and Figure 26.

Throughout the chamber, C65F35 presents no detectable C_2 emission, which results in less soot overall. Gaydon et al.'s prediction also holds true for reduced CH emission as well as for the unchanged high OH intensity. An increased production rate for formaldehyde due to the oxidation of DMC, before transitioning into the flame propagation phase, could also be verified, [15].

There is a prominent Na-signal detectable under all testing conditions and for both tested fuels. Sodium luminescence in engine combustion has been carefully analyzed by Merola et al., [28]. However, those investigations were based on combustion with water addition, while in the present study no additional water is used. Therefore, both fuels are currently being tested for their sodium content, since fuel contained sodium seems to be the most likely cause for this observation.

FIGURE 21 ROI = 3, spark-plug, RON95, λ = 0.8

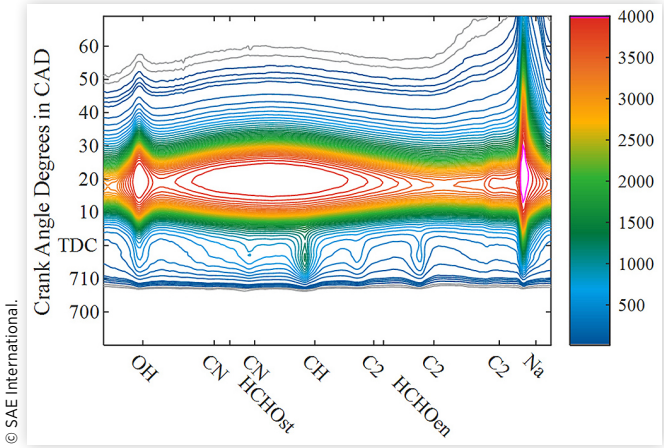

FIGURE 23 ROI = 4 intake valves, RON95, λ = 0.8

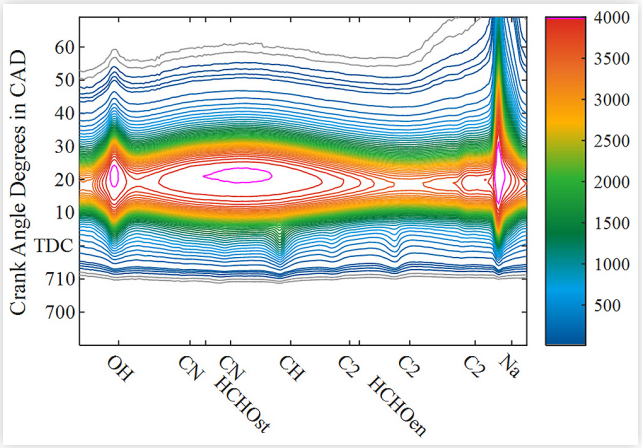

FIGURE 24 ROI = 4, intake valves, C65F35, λ = 0.8

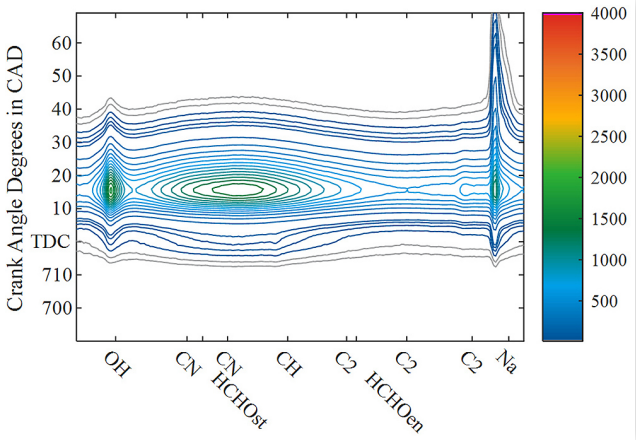

FIGURE 25 ROI = 2, exhaust valves, RON95, λ = 0.8

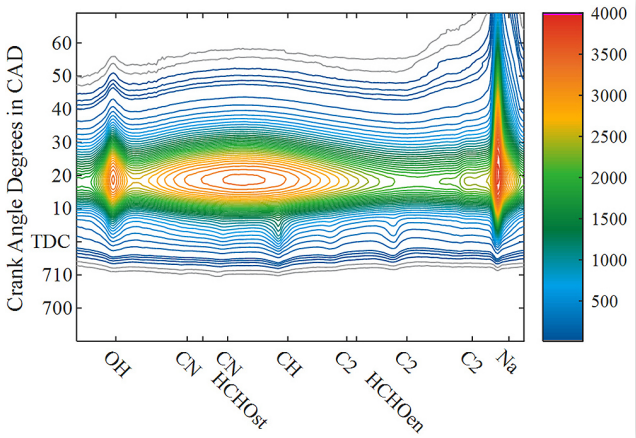

FIGURE 26 ROI = 2, exhaust valves, C65F35, λ = 0.8

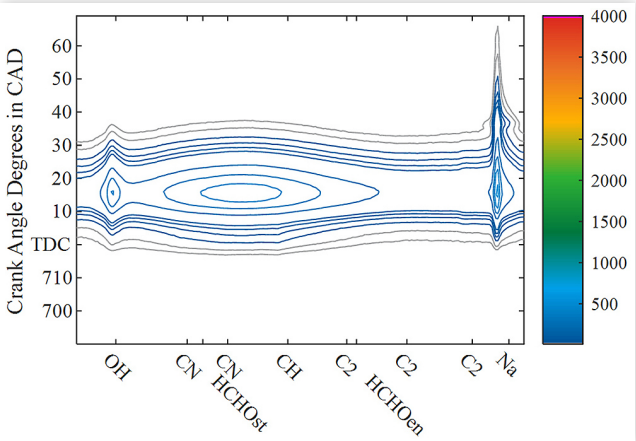

Summary/Conclusions

In this study, a thermodynamic and optical comparison of the oxygenate mixture 65 vol-% Dimethyl Carbonate and 35vol-% Methyl Formate with regular RON95 as a reference was performed.

The recorded natural flame luminescence provided insight into the overall combustion processes, while the simultaneously recorded OH*-chemiluminescence characterized the reaction zone growth. A sweep of the equivalence air fuel ratio λ from 0.8 to 1.4 concluded strong diffusive combustion for RON95 at lambda = 0.8. A sweep of the SOI from 390 to 630 CAD presented another limit at SOI = 630 CAD for RON95, since intense diffusion flames were again present. The late SOI led to a spike in the CoV of the IMEP; valued at 13.4%, deeming the operating point unusable in actual application. Spatial analysis of the OH*-chemiluminescence substantiated significant local in-cylinder cooling due to the prolonged injection time and increased total enthalpy of vaporization for the increased necessary mass of C65F35. Furthermore, spatial position indicated a shift towards the exhaust valves for lean operation and towards the intake valves for late start of injection and rich mixture conditions.

Detailed information about the involved radicals could be achieved by spectrally resolving the flame with high temporal and spatial resolution. The lack of detectable C_2 emission compared to RON95 can be traced back to the missing C-C bonds, as does the reduction in CH emission. Also indicative of reduced in-cylinder temperatures is the diminished signal intensity for C65F35 at identical recording parameters. To exclude a false conclusion, however, a relative investigation of the radicals' production rates in the chemical reaction path of RON95 and C65F35 is required.

Even at rich conditions, where regular gasoline already suffers from soot emission, a significantly cleaner combustion could be observed.

The spatially and temporally resolved spectral distribution grants possibilities for the validation of chemical kinetic simulations.

In summary, the oxygenate fuel granted enhanced operating limits towards leaner mixtures and more flexibility in the available injection timing range, enabling later injections.

To evaluate the oxygenate's potential in more detail, further investigations - including mixtures incorporating methanol and ethanol - are planned for the near future.

References

1. European Community, "REGULATION (EU) 2019/631 OF THE EUROPEAN PARLIAMENT AND OF THE COUNCIL of 17 April 2019 Setting CO2 Emission Performance Standards for New Passenger Cars and for New Light Commercial Vehicles, and Repealing Regulations (EC) No 443/2009 and (EU) No 510/2011," 2019.
2. European Community, "DIRECTIVE 2014/94/EU OF THE EUROPEAN PARLIAMENT AND OF THE COUNCIL of 22 October 2014 on the Deployment of Alternative Fuels Infrastructure," 2014.
3. Härtl, M., Stadler, A., Blochum, S., and Pélerin, D., "DMC+ as Particulate Free and Potentially Sustainable Fuel for DI SI Engines," Geringer, B. and Lenz, H.P. (eds.), in *39. Internationales Wiener Motorensymposium* April 26-27, 2018: In zwei Bänden, Fortschritt-Berichte VDI Reihe 12,

Verkehrstechnik, Fahrzeugtechnik, Nr. 807, 2, VDI-Verlag, Düsseldorf, ISBN 978-3-18-380712-3:202-229, 2018.

4. Menrad, H., Haselhorst, M., and Erwig, W., "Pre-Ignition and Knock Behavior of Alcohol Fuels," , doi:10.4271/821210.
5. Bargende, M., "Schwerpunkt-Kriterium und automatische Klingelerkennung. Bausteine zur automatischen Kennfeldoptimierung bei Ottomotoren," *Motortechnische Zeitschrift (MTZ)* 56:632-638, 1995.
6. Kalghatgi, G.T., "The Outlook for Fuels for Internal Combustion Engines," *International Journal of Engine Research* 15(4):383-398, 2014, doi:10.1177/1468087414526189.
7. Badra, J.A., Bokhumseen, N., Mulla, N., Sarathy, S.M. et al., "A Methodology to Relate Octane Numbers of Binary and Ternary N-Heptane, Iso-Octane and Toluene Mixtures with Simulated Ignition Delay Times," *Fuel* 160:458-469, 2015, doi:10.1016/j.fuel.2015.08.007.
8. Heywood, J.B., "*Internal Combustion Engine Fundamentals*," Mechanical Engineering, ISBN 978-1260116106, 2018.
9. Mei, D., Hielscher, K., and Baar, R., "Study on Combustion Process and Emissions of a Single-Cylinder Diesel Engine Fueled with DMC/Diesel Blend," *J. Energy Eng.* 140(1):4013004, 2014, doi:10.1061/(ASCE)EY.1943-7897.0000168.
10. Pastor, J.V., García-Oliver, J.M., García, A., Micó, C. et al., "A Spectroscopy Study of Gasoline Partially Premixed Compression Ignition Spark Assisted Combustion," *Applied Energy* 104:568-575, 2013, doi:10.1016/j.apenergy.2012.11.030.
11. Pélerin, D., Gaukel, K., Härtl, M., Jacob, E. et al., "Potentials to Simplify the Engine System using the Alternative Diesel Fuels Oxymethylene Ether OME1 and OME3−6 on a Heavy-Duty Engine," *Fuel* 259:116231, 2020, doi:10.1016/j.fuel.2019.116231.
12. Pöllmann, S., Härtl, M., and Wachtmeister, G., "Injection Process of the Synthetic Fuel Oxymethylene Ether: Optical Analysis in a Heavy-Duty Engine," , doi:10.4271/2020-01-2144.
13. Liu, J., Wang, H., Li, Y., Zheng, Z. et al., "Effects of Diesel/PODE (Polyoxymethylene Dimethyl Ethers) Blends on Combustion and Emission Characteristics in a Heavy Duty Diesel Engine," *Fuel* 177:206-216, 2016, doi:10.1016/j.fuel.2016.03.019.
14. Ma, Y., Cui, L., Ma, X., and Wang, J., "Optical Study on Spray Combustion Characteristics of PODE/Diesel Blends in Different Ambient Conditions," *Fuel* 272:117691, 2020, doi:10.1016/j.fuel.2020.117691.
15. Abdalla, A. and Liu, D., "Dimethyl Carbonate as a Promising Oxygenated Fuel for Combustion: A Review," *Energies* 11(6):1552, 2018, doi:10.3390/en11061552.
16. Chan, J.H., Tsolakis, A., Herreros, J.M., Kallis, K.X. et al., "Combustion, Gaseous Emissions and PM Characteristics of Di-Methyl Carbonate (DMC)-Gasoline Blend on Gasoline Direct Injection (GDI) Engine," *Fuel* 263:116742, 2020, doi:10.1016/j.fuel.2019.116742.
17. Wagner, C., Keskin, M.-T., Grill, M., Bargende, M. et al., "Potential Analysis and virtual Development of SI Engines Operated with DMC+," Bargende, M., Reuss, H.-C., and Wagner, A. (eds.), in *20. Internationales Stuttgarter Symposium: Automobil- und Motorentechnik, Proceedings*, 1st ed., Springer Fachmedien Wiesbaden, Wiesbaden, ISBN 9783658309954:49-74, 2020.
18. Blochum, S., Gadomski, B., Retzlaff, M., Thamm, F. et al., "Potential Analysis of a DMC/MEFo Mixture in a DISI Single and Multi-Cylinder Light Vehicle Gasoline Engine," in *SAE Technical Paper Series, SAE Technical Paper Series, WCX SAE World Congress Experience*, Apr. 13, 2021, Warrendale, PA, 2021.
19. Härtl, M., Pélerin, D., Dworschak, P., Maier, T. et al., "Potential of the Sustainable C1 Fuels OME, DMC, and MeFo for Particle-Free Combustion in SI and CI Engines," 459-478.
20. Gaydon, A.G., *The Spectroscopy of Flames* (Dordrecht: Springer Netherlands, 1974).
21. Krishnamachari, S.L.N.G., and Broida, H.P., "Effect of Molecular Oxygen on the Emission Spectra of Atomic Oxygen-Acetylene Flames," *The Journal of Chemical Physics* 34(5):1709-1711, 1961, doi:10.1063/1.1701067.
22. Irimescu, A. and Merola, S.S., "Spark Discharge and Flame Inception Analysis through Spectroscopy in a DISI Engine Fuelled with Gasoline and Butanol," *IOP Conf. Ser.: Mater. Sci. Eng.* 252:12093, 2017, doi:10.1088/1757-899X/252/1/012093.
23. Irimescu, A., Merola, S.S., Di Iorio, S., and Vaglieco, B.M., "Opto-Thermal Analysis of the Combustion Process in a DISI Engine Fueled with Gasoline and Ethanol," , 2009, doi:10.1063/1.5138827.
24. Sheinson, R.S. and Williams, F.W., "Chemiluminescence Spectra from Cool and Blue Flames: Electronically Excited Formaldehyde," *Combustion and Flame* 21(2):221-230, 1973, doi:10.1016/S0010-2180(73)80026-4.
25. Catapano, F., Di Iorio, S., Sementa, P., and Vaglieco, B.M., "Characterization of CH 4 and CH 4 /H 2 Mixtures Combustion in a Small Displacement Optical Engine," *SAE Int. J. Fuels Lubr.* 6(1):24-33, 2013, doi:10.4271/2013-01-0852. https://doi.org/10.4271/2013-01-0852.
26. Merola, S.S., Sementa, P., Tornatore, C., and Vaglieco, B.M., "Knocking Diagnostics in the Combustion Chamber of Boosted Port Fuel Injection Spark Ignition Optical Engine," *IJVD* 49(1/2/3):70, 2009, doi:10.1504/IJVD.2009.024241.
27. Merola, S.S., Di Iorio, S., Irimescu, A., Sementa, P. et al., "Spectroscopic Characterization of Energy Transfer and Thermal Conditions of the Flame Kernel in a Spark Ignition Engine Fueled with Methane and Hydrogen," *International Journal of Hydrogen Energy* 42(18):13276-13288, 2017, doi:10.1016/j.ijhydene.2017.03.219.
28. Merola, S.S., Irimescu, A., and Vaglieco, B.M., "Influence of Water Injection on Combustion Identified through Spectroscopy in an Optical Direct Injection Spark Ignition Engine," *Fuel* 273:117729, 2020, doi:10.1016/j.fuel.2020.117729.
29. Martinez, S., Irimescu, A., Merola, S., Lacava, P. et al., "Flame Front Propagation in an Optical GDI Engine under Stoichiometric and Lean Burn Conditions," *Energies* 10(9):1337, 2017, doi:10.3390/en10091337.
30. Tang, Q., Liu, H., Li, M., Yao, M. et al., "Study on Ignition and Flame Development in Gasoline Partially Premixed Combustion Using Multiple Optical Diagnostics,"

Combustion and Flame 177:98-108, 2017, doi:10.1016/j.combustflame.2016.12.013.

31. Merola, S.S. and Vaglieco, B.M., "Knock Investigation by Flame and Radical Species Detection in Spark Ignition Engine for Different Fuels," *Energy Conversion and Management* 48(11):2897-2910, 2007, doi:10.1016/j.enconman.2007.07.011.
32. Merola, S.S., Valentino, G., Tornatore, C., and Marchitto, L., "In-Cylinder Spectroscopic Measurements of Knocking Combustion in a SI Engine Fuelled with Butanol-Gasoline Blend," *Energy* 62:150-161, 2013, doi:10.1016/j.energy.2013.05.056.
33. Bowditch, F.W., "A New Tool for Combustion Research A Quartz Piston Engine," SAE Technical Paper 610002, 1961, https://doi.org/10.4271/610002.
34. Peer, J., Backes, F., Sauerland, H., Härtl, M. et al., "Development of a High Turbulence, Low Particle Number, High Injection Pressure Gasoline Direct Injection Combustion System," *SAE Int. J. Engines* 9(4):2301-2311, 2016, doi:10.4271/2016-01-9046. https://doi.org/10.4271/2016-01-9046.
35. Stadler, A., Sauerland, H., Härtl, M., and Wachtmeister, G., "The Potential of Gasoline Fueled Pre Chamber Ignition Combined with Elevated Compression Ratio," in *SAE Technical Paper Series, SAE Technical Paper Series, WCX SAE World Congress Experience*, Apr. 21, 2020, Warrendale, PA, 2020, https://doi.org/10.4271/2020-01-0279.
36. Gleis, S., Frankl, S., Waligorski, D., Prager, D.-I.M. et al., "Investigation of the High-Pressure-Dual-Fuel (HPDF) Combustion Process Of Natural Gas on a Fully Optically Accessible Research Engine," , doi:10.4271/2019-01-2172.
37. Verhelst, S., Turner, J.W.G., Sileghem, L., and Vancoillie, J., "Methanol as a Fuel for Internal Combustion Engines," *Progress in Energy and Combustion Science* 70:43-88, 2019, doi:10.1016/j.pecs.2018.10.001.

Contact Information

Markus Mühlthaler
Insitute of Internal Combustion Engines
Technical University of Munich
Schragenhofstraße 31, 80992 Munich, Germany
muehlthaler@lvk.mw.tum.de

Acknowledgments

Markus Mühlthaler - Conceptualization, Methodology, Software, Validation, Investigation, Formal analysis, Writing - Original Draft, Visualization **Sebastian Blochum** - Conceptualization, Methodology, Investigation, Formal analysis, Validation, Writing - Review & Editing **Andreas Stadler** - Methodology, Investigation **Martin Härtl** - Project administration, Writing - Review & Editing **Georg Wachtmeister** - Supervision, Funding acquisition **Akiyasu Miyamoto** - Project administration **Henning Sauerland** - Writing - Review & Editing, Project administration, Funding acquisition

Definitions/Abbreviations

aFTDC - after Fired Top Dead Center
bFTDC - before Fired Top Dead Center
AFR - Air-Fuel Equivalence Ratio
AHRR - Apparent Heat Release Rate
AR - Anti-Reflection
BBAR - Broadband Anti-Reflection
BP - Bandpass
C65F35 - Fuel with 65 vol-% DMC, 35 vol-% MeFo
C - Carbon
C2 - Diatomic Carbon
CAD - Crank Angle Degree
CFPP - Cold Filter Plugging Point
CH - Methylidyne Radical
CH4 - Methane
CMOS - Complementary Metal-Oxide-Semiconductor
CN - Cyano Radical
CO - Carbon Monoxide
CO_2 - Carbon Dioxide
CoV - Coefficient of Variation
DI - Direct Injection
DISI - Direct Injection Spark Ignited
DMC - Dimethyl Carbonate
DOHC - Double Overhead Camshaft
DVPE - Dry Vapor Pressure Equivalent
ECU - Electronic Control Unit
EtOH - Ethanol
FTDC - Fired Top Dead Center
H2 - Hydrogen
HC - Hydrocarbon
HCHO - Formaldehyde
HCO - Triatomic Formyl Radical
HPP - High Pressure Pump
HS - High-Speed
HSC - High-Speed Camera
IGN - Start of Ignition
IRO - Intensified Relay Optics
IMEP - Indicated Mean Effective Pressure
LHV - Lower Heating Value
MeFo - Methyl Formate
MeOH - Methanol

MFB - Mass Fraction Burned
Na - Sodium
NOx - Oxides of Nitrogen (NO and NO_2)
O_2 - Oxygen
OD - Optical Density
OH* - Electronically Excited Hydroxil Radical
PFI - Port Fuel Injection
PM - Particle Matter
PN - Particle Number
POMDME - Poly Oxymethylene Dimethyl Ethers
RGB - Red/Green/Blue
ROI - Region of Interest
RON - Research Octane Number
RPM - Revolutions per Minute
SI - Spark Ignited
SOI - Start of Injection
TDC - Top Dead Center
THC - Total Hydrocarbons
UV - Ultraviolet
°CA - Crank Angle Degree
λ - Air-Fuel Equivalence Ratio

ISSN 0148-7191

B.3 Comparison of Promising Sustainable C1-Fuels Methanol, Dimethyl Carbonate, and Methyl Formate in a DISI Single-Cylinder Light Vehicle Gasoline Engine

2021-01-1204 Published 21 Sep 2021

Comparison of Promising Sustainable C1-Fuels Methanol, Dimethyl Carbonate, and Methyl Formate in a DISI Single-Cylinder Light Vehicle Gasoline Engine

Sebastian Blochum, Felix Fellner, Markus Mühlthaler, Martin Härtl, and Georg Wachtmeister
Technical University of Munich

Naoki Yoneya Hitachi Ltd

Henning Sauerland Hitachi Europe GmbH

Citation: Blochum, S., Fellner, F., Mühlthaler, M., Härtl, M. et al., "Comparison of Promising Sustainable C1-Fuels Methanol, Dimethyl Carbonate, and Methyl Formate in a DISI Single-Cylinder Light Vehicle Gasoline Engine," SAE Technical Paper 2021-01-1204, 2021, doi:10.4271/2021-01-1204.

Abstract

On the way to a climate-neutral mobility, synthetic fuels with their potential of CO_2-neutral production are currently in the focus of internal combustion research. In this study, the C1-fuels methanol (MeOH), dimethyl carbonate (DMC), and methyl formate (MeFo) are tested as pure fuel mixtures and as blend components for gasoline. The study was performed on a single-cylinder engine in two configurations, thermodynamic and optical. As pure C1-fuels, the previously investigated DMC/MeFo mixture is compared with a mixture of MeOH/MeFo. DMC is replaced by MeOH because of its benefits regarding laminar flame speed, ignition limits and production costs. MeOH/MeFo offers favorable particle number (PN) emissions at a cooling water temperature of 40 °C and in high load operating points. However, a slight increase of NO_x emissions related to DMC/MeFo was observed. Both mixtures show no sensitivity in PN emissions for rich combustions. This was also verified with help of the optical engine. DMC was also used as a blend component for gasoline. Advantages in PN emissions, knock resistance and injector tip coking were observed. Furthermore, to evaluate resistance against abnormal combustions of pure C1-fuels, two knock resistant fuels, toluene and pure MeOH were used as reference. Resistance against abnormal combustions was investigated at the operating point at 1500 rpm / 17 bar IMEP / ε = 14.91 with the T_{intake} increased until initial abnormal combustions were detected. Finally, DMC/MeFo was used in a scavenged pre-chamber to determine the potential of the ultra-low soot combustion inside the pre-chamber. Therefore, the lean limit of DMC/MeFo was extended to λ = 2.2 and an indicated efficiency of more than 41 % was achieved at 7 bar IMEP.

Keywords

DISI engines, light-vehicle, single-cylinder, optical engine, future combustion engine, particle number emissions, PN, harmful emissions, climate emissions, NO_x, CO, CO_2, gasoline, alternative fuels, C1-fuels, E-fuels, synthetic fuels, oxygenates, blends, DMC, MeFo, MeOH, methanol, toluene, abnormal combustion, engine knock, pre-ignition, low speed pre-ignition, LSPI, RON, MON, high compression ratio, scavenged pre-chamber, injector tip coking,

Introduction

The European Commission proposed the 'European Climate Law' in 2020, with the goal of making Europe the first climate-neutral continent by 2050 [1]. The proposal includes an increase of the EU's GHG emission reduction target for 2030 by 5 to 55 % compared with 1990 levels. To achieve this ambitious target, synthetic fuels on a non-fossil basis have to be introduced into the market for future internal combustion engines (ICEs) to reduce CO_2 emissions [2]. The possibility of tailoring these fuels to the specific demands of the application unlocks an additional degree of freedom in ICE research to optimize efficiency [3], while also minimizing pollutant emissions [4, 5]. In 2017, the transport sector was responsible for approx. 32 % of the total CO_2 emissions in the EU, whereof over 31 % were emitted by passenger cars [6]. In 2019, about 53 % of the EU´s passenger car fleet used gasoline engines and approx. 59 % of new car registrations were delivered with a gasoline powertrain (exclusive of hybrid ICE cars 7 %) [7]. This circumstance highlights the urgent need to especially replace fossil gasoline fuel in the near future.

Therefore, two promising alternative fuel types for gasoline direct injection (DI) spark-ignition (SI) engines were investigated. One type is gasoline blended with a synthetic C1-fuel, with the intention to launch to the market and reduce CO_2 emissions of the existing car fleet in a short-term scenario [8]. The second type uses only C1-fuel mixtures, which leads to soot-less combustion due to missing C-C bonds in the molecular structure [9]. Furthermore, these fuels offer the possibility of launching a closed CO_2-cycle, which allows for ICE climate-neutral operation. This solution is intended for a long-term scenario.

In this study, the C1-fuels dimethyl carbonate (DMC), methyl formate (MeFo) and methanol (MeOH) were investigated. These fuels feature the possibility of sustainable production [10, 11]. In general, MeOH can be produced using renewable hydrogen (H_2) for the chemical reduction of CO_2 [12]. In a next step, DMC as well as MeFo can be produced from MeOH and the oxides of carbon [13]. Ideally, the sustainable "green" CO_2 will be captured from the air to close the CO_2-cycle [14]. However, if flue gas from e.g. power-, cement-, industrial-, chemical plants is available, this CO_2 source should be preferred to increase production efficiency [15].

DMC is a clear colorless liquid carbonate ester, which is non-toxic and biodegradable. It is commonly used as a solvent or methylating agent [16]. However, in several publications it has already been used as a blend component for gasoline engines [17, 18] as well as a fuel additive in diesel engines [19, 20] because of its high knock resistance [21] and its positive effects on particle formation, respectively [13]. Pure DMC is not suitable for DISI engines, because of its low dry vapor pressure equivalent (DVPE) of 10.8 kPa and a freezing point at 4 °C. Thus, DMC has to be blended with more volatile components to improve the mixture formation and ensure low temperature stability.

MeOH is a clear colorless liquid alcohol and it is the simplest liquid carbonaceous molecule at STP [22]. It is highly toxic to the human body [23], but biodegradable and one of the most widely used chemicals. Nevertheless, it has already been extensively investigated in the ICE as a gasoline replacement as well as a blend component [22]. Furthermore, MeOH has also been successfully tested in field studies [24] and is still an important topic in ICE research [25, 26]. The DVPE of MeOH is approximately 3 times higher than for DMC, but still only half of that of conventional gasoline. As for DMC, blending MeOH with volatile components to improve the mixture formation is commonly recommended.

MeFo is the methyl ester of formic acid. It is a clear, colorless liquid, which is used as a solvent and cooling agent [27]. MeFo has already been investigated in a baseline DISI engine test [13] and its basic combustion properties have been determined [28]. From its usage as a cooling agent, it can be concluded that MeFo has a very high DVPE of 119.8 kPa, which is twice as high as for gasoline, and a relatively low boiling point of 31.5 °C. Originating from these properties, MeFo is suitable as a blend component to enhance mixture formation in gasoline engines.

Hence, for the C-1, fuel mixtures of DMC and MeOH are used as base fuels, while MeFo is added as a blend component to raise the relatively low DVPE of the base fuels. For the mixture of DMC/MeFo, a ratio of 65:35 was chosen since its potential has already been demonstrated [29, 30]. The mixture is patented [31] and has been extensively tested in single- and 4-cylinder DISI engines [32]. Throughout these investigations, the following advantages and disadvantages compared to conventional gasoline fuel were determined:

TABLE 1 Advantages and disadvantages of DMC/MeFo over Gasoline

Advantages	Disadvantages
• High knock resistance • Low NO_x, PN and VOC raw emissions • Low toxicity • Low coking deposits • Low stoichiometric air-fuel ratio (AFR stoich.) • Liquid at standard temperature and pressure (STP)	• Only ~ 36 % of the gasoline lower heating value (LHV) • Lower laminar flame speed • Incompatible with several common sealing materials

The second C1-fuel mixture option, MeOH/MeFo, was selected because of the higher laminar flame speed and the lower production costs of MeOH. The reason for the costs are explained by the shorter manufacturing process [33]. The main disadvantage of MeOH is its high toxicity, which has to be taken into account. During this study, the knock resistance of the C1-fuel mixtures in relation to the well-known high knock resistant fuels, pure MeOH and toluene, was determined.

From the C1-fuels, DMC was chosen as a blend candidate in this study primarily because of its positive effects on particulate emissions, even with a low blend ratio of 8 vol.-% [34]. Secondarily, the chemical stability and miscibility with gasoline has already been documented [35]. In turn, a stabilizer has to be found for MeFo, because it hydrolyzes if water is present [36]Investigation of the DMC blend has not only been focused on combustion behavior and exhaust emissions, but also on the influence of the DMC ratio on the injector tip coking phenomenon. This injector tip coking deposit results in a PN drift towards higher emissions [37].

To simplify the naming of the different fuels, a naming convention is introduced. Each fuel is abbreviated with one letter followed by its ratio in vol.-%. The letters are G for gasoline, M for MeOH, C for DMC and F for MeFo. So, for example, G70C30 represents a mixture of 70 vol.-% gasoline and 30 vol.-% DMC. Table 2 shows the fuel properties of all of the used fuels in this study. The LHV is calculated using DULONG's formula modified by GUMZ [38]. Not referenced values written in *italic* are calculated, and numbers marked with a * are identified by fuel analysis.

In summary, the study evaluates the impact of the DMC ratio in a gasoline fuel blend on raw emissions, engine performance and coking behavior. The advantages aim to reduce well-to-wheel CO_2 and pollutant emissions in a short-term scenario in the existing light-vehicle car fleet Additionally, the extensively tested oxygenate mixture C65F35 is evaluated against an MeOH blend with MeFo to identify the strengths of each base fuel as a renewable gasoline replacement for a long-term scenario. Therefore, engine performance, emissions and economic factors are taken in account.

TABLE 2 Fuel properties - references: [1] = [22], [2] = [28], [3] = [39], [4] = [40], [5] = [41], [6] = [42], [7] = [43], [8] = [44], [9] = [45], [10] = [46], [11] = [47]

Name	Unit	G100	G85C15	G70C30	MeFo	DMC	C65F35	M100	M85F15	M70F30	Toluene
Gasoline RON95 E5	vol. %	100	85	70	-	-	-	-	-	-	-
Dimethyl Carbonate		-	15	30	-	100	65	-	-	-	-
Methyl Formate		-	-	-	100	-	35	-	15	30	-
Methanol		-	-	-	-	-	-	100	85	70	-
Toluene		-	-	-	-	-	-	-	-	-	100
LHV	MJ/kg	*42.14*	*36.67*	*31.85*	*15.2*			*19.8*	*19.68*	*18.78*	*39.92*
Density @ 15 °C	kg/m³	750*	*~ 799*	*~ 848*	957[3]	1079[3]	1041*	790[1]	*~ 817*	*~ 842*	866[8]
Gasoline equivalent	m³/m³	*1.0*	*1.08*	*1.17*	*2.17*	*1.93*	*2.0*	*2.02*	*1.97*	*2.0*	*0.91*
RON	-	95.9*	*> 95.9*		115[3]	109[3]	117*	109[1]	-	-	111[8]
MON		85.8*	*> 85.8*		114[3]	102[3]	> 120*	92[1]	-	-	95[8]
Oxygen content	wt. %	1.86*	*12.35*	*21.54*	*53.29*			*49.93*	*50.52*	*51.08*	*0*
Hydrogen content		13.25*	*11.94*	*10.77*	*6.71*			*12.58*	*11.55*	*10.58*	*8.75*
Carbon content		84.89*	*75.71*	*67.69*	*40*			*37.48*	*37.93*	*38.34*	*91.25*
AFR stoich.	kg/kg	*14.28*	*12.31*	*10.58*	*4.64*			*6.47*	*6.16*	*5.85*	*13.54*
Boiling range	° C	31.3-192.2*	*~ 31.3-192.2*		31.5[3]	90[3]	37.5-94*	65[1]	*~ 31.5-65*		110.6[10]
DVPE @ 37.8 °C	kPa	59.8*	-	-	> 100[3]	10.8[3]	57[3]	30.7*	60.1*	80.0*	~ 70[7]
Enthalpy of vaporization	kJ/kg	~ 420[1]	*~ 420*	*~ 419*	464[3]	418[3]	433[3]	1100[1]	*1005*	*911*	413[11]
Surface tension	mN/m	~ 24[1]	-	-	25[3]	28.5[3]	27.7[3]	22.1[1]	-	-	28.5[10]
Auto-ignition temperature	° C	~ 220[1]	-	-	450[3]	458[3]	-	465[1]	-	-	480[9]
Ignition limits in air	vol.-%	1.3-7.6[1]	-	-	5-20[3]	4.2-12.9[3]	-	6.7-36[1]	-	-	1.27-7.8[9]
Min. ignition energy (MIE)	mJ	0.25[1]	-	-	0.5[6]	-	-	0.14[1]	-	-	0.24[5]
Laminar flame speed @ NTP	m/s	0.4[4]	-	-	0.33[2]	0.3[4]	-	0.68[4]	-	-	-

Experimental Setup and Methodology

Single Cylinder Engine

In this study, an in-house designed gasoline 4-stroke single-cylinder engine (SCE) was used as in previous publications [4, 13, 29, 30, 32, 39, 48, 49, 50]. The SCE has two basic configurations - thermodynamic and optical. Both configurations were used in this investigation and the specifications are listed in Table 3. This study uses a fixed standard valve timing with a moderate lift and a small overlap.

Thermodynamic Configuration The thermodynamic configuration of the SCE uses two different pistons to vary the compression ratio (CR) between 10.92 and 14.91. The high compression ratio (HCR) is used to determine the knock resistance of the oxygenated fuels. For ignition a serial spark plug and ignition coil is used. Detailed information about the thermodynamic configuration e.g. sensors and actors are explained in a previous study [32], which used the identical setup.

To identify the potential of an ultra-lean combustion using an oxygenated fuel, a brief campaign employing a scavenged pre-chamber ignition system introduced by Stadler et al. [50] was performed. Thereby, the ignition system replaced the spark plug and the HCR piston was used. The setup was

TABLE 3 SCE specifications

	Thermodynamic	Optical
Engine base	AUDI EA888	
Bore	82.51 mm	
Stroke	86.6 mm	
Connecting rod length	144 mm	
Displacement	463 cm³	
Compression ratio	10.92:1 or 14.91:1 (varied by piston design)	9.36:1
Number of valves (intake/exhaust)	2 for each	
Exhaust valve lift	7 mm @ 250 °CA aTDC	
Exhaust open	132 °CA aTDC	
Exhaust close	368 °CA aTDC	
Intake valve lift	6 mm @ 460 °CA aTDC	
Intake open	348 °CA aTDC	
Intake close	572 °CA aTDC	
Max. IMEP	17 bar	6 bar
Max. speed	3500 1/min	2000 1/min
Oil temp.	25 - 80° C	80° C
Coolant temp.	-7 - 80° C	80° C

TABLE 4 Pre-chamber Ignition system specifications

Orifices	6
Diameter	1.3 mm
Cross-sectional area	7.96 mm^2
Area to volume ratio	0.038 1/cm
Pre-Chamber volume	2.1 cm^3
Compression Ratio with HCR Piston	14.18:1

slightly modified employing standard DI instead of port fuel injection (PFI). Additionally, an optimized injector for the injection into the pre-chamber was launched. The main specifications of the pre-chamber ignition system are listed in Table 4.

Optical Configuration The main differences between the standard and the optical configuration on the hardware side is the elongated, hollow piston derived from the Bowditch principle [51]. This quartz piston has a flat piston crown and employs two different ring packs with a second dry-running liner. Therefore, the optical engine has a lower CR of 9.36 and a different combustion chamber sealing concept. Based on this design, the engine operates with a lower maximum engine speed and load. The standard spark plug, and ignition coil were applied for all shown results. Additionally, the fired operation time was limited because of a combination of thermal and mechanical loads. Therefore, the typical fired runs included a few hundred working cycles. A high-speed CMOS RGB camera (Phantom v2012, RGB) recorded the natural flame luminescence presented in this study. Further details of an equal optical configuration and data acquisition can be extracted from Mühlthaler et al. [30] and more details about the engine hardware are published by Peer et al. [49].

Fuel Direct Injection Two different types of injectors, specific to their tasks were used in this investigation. The first DI injector was used for the main injection. This multi-hole injector is side mounted in between the intake valves. The second injector is in use, if the SCE operates with the pre-chamber ignition system. This single-hole DI injector is mounted in the pre-chamber body and injects a small amount of fuel directly into the pre-chamber. The specifications of the injectors are listed in Table 5.

TABLE 5 DI Injector Specifications

Name	DI	DI-preCh
Injection	Main	Pre-chamber
Used fuel pressures	25 MPa & 35 MPa	35 MPa
Injector type	Multi-hole DI	Single-hole DI
Nozzle size	6 mm	
Actuation	Solenoid	
Number of orifices	6	1
Orifice shape	Convergent	Straight
Spray pattern	Series	Prototype
Injector position	Side mounted	Pre-chamber
Static flowrate @ 10 MPa	13.8 cm^3/s	0.99 cm^3/s

Auxiliary Units The auxiliary units are separated into four systems, namely intake, fuel, indication and exhaust system. The systems are only introduced briefly because they are already explained in detail (incl. structure diagram) in previous studies [4, 32].

With the intake air system, the charge air is filtered, compressed, cooled and dried. After the intake throttle, an air heater regulates the desired charge air temperature, followed by a plenum to calm the air motion.

The mobile fuel system is used because of the reduced effort for fuel changes and its resistance against all used fuels in this study. A cam box with a series high pressure pump generates a maximum fuel pressure (FUP) of 35 MPa. The mobile fuel system is connected via a flexible high-pressure hose to the fuel rail.

The exhaust system includes a Bosch LSU 4.9 wideband lambda probe and several exhaust measurement systems. The used devices vary between the thermodynamic and optical engine configuration. In the thermodynamic configuration, a Horiba MEXA-ONE-D1 measures the gaseous emissions of CO, CO_2, O_2, NO_X and THC (in C_3H_8 equivalent). For some fuels employed during this investigation, the unburnt fuel and intermediate molecules evince a significantly high oxygen ratio. Therefore, the more convenient 'volatile organic compound' (VOC) term is used rather than THC, in accordance to previous publications [4, 32]. However, the flame ionization detectors' (FID) response factor is generally decreased by VOCs with high oxygen ratios, and the results can therefore be misinterpreted. The VOC emissions are therefore not discussed in this study. Recently, investigations at the engine laboratory of the Technical University of Munich are carried out to measure the exhaust emissions via an FTIR (Fourier-transform infrared spectroscopy) analyzer with specific tailored methods for each fuel. This will be helpful for future investigations to clearly identify the exhaust emissions of these fuel mixtures. In the end, the Horiba MEXA-2300SPCS detects the solid-state emissions by counting non-volatile PN concentration with two condensation particle counters (CPC). The CPCs have different cut-off sizes of 23 nm and 10 nm.

The indication system includes two piezoresistive absolute pressure sensors - a Kistler 4045A10 for intake pressure and a Kistler 4075A10 for exhaust pressure. A Kistler 6056A-3-2 piezo-electric sensor measures the relative in-cylinder pressure. A magnetic incremental encoder detects the crank angle position offering a resolution of 0.1 °CA.

Engine Control and Data Acquisition

The in-house designed ECU employs a dSPACE platform. During the investigation, the λ and engine load controller were in use simultaneously. The load controller regulates the air mass flow via the intake throttle to adjust the desired engine load in indicated mean effective pressure (IMEP). The λ controller regulates the injection duration to adjust the desired λ value measured by the λ probe. For each fuel, the ETAS lambda meter settings were adopted by changing H/C-ratio, O/C-ratio, and AFR. The 50 % burnt mass fraction (MFB50) is controlled manually via the ignition timing.

The LabVIEW based data acquisition gathers all measured values and calculates further values, for example combustion parameters like the MFB50, apparent heat release rate (AHRR) and η_i. When a snapshot is triggered, the values are averaged over the following 200 cycles and stored in a snapshot file including the average pressure traces of intake, exhaust and in-cylinder. A separate snapshot file stores the pressure traces of each cycle on a crank angle base. For the optical configuration, the used high-speed cameras are triggered separately crank angle based via the ECU shortly after the snapshot. The camera records 50 working cycles approximately twenty seconds after the first fired cycle. During post-processing, the images are averaged over the middle 20 working cycles of each recording. Furthermore, different in-house designed MATLAB tools are used to analyze and evaluate the test results via different diagrams and pictures.

Results and Discussion

Standard Engine Parameters and Reference Points

During the investigation, two engine reference points were used, one for the thermodynamic and another for the optical configuration. The reference points are mid-load points, which are representing a typical engine operating point in the NEDC and they were already used in previous investigations [4, 32]. The parameters for each point are listed in Table 6. Subsequently, if parameters differ from the reference points, this is noted in the respective diagram or text passage. The start of injection (SOI) is adjusted to 430 °CA after top dead center (aTDC) to get a homogeneous mixture formation without piston wetting. For the theoretical optimum of the η_i,the MFB50 is located at 8 °CA aTDC.

In opposite to a production multi-cylinder engine, no three-way catalyst (TWC) or gasoline particulate filter (GPF) is in use. Owing to this, all discussed emissions are untreated raw emissions.

TABLE 6 Reference points parameters

Engine configuration	Thermodynamic	Optical
Engine speed in 1/min	2000	1500
Engine load IMEP in bar	7	6
λ	1.0	
MFB50 in °CA aTDC	8	
SOI in °CA aTDC	430	
Number of injections	1	
Fuel pressure	35 MPa	25 MPa
Oil temperature in °C	80 °C	
Piston cooling jet active	IMEP ≥ 11 bar	Not available
Water temperature in °C	80 °C	
Intake air temperature in °C	30 °C	

Gasoline vs. Gasoline + DMC

Pre-Investigation of Different DMC Ratios At first, some base investigations with different DMC blends were performed to identify the most promising blend ratio. Initialized from the DMC's low melting point and related to Scharrer´s investigations [35], the DMC ratio was limited to 30 vol.-%, to hold the freezing point of the mixture below - 15 °C. With this knowledge, a baseline investigation with two ratios, 15 and 30 vol.-%, was carried out. Figure 1 shows an excerpt of the baseline investigation from the thermodynamic SCE in hot conditions.

The left side shows the PN10 concentration (particle diameter > 10 nm) over a SOI variation. For a homogeneous stoichiometric combustion and a DI during intake stroke, G70C30 shows the lowest PN emissions for an SOI between 390 and 510 °CA and an averaged PN10 reduction of 58 % compared to G100 over the SOI variation. The trend of increasing PN10 emissions towards a later SOI timing is explained by less homogeneity due to reduced time for mixture formation. The right side shows the η_i over the IMEP variation. For all points marked in Figure 1 with a *, the MFB50 was shifted from 8 ° CA to later times to prevent knocking. Therefore, G70C30 shows the highest η_i benefit of relatively 4.9 % at 17 bar IMEP. The center of combustion was shifted for G70C30 only at 17 bar IMEP because of initial knocking combustions. Derived from the baseline investigation, G70C30 was chosen for the comparison because of the benefits in the η_i, PN and NO_x emissions.

Variation of Engine and Combustion Parameters In this sub-section, the engine load, the SOI and the air-fuel equivalence ratio (λ) were varied.

The lambda variation was performed with the thermodynamic engine as well as with the optical engine. The PN emissions of the thermodynamic engine tests are shown in Figure 2. In the left diagram, the PN concentration with a cut-off size of 23 nm (PN23) is shown over λ. The right diagram shows the ratio between PN10 and PN23. G100 shows the characteristic bathtub curve with its lowest PN23 level around λ = 1.3 and operates with lean mixtures up to λ = 1.6. In turn, G70C30 already reached the lean misfire limit at λ = 1.4. This is related to the worse mixture formation because of the increased DVPE and the lower combustion temperatures

FIGURE 1 DMC blends - PN10 over SOI and η_i over IMEP @ 2000 rpm / λ = 1.0 / ε = 10.92 / MFB50 = 8 °CA aTDC

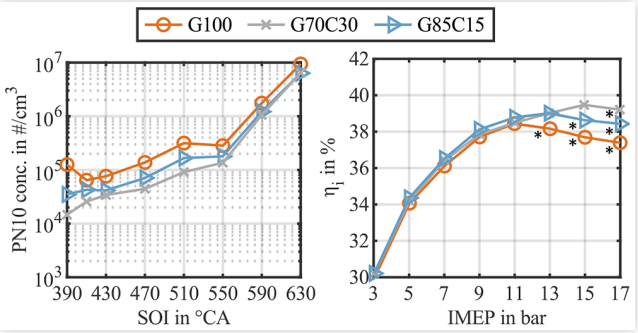

FIGURE 2 PN emissions over lambda variation with the thermodynamic engine @ 2000 rpm / 7 bar IMEP / SOI = 430 °CA a TDC / ε = 10.92 / MFB50 = 8 °CA aTDC

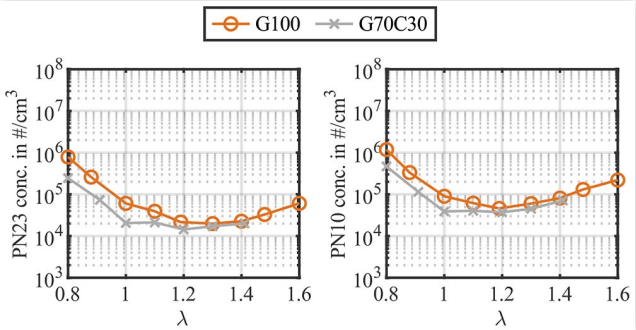

due to the need for increased heat of vaporization. However, DMC are visible for G70C30 benefits caused by the C-1 oxygenate. Up to λ = 1.3, a clear reduction in PN emissions was observed.

In general, a more incomplete combustion can take place with a homogeneous leaner mixture. Therefore, a higher unburnt or partly burnt fraction exits the combustion chamber with the exhaust gas stream and emits particles. In turn, the PN increases more significantly under rich conditions initialized by missing O_2. This effect was confirmed with the optical engine. Figure 3 shows four images recorded through the glass piston of the optical engine. For both fuels. two operating points with λ = 0.8 (left column) and λ = 1.0 (right column) are shown at 11 °CA aTDC. In each picture, the two intake and two exhaust valves are visible; the exhaust valves are located on the left and the intake valves on the right. In the picture center, the spark plug with its side electrode is apparent. The engine load and speed are slightly decreased to

FIGURE 3 λ = 0.8 (left column) and λ = 1.0 (right column) for G100 and G70C30 @ 1500 rpm / 6 bar IMEP / SOI = 430 °CA a TDC / ε = 9.36 / MFB50 = 8 °CA aTDC

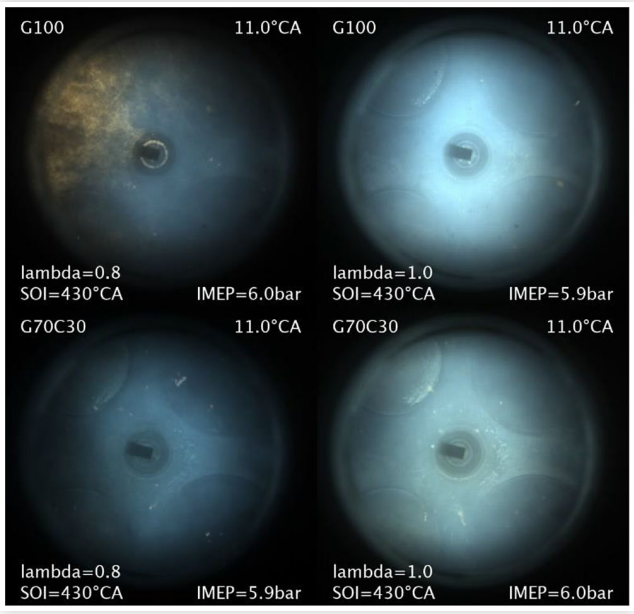

6 bar IMEP and 1500 rpm because of the already explained limited load capacity with the optical configuration. For rich mixtures, G100 in the first row shows a clearly visible yellow diffusion flame on the left top quarter of the combustion chamber, which is an indicator for an inhomogeneous mixture.

These diffusion flames normally lead to increased PN and particulate matter PM emissions in gasoline or diesel fueled engines. If soot emissions are present, the soot self-luminosity emits thermal broadband radiation. Its intensity depends on the number, temperature and diameter of the soot particles [52]. This optical result fits very well with thermodynamic testing, where G100 emits the most PN emissions for λ = 0.8. For the stoichiometric mixture, only a very few diffusion spots are detected in the picture (right side, first row). Care has to be taken since some slight details are possibly washed out during the averaging in post-processing. Overall, the record shows a bluish flame with the highest luminosity of all four recordings in Figure 3. The bluish flame is an indicator for a premixed homogeneous combustion [53] as a result of a good mixture preparation. Disregarding the soot particle radiation, a relatively higher luminosity is an indicator for an increase in gas temperatures, turbulence or flame thickness [54]. In this case, it is conclusive that the temperature increases with stoichiometric combustion as a result of less in-cylinder evaporation cooling from the injected fuel mass. The second row in Figure 3 shows G70C30 with roughly the same results as G100. Only a slightly decreased luminosity, and for λ = 0.8, only few diffusion spots are recorded. This matches well with the thermodynamic results, where G70C30 shows a decrease in PN concentration. The decreased luminosity is also conclusive due to more evaporation cooling from the increased fuel mass.

Back at the thermodynamic engine, a load and cooling water temperature variation was performed. The load was varied between 3 to 17 bar IMEP in 2 bar steps and the cooling water temperature was reduced from 80° C to 40° C and -5° C. In Figure 4, the PN23 concentration and the ratio of PN10 / PN23 for all three temperatures are illustrated under thermodynamic reference point engine conditions.

For the PN23 concentration, a clear trend of increasing particle numbers with higher engine loads and lower coolant

FIGURE 4 PN23 emissions and PN10/PN23 ratio over IMEP in bar for 80° C, 40° C and -5° C coolant temperature @ 2000 rpm / λ = 1.0 / SOI = 430 °CA a TDC / ε = 10.92 / MFB50 = 8 °CA aTDC

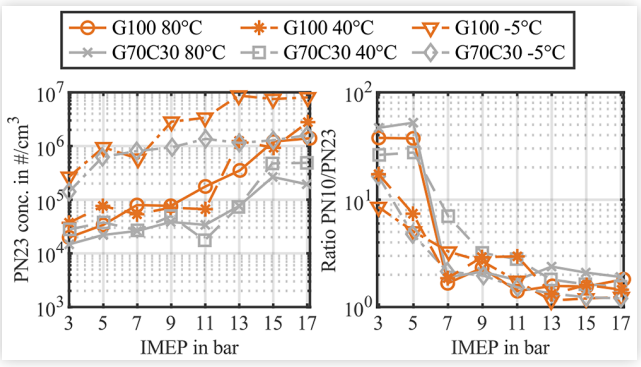

temperatures (T_c) is seen. However, the benefit of G70C30 in PN23 emissions increases with higher engine loads and T_c = 80 °C. Averaged over the load variation, a PN23 reduction of more than 62 % could be achieved. The maximum reduction of 86 % was observed at 17 bar IMEP. The PN10/PN23 ratio is extremely high for both fuels at the low load points of 3 and 5 bar IMEP. At these points, G70C30 has only a slight benefit for PN10 of around 8 %. For all other loads. the PN10 reduction by G70C30 of approx. 50 % is quite constant, except for the PN10 emissions at T_c = 40 °C. The G70C30 has fewer volatile components and needs more heat to evaporate. It is expected that the better mixture formation and the higher combustion temperatures of G100 overcomes DMCs benefit of the soot-less combustion. In turn, a larger portion of gasoline is also not evaporated at $T_{c\,=}$ -5 °C, because of the significantly lower temperature. This ends in a huge particle increase for PN23 and PN10. Summarized, DMC confirmed its big potential of soot-less combustion, especially at high loads. The gaseous NO_X emissions shown in Figure 5 increased by almost 10 % in hot conditions over the load variation for G70C30. This increase is attributed to the earlier located MFB50 at the higher engine loads, owing to the higher knock resistance of G70C30. With decreasing T_c, the NO_X emissions are increasing for both fuels and load points greater than 5 bar IMEP. This is attributed to the easier available oxygen during combustion because of the increased inhomogeneity of the air/fuel mixture at a lower T_c. As a side effect, less fuel evaporates, and the in-cylinder cooling therefore decreases. Additionally, the prompt-NO, which is formed by the Fenimore-mechanism, is mainly driven by local rich areas in the flame front [55]. The appearance of these local rich areas is increased with lower T_c. Owing to these effects, an increase of the NO_x emissions in mid and high load points is possible by decreasing the T_c. In turn, at low loads and low T_c, the decreasing peak temperatures during the combustion process inhibit the Zeldovich mechanism. This effect dominates under these operating conditions and therefore the overall NO_x emissions decrease. However, the overall rise of NO_x is much less for G70C30.

This is justified with the lower combustion peak temperatures of G70C30. Compared to G100, these are in a range where the temperature driven Zeldovich mechanism is less prominent compared to G100. Additionally for G100, the MFB50 is shifted to earlier timings because the knock tendency decreases with a lower T_c. Therefore, the lower NO_X emissions of G100 at high loads are diminished. This results in an averaged NO_x reduction of 9 % at 40 °C and 11.5 % at a -5 °C coolant temperature with G70C30.

The author already published an investigation [32] focusing on the positive effect of DMC/MeFo on combustion stability using late injections during the compression stroke. This property is favorable at low-speed operating points to sustain the tumble flow and enhance the turbulent kinetic energy (TKE) with this late fuel injection. But it is also beneficial in special combustion modes with possibly local rich areas, e.g. catalyst heating, HCCI, stratification or GPF regeneration. For example, Golzari et al. [56] also reported that with low engine speed, a late DI combined with a PFI increases efficiency compared to a single early DI. Therefore, a late SOI variation was performed during the compression stroke to identify the influence of the DMC ratio. In Figure 6, the PN23 emissions and the COV of IMEP are shown over the SOI. It was not possible to operate the SCE with G100 and SOI timing later than 610 °CA under standard operating conditions because of multiple misfires. Figure 6 shows that by increasing the DMC ratio, the operating range for the SOI can be extended by 40 °CA to an SOI up to 650 °CA. At this operating point, the ignition timing was set to 13 °CA before TDC (bTDC) to shift the MFB50 to 8 °CA aTDC. This means that there is only a gap of 41 °CA between End of Injection (EOI) and start of ignition. It is also remarkable that with G70C30 and an SOI timing of 630 °CA, the combustion stability improves again compared to the SOI at 610 °CA.

This is also noticeable in the 9 °CA later ignition timing and a shortened combustion duration. The authors expect that with the later injection the fuel is wall-guided to the spark plug. With this expectation and the fact that DMC has a broader ignition range, especially towards rich mixtures, the combustion stability rises again. Also, a significant PN23 reduction of an average of 80 % was observed between SOI 570 and SOI 610, as shown in Figure 6. This investigation was also performed on the optical configuration at the SCE. In Figure 7, an excerpt of this testing campaign presents two different operating points for both fuels with an engine speed of 1500 rpm and a 6 bar IMEP load. The left column displays the standard operating point

FIGURE 5 NO_X emissions over IMEP in bar for 80° C, 40° C and - 5° C coolant temperature @ 2000 rpm / λ = 1.0 / SOI = 430 °CA a TDC / ε = 10.92 / MFB50 = 8 °CA aTDC

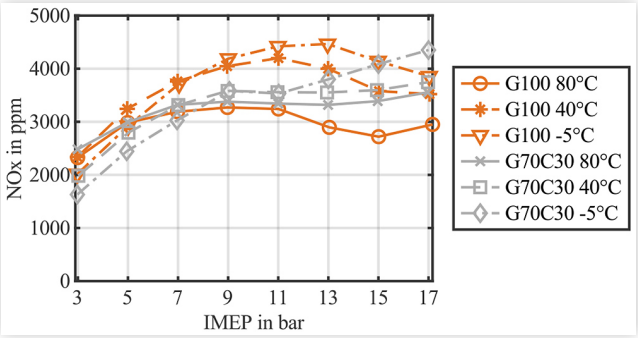

FIGURE 6 PN23 emissions and COV of IMEP over super late SOI @ 2000 rpm / 7bar IMEP / λ = 1.0 / ε = 10.92 / MFB50 = 8 °CA aTDC

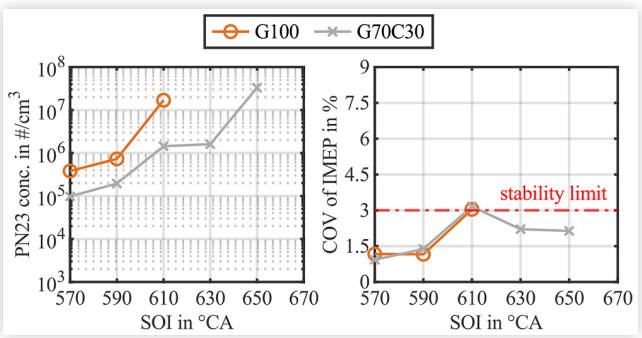

FIGURE 7 SOI = 430 °CA (left column) and SOI = 630 °CA (right column) for G100 and G70C30 @ 1500 rpm / 6 bar IMEP / λ = 1.0 / ε = 9.36 / MFB50 = 8 °CA aTDC

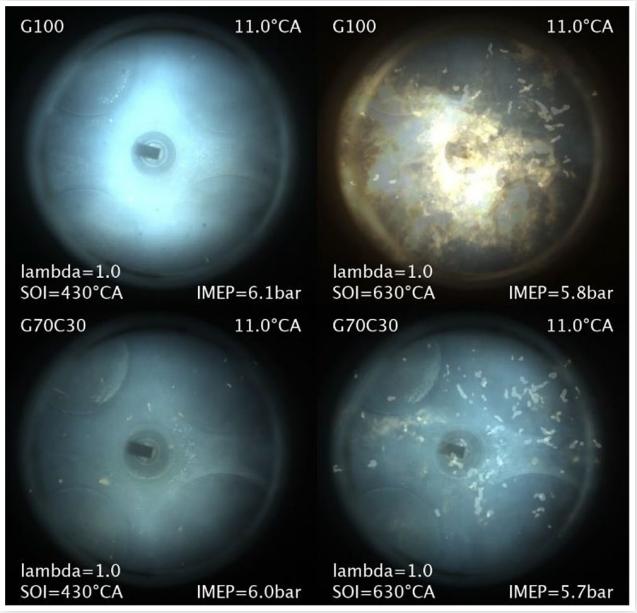

FIGURE 8 PN23 conc. and PN10/PN23 ratio over 90 minutes @ 2000 rpm / 7 bar IMEP / FUP 25 MPa / λ = 1.0 / SOI = 430 °CA a TDC / ε = 10.92 / MFB50 = 8 °CA aTDC

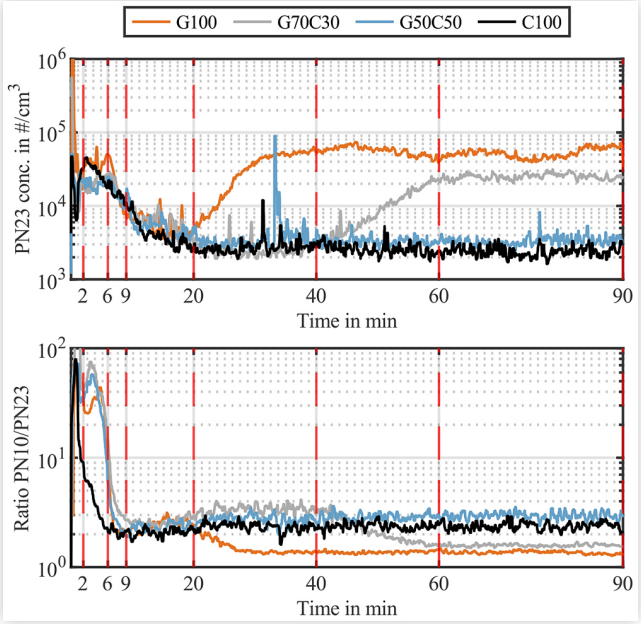

with the standard SOI timing of 430 °CA during the intake stroke. The images of the right column show the operating point with an SOI of 630 °CA, which is the latest injection timing in which the G100 mixture was ignitable. However, first misfires occurred under this operating condition, and the combustion was quite unstable with G100. For G100 and the SOI of 630 °CA, most of the image is covered with diffusion flames, again confirming the high level of PN23 emissions from Figure 6. For G70C30, only diffusion spots are detected matching the results of the thermodynamic investigations very well, whereby the DMC ratio reduces the PN23 emissions by around 80 %. In general, similarly as during the lambda variation in Figure 3, G100 shows a significantly higher intensity with the standard operating parameters. This is explained by the higher temperatures of G100 during combustion.

Direct Injector Tip Coking In this subsection, the effect of the DMC blend ratio on the injector tip coking phenomenon is investigated. For this, the engine is operated stationary under reference conditions (2000 rpm & 7 bar IMEP), except for the DI FUP, which is reduced from 35 MPa to 25 MPa to promote the coking procedure. These coking runs started with a clean injector tip and the PN record starts with the first fire of the engine. To exclude the influence of the common step hole geometry of the injector orifices, an injector without step holes was selected. Figure 8 shows the trace of the PN23 concentration and the PN10/PN23 ratio from the 90 minutes coking runs. The marks on the x-axis highlight the time stamps when the engine was stopped to remove the injector to take a picture of the injector tip with a digital microscope. Afterwards, the injector was cleaned and re-installed for the next coking run to keep the conditions similar. The close-up images of the injector tip are presented in Figure 9. Each column displays one fuel, and each row shows the tip condition at the respective time. For a more representative result, pure DMC and the additional G50C50 mixture were used. Figure 9 also shows an exemplary side-DI injector in side- and front-view with a magnified section-view of the injector tip. The PN23 concentration trace in Figure 8 is quite close for each fuel for the first 9 minutes of the coking run, except during the first second of the trace. This initial particle peak from engine start decreases with higher DMC ratios. However, the injector tips are on a variously advanced coking stage after the first 9 minutes, as can be seen in Figure 9. The image of G100 already has a strongly coked injector tip and those of C100 are completely clean. So, the coking state of the injector tip at 9 min has no influence on the PN23 concentration. Nevertheless, the PN10/PN23 ratio of C100 is significantly different from the other fuels after only 2 minutes. It is assumed that the DMC ratio inhibits the mixture formation because of its higher needed heat of vaporization and its higher vapor pressure. This is most noticeable after the first fired cycles, when the combustion chamber walls, and the piston are not heated up yet. Therefore, fuel droplets are present during combustion and possibly also afterwards. These local rich areas emit PN emissions depending on their droplet size, number, and present fuel. This is most problematic for fuels containing gasoline because of the high number of C-C bonds in its molecules and the existing high boiling components in gasoline. In turn, DMC has no C-C bonds and a wider ignition range towards rich mixture, whereas fewer PN emissions are emitted, even when fuel droplets are present during combustion.

So, the combination of DMC, which inhibits the mixture formation and gasoline that tends to sooty combustion under rich conditions, has an adverse effect on sub-23 nm particles in the first 6 minutes of the coking run. After 9 minutes of the coking run, the PN10/PN23 ratio strongly drops to a value

FIGURE 9 Exemplary injector with scope on injector tip at the top / injector tip microscope images during coking run @ 2000 rpm / 7 bar IMEP / FUP 25 MPa / λ = 1.0 / SOI = 430 °CA a TDC / ε = 10.92 / MFB50 = 8 °CA aTDC

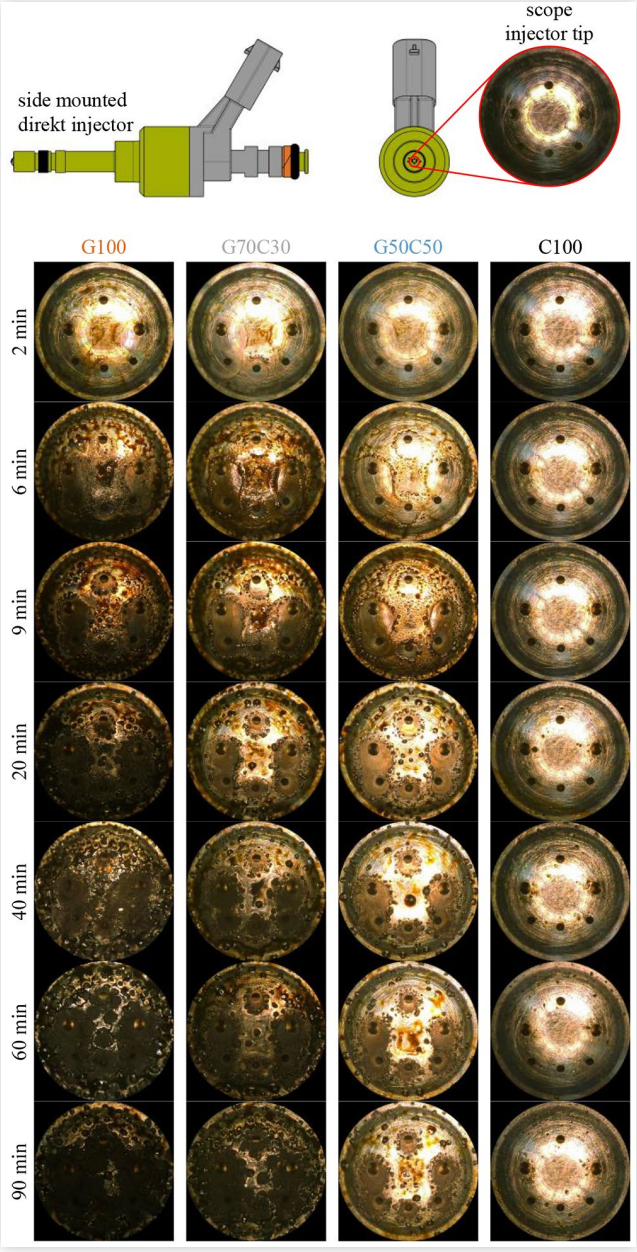

between 2 to 3 for all fuels. This is an indicator that the combustion chamber is heated up enough to evaporate most of the injected fuel after 9 minutes. At around 20 min. the PN23 drift starts for G100. and after another 20 min, the PN23 concentration is roughly 12 times higher. Hereinafter, the PN23 concentration for G100 wobbles between $4{\cdot}10^4$ and $7{\cdot}10^4$ #/cm^3. However, during this process, the PN10 concentration increases only 2 times. Therefore, the PN10/PN23 ratio is falling simultaneously, and the injector tip coking phenomenon is primary influencing the PN23 concentration.

Operating the engine with G70C30, a similar drift occurs roughly 20 min later and ends approximately on a 50 % lower PN23 level. For higher DMC ratios, no PN drift was observed during the 90 min run. In general, tip coking seems to start with the so called "coffee-ring effect" for all fuels except for C100. This is clearly visible in Figure 9 in the images from the first 9 minutes. After the injection, fuel remains on the injector tip around the spray hole edges depending on the operating conditions, e.g. FUP, engine load, tumble flow, injection strategy, and injector design [48]. If this fuel drop evaporates, the outer edge of the droplet is stable and somehow pinned on the tip's surface because of the fuel drop´s surface tension. Consequently, fuel that evaporates from the edge is replenished by fuel from the interior [57]. So, most of the fuel droplets are transported to the outer ring edge. At some time during this phenomenon, combustion takes place and the non-evaporated fuel is diffusively burned. The fuel portion that is not completely oxidized remains on the injector tip as a deposit. This process repeats with the following injection, and the deposit is partly transported to the fuel drop edge. This forms a clear coking layer ring around the spray-holes. However, over time the coking layer inside the fuel drop also rises and prevents the transport of the deposit on the fuel drop edge. In this process, the inner coking layer reaches the outer rings' stage at some time. At that moment, the PN23 drift starts for G100 and G70C30 because this deposit around the injection holes acts as a sponge. This sponge increases the amount of adhered fuel and deteriorates its evaporation [58]. Finally, this ends in a self-reinforcing process until the deposit reaches a stage where it is partly burned by combustion. The slight low-frequency oscillation of the PN23 level after the PN drift in Figure 8 is explained with this process.

MeOH/MeFo vs. DMC/MeFo

Pre-Investigation of Different MeOH/MeFo Ratios Similar to DMC, MeFo is used as a blend for MeOH to eliminate the disadvantages of the relatively low DVPE of 30.7 kPa of MeOH. Just like for the DMC blends, two fuel candidates were investigated in a baseline testing with M85F15 and M70F30. Figure 10 compares M100 compared with the MeFo blends, and G100 is shown as a reference.

With the SOI variation, the benefit of the increased DVPE of M70F30 was observed by decreasing PN emissions. With a

FIGURE 10 MeOH / MeFo blends - PN10 over SOI and η_i over IMEP @ 2000 rpm / λ = 1.0 / ε = 10.92 / MFB50 = 8 °CA aTDC

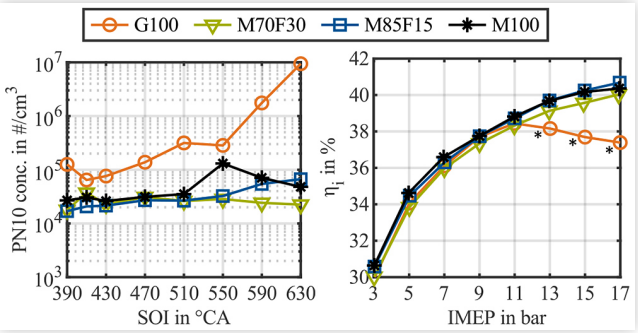

late DI during compression stroke, less time for mixture formation is left, so that the high DVPE of MeFo is beneficial, especially for an SOI timing after 550 °CA aTDC. Owing to the high knock resistance of MeOH as well as MeFo, the MFB50 was kept at 8 °CA during the IMEP variation. This leads to the significant increase of η_i at high load points starting at 13 bar IMEP compared to G100. As a result of the 46 % lower laminar flame speed by ~ 0.3 m/s of MeFo, η_i decreases slightly for an increased MeFo ratio. The author chose the fuel M70F30 for the comparison with C65F35 because of its benefits in PN emissions and the expectation that the higher DVPE leads to better engine performance in cold conditions, especially at low loads.

Variation of Engine and Combustion Parameters

Equal to the DMC-blend testing, a variation of engine load of late SOI and λ was performed.

The lambda variation was performed in the thermodynamic engine as well as in the optical engine. Figure 11 shows the ratio of PN10/PN23 and the PN23 concentration of the thermodynamic engine testing over λ.

Additionally, the overall level is close to the ambient level. Contrary to the expectations, the PN23 emissions of M70F30 decrease continuously with richer mixtures. For the PN10/PN23 ratios, the reversed order between λ = 0.8 - 1.2 is observed when compared to the PN23 emissions. Thereby, M70F30 and C65F35 have higher PN10 emissions relative to their very low PN23 level compared to G100. Towards leaner mixtures, the gap between G100 and the oxygenated fuels in PN emissions tapers, especially for λ = 1.3 and λ = 1.4. During the λ variation, C65F35 shows the lowest PN23 emissions. Compared to M70F30, C65F35 emits 8 % less PN23 emissions on the average, although M70F30 shows 60 % fewer PN23 emissions in operation with a rich or a stoichiometric global mixture. Moreover, M70F30 shows an average of 3 % fewer PN10 emissions compared to C65F35. For the oxygenated fuels, the homogeneous spark ignition limit is reached with λ = 1.5. This is slightly earlier than for G100, and this is explained with the overall colder combustion temperatures combined with a shorter ignition limit range towards lean

FIGURE 11 PN emissions over lambda variation with the thermodynamic engine @ 2000 rpm / 7 bar IMEP / SOI = 430 °CA a TDC / ε = 10.92 / MFB50 = 8 °CA aTDC

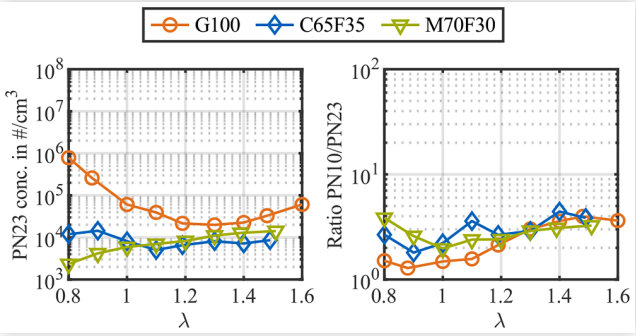

FIGURE 12 Time-series surface plot, spatially averaged over the combustion chamber. The plotted surface is the calculated difference of luminous emission for M100 minus C65F35 between an equal operating point @ 1500 rpm / 6 bar IMEP / λ = 1.0 / SOI = 430 °CA a TDC / ε = 9.36 / MFB50 = 8 °CA aTDC

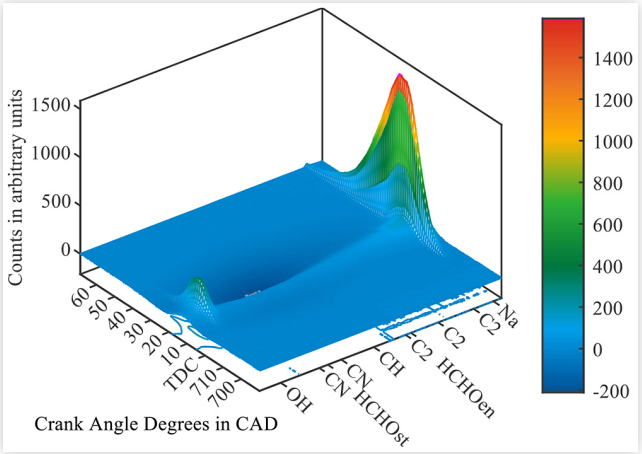

mixtures for both oxygenates. Some effects were also confirmed by the optical engine for the blends. Figure 13 shows the two operating points with λ = 0.8 and λ = 1.0 at 11 °CA aTDC for C65F35 and M70F30 at the optical reference point. Overall, C65F35 exhibits a bluish flame with a very low luminosity for λ = 0.8. As already explained, the relative lower luminosity is an indicator for a decreased gas temperature. In this case, it is conclusive that the temperature decreases with rich combustion as a result of higher in-cylinder evaporation cooling from the injected fuel mass. Additionally, the

FIGURE 13 λ = 0.8 (left column) and λ = 1.0 (right column) for C65F35 and M70F30 @ 1500 rpm / 6 bar IMEP/ SOI = 430 °CA a TDC / ε = 9.36 / MFB50 = 8 °CA aTDC

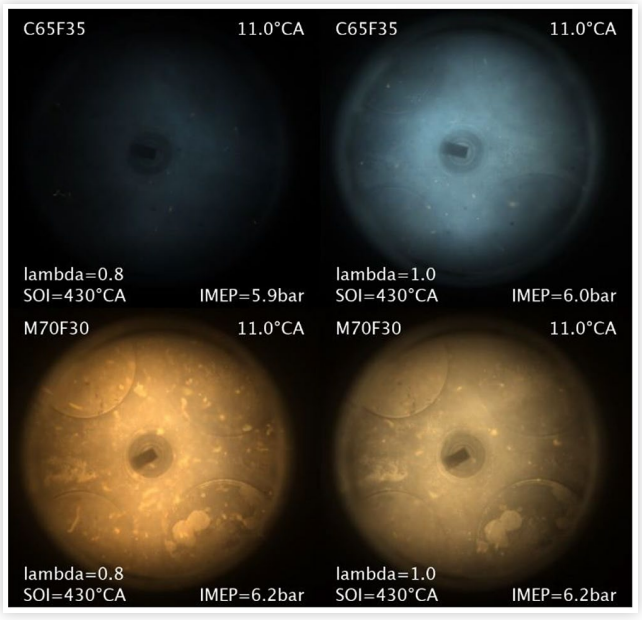

luminosity is significantly lower than for G100 and G70C30, as seen in Figure 7. This is justified with the ~ 2.8 times higher in total enthalpy of vaporization of C65F35. The low PN level from the thermodynamic investigation is also confirmed by detecting only a few diffusion spots, even for λ = 0.8. M70F30 is displayed in the last row. The dominant color of all recordings containing MeOH is yellow. Unfortunately, a technical MeOH with a purity ≥ 98.5 % was used for the investigation that was apparently contaminated by Sodium (Na). Even trace amounts due to impurities result in strong spectral emissions on the D line close to 589.3 nm, dyeing the flame yellow. The presence of Na was confirmed by application of a high-speed 1D flame emission spectroscopy, see Figure 12.

On the x-axis, the recorded signal is spectrally resolved and already matched to probable species, while along the y-axis, combustion is temporally resolved in high resolution. Thus, a whole working cycle is depicted. The z-axis contains the calculated difference in averaged signal intensity for each time-step, when DMC/MeFo is subtracted from an equal operating point applying MeOH. The difference highlights only minor differences in intensity for most of the observed spectrum, except for a strong peak centered on the Na line. Since no optical filtering was applied in the recordings, care has to be taken to not falsely attribute the yellow hue of the flame. Further details on the methodology and experimental setup are available in [30]. Therefore, the color information from the images of M70F30 is distorted and is consequently not used to analyze the combustion. One information that was extracted from the recordings is that a lot more liquid droplets are visible compared to the stoichiometric mixture.

However, it cannot be clarified to this moment whether the droplets would also be visible without the presence of Na. However, M70F30 shows the lowest PN23 and PN10 concentrations in Figure 11. Therefore, it is expected that the M70F30 liquid fuel droplets do not result in solid PN emissions, even if they burn under extremely rich conditions. To confirm these results. the same testing methodology process from the optical engine was transferred to the thermodynamic configuration. This means that the engine was motored for 100 seconds with wide-open throttle (WOT) before every snapshot. By WOT, operation oil aspiration through the piston ring group was avoided because of vacuum pressure during the intake stroke. The snapshot was subsequently triggered after 10 seconds under fired engine conditions. Figure 14 contains the results of the PN23 and PN10 concentrations. The PN23 emissions show roughly the same trend and level as under stationary conditions in Figure 11. But the PN10 emissions increased over a wide range by two orders of magnitude for all fuels. Especially M70F30 increased conspicuously close to the level of G100. Particles below 20 nm diameter are mostly volatile particles and branded as nucleation mode [59].

The authors expect that lots of unburnt and partly burnt liquid fuel particles are counted by the CPC system, even though they had to pass through the 300 to 400 °C hot evaporation tube of the solid particle counting system (SPCS). The expectation is that the tube cannot deliver enough energy to evaporate all volatile particles.

This effect is intensified for M70F30 compared to C65F35 because of its more than 70 % higher heat of vaporization related to the LHV. Additionally, if the engine is fired for

FIGURE 14 PN emissions over lambda variation with the thermodynamic engine with optical testing methodology @ 1500 rpm / 6 bar IMEP / SOI = 430 °CA a TDC / ε = 10.92 / MFB50 = 8 °CA aTDC

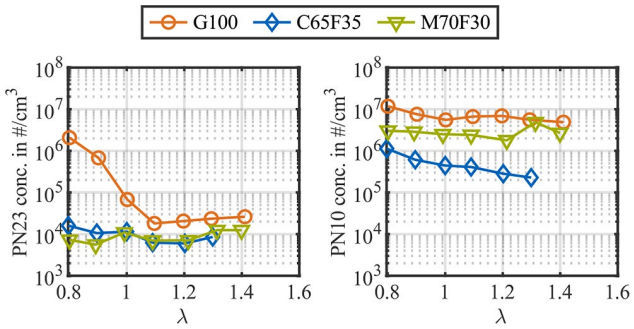

almost 10 seconds, this effect is also forced by lower combustion chamber temperatures during the mixture preparation and combustion process. Also, at this low load and engine speed, less TKE is present to enhance evaporation of the fuel. Therefore, the high number of fuel droplets with λ = 0.8 in Figure 13 and the rise of the PN10 emissions in Figure 14 of M70F30 is conclusive. The assumption of the high volatile particle ratio at the PN10 concentration is strengthened by Liu et al. [60]. They utilized a V6 DISI light vehicle engine fueled with a displacement volume of 500 ccm per cylinder. The engine operated with an engine speed of 1500 rpm and an engine load between 2.9 - 6.1 brake mean effective pressure (BMEP), which is very close to this study. They used gasoline at a stoichiometric mixture and a similar early SOI timing of 420 - 439 °CA aTDC. Particle measurements were executed pre- and post-TWC in four particle size ranges. It was demonstrated that the TWC reduces the PN concentration extremely by converting the VOC particles. With an engine load of 6.1 bar BMEP, the reduction efficiency was greater than 90 % for the particle size range of 8 - 25 nm.

The following section discusses the load and cooling water temperature variation in the thermodynamic engine, which is similar to the already discussed one with G100 and G70C30. Figure 15 shows the PN23 concentration and the ratio of PN10 / PN23 over the load in IMEP for 80 °C, 40 °C and -5 °C coolant temperature at a 2000 rpm engine speed and a FUP of 35 MPa. With T_c = 80 °C, the oxygenates show their benefits of low-soot combustion. However, for C65F35, the PN23 concentration increases with higher loads beginning with 13 bar IMEP instead of M70F30, which shows the reverse behavior. But averaged over the load variation, M70F30 has 14 % more PN23 and 37 % more PN10. It is expected that due to the approximately doubled injected fuel volume of the oxygenates, combined with a roughly 10 % decrease in required air mass flow, lots of local rich areas are present in the combustion chamber. This is reinforced at high engine loads because of a larger spray penetration length, which results in liner and piston wetting.

These rich areas are more reactive using M70F30 because MeOH has a wider ignition range towards rich mixtures. Moreover, with the higher laminar flame speed of MeOH, the combustion intensity and the peak temperatures increase.

FIGURE 15 PN23 emissions and PN10/PN23 ratio over IMEP in bar for 80° C, 40° C and -5° C coolant temperature @ 2000 rpm / λ = 1.0 / SOI = 430 °CA a TDC / ε = 10.92 / MFB50 = 8 °CA aTDC

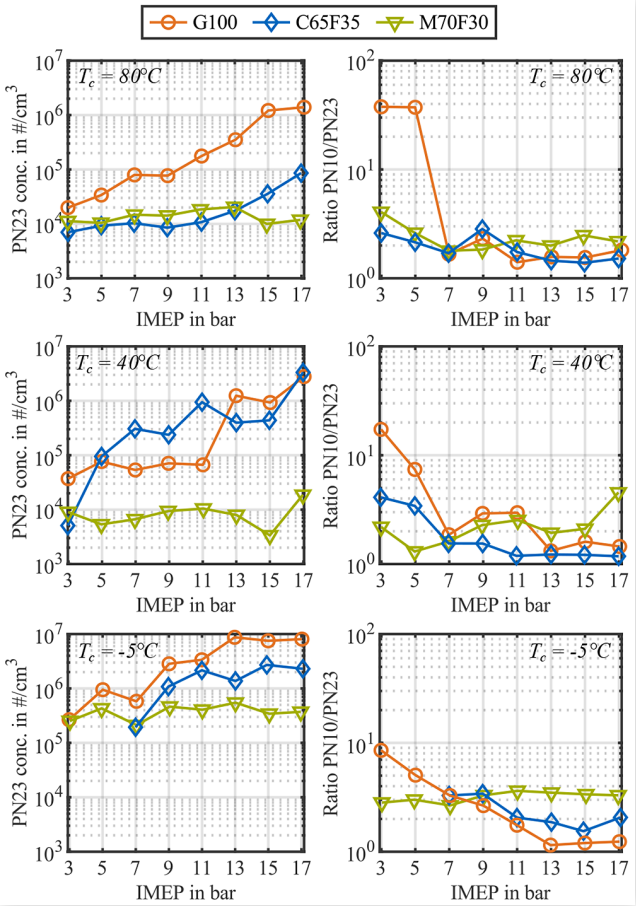

These effects also lead to low PN23 emissions for M70F30 at higher loads. In hot conditions, no significant differences between the oxygenates were observed in the PN10/PN23 ratio. Both oxygenated mixtures show an increase in the PN10/PN23 ratio for 3 and 5 bar IMEP, but on a significantly lower level than for G100. For the PN23 emissions, a trend of increasing particles for lower T_c is seen, except for M70F30. M70F30 shows an average decrease of 33 % in PN23 emissions at a 40 °C coolant temperature compared to hot conditions. The overall lower combustion chamber temperatures lead to a more inhomogeneous mixture formation with local richer areas. As already shown with the λ variation in Figure 11, rich mixtures for M70F30 lead to lower PN23 concentrations, and this explains the drop of the PN23 emissions at a 40 °C coolant temperature. At a further decrease of the T_c to -5 °C, the PN emissions even for M70F30 rise compared to T_c = 80 °C by a factor of 2.7 for PN23 and a factor 3.9 for PN10. It is expected that the flame front is quenched at the cold combustion chamber walls, and that therefore lots of unburnt fuel crosses the combustion chamber with the raw exhaust stream, which in turn is counted in the CPC. However, compared to hot conditions, for C65F35 a conspicuous increase at T_c = 40 °C by 2.8 times for PN23 and 2.1 times for PN10 emissions was examined for C65F35. Similar to M70F30, more fuel droplets are present at a lower T_c, but DMC`s ignition limits allow up to 12.9 vol.-% fuel inside the mixture with air. The maximum ignition limit for MeOH is found at 36 vol.-% (see Table 2). Furthermore, the laminar flame speed of DMC is approximately 56 % slower than of MeOH. With regard to these facts, it is expected that the amount of unburnt fuel in the exhaust stream is higher for C65F35 than for M70F30 if a significant portion of fuel is not evaporated during the mixture formation. When the T_c was regulated at -5 °C, it was not possible to operate the engine at the low load points 3 and 5 bar IMEP with C65F35 under reference conditions. As expected, the PN emissions for the remaining points of the load variation increased again by an average of 67 % for PN23 and 95 % for PN10. For the low load points, no ignitable local mixture is present at the spark plug because of the bad mixture formation initialized by the combination of less TKE and extremely low combustion chamber temperatures. In spite of this issue, it is possible to operate the engine under these conditions if the SOI is shifted to 655 °CA during the compression stroke close to the ignition timing. Another possibility is to actuate a tumble flap to increase the TKE and therefore enhance the mixture formation. This is only possible at the SCE if the intake manifold is replaced. However, the focus of this study is to compare the base fuels DMC and MeOH to identify potentials and differences. Therefore, the operating conditions were kept equal for C65F35 and M70F30.

Figure 16 plots the NO_x and CO emissions over the engine load in IMEP with the three different T_c. The oxygenates show a significantly lower NO_x level than gasoline, except at high loads at T_c = 40 °C and T_c = 80 °C, where only a slight benefit is observed. At 40 °C, M70F30 emits slightly more NO_x emissions than C65F35 by an average of 5 %. Also, in hot conditions under enhanced mixture formation, the NO_x emissions are quite similar, and M70F30 emits an average of 1.9 % more NO_x emissions. However, similar to the DMC blends investigation, a rise in NO_x emissions was also observed for the oxygenates by decreasing the T_c, except when reducing T_c from 40 °C to -5 °C. As already discussed, easier accessible oxygen is available for the NO_x formation with the lower T_c because of an increase of local rich and lean areas. Additionally, prompt-NO_x formation is forced, and the evaporation cooling decreases. Similar to the DMC blends, the decelerated Zeldovich mechanism is possibly dominant, and the NO_x emissions partly decrease slightly with lower loads (3 to 5 bar IMEP) and lower T_c.

But with the decrease of T_c to -5 °C, the portion of unburnt fuel increases with the worse mixture formation and NO_x emissions decline with the combustion peak temperatures. The CO emissions during almost all points are on a higher level for the oxygenated fuels as shown in Figure 16. This is a result of the fact that both oxygenates emit more CO_2 emissions locally than gasoline due to their elemental composition. This difference is significant with an average increase of 32 % for C65F35 in hot conditions. In turn, only a slight increase of more than 4 % was determined under the same conditions for M70F30. Therefore, more intermediate CO must be oxidized during combustion. In general, the oxidation of CO is temperature driven and depends on the available oxygen, especially in the flame front area, where a

FIGURE 16 NO_X and CO emissions over IMEP in bar for 80 °C, 40 °C and -5 °C coolant temperature @ 2000 rpm / λ = 1.0 / SOI = 430 °CA a TDC / ε = 10.92 / MFB50 = 8 °CA aTDC

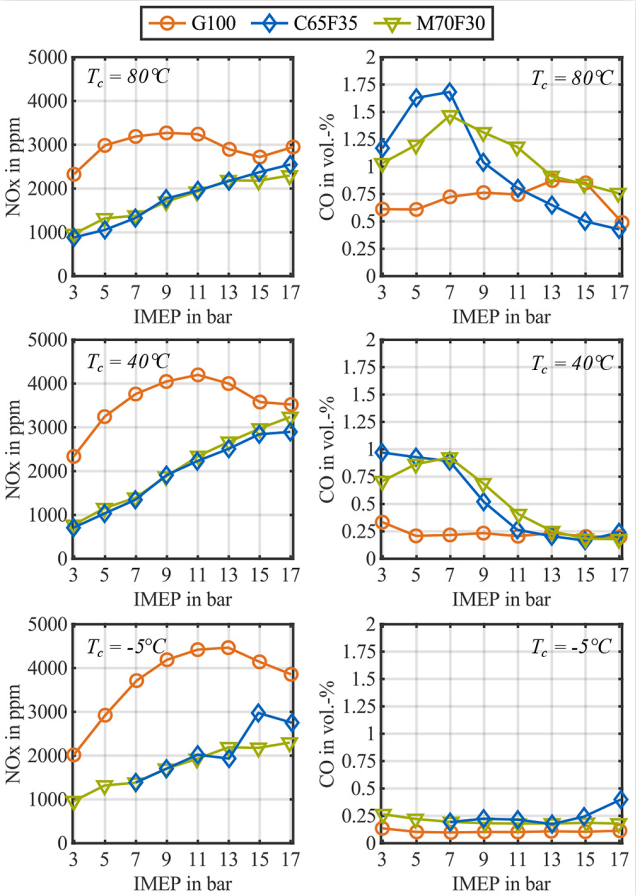

self-adjusted equilibrium is present between CO and CO_2. With the expansion stroke, the gas temperature decreases and the present balance of CO and CO_2 in the flame front is mostly frozen. Therefore, lower combustion temperatures caused by low engine loads and higher in-cylinder cooling from DI generally lead to higher CO emissions. This is clearly visible for C65F35 and M70F30 in Figure 16 for engine loads below 11 bar IMEP and a T_c of 80 °C and 40 °C. Across the board, the oxygenates show the same trend, but M70F30 emits an average of +26 % CO with 80 °C T_c, +16 % CO with 40 °C T_c and -18 % CO with 80 °C T_c. Since the combustion temperatures are higher with G100, no clear increase of CO is therefore monitored at low loads. But the shift of the MFB50 increases CO emissions beginning with 13 bar IMEP under hot conditions. However, at 17 bar IMEP, CO emissions drop clearly. It is expected that the extreme shift of the MFB50 at 13 °CA lifts the exhaust gas temperatures to a level where lots of post-oxidations reduce CO emissions when using G100. For all fuels, the reduction of CO emissions with decreasing T_c is quite clear in Figure 16. This is explained with more accessible oxygen in the flame front area by decreasing the T_c. As already mentioned, the inhomogeneity and the unburnt fuel portion increase, whereby an oversupply of oxygen is present in the combustion chamber due to the global stoichiometric mixture.

FIGURE 17 PN23 emissions and COV of IMEP over super late SOI @ 2000 rpm / 7 bar IMEP / λ = 1.0 / ε = 10.92 / MFB50 = 8 °CA aTDC

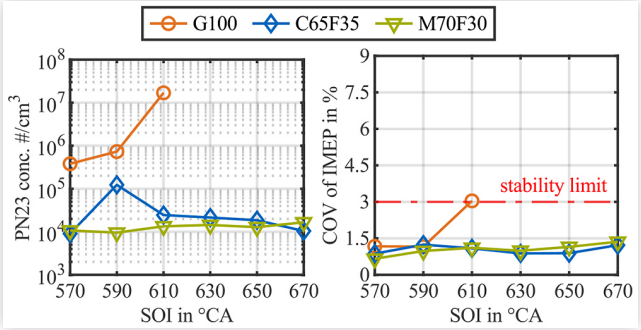

Equal to the DMC blend investigations, a super late SOI variation during the compression stroke was performed with both SCE configurations. Figure 17 shows the PN23 concentration and the COV_{IMEP} over the super late SOI variation. The stable combustion and the low PN23 emissions behavior of C65F35 from previous studies were confirmed. With an SOI between 570 and 610 °CA, the oxygenates on average show significantly lower PN23 concentration than G100, namely -94 % for C65F35 and - 99 % for M70F30. M70F30 also exhibits positive behavior when SCE operates with the single DI during the compression stroke. Thereby, M70F30 enables another PN23 reduction of an average of 12 % with a similar combustion stability compared to C65F35. With C65F35 and an SOI of 670 °CA, fuel injection ends 6 °CA before ignition if the MFB50 is regulated to 8 °CA aTDC.

Operating the engine under equal conditions but using M70F30, the gap between EOI and ignition is 12.5 °CA. If the injection is shifted another 20 °CA later, no stable engine operation is possible with either C65F35 or with M70F30. So, as expected, the C1-oxygenates are completely insensitive for PN23 emissions, even if an extreme inhomogeneous mixture including a high portion of unevaporated fuel is ignited. These observations were confirmed by the optical configuration as well. In Figure 18, the standard SOI of 430 °CA during the intake stroke is compared with a late SOI of 630 °CA during the compression stroke for C65F35 and M70F30. The first row shows the images of C65F35, both images have a bluish color, the same intensity and only a few diffusion flame-spots.

However, one difference was observed in the main location of the combustion flame. While the flame is centered for the SOI 430 °CA, an SOI at 630 °CA shows an asymmetric flame location shifted towards the intake valves and the side mounted DI injector. This phenomenon is attributed to the extremely late fuel injection with its resulting mixture inhomogeneity and its rich area around the fuel injector. Equal to the lambda variation, the color and the intensity of M70F30 in the second row is not valued. However, some information about the mixture formation was extracted. With the standard SOI = 430 °CA, the image shows numerous additional diffusion spots compared to the injection during the compression stroke. It is assumed that more fuel hits the hot piston during late injection. This possibly enhances the mixture formation of M70F30 at this operating point because more heat of

FIGURE 18 SOI = 430 °CA (left column) and SOI = 630 °CA (right column) for C65F35 and M70F30 @ 1500 rpm / 6 bar IMEP/ λ = 1.0 / ε = 9.36 / MFB50 = 8 °CA aTDC

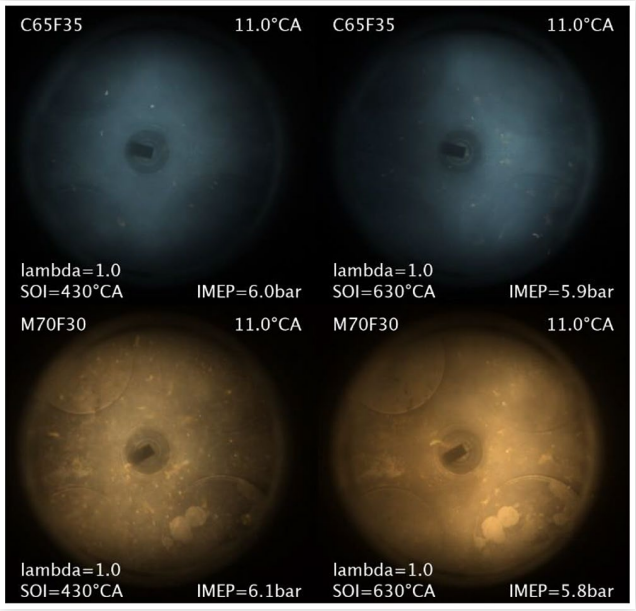

vaporization is needed compared to C65F35 as already mentioned. In addition, the flame location is asymmetric and concentrated towards the DI injector, just like with C65F35.

Lastly, M70F30 also shows this positive behavior for an inhomogeneous mixture formation initialized by a super late single injection. This opens an additional degree of freedom for several combustion modes in ICEs application, as previously mentioned in the blend's super late SOI variation.

Abnormal Combustion Behavior In this sub-section, an abnormal combustion testing was performed with the thermodynamic engine configuration to classify the resistance against abnormal combustions compared to the well-known fuels toluene and M100. This information is useful for future investigations, especially for 3D-CFD simulations. In order to provoke abnormal cycles, some changes compared to the reference point and the thermodynamic engine's hardware were initialized. The standard piston was replaced with an in-house designed piston from Stadler et al. [50] to raise the CR from 10.92 to 14.91. The engine speed was reduced to 1500 rpm and the engine load was raised to 17 bar IMEP, while all other parameters, except the T_{intake}, were maintained from the reference point. The T_{intake} was gradually increased in 50 °C steps, starting at 30 °C until= abnormal combustion cycles occurred. When abnormal cycles were detected, a snapshot was triggered to record the cylinder pressure traces of the following 200 cycles. During post-processing with a MATLAB-routine, the abnormal combustion cycles were alternatively categorized as two different types, namely knocking and pre-ignition cycles. The pre-ignition cycles are combustion cycles where the mixture formation is ignited before the start of ignition is triggered. Dahnz et al. [61] described several different mechanisms leading to pre-ignitions. The pre-ignition cycles are simply identified by comparing the cylinder pressure of each cycle with the lowest pressure of all 200 recorded cycles at the point of ignition. If the pressure difference is greater than 0.5 bar, it is defined as pre-ignition. The threshold value set at 0.5 bar was chosen by analyzing similar engine operating points without pre-ignitions. Thereby, a maximum cylinder pressure deviation of ± 0.25 bar at the point of ignition was identified. This result fits with the in-cylinder pressure sensor's specified accuracy and the expected pressure oscillations inside the combustion chamber. On the other hand, the knocking cycles were detected using the band-pass filtered pressure trace, close to the methodology of Panzani et al. [62]. The evaluation software was fine tuned to detect knocking cycles when the maximum amplitude of pressure oscillations was ≥ 5 bar. This amplitude is defined as conventional knock by Wang et al. [63].

In the following, the 200 pressure traces for each fuel are plotted, starting with M70F30 in Figure 19, which shows at first abnormal combustion cycles by raising the T_{intake}. The figures visualize the cylinder pressure plotted over ° CA in the range of 700 - 60 °CA after fired TDC (aFTDC). At the top of the figure, the key parameters and the fuel name are listed in a table. The black line represents the mean pressure trace of all 200 cycles. The vertical red dashed line marks the ignition timing. The single pressure traces are colored red if a knocking cycle was detected and are colored blue if a pre-ignition cycle was determined. All other single pressure traces are displayed in grey. Additionally, the number of counted abnormal combustions for each type is listed in the legend. With M70F30 in Figure 19, first pre-ignitions occurred with a T_{intake} of 80 °C and the SCE getting uncontrollable. The maximum pressures of the single cycles ranged between 140 - 69 bar.

The maximum pressure of 140 bar was reached by a single pre-ignition cycle. Overall, 25 pre-ignition and no knocking cycles were detected. The authors expect that with the in total extreme high enthalpy of evaporation of MeOH (+ 457 % compared to G100 and + 96 % compared to C65F35), a high portion of fuel is not evaporated due to the low engine speed of 1500 rpm generating only a relatively small TKE and

FIGURE 19 200 single cylinder pressure traces of M70F30 from 700 °CA to 60 °CA aTDC with highlighted pre-ignitions traced in blue

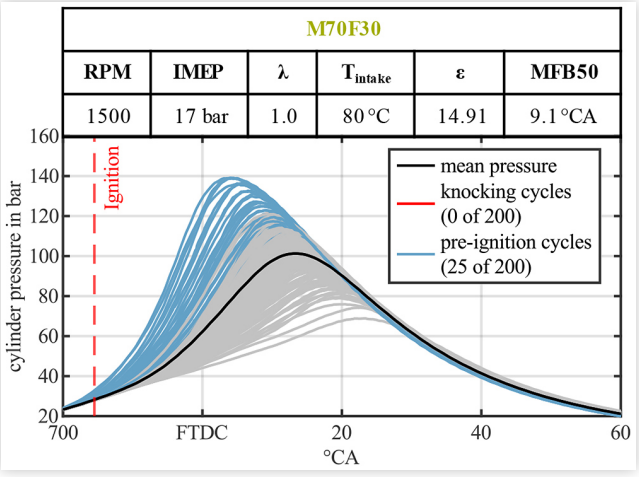

simultaneously high quantities of fuel being injected at high load operation. Thus, lots of fuel droplets are possibly present during the compression stroke. As published by Dahnz et al. [64], not evaporated droplets form significant sources for pre-ignition because this non-evaporated fuel is already ignitable at lower gas temperatures when the liquid droplets reach specific temperatures. Dahnz et al. reported that with a 20 °C decrease of T_c, approximately 15 % less fuel is evaporated and thereby the number of detected pre-ignitions using gasoline is raised by 100 %. Additionally, the longer injection duration using M70F30 results in a larger penetration length of the fuel spray, as a following wall wetting is likely. This may then lead to an oil dilution by the fuel and decreases viscosity and surface tension of the lubricant oil. Thereby, oil/fuel droplets can be easier blown or thrown into the combustion chamber by the piston movement [65]. The combination of the significant wider ignition limits, the higher laminar flame speed, and the low ignition energy requirement of MeOH will finally lead to pre-ignitions. In literature this phenomenon is called low speed pre-ignition (LSPI) [65] and these pre-ignitions are often initialized by a hot surface like the spark plug electrode [66]. LSPI occurs in turbocharged DISI engines with high compression ratios, and it is reinforced by alcohol fuels [65, 66, 67, 68, 69, 70]. Similar to Haenel et. al [65], no knocking combustion is detected after pre-ignition with a high ratio of alcohol fuels. This indicates that the energy level of the mixture itself is still below the auto-ignition level. The fact that M70F30 is pre-ignited earlier than M100 is explained by the lower enthalpy of vaporization of MeFo, whereby the gas phase's and fuel/oil droplets' temperatures are higher.

When the intake air is heated up to 130 °C, abnormal combustion occurs also for M100 and toluene, shown in Figure 20 and Figure 21.

For M100, one knocking cycle and 33 pre-ignition cycles were detected. The maximum pressure for the single cycles ranged from 144 to 77 bar. Similarly to M70F30, the maximum pressure of 144 bar was induced by a pre-ignition cycle. As already explained, the higher enthalpy of vaporization of MeOH increases with the in-cylinder cooling.

FIGURE 20 200 single cylinder pressure traces of M100 from 700 °CA to 60 °CA aTDC with highlighted pre-ignitions traced in blue and knocking cycles in red

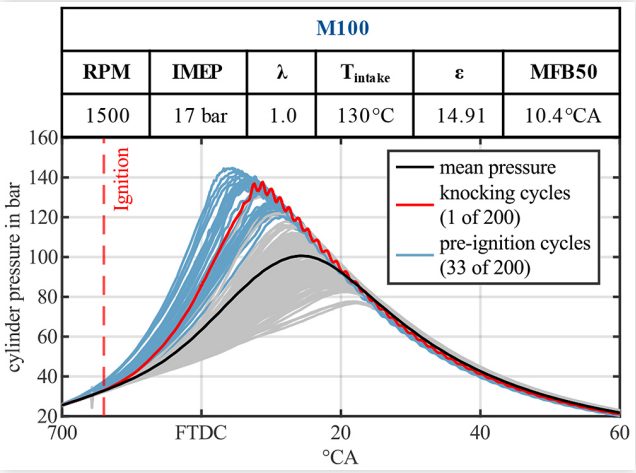

FIGURE 21 200 single cylinder pressure traces of toluene from 700 °CA to 60 °CA aTDC with highlighted knocking cycles in red

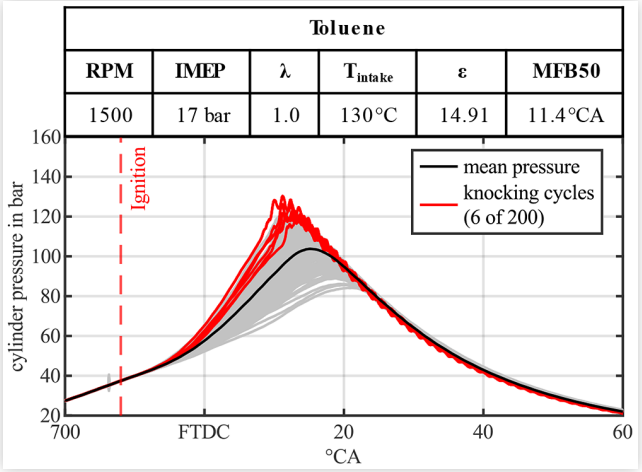

Therefore, M100 showed a higher resistance against abnormal combustion compared to M70F30 during this campaign. In turn, only six knocking cycles and no pre-ignition cycles were detected for toluene. The maximum pressures of the single cycles were in the range of 130 - 84 bar. For toluene, the maximum pressure peak of 130 bar was reached by a knocking cycle, even though the auto-ignition temperature of toluene is 480 °C, which is 15 °C higher than for MeOH. However, the enthalpy of evaporation is close to G100 and in total equals only 16 % of the one from MeOH. Therefore, it is expected that most of the fuel is evaporated, and the gas phase temperature is significantly higher compared to M100. However, the ignition limit of toluene in air is narrow, ranging from 1.1 - 7.1 vol.-% compared to MeOH with 5.5 - 36.5 vol.-% and the MIE is over 40 % lower for MeOH. Therefore, the higher mixture temperature rises the probability for a pre-ignition, but this tendency is overcompensated by the narrower ignition limit and the higher MIE. Hence, no pre-ignition occurred. However, when the mixture is ignited by the spark plug, the pressure increases rapidly in the combustion chamber and even in unburnt zones. Thereby, at several different points in the unburnt zones, the mixture reaches the auto-ignition energy level because of the higher gas phase temperatures. Thus, a knocking cycle with the prominent pressure oscillations occurs. This in turn also explains that the fuel with high MeOH ratio shows mostly pre-ignitions and hardly any knocking cycles. Due to the MeOH share, the gas phase temperature is lower and therefore the pressure increase from the spark-ignited combustion is insufficient to exceed the auto-ignition energy level.

Based on the fact, that C65F35 showed no abnormal combustions with a T_{intake} of 180 °C, the T_{intake} was raised by another 20 °C. Finally, with T_{intake}= 200 °C, the first knocking cycles were observed, as shown in Figure 22. In total, 3 knocking cycles were identified. However, no pre-ignitions were observed, just like for toluene.

The highest maximum cylinder pressure in a single cycle of 137 bar was reached with normal combustion. Overall, the maximum cylinder pressure ranged from 137 to 83 bar. In this

FIGURE 22 200 single cylinder pressure traces of C65F35 from 700 °CA to 60 ° CA aTDC with highlighted knocking cycles in red

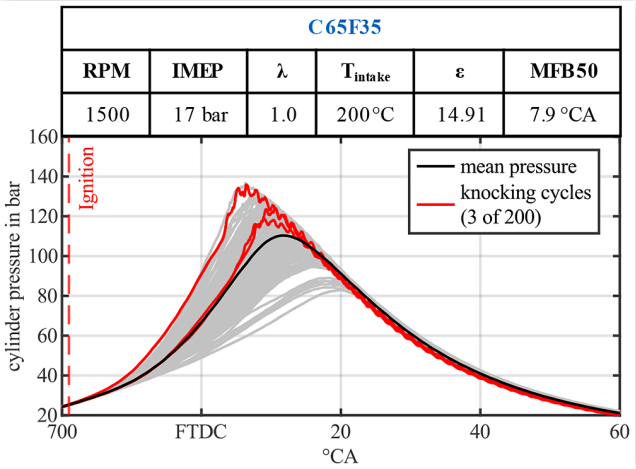

study, C65F35 showed the highest resistance against abnormal combustions of all investigated fuels, even though DMC and MeFo have lower auto-ignition temperatures than MeOH and toluene. Moreover, C65F35 needs half the total heat for evaporation than M100. This leads to the assumption that most of the fuel is evaporated for C65F35 as well, especially in this high engine load case with the increased T_{intake}. Thus, with the relatively low gas phase temperature, the possibly low number of fuel droplets and primarily the small ignition limit range, no pre-ignition occurred. However, the gas phase temperature is at a level where the pressure shock wave from the spark-ignited combustion initializes a knocking cycle. The higher resistance against an abnormal combustion from C65F35 compared to toluene is explained by the lower gas phase temperature due to the three times higher total enthalpy of evaporation of C65F35, and the more than doubled MIE of MeFo. The main difference between C65F35 and M100 lies in the fact that C65F35 needs half the total heat for evaporation. Furthermore, MeOH has a significantly wider ignition limit range in air and a relatively low MIE. Derived from these facts, C65F35's higher resistance against abnormal combustions is explainable. Unfortunately, no reliable data for the MIE of DMC is accessible, but it is expected that the MIE is close to MeFo.

Scavenged Pre-Chamber The advantages of the C65F35 synthetic fuel blend in terms of raw engine-out emissions, especially considering PN emissions, suggest the development of strategies may lead to their full exploitation. One considerable strategy to further increase the efficiency of ICEs is moving the λ to leaner regions. As shown earlier in this publication, operations leaner than λ = 1.5 are not suitable for C65F35. A remedy for this restriction is found in replacing the standard ignition coil with a scavenged pre-chamber as ignition element.

This setup is already presented by Stadler et al. [50] employing gasoline as fuel and PFI as main energy source for combustion. With this mode of operation, Stadler found a share of 5 % of the overall injected fuel into the pre-chamber to yield most favorable results in terms of engine-out emissions. Furthermore, operation at λ of 2 outperformed other air/fuel ratios regarding engine efficiency while still maintaining favorable emissions. With respect to these results, λ and share of injected mass to the pre-chamber are varied in a range of comparable values in this work.

To ensure comparability to the other measurements in this publication, the engine was operated at 2000 rpm, which is not corresponding to [50]. Furthermore, the main portion of the injected fuel was injected directly into the combustion chamber during the measurements presented in the following section. To enable the injection of increased amounts of fuel into the pre-chamber to compensate for C65F35's smaller lower heating value, a specifically designed single-hole injector was employed. Pre-chamber operation is compared to G100 as a reference and to show C65F35's potentials and possible restrictions.

The increased number of engine-out particle emissions resulting from the locally hyperstoichiometric mixture inside the pre-chamber is a major drawback for engine operation with a gasoline scavenged pre-chamber. As already described, C65F35 as a fuel is a possible key to solve this problem. Figure 23 shows the raw emissions of PN23 and PN10 for one operation point while increasing the amount of energy injected into the pre-chamber.

While on one hand the difference between G100 and C65F35 is remarkable in itself, the absence of an increasing tendency towards higher amounts of C65F35 confirms its suitability for pre-chamber operations on the other hand. While for standard spark ignition, λ = 1.4 is an operation point considered to be near the ignitability limits, the scavenged pre-chamber ensures stable operation. The share of the pre-chamber energy up to 3.93 % of the overall injected energy leads to a two-step combustion process presented in Figure 24. The first peak of pressure results from the pre-reactions of fuel inside the pre-chamber, while the second increase of pressure results from the combustion inside the engine's main chamber. During main combustion, both pressures extend identically. The potential for efficiency increases while decreasing engine out-emissions by moving the λ to leaner regions is presented in Figure 25. Ignition via the pre-chamber ignition system enables operation up to λ = 2. Emphasis should be placed on the fact that due to the higher cooling effect of the injected

FIGURE 23 Engine- out particle emissions over injected fuel mass in pre-chamber @ 2000 rpm / 7 bar IMEP / λ = 1.0 / ε = 14.18 / MFB50 = 8 °CA aTDC

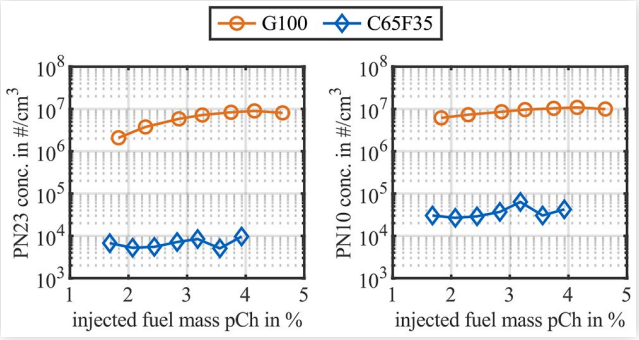

FIGURE 24 Visualization of two-step ignition process over crank angle at the given engine operation parameters

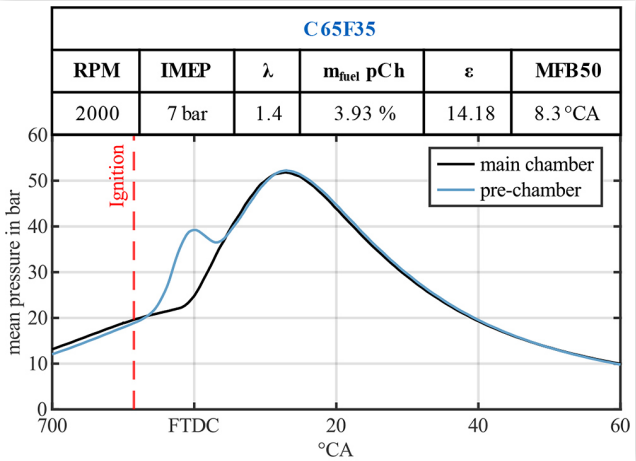

FIGURE 25 η_i, COV_{IMEP} and engine-out emissions (NO_x, CO) over λ @ 2000 rpm / 7 bar IMEP / ε = 14.18 / MFB50 = 8 °CA aTDC

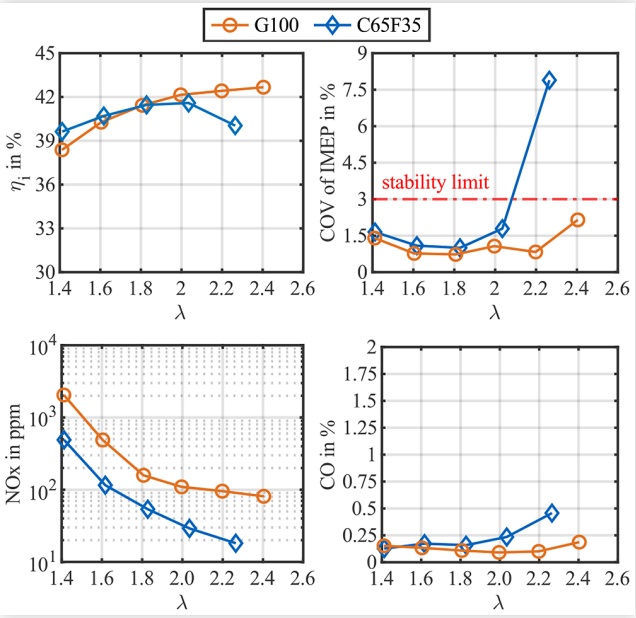

C65F35, the ignition limits of this fuel are narrower than for gasoline. Operating the engine under conditions of lambda higher than 2 yields COV_{IMEP} up to 8 % with a tendency for even higher instabilities at leaner conditions. The engine-out emissions show favorable tendencies with increased λ. While NO_x emissions decrease continuously, CO emissions show increasing tendencies beginning from λ 1.8 for C65F35 and 2 for G100. The improvements of NO_x emissions are driven by the decreased combustion peak temperatures. Owing to the already described unstable and incomplete combustion under these conditions, the engine-out emissions of CO deteriorate, especially when C65F35 is used as fuel.

Nonetheless, the efficiency gains at decreased engine-out emissions compared to operation at λ = 1 proves the suitability for C65F35 to be operated under lean conditions by employing an adapted ignition strategy. Comparisons with measurements of efficiency and engine-out emissions of conventionally ignited operations further underline the advantages of the scavenged pre-chamber for ignition.

Therefore, the matching, most favorable operation point employing C65F35 from this paper's section focusing on spark ignited combustion (IMEP = 7 bar / 2000 rpm / λ = 1.5) was compared to the presented operation point at λ = 2.0. Special emphasis should be placed on the reduction of NOx emissions by 97 % to a value of only 27 ppm. In terms of $\eta_{i,,}$ a relative increase by 10 % to 41.6 % even at low load of 7 bar IMEP could be realized. These outstanding results are partly diminished by increased CO (55 % higher) and PN (34.6 % higher) emissions. However, both exhaust gas components' absolute values are on a remarkably low level of 0.25 % CO and 10500 counted particles per ccm^3 (PN23). The CO level is significantly lower than under stoichiometric operating conditions and the PN23 emissions are slightly above the average ambient concentration range in Germany [71]. Furthermore, compared to operations at global λ = 1, the scavenged pre-chamber operation proves to be preferable due to simultaneously reduced emissions and increased efficiency. Summarized, reaching efficiencies of this magnitude at low emission levels with a spark ignited engine is considered exceptional. The promising results of the presented investigations suggest further testing of C65F35 as pre-chamber injected fuel. To enable an overall leaner operation than in this publication, the employment of a second fuel offering wider ignition limits and thereby the ability to be burned in even leaner conditions should be considered. The absence of unfavorable emissions when igniting a hyper-stoichiometric mixture inside the pre-chamber recommends that C65F35 is used as ignition source for lean mixtures of arbitrary fuels inside the main chamber. Such a dual-fuel pre-chamber ignited combustion could offer high efficiency as well as low emissions at the same time. This appears to be a promising approach to fulfill future requirements for ICEs.

Summary and Conclusions

In this study, two alternative fuel types for DISI engines were investigated, namely gasoline blends with DMC and pure C1-mixtures containing DMC, MeOH, and MeFo. Throughout a brief pre-investigation the most promising candidates for both types were determined.

Based on this pre-investigation of the DMC blends, G70C30 was identified as the most promising blend, because of the following advantages:

- Freezing point still below - 15 °C, even with the high freezing point of 4 °C of DMC
- Highest benefit in η_i of 4.9 % at 17 bar IMEP and 2000 rpm engine speed compared to G100
- Highest reduction of PN10 emissions of an average of 58 % during the SOI variation compared to G100

Subsequently, by an engine load, SOI and λ variation G70C30 were compared to G100 using the optical and thermodynamic configuration of the SCE. Thereby, the following facts were pointed out:

- Averaged PN23 reduction during the variations by 59 % @ λ, 53 % @ T_c and 80 % @ late SOI
- Averaged slight NO_x reduction of 3.5 % over IMEP and the T_c variation, even with the earlier located MFB50 with enhanced η_i
- The ignitable λ lean limit with spark plug is lowered from 1.6 to 1.4
- Widened range for a super late SOI during compression stroke by 40 °CA

The benefits in PN emissions, NOx emissions and indicated efficiency are related to the C1-molecule structure, the higher overall enthalpy of vaporization and the higher knock resistance of DMC.

Finally, the injector tip coking phenomenon was investigated by increasing the DMC ratio in three steps up to 100 vol.-%. Thereby, the SCE was operated with reference conditions over 90 min, except that the FUP was reduced to 25 MPa to force tip coking. To evaluate the different blends, several injector tip images were recorded with a microscope and the PN emissions were tracked over time. The main findings were:

- A coking layer on the injector tip was observed for all fuels containing gasoline
- The coking process always started with the "coffee-ring effect"
- The coking layer decreases with the increase of DMC and disappears with pure DMC
- The coking drift is already delayed by around 20 minutes with a ratio of 30 % DMC
- Beginning with a ratio of 50 % DMC, no coking drift was observed during the coking run

For the pure C1-mixtures, M70F30 was selected from the fuels with an MeOH base because of its benefits in PN emissions using late SOI´s during the compression stroke. Furthermore, it was expected that the high ratio of MeFo enhances the mixture formation under cold conditions and low loads. In addition, similar variations as for the blend investigations were performed to compare M70F30 with the already investigated C65F35 mixture in detail. The main findings are as follows:

- C65F35 emits on average fewer PN23 emissions by 8 % @ λ variation and 14 % @ IMEP variation
- M70F30 shows fewer PN23 emissions operating
  - with an λ between 0.8 - 1.0 by an average of 60 %
  - in high load points during the load variation
  - with T_c below 80 °C e. g. 60 % with T_c= -5 °C
  - with a single late SOI by an average of 12 %
- Operation of the SCE with 3 and 5 bar IMEP was not possible using C65F35 at a T_c= -5 °C under reference engine conditions in contrast to M70F30
- The observed NO_x of the oxygenates were quite similar
- M70F30 operates as well as C65F35 with a single super late DI during the compression stroke

The resistance against abnormal combustion was observed with an increase of the CR to ε = 14.91. Therefore, the SCE was operated with an engine speed of 1500 rpm and an engine load of 17 bar IMEP. In addition, the intake air was heated subsequently. For an improved comparability, the two well-known high knock resistant fuels toluene and MeOH were added. M70F30 and M100 showed foremost abnormal combustions in form of almost solely pre-ignitions at 80 °C and 130 °C. This is attributed to MeOH´s wide ignition limits in air combined with low MIE and high need for heat to evaporate. With a T_{intake} of 130 °C, toluene also exhibits abnormal combustion, however only knocking cycles. This is explained with its lowest need of heat for evaporation, which results in a higher gas phase temperature. Combined with the highest auto-ignition, high MIE and short ignition-limit range, only knocking combustions occurred. Finally, C65F35 offers knocking cycles with a T_{intake} of 200 °C for the first time. This is related to its relatively high enthalpy of vaporization combined with short ignition limits and the high MIE of MeFo.

In the end, an already launched scavenged pre-chamber ignition system was briefly tested with C65F35 and the HCR to estimate its potential. The low-soot combustion properties of C65F35, even under local rich conditions, enables the possibility to scavenge a pre-chamber by nevertheless having low PN emissions. The wider ignition limits in air towards rich mixtures of C65F35 further extend the operating range of the pre-chamber. Therefore, at the reference point (2000 rpm / 7 bar IMEP) and an λ of 2.0, an increase of η_i by a relative 10 % to 41.6 % was achieved compared to conventional spark plug operation at its lean limit of λ = 1.5. In addition, a reduction of NOx emissions of 97 % to 27 ppm was examined by holding the CO and PN emissions in the range of the stoichiometric operation mode.

For future investigations in terms of using alternative C1-oxygenates in SI engines, several topics are intended to be investigated in the engine laboratory of TUM. Firstly, improvements regarding exhaust measurement methodology of FTIR technique to identify all exhaust emissions precisely, including the unburnt fuel portions are necessary. Another topic is to launch a dual fuel combustion process with the scavenged pre-chamber to demonstrate the potential of using only a small amount of C1-oxygenates for the ignition system. Also, improvements on the engine's hardware side are planned to further increase combustion efficiency and stability. With the already performed and intended investigations, the possibility of a highly efficient, CO_2-neutral, future gasoline powertrain with low harmful exhaust emissions is feasible.

Contact Information

Sebastian Blochum
Chair of Internal Combustion Engines
Technical University of Munich
Schragenhofstraße 31, 80992 Munich, Germany
blochum@lvk.mw.tum.de

Abbreviations

aTDC - after Top Dead Center
AFR - Air-Fuel Ratio
BMEP - Brake Mean Effective Pressure
bTDC - before Top Dead Center
C100 - Fuel with 100 vol.-% DMC
C1-fuel - Fuel without C-C bond
CFD - Computational Fluid Dynamics
CR - Compression Ratio
C65F35 - Fuel with 65 vol.-% DMC / 35 vol.-% MeFo
CO - Carbon Monoxide
CO_2 - Carbon Dioxide
COV - Coefficient Of Variation
CPC - Condensation Particle Counter
DI - Direct Injection
DISI - Direct Injection Spark-Ignition
DMC - Dimethyl Carbonate
DVPE - Dry Vapor Pressure Equivalent
ECU - Electronic Control Unit
EOI - End Of Injection
FID - Flame Ionization Detector
FTDC - Fired Top Dead Center
FTIR - Fourier-Transform InfraRed spectroscopy
FUP - FUel Pressure
G100 - Fuel with 100 vol.-% RON95 E5
G85C15 - Fuel with 85 vol.-% RON95 E5 / 15 vol.-% MeFo
G70C30 - Fuel with 70 vol.-% RON95 E5 / 30 vol.-% MeFo
G50C50 - Fuel with 50 vol.-% RON95 E5 / 50 vol.-% MeFo
GHG - GreenHouse Gas
GPF - Gasoline Particulate Filter
HCCI - Homogeneous Charge Compression Ignition
HCR - High Compression Ratio
ICE - Internal Combustion Engine
IMEP - Indicated Mean Effective Pressure
LHV - Lower Heating Value
LSPI - Low Speed Pre-Ignition
M100 - Fuel with 100 vol.-% MeOH
M85F15 - Fuel with 85 vol.-% MeOH / 15 vol.-% MeFo
M70F30 - Fuel with 70 vol.-% MeOH / 30 vol.-% MeFo
MeFo - Methyl Formate
MeOH - Methanol
MFB50 - 50 % Mass Fraction Burned
MIE - Minimum Ignition Energy
MON - Motor Octane Number
NO_x - Oxides of Nitrogen (NO and NO2)
NTP - Normal Temperature and Pressure
O_2 - Oxygen
PFI - Port Fuel Injection
PN - Particle Number
PN10 - Particle Number with cut off at 10 nm
PN23 - Particle Number with cut off at 23 nm
PPM - Parts Per Million
RGB - Red Green Blue
RON - Research Octane Number
RPM - Revolutions Per Minute
SCE - Single Cylinder Engine
SI - Spark-Ignition
SOI - Start Of Injection
SPCS - Solid Particle Counting System
STP - Standard Temperature and Pressure
T_c - Coolant Temperature
T_{intake} - Intake Air Temperature
TDC - Top Dead Center
THC - Total HydroCarbons
TKE - Turbulence Kinetic Energy
TUM - Technical University of Munich
TWC - Three-Way Catalyst
VOC - Volatile Organic Compounds
WOT - Wide-Open Throttle
°CA - Crank Angle Degree

References

1. European Commission, "*Amended Proposal for a Regulation of the European Parliament and of the Council on Establishing the Framework for Achieving Climate Neutrality and Amending Regulation (EU) 2018/1999 (European Climate Law): COM(2020) 563 Final*," 2020.
2. Schulmeister, U., Eppler, S., and Christ, A., "Roadmap to a De-fossilized Powertrain," in: Bargende, M., Reuss, H.-C., and Wiedemann, J. (eds.), in *17. Internationales Stuttgarter Symposium, Proceedings, Springer Fachmedien Wiesbaden*, Wiesbaden, ISBN 978-3-658-16987-9: 279-291, 2017.
3. Wagner, C., Grill, M., Keskin, M.-T., Bargende, M., et al., "Potential Analysis and Virtual Developament of SI Engines Operated with Synthetic Fuel DMC+," in *SAE Technical Paper Series, WCX SAE World Congress Experience*, APR. 21, 2020, SAE International400 Commonwealth Drive, Warrendale, PA, United States, 2020, https://doi.org/10.4271/2020-01-0342.
4. Blochum, S., Ruch, F.H., Bastuck, T., Härtl, M. et al., "Identification of In-cylinder Aerosol Flow Induced Emissions due to Piston Ring Design in a DISI Single Cylinder LV Engine using Oxygenated Synthetic Fuels," in *SAE Technical Paper Series, WCX SAE World Congress Experience*, APR. 13, 2021, SAE International400 Commonwealth Drive, Warrendale, PA, United States, 2021, https://doi.org/10.4271/2021-01-0625.

5. Pélerin, D., Gaukel, K., Härtl, M., and Wachtmeister, G., "Nitrogen Oxide Reduction Potentials using Dimethyl Ether and Oxymethylene Ether in a Heavy-duty Diesel Engine," SAE Technical Paper Series, SAE Technical Paper Series, Automotive Technical Papers, JAN. 01, 2020, SAE International400 Commonwealth Drive, Warrendale, PA, United States, 2020, https://doi.org/10.4271/2020-01-5084.
6. "Monitoring CO2 Emissions from New Passenger Cars and Vans," *EEA Report, no 2020, 2, Publications Office of the European Union*, Luxembourg, ISBN 978-92-9480-222-4, 2020.
7. European Automobile Manufacturers Association, "Making the Transition to Zero-Emission Mobility: 2020 Progress Report-Enabling Factors for Alternatively-Powered Cars and Vans in the European Union," https://www.acea.be/uploads/publications/ACEA_progress_report_2020.pdf.
8. Scharrer, O., "The Powertrain in 2030 Shaped by Diversification," *ATZ Worldw* 120, no. S1 (2018): 52-57, doi:10.1007/s38311-018-0090-z.
9. Härtl, M., Pélerin, D., Dworschak, P., Maier, T. et al., "Potential of the Sustainable C1 Fuels OME, DMC, and MeFo for Particle-Free Combustion in SI and CI Engines," in: Liebl, J., Beidl, C., and Maus, W. (eds.), *Internationaler Motorenkongress 2018, Proceedings*, Springer Fachmedien Wiesbaden, Wiesbaden, ISBN 978-3-658-21014-4:459-478, 2018.
10. Fallah Ramezani, S., Karimi, M., Panahi, M., and Rafiee, A., "Sustainable Dimethyl Carbonate Production from Ethylene Oxide and Methanol," *Chem. Eng. Technol.* 43, no. 12 (2020): 2484-2492, doi:10.1002/ceat.202000150.
11. Kishi, R., Ogihara, H., Yoshida-Hirahara, M., Shibanuma, K. et al., "Green Synthesis of Methyl Formate via Electrolysis of Pure Methanol," *ACS Sustainable Chem. Eng.* 8, no. 31 (2020): 11532-11540, doi:10.1021/acssuschemeng.0c02281.
12. Effenberger, F.X., "Vision: "Technical Photosynthesis"," in: Bertau, M., Offermanns, H., Plass, L., Schmidt, F. et al. (eds.), *Methanol: The Basic Chemical and Energy Feedstock of the Future*, Springer Berlin Heidelberg, Berlin, Heidelberg, ISBN 978-3-642-39708-0:39-50, 2014.
13. Härtl, M., Stadler, A., Backes, F., Wachtmeister, G. et al., "Potentially CO2-neutral Fuels for Clean SI Engines," *MTZ Worldw* 78, no. 7-8 (2017): 76-83, doi:10.1007/s38313-017-0058-1.
14. Liu, C.M., Sandhu, N.K., McCoy, S.T., and Bergerson, J.A., "A Life Cycle Assessment of Greenhouse Gas Emissions from Direct Air Capture and Fischer-tropsch Fuel Production," *Sustainable Energy Fuels* 4, no. 6 (2020): 3129-3142, doi:10.1039/c9se00479c.
15. Kotowicz, J., Węcel, D., and Brzęczek, M., "Analysis of the Work of a "Renewable" Methanol Production Installation Based ON H2 from Electrolysis and CO2 from Power Plants," *Energy* 221 (2021): 119538, doi:10.1016/j.energy.2020.119538.
16. Tundo, P. and Selva, M., "The Chemistry of Dimethyl Carbonate," *Accounts of Chemical Research* 35, no. 9 (2002): 706-716, doi:10.1021/ar010076f.
17. Abdalla, A. and Liu, D., "Dimethyl Carbonate as a Promising Oxygenated Fuel for Combustion: A Review," *Energies* 11, no. 6 (2018): 1552, doi:10.3390/en11061552.
18. Schifter, I., González, U., and González-Macías, C., "Effects of Ethanol, Ethyl-tert-butyl Ether and Dimethyl-carbonate Blends with Gasoline on SI Engine," *Fuel* 183 (2016): 253-261, doi:10.1016/j.fuel.2016.06.051.
19. Yang, J., Jiang, Y., Karavalakis, G., Johnson, K.C. et al., "Impacts of Dimethyl Carbonate Blends on Gaseous and Particulate Emissions from a Heavy-duty Diesel Engine," *Fuel* 184 (2016): 681-688, doi:10.1016/j.fuel.2016.07.053.
20. Mei, D., Wu, H., Ren, H., Hielscher, K. et al., "Combustion Cycle-by-cycle Variations in a Common Rail Direct Injection Engine Fueled with Dimethyl Carbonate-Diesel Blend," *J. Energy Eng* 142, no. 1 (2016): 4014059, doi:10.1061/(ASCE)EY.1943-7897.0000259.
21. Pacheco, M.A. and Marshall, C.L., "Review of Dimethyl Carbonate (DMC) Manufacture and its Characteristics as a Fuel Additive," *Energy Fuels* 11, no. 1 (1997): 2-29, doi:10.1021/ef9600974.
22. Verhelst, S., Turner, J.W.G., Sileghem, L., and Vancoillie, J., "Methanol as a Fuel for Internal Combustion Engines," *Progress in Energy and Combustion Science* 70 (2019): 43-88, doi:10.1016/j.pecs.2018.10.001.
23. Najari, F., Baradaran, I., and Najari, D., "Methanol Poisoning and its Treatment," *Int J Med Toxicol Forensic Med* 10, no. 1 (2020): 26639, doi:10.32598/ijmtfm.v10i1.26639.
24. Naman, T.M. and Striegler, B.C., "Engine and Field Test Evaluation of Methanol as an Automotive Fuel," in *SAE Technical Paper Series*, SAE Technical Paper Series, 1983 SAE International Fall Fuels and Lubricants Meeting and Exhibition, OCT. 31, 1983, SAE International400 Commonwealth Drive, Warrendale, PA, 1983, https://doi.org/10.4271/831703.
25. Divakar Shetty, A.S., Sahu, D., Arthur Davis, J., and Kumar, R., "Comparative Study on Gasoline and Methanol in a Twin Spark IC Engine," in: Pant, P., Mishra, S.K., and Mishra, P.C. (eds.), in *Advances in Mechanical Processing and Design*, Lecture Notes in Mechanical Engineering, Springer Singapore, Singapore, ISBN 978-981-15-7778-9:191-201, 2021.
26. Mishra, P.C., Gupta, A., Kumar, A., and Bose, A., "Methanol and Petrol Blended Alternate Fuel for Future Sustainable Engine: A Performance and Emission Analysis," *Measurement* 155 (2020): 107519, doi:10.1016/j.measurement.2020.107519.
27. Lee, J.S., Kim, J.C., and Kim, Y.G., "Methyl Formate as a New Building Block in C1 Chemistry," *Applied Catalysis* 57, no. 1 (1990): 1-30, doi:10.1016/S0166-9834(00)80720-4.
28. Dooley, S., Burke, M.P., Chaos, M., Stein, Y. et al., "Methyl Formate Oxidation: Speciation Data, Laminar Burning Velocities, Ignition Delay Times, and a Validated Chemical Kinetic Model," *Int. J. Chem. Kinet.* 42, no. 9 (2010): 527-549, doi:10.1002/kin.20512.
29. Härtl, M., Stadler, A., Blochum, S., Pélerin, D. et al., "DMC+ as Particulate Free and Potentially Sustainable Fuel for DI SI Engines," in: Geringer, B. and Lenz, H.P. (eds.), *39. Internationales Wiener Motorensymposium 26.-27. April 2018*, Fortschritt-Berichte VDI. Reihe 12, Verkehrstechnik, Fahrzeugtechnik, ISBN 978-3-18-380712-3:202-229, 2018.
30. Mühlthaler, M., Blochum, S., Stadler, A., Härtl, M. et al., "Optical Investigations of Oxygenated Alternative Fuels in a Single Cylinder DISI Light Vehicle Gasoline Engine," in *SAE*

Technical Paper Series, WCX SAE World Congress Experience, APR. 13, 2021, SAE International400 Commonwealth Drive, Warrendale, PA, 2021, https://doi.org/10.4271/2021-01-0557.

31. Wilharm, T., Seidenspinner, P., and Jacob, E., "Potentially Co2-Neutral and Ecological Gasoline Based on C1-Chemistry," EP3399008A1, January 26, 2018.
32. Blochum, S., Gadomski, B., Retzlaff, M., Thamm, F. et al., "Potential Analysis of a DMC/MeFo Mixture in a DISI Single- and Multi-Cylinder Light Vehicle Gasoline Engine," in *SAE Technical Paper Series, WCX SAE World Congress Experience, APR. 13, 2021, SAE International400 Commonwealth Drive*, Warrendale, PA, 2021, https://doi.org/10.4271/2021-01-0561.
33. Jacob, E., Stark, M., Härtl, M., and Wachtmeister, G., "C1-Oxygenate als zukünftige Kraftstoffe," in: Tschöke, H. and Marohn, R. (eds.), *11. Tagung Einspritzung und Kraftstoffe 2018*, Proceedings, Springer Fachmedien Wiesbaden, Wiesbaden, ISBN 978-3-658-23180-4:17-55, 2019.
34. Chan, J.H., Tsolakis, A., Herreros, J.M., Kallis, K.X. et al., "Combustion, Gaseous Emissions and PM Characteristics of Di-Methyl Carbonate (DMC)-Gasoline Blend on Gasoline Direct Injection (GDI) Engine," *Fuel* 263 (2020): 116742, doi:10.1016/j.fuel.2019.116742.
35. Scharrer, O., Wieske, P., Warth, M., Schwarzenthal, D. et al., "Uncompromisingly Fun to Drive Thanks to Synthetic Fuel Blend," in: Geringer, B. and Lenz, H.P. (eds.), *40. Internationales Wiener Motorensymposium 15.-17. Mai 2019*, Fortschritt-Berichte VDI. Reihe 12, Verkehrstechnik, Fahrzeugtechnik, vol. 811, ISBN 978-3-18-381112-0:84-102, 2019.
36. Forbes, A.D., and Powell, K.G., "Gasoline Composition," GB000001411947A.
37. Zhang, W., Zhang, Z., Ma, X., Awad, O.I. et al., "Impact of Injector Tip Deposits on Gasoline Direct Injection Engine Combustion, Fuel Economy and Emissions," *Applied Energy* 262 (2020): 114538, doi:10.1016/j.apenergy.2020.114538.
38. Gumz, W., "Eine neue Heizwertformel für feste Brennstoffe," *Feuerungstechnik* 26, no. 10 (1938): 322-323.
39. Härtl, M., Stadler, A., Blochum, S., Pélerin, D., et al., "DMC+ as Particulate Free and Potentially Sustainable Fuel for DI SI Engines," in: Maus, W. (ed.), *Zukünftige Kraftstoffe: Energiewende des Transports als ein weltweites Klimaziel*, ATZ/MTZ-Fachbuch, 1st ed., Springer Berlin, Berlin, ISBN 978-3-662-58006-6, 2019.
40. Kraus, C., Fellner, F., Härtl, M., Blochum, S. et al., "Review of Potential CO2-Neutral Fuels in Passenger Cars in Context of a Possible Future Hybrid Powertrain," SAE Technical Paper Series (2022).
41. Babrauskas, V., "*Ignition Handbook: Principles and Applications to Fire Safety Engineering, Fire Investigation, Risk Management and Forensic Science*," Fire Science Publishers, Issaquah, Wash., ISBN 978-0972811132, 2003.
42. McAllister, S., Chen, J.-Y., and Fernandez-Pello, A.C., "*Fundamentals of Combustion Processes*," Springer New York, New York, NY, ISBN 978-1-4419-7942-1, 2011.
43. Aprentas (ed.), "*Laborpraxis Band 3: Trennungsmethoden*," Springer International Publishing, Cham, ISBN 978-3-0348-0969-6, 2017.
44. Heywood, J.B., "Internal Combustion Engine Fundamentals," *McGraw-Hill Series in Mechanical Engineering, McGraw-Hill, New York, ISBN* 9780070286375 (1988).
45. Lee, H.E., Yoon, S.J., Sohn, J.-R., Huh, D.-A. et al., "Flammable Substances in Korea Considering the Domino Effect: Assessment of Safety Distance," *International Journal of Environmental Research and Public Health* 16, no. 6 (2019), doi:10.3390/ijerph16060969.
46. Dehdashti, A.R., Khavanin, A., Rezaei, A., Assilian, H. et al., "Using Microwave Radiation to Recover Granular Activated Carbon Exposed to Toluene Vapor," *Iranian Journal of Chemistry and Chemical Engineering (IJCCE)* 30, no. 1 (2011): 55-64, doi:10.30492/ijcce.2011.6277.
47. Bormashenko, E., "Why are the Values of the Surface Tension of Most Organic Liquids Similar?" *American Journal of Physics* 78, no. 12 (2010): 1309-1311, doi:10.1119/1.3471939.
48. Backes, F., Blochum, S., Härtl, M., and Wachtmeister, G., "Experimental Analysis of Gasoline Direct Injector Tip Wetting," *SAE Int. J. Engines* 13, no. 1 (2020), https://doi.org/10.4271/03-13-01-0006.
49. Peer, J., Backes, F., Sauerland, H., Härtl, M. et al., "Development of a High Turbulence, Low Particle Number, High Injection Pressure Gasoline Direct Injection Combustion System," *SAE Int. J. Engines* 9, no. 4 (2016): 2301-2311. https://doi.org/10.4271/2016-01-9046.
50. Stadler, A., Sauerland, H., Härtl, M., and Wachtmeister, G., "The Potential of Gasoline Fueled Pre Chamber Ignition Combined with Elevated Compression Ratio," in:, SAE Technical Paper Series, WCX SAE World Congress Experience, APR. 21, 2020, SAE International400 Commonwealth Drive, (Warrendale, PA, 2020), https://doi.org/10.4271/2020-01-0279.
51. Bowditch, F.W., "A New Tool for Combustion Research A Quartz Piston Engine," in *SAE Technical Paper Series, SAE Technical Paper Series, Pre-1964 SAE Technical Papers, JAN. 01, 1961, SAE International400 Commonwealth Drive*, Warrendale, PA, 1961, https://doi.org/10.4271/610002.
52. Dec, J.E., and Espey, C., "Ignition and Early Soot Formation in a DI Diesel Engine Using Multiple 2-D Imaging Diagnostics," in *SAE Technical Paper Series, SAE Technical Paper Series, International Congress & Exposition, FEB. 27, 1995, SAE International400 Commonwealth Drive*, Warrendale, PA, 1995, https://doi.org/10.4271/950456.
53. Vedharaj, S., Vallinayagam, R., An, Y., Izadi Najafabadi, M. et al., "Combustion Homogeneity and Emission Analysis during the Transition from CI to HCCI for FACE I Gasoline," in *SAE Technical Paper Series, SAE Technical Paper Series, International Powertrains, Fuels & Lubricants Meeting, OCT. 16, 2017, SAE International400 Commonwealth Drive*, Warrendale, PA, 2017, https://doi.org/10.4271/2017-01-2263.
54. Sheikhani, H., Ajam, H., and Ghazikhani, M., "A Review of Flame Radiation Research from the Perspective of Factors Affecting the Flame Radiation, Measurement and Modeling," *Eur. Phys. J. Plus* 135, no. 4 (2020), doi:10.1140/epjp/s13360-020-00350-7.
55. Fenimore, C.P., "Formation of Nitric Oxide in Premixed Hydrocarbon Flames," *Symposium (International) on*

Combustion 13, no. 1 (1971): 373-380, doi:10.1016/s0082-0784(71)80040-1.

56. Golzari, R., Li, Y., and Zhao, H., "Impact of Port Fuel Injection and In-Cylinder Fuel Injection Strategies on Gasoline Engine Emissions and Fuel Economy," in *SAE Technical Paper Series*, SAE Technical Paper Series, SAE 2016 International Powertrains, Fuels & Lubricants Meeting, OCT. 24, 2016, SAE International 400 Commonwealth Drive, Warrendale, PA, United States, 2016, https://doi.org/10.4271/2016-01-2174.
57. Deegan, R.D., Bakajin, O., Dupont, T.F., Huber, G. et al., "Capillary Flow as the Cause of Ring Stains From Dried Liquid Drops," *Nature* 389, no. 6653 (1997): 827-829, doi:10.1038/39827.
58. Zhang, H., Achleitner, E., Jovovic, D., Kull, E. et al., "Herausforderungen an die Benzindirekteinspritzsysteme zur Einhaltung der EU6c Benzindirekteinspritzung," in: Tschöke, H. (ed.), *9. Tagung Diesel- und Benzindirekteinspritzung 2014*, Proceedings, Springer Vieweg, Wiesbaden, ISBN 978-3-658-07649-8:251-286, 2015.
59. "Fundamentals," in: Eastwood, P. (ed.), *Particulate Emissions from Vehicles*, Wiley-Professional Engineering Publishing Series, John Wiley & Sons, Ltd, Chichester, UK, ISBN 9780470986516:9-59, 2007.
60. Liu, H., Li, Z., Xu, H., Ma, X. et al., "Nucleation Mode Particle Evolution in a Gasoline Direct Injection Engine with/without a Three-Way Catalyst Converter," *Applied Energy* 259 (2020): 114211, doi:10.1016/j.apenergy.2019.114211.
61. Dahnz, C., Han, K.-M., Spicher, U., Magar, M. et al., "Investigations on Pre-Ignition in Highly Supercharged SI Engines," *SAE Int. J. Engines* 3, no. 1 (2010): 214-224. https://doi.org/10.4271/2010-01-0355.
62. Panzani, G., Pozzato, G., Savaresi, S.M., Rösgren, J. et al., "Engine Knock Detection: An Eigenpressure Approach," *IFAC-PapersOnLine* 52, no. 5 (2019): 267-272, doi:10.1016/j.ifacol.2019.09.043.
63. Wang, Z., Liu, H., Song, T., Qi, Y. et al., "Relationship Between Super-knock and Pre-ignition," *International Journal of Engine Research*, 16(2):166-180, 2015, doi:10.1177/1468087414530388.
64. Dahnz, C. and Spicher, U., "Irregular Combustion in Supercharged Spark Ignition Engines - Pre-ignition and other Phenomena," *International Journal of Engine Research* 11, no. 6 (2010): 485-498, doi:10.1243/14680874jer609.
65. Haenel, P., Kleeberg, H., Bruijn, R., and Tomazic, D., "Influence of Ethanol Blends on Low Speed Pre-Ignition in Turbocharged, Direct-Injection Gasoline Engines," *SAE Int. J. Fuels Lubr.* 10, no. 1 (2017): 95-105. https://doi.org/10.4271/2017-01-0687.
66. Ebersole, R.E., Matusz, L.C., Modi, M.S., and Orlando, R.E., "Hot Surface Ignition of Gasoline-Ethanol Fuel Mixtures," *SAE Int. J. Engines* 2, no. 1 (2009): 1-8. https://doi.org/10.4271/2009-01-0016.
67. Hamilton, L.J., Rostedt, M.G., Caton, P.A., and Cowart, J.S., "Pre-Ignition Characteristics of Ethanol and E85 in a Spark Ignition Engine," *SAE Int. J. Fuels Lubr.* 1, no. 1 (2009): 145-154. https://doi.org/10.4271/2008-01-0321.
68. Menrad, H., Haselhorst, M., and Erwig, W., "Pre-Ignition and Knock Behavior of AIcohol Fuels," SAE Technical Paper Series, SAE Technical Paper Series, 1982 SAE International Fall Fuels and Lubricants Meeting and Exhibition, OCT. 18, 1982, SAE International400 Commonwealth Drive, Warrendale, PA, United States, 1982, https://doi.org/10.4271/821210.
69. Haenel, P., Seyfried, P., Kleeberg, H., and Tomazic, D., "Systematic Approach to Analyze and Characterize Pre-ignition Events in Turbocharged Direct-injected Gasoline Engines," SAE Technical Paper Series, SAE Technical Paper Series, SAE 2011 World Congress & Exhibition, APR. 12, 2011, SAE International400 Commonwealth Drive, Warrendale, PA, United States, 2011, https://doi.org/10.4271/2011-01-0343.
70. Kalghatgi, G., "Fuel/Engine Interactions," *SAE International*, Warrendale, PA, ISBN 978-0-7680-8043-8, 2013.
71. Birmili, W., Weinhold, K., Rasch, F., Sonntag, A. et al., "Long-term Observations of Tropospheric Particle Number Size Distributions and Equivalent Black Carbon Mass Concentrations in the German Ultrafine Aerosol Network (GUAN)," *Earth Syst. Sci. Data* 8, no. 2 (2016): 355-382, doi:10.5194/essd-8-355-2016.

ISSN 0148-7191

B.4 Identification of In-Cylinder Aerosol Flow Induced Emissions due to Piston Ring Design in a DISI Single Cylinder LV Engine Using Oxygenated Synthetic Fuels

2021-01-0625 Published 06 Apr 2021

Identification of In-Cylinder Aerosol Flow Induced Emissions due to Piston Ring Design in a DISI Single Cylinder LV Engine Using Oxygenated Synthetic Fuels

Sebastian Blochum Technical University of Munich

Fabian H. Ruch Technical University of Munich / Tenneco

Thomas Bastuck Tenneco

Martin Härtl Technical University of Munich

Richard Mittler Tenneco

Georg Wachtmeister Technical University of Munich

Citation: Blochum, S., Ruch, F.H., Bastuck, T., Härtl, M. et al., "Identification of In-Cylinder Aerosol Flow Induced Emissions due to Piston Ring Design in a DISI Single Cylinder LV Engine Using Oxygenated Synthetic Fuels," *SAE Int. J. Advances & Curr. Prac. in Mobility* 3(5):2395-2409, 2021, doi:10.4271/2021-01-0625.

This article was presented at the WCX World Congress Experience Digital Summit, April 13-15, 2021.

Abstract

In the near future, pollutant and GHG emission regulations in the transport sector will become increasingly stringent. For this reason, there are many studies in the field of internal combustion research that investigate alternative fuels, one example being oxygenated fuels. Additionally, the design of engine components needs to be optimized to improve the thresholds of clean combustion and thus reduce particulates. Simulations based on PRiME 3D® for dynamic behaviors inside the piston ring group provide a guideline for experimental investigation. Gas flows into the combustion chamber are controlled by adjusting the piston ring design. A direct comparison of regular and synthetic fuels enables to separate the emissions caused by oil and fuel. This study employed a mixture of dimethyl carbonate (DMC) and methyl formate (MeFo). These two components have no C-C bonds, and the mixture displayed extremely good performance in terms of the particle number (PN) emissions on an ambient level published in previous studies. This fuel property is employed in this study to identify oil induced, engine-out PN-emissions, while the combustion process remains almost identical to that of conventional gasoline. The PN-emissions are measured and subdivided into two ranges: larger than 10 nm and larger than 23 nm.

It was demonstrated that merely changing the piston ring design has an impact on raw PN engine emissions and gas flow behavior in the piston assembly. An increase in PN-emissions and lower blow-by level could only be detected by changing the piston ring design. With reduced, predicted fluid flows into the combustion chamber, lower VOC emissions could be observed during motored runs. The adaptations in the tested piston ring design demonstrate that it is possible to improve particulate emissions by modifying the piston ring group.

Keywords

DISI engines, future combustion engine, piston ring, piston ring pack, piston ring design, piston assembly, oil induced emissions, particle number emissions, PN, alternative fuels, e-fuels, synthetic fuels, oxygenates, DMC, MeFo, blow-by, reverse blow-by, blow-back, aerosol, gas flow, second land pressure

Introduction

The global trend towards urbanization is still ongoing. The world´s 400 biggest cities occupy around 2 % of the earth´s surface and account for more than 60 % of global energy consumption. Over the course of the twentieth century, the worldwide urban population figure increased from 220 million to around 2.8 billion. It is expected that by 2050, the urban population will have increased to 6.9 billion. By then, around 70 % of the global population will be living in cities [1]. Increasing attention is therefore being paid to the

subject of air pollution exposure. Particle number (PN) emissions make up a significant proportion of total air pollution, resulting in negative effects on both the environment and human health.

All of this points towards big challenges for the transport sector due to the need to reduce local PN emissions. In turn, emission regulations throughout all sectors and regions are becoming increasingly stringent [2, 3, 4]. The potential exists to reduce particle formation by optimizing the piston, piston ring and crankcase assembly in terms of gas, fuel and oil flow under conditions that prevail in an internal-combustion engine [5]. As an example of synthetic fuels, the class of oxygenated fuels produced promising results in relation to particulate matter (PM) and PN emissions in both the diesel and the gasoline combustion process. In previous studies, Härtl et al. and Jacob [6, 7] demonstrated the benefit of the molecular structure of C1 oxygenates. They are so called because they lack a C-C bond in their molecules. This means that even a diffusive combustion emits low-soot emissions, as shown by Pelerin et al. [8] for a heavy-duty diesel engine.

Owing to the extreme reduction of fuel-related particle emissions - by a factor of 10 for dimethyl carbonate (DMC) and 100 for methyl formate (MeFo) [9] - the synthetic fuel described is suitable for a comparative study of regular and synthetic fuels. This allows the direct effect of oil-related particulates to be determined. On the other hand, interactions of oil, fuel and additional fluid components can vary from one fuel to another. Piston ring designs are modified to influence these interactions and thus impact on the total PN concentration. A comparison of synthetic and conventional fuels reveals that these interactions exist and can be influenced by piston ring design.

Background

Influence of Piston Rings on Fluid Flow and Emission Control

It is well known that the aerosol flow between the combustion chamber and crankcase caused by the piston ring pack is a significant source of oil emissions [10]. There are a great number of parameters which influence the interaction of the piston ring pack and oil-gas flow, for example, piston ring radial thickness, piston ring closed gap, tangential elastic force, cylinder bore match clearance, piston ring land clearance and many other design parameters [11]. Moreover, oil quality and operating conditions also affect the behavior of the complex system [12]. There are several non-trivial phenomena of oil consumption associated with gas flow in the piston ring pack. In-cylinder oil transport between combustion chamber and crankcase is divided into five different fields derived from [13, 14] as follows:

1. Throw-off - inertia forces throw oil droplets in the direction of the combustion chamber from the first ring surface and the top land. 'Top land' is defined as the area between the piston crown and the first ring.
2. Transport with reverse blow by - this is the aerosol flow from the crankcase to the combustion chamber caused by a difference in pressure. This study defines a subtype of reverse blow-by, called blow-back. This is the gas flow which originates in the area between the first and second ring, referred to as the second land. The flow is initialized by the combustion process and influenced by the piston ring design. Hence, it is possible for the second land pressure to exceed the combustion chamber pressure during the expansion stroke.
3. Entrainment in blow-by flow - oil mist is entrained by the blow-by gas flow into the crankcase. Depending on the engine design, a varying quantity of oil mist finds its way back into the combustion chamber through the intake manifold by way of the crankcase breather.
4. Evaporation - this refers to the evaporation of oil on the surfaces of the piston-ring-liner system, originating mainly from the liner.
5. Oil scraping from piston top land - oil is scraped from the liner by the top land of the piston. This is generally only the case if there are carbon deposits on the piston crown or top land [15].

As discussed above, gas flow in the form of blow-by, reverse blow-by, and blow-back has the capability to transport liquid and mist oil. Aerosol flow is obviously related to the pressure levels in the combustion chamber, inter-ring areas and crankcase. Essential for the inter-ring pressures are the ring gap areas and their ratios, because they function like a throttle and delay pressure equalization in the direction of the crankcase and combustion chamber. Tomanik et al. [16] pointed out that area of the first ring closed gap has an extreme effect on blow-by. It was shown in a 1.6L 4-cylinder gasoline engine that with a 50 % reduction of the first closed gap, average blow-by is reduced by 38 %. The reduction in closed gap was achieved by removing the chamfer of the outer diameter of the closed gap. As published previously, in 1984 Miyachika et al. [17] varied only the second ring gap area to manipulate the pressure level on the second land, in which two different ring gaps were used. The experiment showed that the second land pressure was higher than the combustion pressure. This generated a blow-back from the second land to the combustion chamber. This reverse aerosol flow was confirmed by the oil consumption measurement, which showed an increase. The configuration with blow-back resulted in higher oil consumption over the field-operating conditions and thus verified the transport of oil via gas flow. Overall, the results of the experiment and simulation show that the second land pressure is the crucial parameter of blow-back flow, although it has a significant effect on oil flow towards the combustion chamber [17].

The concept of manipulating gas flows using different closed gaps is applied in this study to change the boundaries in the combustion chamber during particle formation processes. Dynamic piston ring simulations are performed to define the final piston ring designs for test bed validation.

Against this background, the scope of the study is to investigate the opportunities for reducing PN emissions by

fluid flow control in the area between the combustion chamber and the crankcase by way of the piston ring design. The study also investigates the separate effects on PN emissions from lubricant oil and the interaction of all fluid components which are controlled via piston ring design.

In this study, the aerosol flow was also specifically adjusted by varying the second closed gap clearance on the basis of previous simulations. However, a direct comparison of PN emissions using regular and synthetic fuels was carried out to separate the effects of the piston ring assembly causing PN.

Lubricant Oil-Related Particle Emissions

The typical emitted particles from direct-injection (DI) and spark-ignited (SI) engines can be separated by the particle size in the two distinctive types. Particles with a mean diameter of less than 50 nm are combined in the nucleation mode and the size range from 50 - 200 nm is labeled as accumulation mode [18]. Different publications showed that lubricant oil-related particles are mainly emitting particles in the nucleation mode for DISI engines [19, 20, 21, 22, 23], as well as for diesel engines [24, 25, 26].

For diesel engines Miller et al. [24] showed the role of lubricant oil in particulate emissions due to a modified CAT 3304 diesel engine fueled with hydrogen. In spite of the absence of fuel-derived soot, because of missing carbon in the fuel, PN emissions were observed. The results showed a higher metal-to-carbon ratio for most of the particles and the particles had a small geometric mean diameter from 18 to 31 nm. The carbon and metal source must be from the lubricant oil, lubricant oil additives or derived from engine wear.

On the SI engine side Tabata et al. [21] varied the lubricant oil and also figured out that lubricant oil increases the PN emissions with a mean diameter of ~ 10 nm. He assumed that the particles are mainly generated through the combustion of metal-based additives used in lubricant oil. It was also observed that a novel molecular design of metal-free lubricant additives can dramatically decrease particles with a mean diameter of less than 50 nm.

With the support of these publications the important link between lubricant oil and fine PN emissions is clearly confirmed.

Synthetic Fuel

The baseline of the investigation is constituted by regular RON 95 E5 fuel. To ensure comparability with low particle generating fuel, a mixture of DMC and MeFo was chosen. The main reason for this was the extremely low PN and THC emissions noted in previous studies [27, 28]. In addition, it should not significantly affect the main combustion process, because the critical fuel properties of a mixture of 65 vol.- % DMC and 35 vol.-% MeFo (C65F35) are sufficiently close to standard RON 95 E5 gasoline [9]. This idea was transferred to a modern internal combustion single-cylinder DISI engine test bed and performed with a self-sufficient mobile fuel support system with an internal cambox.

Experimental Setup and Numerical Methodology

Single Cylinder Engine (SCE)

In the experimental setup a self-designed gasoline four-stroke gasoline research SCE is employed in line with several other publications [9, 27, 29, 30, 31]. The design is based on that of a modern series-production engine. The valve train is equipped with a non-variable double-overhead camshaft (DOHC) with four valves, two each for intake and exhaust. As shown in Table 1 a standard valve timing with a moderate lift and a small overlap is used. In this study, it operates in DISI, homogenous-combustion mode. A serial M14 spark plug and ignition coil is used for SI. All other essential specifications of the internal combustion engine (ICE) are shown in Table 1.

In this study three different variations of engine load, speed and intake manifold pressure were carried out. Finally, some additional points were measured throughout the engine operating map, in order to detect any tendencies in the engine load and speed diagram. For the load variation, only the intake throttle was adjusted, to set the desired IMEP value. During speed variation, the dynamometer speed was changed by the test bench control unit. The intake pressure sweep was recorded under motored operation with injection and ignition enabled.

The structural diagram shown in Figure 1 gives a compact overview of all key auxiliary units of the SCE. It is divided into four groups: air intake, mobile fuel, indication and exhaust system.

Air Intake System The air is aspirated from the environment by a stationary-working screw compressor through an air filter. After the compressor, the charge air passes an oil

TABLE 1 SCE specifications

Engine base	Modern production engine
Bore	82.51 mm
Stroke	86.6 mm
Connecting rod length	144 mm
Displacement	463 ccm
Compression ratio	10.92:1
Number of valves (intake/exhaust)	Two each
Exhaust valve lift	7 mm @ 250 °CA aTDC
Exhaust open	132 °CA aTDC
Exhaust close	368 °CA aTDC
Intake valve lift	6 mm @ 460 °CA aTDC
Intake open	348 °CA aTDC
Intake close	572 °CA aTDC
Max. engine load	17 bar IMEP
Max. rpm	3500 1/min
Oil temperature	80° C
Coolant temperature	80° C

FIGURE 1 Structure diagram

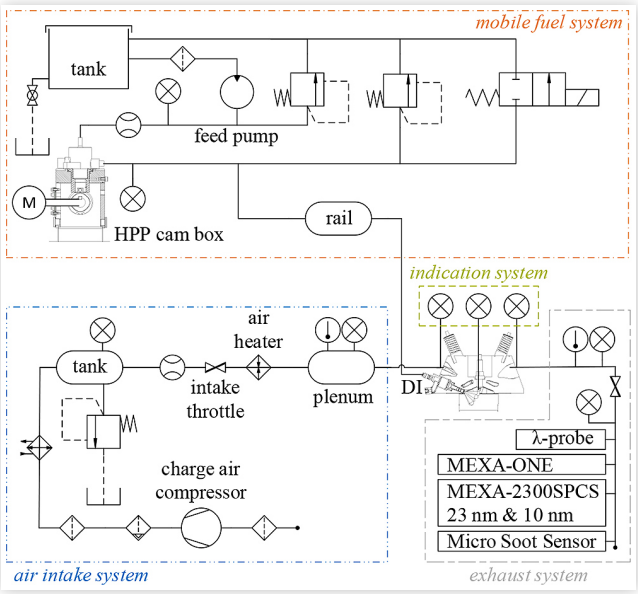

and water separator followed by an intake air cooler. The air tank then stores 150 liters of cleaned and cooled charge air at an absolute pressure of 2 bar. The surplus air mass flow is blown off by a relief valve from the tank. The intake air pressure is then controlled by a throttle, and the volumetric airflow is measured by an Aerzen rotary displacement meter. The desired air temperature in the intake manifold is supplied via an electric heater. A plenum is installed directly ahead of the intake manifold to damp turbulences and pressure oscillations in the charge air stream.

Mobile Fuel System & DI-Injector A compact mobile fuel system was used in the experiment. The main reason for using this system is the reduced effort required in changing and rinsing the fuel system, because of the low fuel capacity in resulting from the short pipe connections. Additionally, all pipes are built from stainless steel, which excludes virtually all potential durability issues resulting from the use of alternative fuels. In general, the mobile fuel system can be divided into a low-pressure and a high-pressure section. The low-pressure section is located before the high-pressure pump (HPP). It contains the fuel tank, fuel filter, feed pump, pressure gauge and pressure relief valve, as well as a flow meter. The low-pressure is set to 6 bar by the relief valve. The HPP is driven by a camshaft, which is connected directly to an electric motor via a clutch and mounted in a bearing housing.

The HPP is also mounted in the sealed housing, i.e. the cambox, to ensure adequate oil sump lubrication. The HPP operates quantitatively at the desired pressure, which is set using the National Instruments CompactRIO-based controller of the mobile fuel system. The pressure is subsequently measured in the high-pressure section using a WIKA S-10 pressure transducer. The maximum fuel pressure of the HPP is limited to 25 MPa and secured by means of an integrated pressure relief valve and an electronically actuated safety valve.

A stub line in the form of a high-pressure hose is connected to the fuel rail, which fits directly on the injector.

TABLE 2 DI-injector specifications

Max. pressure	25 MPa
Injector type	Multi-hole DI
Nozzle size	7.5 mm
Actuation	Solenoid
Number of orifices	6
Orifice shape	Taper
Injector position	Side mounted
Static flowrate @ 10 Mpa with n-Heptane	13.8 ccm/s

As can be seen in Table 2, the side-orientated series DI multi-hole injector is actuated by solenoid and the spray pattern matches the design of the engine base.

Exhaust System The exhaust manifold is followed by the adjustable exhaust throttle and a Bosch LSU 4.9 screw-in wideband lambda probe downstream. All exhaust gas measurement equipment is connected to the exhaust pipe 1.6 meters away from the cylinder by a gas-sampling probe. The probes pipe is trimmed diagonally, and the orifice is orientated downstream.

The gaseous emissions CO, CO_2, O_2, NO_x and THC (in C_3H_8 equivalent) are measured by different analyzers in the Horiba MEXA-ONE-D1 system. The common declaration of THC is ambiguous because it refers to a molecular structure made up exclusively of hydrogen and carbon. If the engine operates on oxygenated fuels such as DMC and MeFo, unburned fuel and intermediate molecules mainly contain oxygen. In accordance with the Directive 1999/13/EC of the European Council the more convenient term 'volatile organic compounds' (VOC) is therefore used rather than THC in this paper [32, 33].

Solid-state PN emissions are measured by a HORIBA MEXA-2300SPCS system [34] equipped with two condensation particle counters (CPC) with a cut-off size of 23 and 10 nm. The HORIBA MEXA-2300SPCS uses a direct sampling unit (DSU), which is connected through a 5.0 meters long heated sample line to the evaporation tube with an average temperature of 300 to 400 °C. The evaporation tube removes the soluble organic fraction and sulfate particles, as required by the emission regulations [35]. Therefore the counted values of the SPCS are mainly non-volatile particles that overcome a temperature greater than 300 °C over a timerange of 0.25 - 0.40 s [36]. Throughout the investigation no constant volume sampling (CVS) was used, but several publications [37, 38, 39] show that the PN emissions, measured from the raw exhaust using a DSU, are comparable. Finally, the PM-emissions are detected by an AVL micro soot sensor.

Engine Control and Data Acquisition The indication system is used to measure the in-cylinder pressure of the engine using the Kistler 6056A-3-2 piezo-electric pressure sensor. To measure the intake and exhaust pressure, the Kistler 4045A10 and Kistler 4075A10 piezo-resistive pressure sensors are mounted directly in the respective manifold. The engine load is calculated using the indicated mean effective pressure (IMEP) with the pressure trace sampling rate of 0.1 crank

angle degrees (°CA). The engine is operated with the intake pressure and air/fuel ratio (AFR) controlled automatically by the injection duration using the in-house dSPACE engine control unit (ECU) software. When an engine operation point is set as requested, the NI LabVIEW based data acquisition is triggered and 200 subsequent cycles are measured. The calculated data is averaged and stored in a data file along with the indicated pressure traces.

Lubricant Oil

The lubricant oil used in this study is the Mobil 1™ ESP 5W- 30 full synthetic engine oil which meets or exceeds lots of car manufacturers' standards for modern ICE's. In Table 3 the properties from the product data sheet are listed

Fuel

The key to separating the PN emission sources of fuel and oil is to use a substitute synthetic fuel, which leads to low-soot combustion. Furthermore, a mixture of 65 vol.-% DMC and 35 vol.-% MeFo was chosen, to match as closely as possible the RON95 E5 (G100) gasoline fuel properties. Table 4 shows the properties of G100 and C65F35.

The imbalances between the fuels are mostly due to the different oxygen content relative to the carbon content, i.e. the O/C-ratio. The lower heating value (LHV) results in a 2.8 times lower mass-based energy content for C65F35 compared to the reference fuel. However, the higher density of C65F35 partially compensates the volumetric energy content. Therefore, the mass-based gasoline equivalent is 2.0. Hence, the stoichiometric AFR is at an extremely low level. Approximately 10 % less intake air is needed with the synthetic fuel to achieve the same energy content. Additionally, the increased fuel mass flow for C65F35 means that the injection duration (t_i) has to be extended. There is also a rise in the total enthalpy of vaporization, equated with the in-cylinder cooling.

TABLE 3 Lubricant oil properties

Grade	SAE 5W-30
Viscosity, cSt @ 100°C, ASTM D445	11.8 mm^2/s
Sulfated Ash mass, ASTM D874	0.8-%
Hi-Temp Hi-Shear Viscosity @ 150 C ASTM D4683	3.5 mPa • s
Pour Point, ASTM D97	- 48 °C
Density @ 15 C, ASTM D4052	0.8458 g / cm^3

TABLE 4 Fuel properties

	Unit	G100	C65F35
Gasoline RON95 E5	vol. %	100	-
Dimethyl **C**arbonate		-	65
Methyl **F**ormate		-	35
LHV	MJ/kg	42.2	15.2
Density @ 15 °C	kg/m^3	750.8	1041.1
Gasoline equivalent	m^3/m^3	1.0	2.0
RON / MON	-	96.8/86.3	117/ >120
Oxygen content	wt. %	1.7	53.3
Hydrogen content	wt. %	13.2	6.7
Carbon content	wt. %	85.1	40
AFR (stoich.)	kg/kg	14.28	4.64
Boiling range	° C	37.5-202.5	37.5-94
CFPP		-	- 30
DVPE @ 37,8 °C	kPa	57.8	57.4
Enthalpy of vaporization	kJ/kg	420	433
Surface tension	mN/m	24	27.7

Engine Performance Using C65F35

The primary focus of this study is on gas blow-back, which is mainly affected by the second land pressure trace. The impact of the combustion side due to inter-ring pressures corresponds to the in-cylinder pressure over °CA. Some slight differences in the exemplary stoichiometric pressure traces can be observed in Figure 2. In all four pressure traces, the center of combustion, namely the mass fraction of burned 50 % (MFB50), is located at 8 °CA after the fired top dead center (FTDC).

During the compression stroke from 630 °CA up to the FTDC, C65F35 shows a lower pressure level for both cases, because less intake air mass flow is needed, and the total enthalpy of vaporization is higher. The 11 bar IMEP engine load point shows a higher pressure gradient around the FTDC. During the expansion stroke, the pressure level of both fuels matches very well. Only the maximum pressure is slightly lower, at the 5 bar IMEP point. This observation matches Figure 3, which shows the apparent heat release rate (AHRR). It can also be seen that the increase in AHRR is more rapid at 11 bar IMEP for C65F35. Overall, the maximum AHRR occurs for G100 shortly after C65F35.

Additionally, Figure 4 shows the maximum pressure and pressure gradient over a load variation. By increasing the load, the deviation of the maximum pressure gradient between G100 and C65F35 increases. This coincides with a better mixture formation, originating from a higher air mass flow at higher load points and differences in the final boiling point of 94° C for C65F35 and 202.5° C for G100. As a result, the

FIGURE 2 In-cylinder pressure trace of G100 and C65F35 @ 2000 rpm

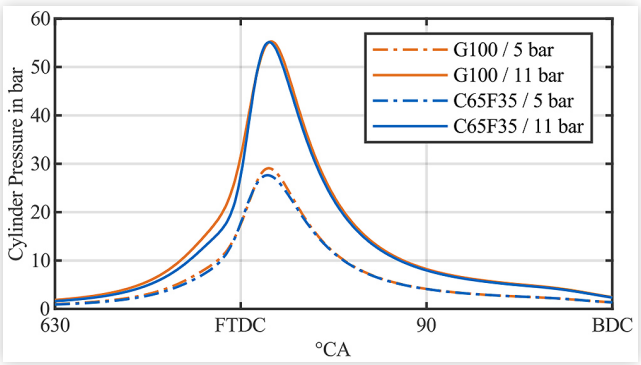

FIGURE 3 AHRR of G100 and C65F35 at 5 and 11 bar IMEP @ 2000 rpm

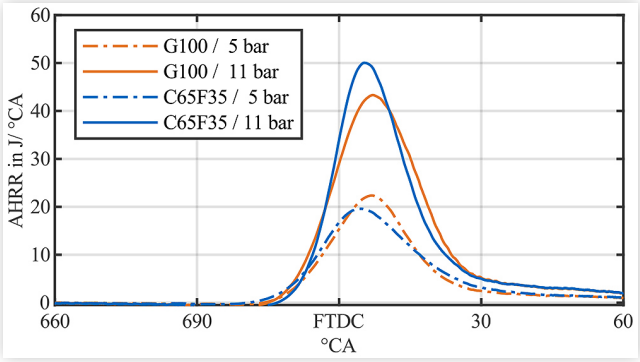

FIGURE 4 Max. pressure gradient & chamber pressure over IMEP

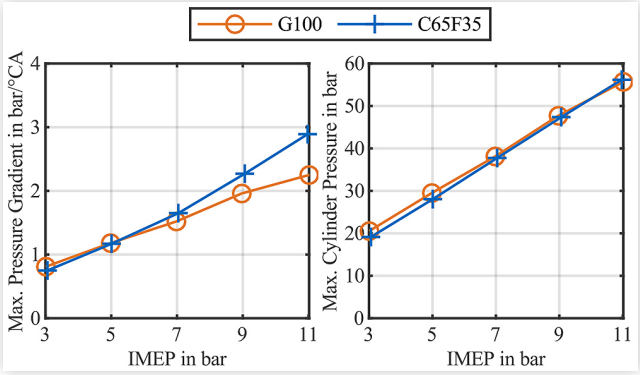

combustion duration of C65F35 decreases in comparison with G100 and C65F35 therefore displays a higher pressure gradient. No significant deviation in the maximum combustion chamber pressure was detected over all five load points. To sum up, the oxygenated fuel selected is suitable as a replacement for gasoline fuel in the DISI engine and for maintaining virtually the same pressure conditions in the combustion chamber, as well as the correlating land pressures of the piston assembly.

The main purpose of using C65F35 is the very low PN level involved - up to two orders of magnitude lower than for standard gasoline fuel. This significant decrease in PN 23 and 10 nm cut off size is described in Figure 5. The PN-level for C65F35 up to an engine load of 7 bar IMEP is roughly at an ambient level. With such an extreme decrease in the basic particle level, it is possible to detect small changes on the combustion mode side in terms of PN emissions.

The atmospheric emission level in this study is derived from long-term observation in Germany. The measurement by Birmili et al. [40] covered 17 different monitoring stations across four different region types, namely roadside, urban background, rural and alpine mountain. The average PN of 20-800 nm particle size level over several years was between $1.12x10^3$ at the Zugspitze (alpine mountain) and $1.05x10^4$ in the downtown area of Leipzig (roadside).

As is common in the measurement of atmospheric PN concentrations, volatile particles are included. This

FIGURE 5 PN of 23 and 10 nm over IMEP with G100 and C65F35

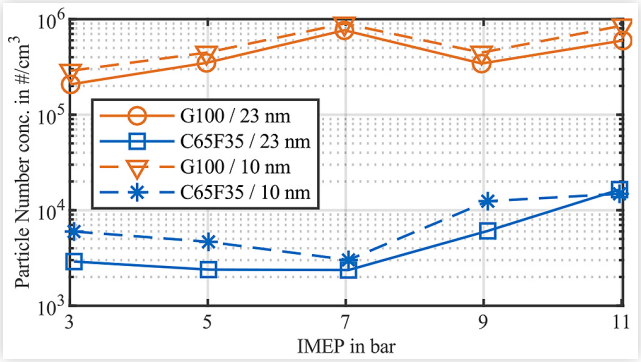

publication compares this figure with the non-volitle particles of the raw exhaust stream, as no significant share of non-volatile PN23 can be detected in the tailpipe under hot engine conditions after a three-way catalytic converter [41]. The impact of tailpipe PN-emissions on the environment is almost exclusively taken from non-volatile PN emissions. One of the few studies dealing with total atmospheric non-volatile PN (30-800 nm) was carried out in Augsburg Germany under urban background conditions. It determined an ambient non-volatile PN level of $1.9x10^3$ to 6.4 $x10^3$ in the city centre of Augsburg, with the nearest street about 100 meters away [42]. All shown PN concentrations in this study are described in #/cm^3. Because in the ICE´s research the emission target will be to have no impact on the environment. Therefore, specific emissions based on engine power are obsolete.

Figure 6 shows a clear drop in VOC-emissions using C65F35. This phenomenon can be explained by the measurement technique employed in the MEXA-ONE-D1. A flame ionization detector (FID) inside the exhaust gas analyzer measures the VOC content. The FID response is highly sensitive to hydrocarbons and is in general proportional to the number of carbon atoms per molecule in the gas stream. However, the signal reduction varies markedly for partially oxidized carbon atoms in compounds which are heteroatomic. As the O/C-ratio of the fuel increases, the response factor decreases. DMC and MeFo have an O/C-ratio of 1.0, which is the same as, for example, methanol (MeOH) or formaldehyde, which, based on a literature study by [43], have a response

FIGURE 6 VOC over IMEP of G100 and C65F35

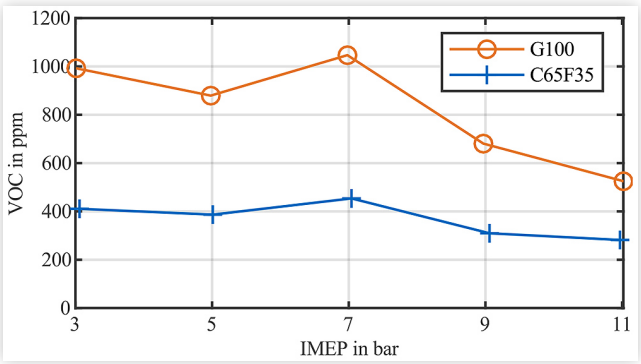

factor of 0.4 - 0.74 and 0, respectively. Depending on the operating conditions, all four components will be present in the exhaust gas to a greater or less extent, because they are intermediate or starting products of the reaction kinetics of the combustion.

Conversely, in this study, G100 has an O/C-ratio of 0.0153, and so the response factor is close to 1.0 for the FID [43, 44]. Ultimately, if the engine operates with C65F35 the base level of the detected VOC emissions over the load variation in Figure 6 are approximately halved. This fits in with the expected response factor range of MeOH, which is between 0.4 and 0.74. The measurement noise of the FID is about ± 1 %. Hence, it is expected that with the overall lower VOC level, the detection of oil-based VOC-emissions in an exhaust gas is increasingly accurate.

Piston Ring Design Using Prime3D® Simulation

This paper examines the variation in raw PN concentration in the ICE resulting from controlling the aerosol flow of the gas, fuel and oil mixture from the second land volume past the first compression ring into the combustion chamber. An aerosol transport increases owing to the change in ratio between the combustion pressure and inter-ring pressure of the top and second compression rings. Changing the closed gap of the piston ring causes a variation in the pressure ratio and enables the transport of aerosol towards the combustion chamber.

The piston ring configurations for the experimental study in this paper are designed on the basis of PRiME 3D® calculations. The ring dynamic simulations performed consist of three main elements:

- Gas flows in piston ring grooves and closed gaps
- Hydrodynamic contact situations
- Dynamic ring motion (translational and rotational / twist)

Gas flow is driven by the resulting clearance of the ring motion and the pressure differences. Hydrodynamic contact is based on the pressure distributions in the ring field and the axial velocities. Axial motion is affected by the resulting forces of the radial contact and the resulting pressure distributions around the ring. The resulting pressures in the ring field are a result of all these effects, which means that everything continuously interacts continuously. All simulation modules are calculated using physical methodologies that do not use any factors to balance out differences between measurements and simulations. This allows engine conditions to be predicted upfront before running the engine on a test bed, when proper input data is given [45, 46, 47]. For an accurate prediction, it is essential to take the three-dimensional effects into account, because the boundary conditions differ around the circumference and do not behave as rigid as often stated in the literature [45]. Additional effects such as bore distortions around the circumference [48] or advanced friction models increase the accuracy of the predictions and allow potential design changes to be identified [49, 50].

Initially, three ring pack configurations were defined for the test runs. Adapting the closed gap of the second ring is assumed to change the resulting inter-ring pressure between the top and second ring. With smaller closed gaps, the inter-ring pressure is increased until its level exceeds the combustion pressure, generating a flow from the land into the combustion chamber. Thermal deflections of liner and piston were derived from FE simulation of another engine from the same engine type with different measurement equipment, where temperatures were measured. The temperatures of the liner surface influence the local viscosity of the engine oil and differs along the stroke.

Table 5 shows the closed gaps that were tested:

Owing to the fact, that the simulations are supposed to represent the average of an engine conditions, the positioning of the gap ends has been neglected. The simulated inter-ring pressures and related top-ring motions can be seen in Figure 7. Configuration V0 with the small gap has a relatively high inter ring pressure (green dashed line in the upper diagram).

TABLE 5 Investigated ring configurations

Configuration	Top	2nd	3rd
V0	Asym. barrel ring	Napier Ring relative gap 0.8	LKZ oil control ring
V1	Asym. barrel ring	Napier Ring relative gap 1.5	LKZ oil control ring
V2	Asym. barrel ring	Napier Ring relative gap 1.0	LKZ oil control ring

FIGURE 7 Simulated interring pressures and top ring motions V0

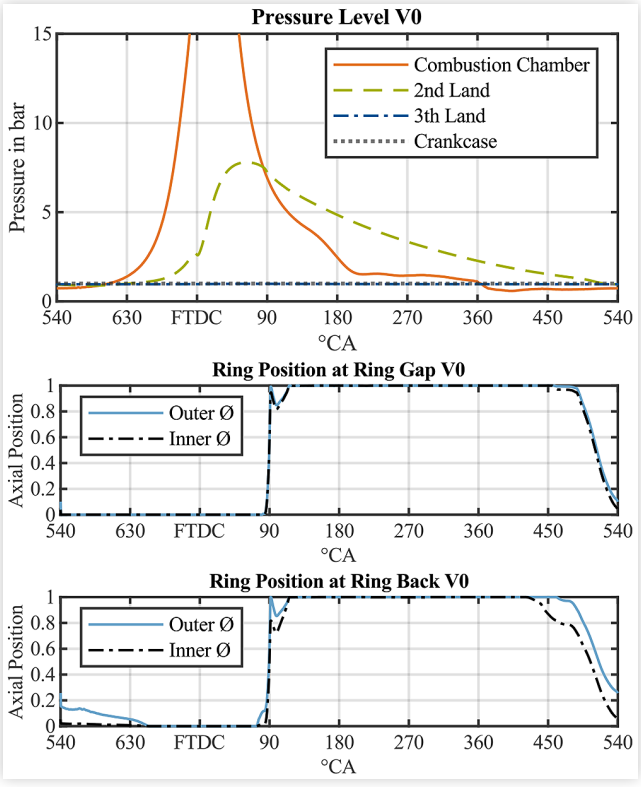

Close to 90 °CA, the inter-ring pressure exceeds the combustion pressure, which generates the blow-back gas flow from the inter ring volume into the combustion chamber. On the other hand, the configuration V1 in Figure 8 with the large second gap generates this gas flow for a very short time only. This increases the total blow-by and decreases the blow-back in comparison to V0.

Additionally, the ring position in the groove in the second and third diagrams from top is different. With high inter-ring pressures from V0, the ring is pushed to the upper flank (axial position = 1.0), where it is able to seal properly. In the V1 version with the low inter-ring pressures, the ring is pushed to the bottom (axial position = 0.0) of the flank owing to the acting inertia forces.

In both situations the sealing capabilities for gas flow through the groove are given. With the medium sized closed gap, the ring motion between 90 and 225 °CA is unstable. Because of the unstable ring motion of V2 shown in Figure 9, which might cause additional and uncontrolled transport of oil or gas, only the configurations V0 and V1 are considered. Figure 10 shows the resulting blow-by and blow-back values for V0 and V1 with a load sweep at 2000 rpm. It is important to notice that only one data set for thermal deflections was available for all load cases, which may result in measurement aberrations at different load points. However, the blow-by values are assumed to increase at higher loads, as expected. The trend of increasing blow-by in Figure 10 is lower when an IMEP of 7 bar is exceeded. The blow-back map confirms the desired trend for aerosol flow from the inter-ring volumes into the combustion chamber. Moreover, the amount blow-back increases at higher load. For V1, the closed gap is big enough to keep the blow-back level low, with a decreasing trend at a higher load of 11 bar IMEP.

FIGURE 8 Simulated interring pressures and top ring motions V1

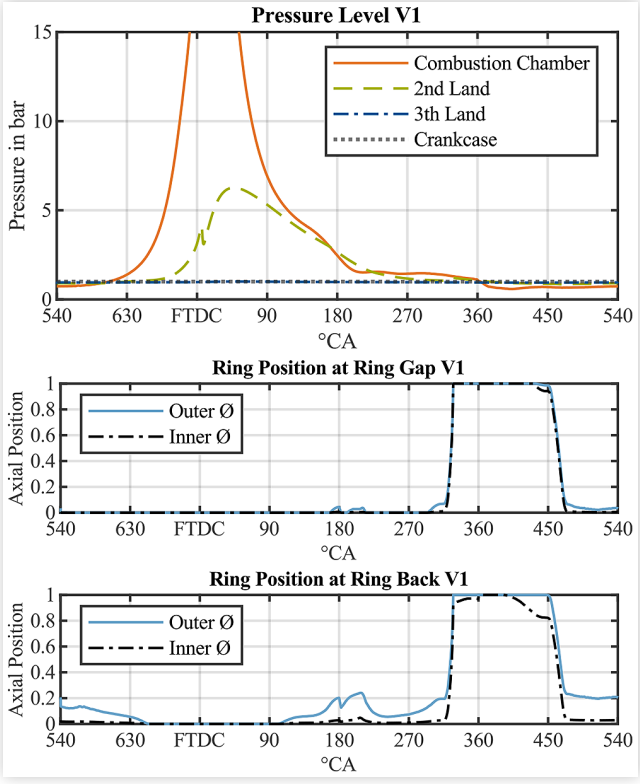

FIGURE 9 Simulated interring pressures and top ring motions V2

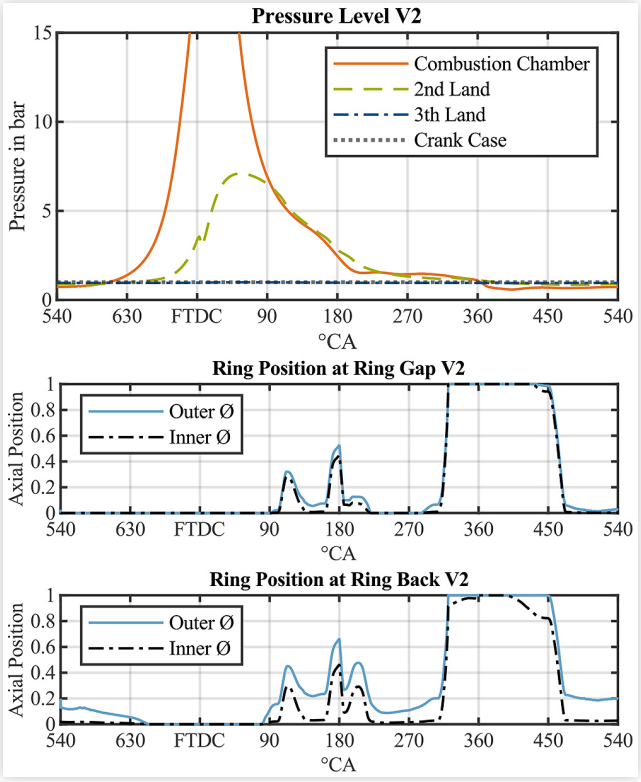

FIGURE 10 Simulated blow-by & blow-back @ 2000 rpm

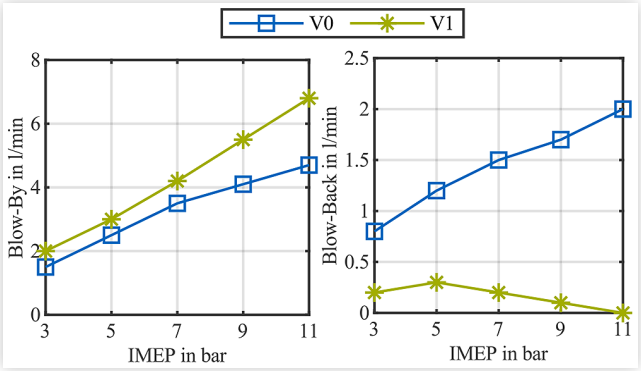

Results and Discussion

Operating Conditions

The reference point used in this study corresponds to an engine speed of 2000 rpm and an engine load of 7 bar IMEP with a global λ=1. The study employs a fixed start of injection (SOI) of 430 °CA and a constant fuel rail pressure of 25 MPa.

TABLE 6 Standard engine operating parameters

Engine Speed	2000 rpm
Engine Load in IMEP	7 bar
Lambda	1.0
MFB50	8 °CA aFTDC
Fuel Injection Pressure	25 MPa
SOI	430 °CA aFTDC
Oil & Water Temp.	80° C
Intake Air Temp.	30° C

This injection timing is adopted from the base engine and ensures the earliest possible injection timing without wetting the piston crown, which in turn implies the lowest possible PN-emissions. The oil and cooling water temperatures were each conditioned to the standard temperature of 80° C. Also, the air in the intake manifold was controlled to the standard temperature of 30° C. The ignition timing was adjusted for an MFB50 at 8 °CA aFTDC, which represents the thermodynamic optimum. All standard parameters shown in Table 6 are valid unless otherwise stated.

A running-in procedure with G100 was performed for both versions V0 and V1 of the second ring. One example run is shown in Figure 11. Only the second piston ring was changed between the two runs. All dimensions of the piston and liner were within the accepted tolerance range given by the manufacturer. The running-in procedure consists of three hours of fired operation at a constant load of 6 bar IMEP and an engine speed of 1000 rpm.

Subsequently, the engine load was shifted to 11 bar IMEP for 30 minutes. Afterwards, the engine load was decreased again to 6 bar IMEP for 10 min.

During this procedure, no significant change in the friction mean effective pressure (FMEP) could be observed, and the blow-by flow showed no anomalies. The PN and VOC emissions during the running-in procedure are shown in Figure 12. Throughout this run, no abnormalities were detected. With an increased engine load of 11 bar IMEP, the PN and VOC emissions are decreasing owing to the increased temperatures, which accelerates the oxidation reaction.

FIGURE 11 IMEP, FMEP and blow-by during running-in

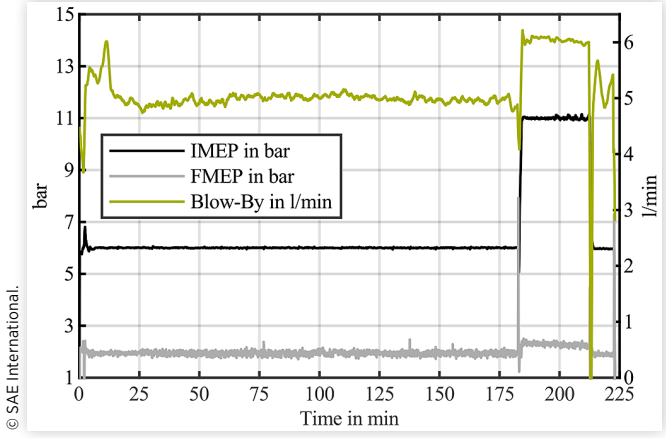

FIGURE 12 PN 23nm, PN 10nm and VOC in ppm during running-in

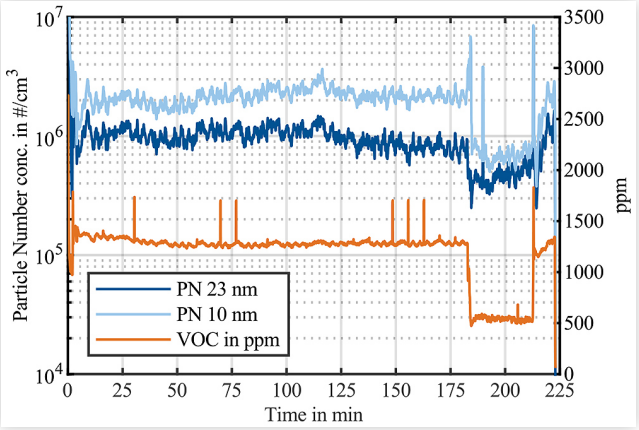

Also, the ratio of PN10 nm to PN23 nm decreases at an IMEP load of 11 bar. After stepping back to 6 bar IMEP, all monitored values were at roughly the same level as before the load increase. Throughout the procedure, no wear-in effect of the second compression ring could be detected.

Influence of Load and Engine Speed Variation The load variation takes in five operation points from 3 to 11 bar IMEP in 2 bar steps. The engine speed was varied from 1000 to 3000 rpm in 500 rpm steps. Some of these stationary measured points represent operating conditions from the NEDC cycle [51]. All other relevant parameters can be found in Table 6. In Figure 13, the clear expected trend of a higher V1 blow-by level could be observed. A repeatability check was pointed out for the reference point at IMEP = 7 bar and 2000 rpm. For all measured variants the error was less than ± 5 %. Because of the increase in the second ring closed gap, the gas flow towards the crankcase housing is less throttled. Averaged over the load sweep, the blow-by increased by 20 %. By elevating the load, Δp also increases during the compression and expansion stroke. Blow-by consequently also rises. In addition, blow-by in the engine speed variation increased by 24 % for V1. In general, boosting the engine speed reduces the blow-by to below 3000 rpm. An increase back to 3000 rpm increases the blow-by aerosol again.

FIGURE 13 Blow-by over IMEP & engine speed of V0 & V1

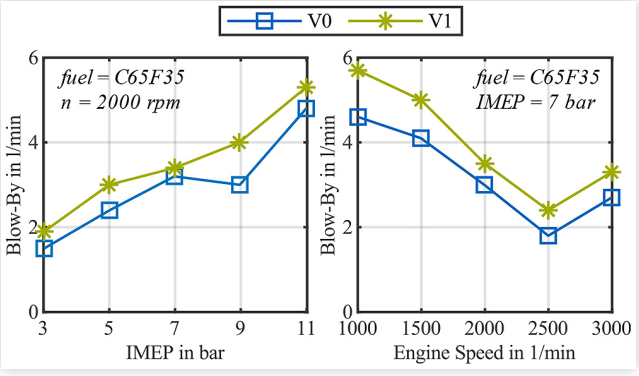

The largest percentage variance was detected for the speed variation at 2500 rpm. PN23 emissions for the load and speed variations in this study are shown in Figure 14. The area of the ambient level is marked in each diagram.

Below 9 bar IMEP, the PN23 emissions of V1 decrease, while V0 is roughly on the same level. When increasing the engine load from 7 to 11 bar IMEP, the PN of both variants rises owing to the longer injection duration. This leads to an increased penetration length for the fuel spray, especially for oxygenated fuel, due to its gasoline equivalent of 2.0. This can lead to increased wetting of the wall and piston. The mixture formation is thus more challenging. It is also necessary to convert the larger air-fuel charge in the same time range. At 9 and 11 bar IMEP, exceeds the ambient PN-level. With the rise in engine speed, the PN increase continuously for both components. This effect is due to the reduction in time remaining for mixture formation and combustion, resulting from the higher engine speed. All stationary points measured in the speed variation show a PN equal to or lower than ambient level. At all points except the 3 bar IMEP V1, it shows a lower PN23 over load and speed variation. An average reduction of 39 % by load and 31 % by speed variation was achieved. The maximum reduction of 83 % is achieved at the 9 bar IMEP load point. This is due to the higher blow-back of V0, which transports more unburned and partly burned aerosol including particles, back into the combustion chamber during the expansion stroke. This effect is more intensive at higher load points because of the higher pressure level and gradient in the combustion chamber. Conversely, an increase in engine speed reduces the time slot for the blow-back gas exchange between the second land and the combustion chamber. Figure 15 compares PN23- and PN10-emissions for both variants.

It is clearly evident that not only PN23, but also the PN10/PN23 ratio of V0 is higher for almost every measured point. Specifically, V0 emits even more PN10 than PN23, driven by more blow-back, which includes lubricant oil. Over the load and speed variation, V0 displays an average increase in PN10/PN23 ratio of 26 %. As Amirante [20] verified previously, a small amount of 1 % lubricant oil in the fuel mainly has an impact on PN sizes below 25 nm, with a maximum at 10 nm. He also used CNG as fuel to minimize the fuel´s influence on PN emissions. For comparison, standard lubricant oil consumption for a light-duty vehicle from the first decade of the twenty-first century ranges between approximately 0.016

FIGURE 15 Ratio of PN 23 nm to PN 10 nm over of V0 & V1

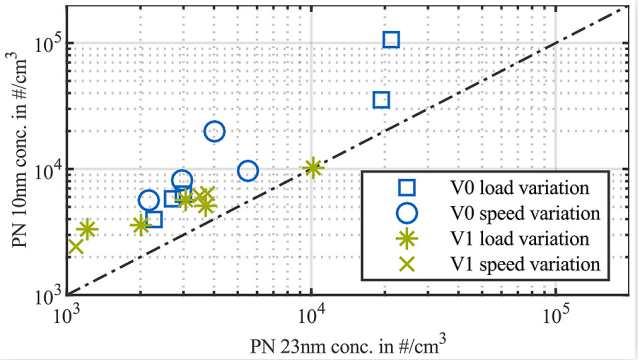

and 0.114 % [52]. Furthermore, the measured increased VOC level in Figure 16 appears to be an effect of the higher blow-back of V0. This is evidence of further unburned fuel and oil in the exhaust stream. Averaged over all points, the V1 ring pack reduced the VOC by 9 %. The exhaust gas temperature rises with the engine load and favors post-reactions in the exhaust. This leads to a reduction in VOC emissions. At a higher engine speed, the turbulent kinetic energy inside the combustion chamber increases, thus promoting the mixture formation. This enhances the combustion process and reduces the VOC emissions. A further indicator of incomplete combustion is the presence of CO in the exhaust gas, as shown in Figure 17. CO occurs in rich areas owing to the lack of oxygen and also if the flame front is quenched by a heat sink initiated by solid surfaces or a flame trap [53].

With the larger second closed gap of V1, an average of 6 % less CO was displayed by the non-dispersive infrared spectrometric (NDIR) analyzer. CO emissions were only higher for V1 at low engine speed points, below 2000 rpm.

The difference between the two variants used grows with higher engine loads. NOx emissions are very sensitive to peak temperatures during the combustion process. During measurement, the average deviation between V0 and V1 was less than 1 %, and the exhaust temperature showed a 1.2 % variance at its maximum. Also, the deviation in combustion duration is less than or equal to 1 °CA. With this information, it can be assumed that no significant change in the combustion process was initiated between the two variants of the piston ring assembly.

FIGURE 14 PN 23 nm over IMEP & engine speed of V0 & V1

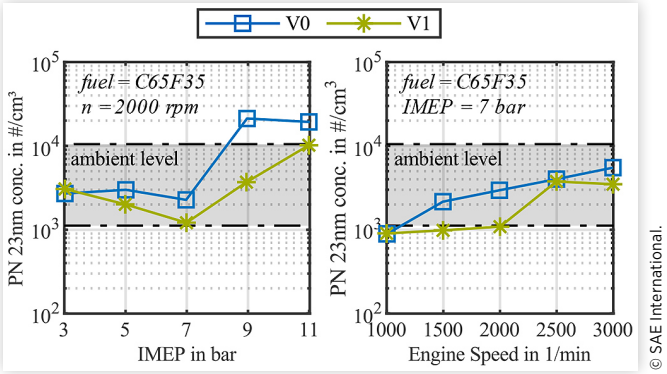

FIGURE 16 VOC over IMEP & Engine Speed V0 & V1

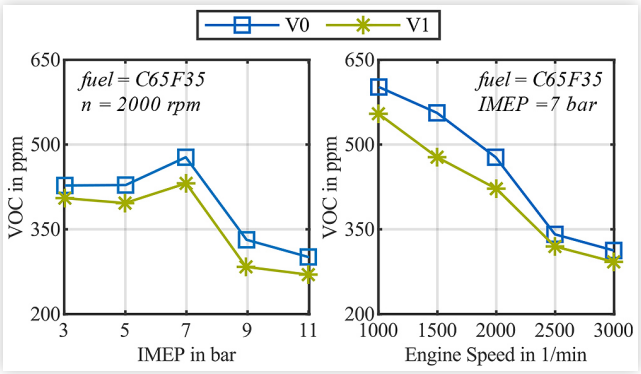

FIGURE 17 CO over engine speed of V0 & V1

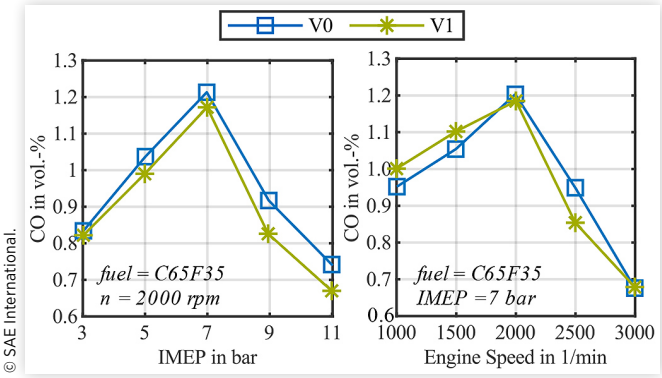

Motored Intake Pressure Variation Despite throttled motored conditions without combustion, PN and VOC emissions are detected by the exhaust analyzers. Figure 18 illustrates that with decreasing intake pressure, beginning at ambient pressure, a logarithmic growth of VOC emissions was identified. It should be considered here that a piston group assembly design is a compromise, intended for use in different operating conditions. As expected, the increased closed gap of V1 generated 25 % or 94 ppm more VOCs at its maximum intake air pressure of 0.25 bar. The reason for that is the increased difference between the ambient pressure in the crankcase housing and vacuum pressure in the combustion chamber. This difference is present at around the bottom dead center (BDC) of expansion as well as in the exhaust stroke.

With this pressure gradient lubricant oil is transported from the crankcase into the combustion chamber owing to the piston ring group. At the beginning of charged operating conditions, VOC emissions are below 60 ppm for both variants. Under naturally aspirated conditions, V1 has a 20 - 26 % higher VOC value. Under normal motored engine conditions, there should be no considerable non-volatile PN to be counted. However, a clear effect on PN could be observed up until ambient pressure level. It is suspected that the evaporation tube of the SPCS is not able to evaporate all volatile lubricant oil droplets at 350 °C. A smaller or larger quantity of PN will be counted, depending on the surface area of the oil droplets, and in turn the diameter. Hence, it is possible that V1 has more VOC but lower PN emissions compared to

FIGURE 18 VOC & PN23 over intake pressure of V0 & V1

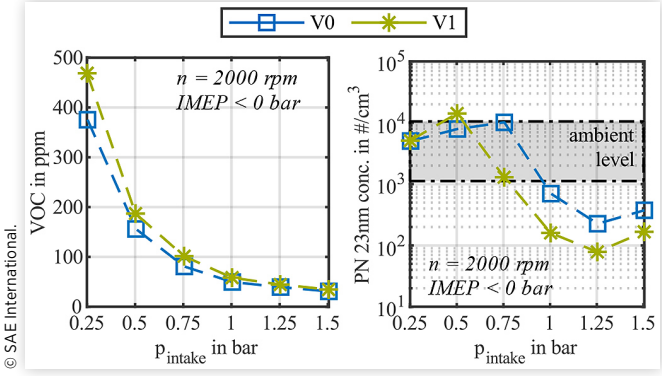

FIGURE 19 PN23 of fired and motored conditions over p_{intake}

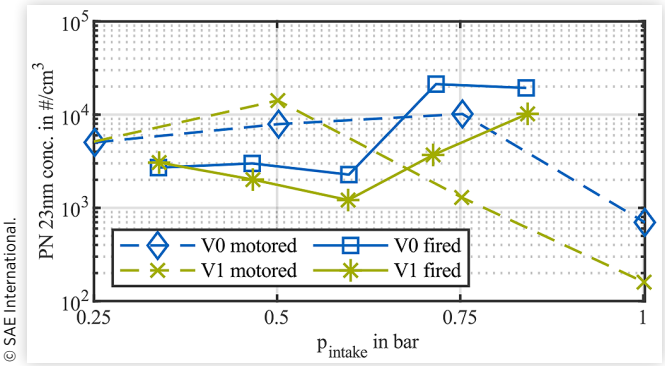

V0. In general, the curve of PN23 over intake pressure is distorted, compared to VOC emissions. Also, the ratio of the gas and liquid phases may change owing to modifications in engine conditions such as engine speed, which varies the impact of reverse blow-by on emissions. PN23 in charged engine mode is below ambient PN level. If the intake port pressure is less than 1 bar, PN23 rises to ambient level and above. For the sake of completeness, Figure 19 compares fired and throttled motored operation. The fired points are for the load variation already discussed for a 3 bar IMEP with 340 mbar p_{intake} to an 11 bar IMEP with 840 mbar p_{intake}. The pressure trace and resulting inter-ring pressures during one cycle naturally differ completely between firing and motored conditions. Therefore, it is not possible to extrapolate, for instance, the quantity of oil in the exhaust from one condition to another. However, it can be seen that under fired conditions below 9 bar IMEP, less PN23 is counted by the SPCS than under motored conditions. Therefore, it must be assumed that the majority of the lubricant oil in the combustion chamber has oxidized as a result of combustion and the higher temperature level.

At 9 and 11 bar IMEP, the intake port pressure increases, with reduced transport of lubricant oil from the crankcase housing to the combustion chamber. Now, the blow-back from the second land dominates under fired conditions. Hence, PN23 in fired operating mode exceeds that in motored mode.

Summary and Conclusions

The experimental investigation of the DISI-SCE confirmed that modifying design of the piston ring pack affects PN-, VOC- and CO-emissions. For this reason, piston ring dynamic simulations with variation of the closed gap of the second ring were performed in PRiME 3D® to analyze the effect on gas-flow and piston ring behavior. The findings demonstrated that aerosol flow between the crank housing and combustion chamber can be manipulated precisely by the second land pressure. If a small closed gap is chosen for the second ring, the pressure at the second land increases during combustion. Under extreme conditions the pressure exceeds that of the combustion chamber and thus an aerosol flow towards the

combustion chamber takes place. The piston ring was designed on the basis of simulations and a test series of three variants was carried out on a DISI-SCE to validate the exhaust emissions. Only the closed gap of the second ring was varied and changed between engine runs. The V0 variant has a small closed gap, whereas V1 has a large one. This means that blow-back is less for V1 and more for V0. With the V2 variant and a medium closed gap, it was demonstrated, that the ring motion has a significant influence on the resulting interactions in the system. The ring pack V2 displayed additional motions and, in turn, gas flows and oil transport mechanisms that changed the overall behavior of the system. Additionally, the load sweep showed a change in behavior at 7 bar IMEP or higher in simulations and measurements. This can be explained by the change in axial ring motion caused by the change from inertia-driven to gas-pressure-driven motion.

The scope of the study was to evaluate the impact of lubricant oil on raw exhaust emissions in a DISI engine. The key method of increasing resolution was to minimize the impact of the fuel-borne emissions. For this purpose, a gasoline replacement mixture of DMC/MeFo was used because of its low-soot combustion and low response factor in the FID analyzer. With these properties, the PN-level is one to two orders of magnitude lower, while VOC emissions are roughly halved. As a result, the proportion of emissions caused by lubricant oil in the exhaust stream increases, as does the resolution. Besides, it was found that the combustion process with DMC/MeFo does not significantly change, particularly with regard to the chamber pressure trace and the maximum combustion pressure, which have a fundamental impact on the investigated phenomena. The investigation showed that with a large closed gap in the second ring, V1 produces the following benefits when varying engine speed and load:

- A 36 % decrease in PN23 and a 51 % decrease in PN10
- A 9 % decrease in VOC emissions
- A 3 % decrease in CO emissions

The following disadvantages were determined as a result of the reduced blow-back:

- With an increased blow-by of 22 %, thermal efficiency theoretically decreases. But averaged over all points, the loss in η_i was less than 0.1 %
- In throttled motored conditions, VOC emissions increase

It was also detected that in fired operation below 9 bar IMEP, less PN could be counted than with to motored mode using the same intake pressure. It is also evident that the performance of the engine can be optimized with predicted piston ring motions and resulting gas flows. Understanding system-relevant interactions is essential to being able to support modern engine development and complying with increasingly stringent legal requirements.

Contact Information

Sebastian Blochum
Chair of Internal Combustion Engines, Technical University of Munich, Schragenhofstraße 31, 80992 Munich, Germany
blochum@lvk.mw.tum.de

Abbreviations

AFR - **Air/Fuel Ratio**
AHRR - Apparent Heat Release Rate
aFTDC - after Fired Top Dead Center
BDC - Bottom Dead Center
C65F35 - Fuel with 65 vol.-% DMC / 35 vol.-% MeFo
CNG - Compressed Natural Gas
CO - Carbon Monoxide
CO2 - Carbon Dioxide
CPC - Condensation Particle Counter
DI - Direct Injection
DISI - Direct Injection Spark Ignition
DMC - Dimethyl Carbonate
DOHC - Double Overhead Camshaft
DVPE - Dry Vapor Pressure Equivalent
ECU - Electronic Control Unit
FID - Flame Ionization Detector
FMEP - Friction Mean Effective Pressure
FTDC - Fired Top Dead Center
G100 - Fuel with 100 vol.-% RON95 E5 Gasoline
HPP - High Pressure Pump
ICE - Internal Combustion Engine
IMEP - Indicated Mean Effective Pressure
LHV - Lower Heating Value
MeFo - Methyl Formate
MeOH - Methanol
MFB50 - Mass Fraction Burned 50%
MON - Motor Octane Number
NDIR - Non-Dispersive InfraRed spectrometer
NEDC - New European Driving Cycle
NOx - Oxides of Nitrogen (NO and NO2)
O2 - Oxygen
PM - Particulate Matter
PN - Particle Number
PN10 - Particle Number with Cutoff at 10 nm
PN23 - Particle Number with Cutoff at 23 nm
RON - Research Octane Number

RPM - Revolutions Per Minute
SCE - Single Cylinder Engine
SI - Spark Ignited
SOI - Start Of Injection
SPCS - Solid Particle Counting System
TDC - Top Dead Center
THC - Total HydroCarbons
VOC - Volatile Organic Compounds
°CA - Crank Angle Degree

References

1. Sodiq, A., Baloch, A.A.B., Khan, S.A., Sezer, N. et al., "Towards Modern Sustainable Cities: Review of Sustainability Principles and Trends," *Journal of Cleaner Production* 227:972-1001, 2019, doi:10.1016/j.jclepro.2019.04.106.
2. Environmental Protection Agency, "Control of Air Pollution From Motor Vehicles: Tier 3 Motor Vehicle Emission and Fuel Standards; Final Rule: EPA-HQ-OAR-2011-0135," 2014.
3. European Community, "REGULATION (EC) No 443/2009 OF THE EUROPEAN PARLIAMENT AND OF THE COUNCIL of 23 April 2009 Setting Emission Performance Standards for New Passenger Cars as Part of the Community's Integrated Approach to Reduce CO2 Emissions from Light-Duty Vehicles," 2009.
4. European Community, "COMMISSION REGULATION (EU) 2017/1347 of 13 July 2017 correcting Directive 2007/46/EC of the European Parliament and of the Council, Commission Regulation (EU) No 582/2011 and Commission Regulation (EU) 2017/1151 Supplementing Regulation (EC) No 715/2007 of the European Parliament and of the Council on Type-Approval of Motor Vehicles with Respect to Emissions from Light Passenger and Commercial Vehicles (Euro 5 and Euro 6) and on Access to Vehicle Repair and Maintenance Information, Amending Directive 2007/46/EC of the European Parliament and of the Council, Commission Regulation (EC) No 692/2008 and Commission Regulation (EU) No 1230/2012 and Repealing Regulation (EC) No 692/2008," 2017.
5. Lensch-Franzen, C., Hadler, J., Gohl, M., Becker, J. et al., "The Interaction Between Tribology and Emissions Under Real Driving Conditions (RDE)," . In: Liebl, J., editor. *Der Antrieb von morgen 2017*, (Wiesbaden, Springer Fachmedien Wiesbaden, 2017), 219-230. ISBN:978-3-658-19223-5.
6. Härtl, M., Pélerin, D., Dworschak, P., Maier, T., et al., "Potential of the Sustainable C1 Fuels OME, DMC, and MeFo for Particle-Free Combustion in SI and CI Engines," in: Liebl, J., Beidl, C., and Maus, W. (eds.), in *Internationaler Motorenkongress 2018, Proceedings*, Springer Fachmedien Wiesbaden, Wiesbaden, 2018), 459-478, ISBN 978-3-658-21014-4.
7. Jacob, E., "C-1 Oxygenate als nachhaltige Kraftstoffe und deren günstige Eigenschaften," in: Maus, W. (ed.), *Zukünftige Kraftstoffe: Energiewende des Transports als ein weltweites Klimaziel*, ATZ/MTZ-Fachbuch, 1st ed., Springer Berlin, Berlin, 2019), 155-180, ISBN 978-3-662-58006-6.
8. Pélerin, D., Gaukel, K., Härtl, M., Jacob, E. et al., "Potentials to Simplify the Engine System Using the Alternative Diesel Fuels Oxymethylene Ether OME1 and OME3−6 on a Heavy-Duty Engine," *Fuel* 259:116231, 2020, doi:10.1016/j.fuel.2019.116231.
9. Härtl, M., Stadler, A., Blochum, S., Pélerin, D., et al., "DMC+ as Particulate Free and Potentially Sustainable Fuel for DI SI Engines," in: Geringer, B. and Lenz, H.P. (eds.), in *39. Internationales Wiener Motorensymposium 26.-27. April 2018*, Fortschritt-Berichte VDI. Reihe 12, Verkehrstechnik, Fahrzeugtechnik, ISBN 978-3-18-380712-3, 202-229, 2018.
10. Santhanamm, P., Sreejith, K., and Anandan, A., "Parametrical and Tribological Investigation of Ring Parameters Using Ring Dynamics Simulation for Blow-By, LOC and Friction Reduction," in *International Conference on Advances in Design, Materials, Manufacturing and Surface Engineering for Mobility*, SAE Technical Paper Series, Jul. 19, 2017, https://doi.org/10.4271/2017-28-1954.
11. Kirner, C., Halbhuber, J., Uhlig, B., Oliva, A. et al., "Experimental and Simulative Research Advances in the Piston Assembly of an Internal Combustion Engine," *Tribology International* 99:159-168, 2016, doi:10.1016/j.triboint.2016.03.005.
12. Lei, J., Zhang, D., Deng, X., Bi, Y., et al., "Influence of Piston Ring Component Structural Parameters on Diesel Engine Blow-By and Oil Consumption," *Nongye Gongcheng Xuebao/Transactions of the Chinese Society of Agricultural Engineering* 34:54-62, 2018, doi:10.11975/j.issn.1002-6819.2018.05.008.
13. Herbst, H.M. and Priebsch, H.H., "Simulation of Piston Ring Dynamics and Their Effect on Oil Consumption," in *SAE 2000 World Congress*, SAE Technical Paper Series, Mar. 6, 2000, 2000, https://doi.org/10.4271/2000-01-0919.
14. Yilmaz, E., Tian, T., Wong, V.W., and Heywood, J.B., "The Contribution of Different Oil Consumption Sources to Total Oil Consumption in a Spark Ignition Engine," in *2004 Powertrain & Fluid Systems Conference & Exhibition*, SAE Technical Paper Series, Oct. 25 2004, https://doi.org/10.4271/2004-01-2909.
15. Johansson, P., and Andersson, S., "Variations in Piston Second Land Pressure as a Function of Ring Gap Position," *International Journal of Engine Research* 11(2):153-161, 2010, doi:10.1243/14680874JER05509.
16. Tomanik, E., Sobrinho, R.M.S., and Zecchinelli, R., "Influence Of Top Ring End Gap Types At Blow-By Of Internal Combustion Engines," SAE Brasil, SAE Technical Paper Series, May 1, 1993, https://doi.org/10.4271/931669.
17. Miyachika, M., Hirota, T., and Kashiyama, K., "A Consideration on Piston Second Land Pressure and Oil Consumption of Internal Combustion Engine," in *SAE International Congress and Exposition*, SAE Technical Paper Series, Feb. 27, 1984, https://doi.org/10.4271/840099.
18. Raza, M., Chen, L., Leach, F., and Ding, S., "A Review of Particulate Number (PN) Emissions from Gasoline Direct Injection (GDI) Engines and Their Control Techniques," *Energies* 11(6):1417, 2018, doi:10.3390/en11061417.

19. Kang, Y., "Role of Selected Dispersants in Gasoline Particulate Emissions under Lubricant Formulations in the Presence of Commercial Package and Dispersant Additives: Its Effect on Emissions, Viscosity, and Soot Morphology," *Fuel* 281:118444, 2020, doi:10.1016/j.fuel.2020.118444.
20. Amirante, R., Distaso, E., Napolitano, M., Tamburrano, P. et al., "Effects of Lubricant Oil on Particulate Emissions from Port-Fuel and Direct-Injection Spark-Ignition Engines," *International Journal of Engine Research* 18(5, 6):606-620, 2017, doi:10.1177/1468087417706602.
21. Tabata, K., Takahashi, M., Takeda, K., Tsurumi, K., et al., "Studies on Characteristics of Nanoparticles Generated in a Gasoline Direct-Injection Engine," in *SAE Technical Paper Series*, SAE Technical Paper Series, 2019 JSAE/SAE Powertrains, Fuels and Lubricants, Aug. 26, 2019, https://doi.org/10.4271/2019-01-2328.
22. Pirjola, L., Karjalainen, P., Heikkilä, J., Saari, S. et al., "Effects of Fresh Lubricant Oils on Particle Emissions Emitted by a Modern Gasoline Direct Injection Passenger Car," *Environmental Science & Technology* 49(6):3644-3652, 2015, doi:10.1021/es505109u.
23. Premnath, V., Khalek, I., Morgan, P., Michlberger, A., et al., "Effect of Lubricant Oil on Particle Emissions from a Gasoline Direct Injection Light-Duty Vehicle," SAE Technical Paper Series, International Powertrains, Fuels & Lubricants Meeting, Sep. 17, 2018, https://doi.org/10.4271/2018-01-1708.
24. Miller, A.L., Stipe, C.B., Habjan, M.C., and Ahlstrand, G.G., "Role of Lubrication Oil in Particulate Emissions from a Hydrogen-Powered Internal Combustion Engine," *Environmental Science & Technology* 41(19):6828-6835, 2007, doi:10.1021/es070999r.
25. Jung, H., Kittelson, D.B., and Zachariah, M.R., "The Influence of Engine Lubricating Oil on Diesel Nanoparticle Emissions and Kinetics of Oxidation," SAE Technical Paper Series, SAE Powertrain & Fluid Systems Conference & Exhibition, Oct. 27, 2003, https://doi.org/10.4271/2003-01-3179.
26. Kytö, M., Aakko, P., Nylund, N.-O., and Niemi, A., "Effect of Lubricant on Particulate Emissions of Heavy Duty Diesel Engines," SAE Technical Paper Series, SAE Powertrain & Fluid Systems Conference & Exhibition, Oct. 21, 2002, https://doi.org/10.4271/2002-01-2770.
27. Härtl, M., Stadler, A., Backes, F., Wachtmeister, G. et al., "Potentially CO2-Neutral Fuels for Clean SI Engines," *MTZ Worldw* 78(7, 8):76-83, 2017, doi:10.1007/s38313-017-0058-1.
28. Maier, T., Härtl, M., Jacob, E., and Wachtmeister, G., "Dimethyl carbonate (DMC) and Methyl Formate (MeFo): Emission Characteristics of Novel, Clean and Potentially CO2 -Neutral Fuels Including PMP and Sub-23 nm Nanoparticle-Emission Characteristics on a Spark-Ignition DI-Engine," *Fuel* 256:115925, 2019, doi:10.1016/j.fuel.2019.115925.
29. Stadler, A., Wessoly, M., Blochum, S., Härtl, M. et al., "Gasoline Fueled Pre-Chamber Ignition System for a Light-Duty Passenger Car Engine with Extended Lean Limit," *SAE Int. J. Engines* 12(3):323-339, 2019, doi:10.4271/03-12-03-0022.
30. Peer, J., Backes, F., Sauerland, H., Härtl, M. et al., "Development of a High Turbulence, Low Particle Number, High Injection Pressure Gasoline Direct Injection Combustion System," *SAE Int. J. Engines* 9(4):2301-2311, 2016, doi:10.4271/2016-01-9046.
31. Baumgartner, L.S., Karmann, S., Backes, F., Stadler, A., et al., "Experimental Investigation of Orifice Design Effects on a Methane Fuelled Prechamber Gas Engine for Automotive Applications," SAE Technical Paper Series, in *13th International Conference on Engines & Vehicles*, Sep. 10, 2017, https://doi.org/10.4271/2017-24-0096.
32. Gelner, A.D., Pastoetter, C., Beck, H.A., Härtl, M. et al., "Fuel Dosing on a Diesel Oxidation Catalyst for After-Treatment System Heating on a Heavy-Duty Engine Powered by Polyoxymethylene Dimethyl Ethers," SAE Technical Paper 2020-01-2157, 2020, https://doi.org/10.4271/2020-01-2157.
33. The Council of the European Union, "Council Directive 1999/13/EC of 11 March 1999 on the Limitation of Emissions of Volatile Organic Compounds due to the Use of Organic Solvents in Certain Activities and Installations," 1999.
34. Wei, Q., Oestergaard, K., Porter, S., Ichiro, A., et al., "Real-Time Measuring System for Engine Exhaust Solid Particle Number Emission - Design and Performance," SAE Technical Paper Series, SAE 2006 World Congress & Exhibition, Apr. 3, 2006, https://doi.org/10.4271/2006-01-0865.
35. United Nations Economic Commission for Europe, "Concerning the Adoption of Uniform Technical Prescriptions for Wheeled Vehicles, Equipment and Parts which can be Fitted and/or be Used on Wheeled Vehicles and the Conditions for Reciprocal Recognition of Approvals Granted on the Basis of these Prescriptions - Addendum 82: Regulation No. 83 - UNIFORM PROVISIONS CONCERNING the Approval of Vehicles with Regard to the Emission of Pollutants According to Engine Fuel Requirements," 2015.
36. Giechaskiel, B., Mamakos, A., Andersson, J., Dilara, P. et al., "Measurement of Automotive Nonvolatile Particle Number Emissions within the European Legislative Framework: A Review," *Aerosol Science and Technology* 46(7):719-749, 2012, doi:10.1080/02786826.2012.661103.
37. Giechaskiel, B., "Differences Between Tailpipe and Dilution Tunnel Sub-23 nm Nonvolatile (Solid) Particle Number Measurements," *Aerosol Science and Technology* 53(9):1012-1022, 2019, doi:10.1080/02786826.2019.1623378.
38. Giechaskiel, B., Lähde, T., and Drossinos, Y., "Regulating Particle Number Measurements from the Tailpipe of Light-Duty Vehicles: The Next Step?" *Environmental Research* 172:1-9, 2019, doi:10.1016/j.envres.2019.02.006.
39. Khan, M.Y., Sharma, S., Liew, C.M., Joshi, A. et al., "Comparison of Full Flow Dilution, Partial Flow Dilution, and Raw Exhaust Particle Number Measurements," *Emiss. Control Sci. Technol* 4(2):103-112, 2018, doi:10.1007/s40825-018-0086-6.
40. Birmili, W., Weinhold, K., Rasch, F., Sonntag, A. et al., "Long-Term Observations of Tropospheric Particle Number Size Distributions and Equivalent Black Carbon Mass Concentrations in the German Ultrafine Aerosol Network (GUAN)," *Earth Syst. Sci. Data* 8(2):355-382, 2016, doi:10.5194/essd-8-355-2016.
41. Tikkanen, J., Janka, K., Rostedt, A., Röbel, M., et al., "Dilution Artifacts. A Significant Source of Error from

Absolute Concentration and Possibly Difficult to Reproduce. PMP vs. Raw Exhaust," in *ETH-Conference on Combustion Generated Nanoparticles, 17th ETH-Conference on Combustion Generated Nanoparticles*, Zürich, Switzerland, June 23-26, 2013.

42. Birmili, W., Heinke, K., Pitz, M., Matschullat, J. et al., "Particle Number Size Distributions in Urban Air Before and After Volatilisation," *Atmos. Chem. Phys.* 10(10):4643-4660, 2010, doi:10.5194/acp-10-4643-2010.
43. Wallner, T., "Correlation Between Speciated Hydrocarbon Emissions and Flame Ionization Detector Response for Gasoline/Alcohol Blends," in *ASME 2010 Internal Combustion Engine Division Fall Technical Conference, ASME 2010 Internal Combustion Engine Division Fall Technical Conference*, ASMEDC, San Antonio, Texas, USA, 119-128, 12.09.2010-15.09.2010, 2010, ISBN 978-0-7918-4944-6.
44. Jorgensen, A.D., Picel, K.C., and Stamoudis, V.C., "Prediction of Gas Chromatography Flame Ionization Detector Response Factors from Molecular Structures," *Anal. Chem.* 62(7):683-689, 2012, doi:10.1021/ac00206a007.
45. Mittler, R., Mierbach, A., and Richardson, D., "Understanding the Fundamentals of Piston Ring Axial Motion and Twist and the Effects on Blow-By," in *ASME 2009 Internal Combustion Engine Division Spring Technical Conference, ASME 2009 Internal Combustion Engine Division Spring Technical Conference*, ASMEDC, Milwaukee, Wisconsin, USA, 721-735, May 3, 2009-May 6 2009, 2009, ISBN 978-0-7918-4340-6.
46. Mittler, R., "Detaillierte 3D-Ringpaketanalyse," *MTZ Motortech Z* 71(7, 8):500-505, 2010, doi:10.1007/BF03225590.
47. Bastuck, T., Böhnke, F., Hoppe, S., and Mittler, R., "Systemic Approach for Piston Ring Designs to Reduce Raw Particle Emissions," *MTZ Worldw* 81(10):50-55, 2020, doi:10.1007/s38313-020-0271-1.
48. Mierbach, A., and Mittler, R., "Einfluss der Auslegung von Kolbenringen auf das Formfüllvermögen in thermisch und mechanisch hoch beanspruchten Motoren," *MTZ Motortech Z* 67(1):32-37, 2006, doi:10.1007/BF03225376.
49. Mittler, R. and Ruch, F., "Friction Tool Development and Validation on the Basis of DuroGlide, Design Changes and their Secondary Physical Effects to Leverage the Highest Friction Potential," in *24th Aachen Colloquium Automobile and Engine Technology, 24th Aachen Colloquium Automobile and Engine Technology*, Aachen, North Rhine-Westphalia, Germany, 1031-1045, 05.10.2015-07.10.2015, 2015.
50. Graf, S., Ruch, F., Mittler, R., and Wachtmeister, G., "Optimization of the Piston Assembly Friction," . In: Liebl, J., Beidl, C., editors. *Internationaler Motorenkongress 2016, Proceedings*, (Wiesbaden, Springer Fachmedien Wiesbaden, 2016), 391-407. ISBN:978-3-658-12917-0.
51. Gottschalk, W., "PKW-Ottomotoren," . In: Merker, G.P., Teichmann, R., editors. *Grundlagen Verbrennungsmotoren*, (Wiesbaden, Wiesbaden, Springer Fachmedien, 2018), 9-45. ISBN:978-3-658-19211-2.
52. West, B. and Sluder, C.S., "Lubricating Oil Consumption on the Standard Road Cycle," SAE Technical Paper Series, SAE 2013 World Congress & Exhibition, Apr. 16, 2013, https://doi.org/10.4271/2013-01-0884.
53. Speight, J.G., "Combustion of Hydrocarbons," . In: *Handbook of Industrial Hydrocarbon Processes*, (Elsevier, 2011), 355-393. ISBN:9780750686327.

e-ISSN 2641-9645

C Anhang

Grenzwerte für Zertifizierungskraftstoff CEC RF-02-08 E5

	Einheit	Limit	
		Min	Max
ROZ	-	95	-
MOZ		85	-
Dichte bei 15 °C	g/l	743	756
DVPE bei 37,8 °C	kPa	56	60
Schwefel	mg/kg	-	10
Wasseranteil	Vol.-%	-	0,015
Aromaten		29	35
Olefine		3	13
Benzol		-	1
Ethanol		4,7	5,3
Oxidationsstabilität	min	480	-
Kupferkorrosion (3h bei 50°C)	Klasse	Klasse 1	-
Abdampfrückstand	mg/100ml	-	4
Blei	mg/l		5
Phosphor			1,3
Sauerstoff	Gew.-%	1,7	2,0
Kondensatvolumen bei 70 °C – E70	Vol.-%	24	44
Kondensatvolumen bei 70 °C – E100		48	60
Kondensatvolumen bei 70 °C – E150		82	90
Siedeende	°C	190	210
Verdampfungsverluste	Vol.-%	-	2,0

D Copyrights für verwendete Veröffentlichungen

Fortfolgend sind die Lizenzvereinbarungen für die verwendeten Veröffentlichungen

Blochum, S., Gadomski, B., Retzlaff, M., Thamm, F. et al., "Potential Analysis of a DMC/MeFo Mixture in a DISI Single and Multi-Cylinder Light Vehicle Gasoline Engine," SAE Int. J. Adv. & Curr. Prac. in Mobility 4(1):15-31, 2022, https://doi.org/10.4271/2021-01-0561.

Blochum, S., Fellner, F., Mühlthaler, M., Härtl, M. et al., "Comparison of Promising Sustainable C1-Fuels Methanol, Dimethyl Carbonate, and Methyl Formate in a DISI Single-Cylinder Light Vehicle Gasoline Engine," SAE Technical Paper 2021-01-1204, 2021, https://doi.org/10.4271/2021-01-1204.

Mühlthaler, M., Blochum, S., Stadler, A., Härtl, M. et al., "Optical Investigations of an Oxygenated Alternative Fuel in a Single Cylinder DISI Light Vehicle Gasoline Engine," SAE Technical Paper 2021-01-0557, 2021, https://doi.org/10.4271/2021-01-0557.

Blochum, S., Ruch, F., Bastuck, T., Härtl, M. et al., "Identification of In-Cylinder Aerosol Flow In-duced Emissions due to Piston Ring Design in a DISI Single Cylinder LV Engine Using Oxygenated Synthetic Fuels," SAE Int. J. Adv. & Curr. Prac. in Mobility 3(5):2395-2409, 2021, https://doi.org/10.4271/2021-01-0625.

zu finden.

Order Date	25-Sep-2022	Type of Use	Republish in a thesis/dissertation
Order License ID	1230384-6		
ISSN	0148-7191	Publisher	SOCIETY OF AUTOMOTIVE ENGINEERS,
		Portion	Chapter/article

LICENSED CONTENT

Publication Title	SAE technical paper series	Rightsholder	SAE International
Article Title	Potential Analysis of a DMC/MeFo Mixture in a DISI Single and Multi-Cylinder Light Vehicle Gasoline Engine	Publication Type	Monographic Series
		Start Page	15
		End Page	31
		Issue	1
Author/Editor	SOCIETY OF AUTOMOTIVE ENGINEERS.	Volume	4
Date	01/01/1970		
Language	English		
Country	United States of America		

REQUEST DETAILS

Portion Type	Chapter/article	Rights Requested	Main product
Page range(s)	1-17	Distribution	Worldwide
Total number of pages	17	Translation	Original language of publication
Format (select all that apply)	Print, Electronic	Copies for the disabled?	No
Who will republish the content?	Author of requested content	Minor editing privileges?	No
		Incidental promotional use?	No
Duration of Use	Life of current edition		
Lifetime Unit Quantity	More than 2,000,000	Currency	EUR

NEW WORK DETAILS

Title	Potentialbewertung von synthetischen, sauerstoffhaltigen C1-Kraftstoffen im direkteinspritzenden Ottomotor	Institution name	Technical University of Munich
		Expected presentation date	2023-02-01
Instructor name	Prof. Georg Wachtmeister		

ADDITIONAL DETAILS

Order reference number	N/A	The requesting person / organization to appear on the license	Sebastian Blochum / Technical University of Munich

REQUESTED CONTENT DETAILS

Title, description or numeric reference of the portion(s)	Potential Analysis of a DMC/MeFo Mixture in a DISI Single and Multi-Cylinder Light Vehicle Gasoline Engine	Title of the article/chapter the portion is from	Potential Analysis of a DMC/MeFo Mixture in a DISI Single and Multi-Cylinder Light Vehicle Gasoline Engine
Editor of portion(s)	Blochum, Sebastian; Gadomski, Bartosch; Retzlaff, Mario; Thamm, Fabian; Kraus, Christoph; Härtl, Martin; Gelhausen, Ralf; Hoppe, Steffen; Wachtmeister, Georg	Author of portion(s)	Blochum, Sebastian; Gadomski, Bartosch; Retzlaff, Mario; Thamm, Fabian; Kraus, Christoph; Härtl, Martin; Gelhausen, Ralf; Hoppe, Steffen; Wachtmeister, Georg
Volume of serial or monograph	4	Issue, if republishing an article from a serial	1
Page or page range of portion	15-31	Publication date of portion	2021-07-21

Marketplace Permissions General Terms and Conditions

The following terms and conditions ("General Terms"), together with any applicable Publisher Terms and Conditions, govern User's use of Works pursuant to the Licenses granted by Copyright Clearance Center, Inc. ("CCC") on behalf of the applicable Rightsholders of such Works through CCC's applicable Marketplace transactional licensing services (each, a "Service").

1) Definitions. For purposes of these General Terms, the following definitions apply:

"License" is the licensed use the User obtains via the Marketplace platform in a particular licensing transaction, as set forth in the Order Confirmation.

"Order Confirmation" is the confirmation CCC provides to the User at the conclusion of each Marketplace transaction. "Order Confirmation Terms" are additional terms set forth on specific Order Confirmations not set forth in the General Terms that can include terms applicable to a particular CCC transactional licensing service and/or any Rightsholder-specific terms.

"Rightsholder(s)" are the holders of copyright rights in the Works for which a User obtains licenses via the Marketplace platform, which are displayed on specific Order Confirmations.

"Terms" means the terms and conditions set forth in these General Terms and any additional Order Confirmation Terms collectively.

"User" or "you" is the person or entity making the use granted under the relevant License. Where the person accepting the Terms on behalf of a User is a freelancer or other third party who the User authorized to accept the General Terms on the User's behalf, such person shall be deemed jointly a User for purposes of such Terms.

"Work(s)" are the copyright protected works described in relevant Order Confirmations.

2) Description of Service. CCC's Marketplace enables Users to obtain Licenses to use one or more Works in accordance with all relevant Terms. CCC grants Licenses as an agent on behalf of the copyright rightsholder identified in the relevant Order Confirmation.

3) Applicability of Terms. The Terms govern User's use of Works in connection with the relevant License. In the event of any conflict between General Terms and Order Confirmation Terms, the latter shall govern. User acknowledges that Rightsholders have complete discretion whether to grant any permission, and whether to place any limitations on any grant, and that CCC has no right to supersede or to modify any such discretionary act by a Rightsholder.

4) Representations; Acceptance. By using the Service, User represents and warrants that User has been duly authorized by the User to accept, and hereby does accept, all Terms.

5) Scope of License; Limitations and Obligations. All Works and all rights therein, including copyright rights, remain the sole and exclusive property of the Rightsholder. The License provides only those rights expressly set forth in the terms and conveys no other rights in any Works

6) General Payment Terms. User may pay at time of checkout by credit card or choose to be invoiced. If the User chooses to be invoiced, the User shall: (i) remit payments in the manner identified on specific invoices, (ii) unless otherwise

specifically stated in an Order Confirmation or separate written agreement, Users shall remit payments upon receipt of the relevant invoice from CCC, either by delivery or notification of availability of the invoice via the Marketplace platform, and (iii) if the User does not pay the invoice within 30 days of receipt, the User may incur a service charge of 1.5% per month or the maximum rate allowed by applicable law, whichever is less. While User may exercise the rights in the License immediately upon receiving the Order Confirmation, the License is automatically revoked and is null and void, as if it had never been issued, if CCC does not receive complete payment on a timely basis.

7) General Limits on Use. Unless otherwise provided in the Order Confirmation, any grant of rights to User (i) involves only the rights set forth in the Terms and does not include subsequent or additional uses, (ii) is non-exclusive and non-transferable, and (iii) is subject to any and all limitations and restrictions (such as, but not limited to, limitations on duration of use or circulation) included in the Terms. Upon completion of the licensed use as set forth in the Order Confirmation, User shall either secure a new permission for further use of the Work(s) or immediately cease any new use of the Work(s) and shall render inaccessible (such as by deleting or by removing or severing links or other locators) any further copies of the Work. User may only make alterations to the Work if and as expressly set forth in the Order Confirmation. No Work may be used in any way that is unlawful, including without limitation if such use would violate applicable sanctions laws or regulations, would be defamatory, violate the rights of third parties (including such third parties' rights of copyright, privacy, publicity, or other tangible or intangible property), or is otherwise illegal, sexually explicit, or obscene. In addition, User may not conjoin a Work with any other material that may result in damage to the reputation of the Rightsholder. Any unlawful use will render any licenses hereunder null and void. User agrees to inform CCC if it becomes aware of any infringement of any rights in a Work and to cooperate with any reasonable request of CCC or the Rightsholder in connection therewith.

8) Third Party Materials. In the event that the material for which a License is sought includes third party materials (such as photographs, illustrations, graphs, inserts and similar materials) that are identified in such material as having been used by permission (or a similar indicator), User is responsible for identifying, and seeking separate licenses (under this Service, if available, or otherwise) for any of such third party materials; without a separate license, User may not use such third party materials via the License.

9) Copyright Notice. Use of proper copyright notice for a Work is required as a condition of any License granted under the Service. Unless otherwise provided in the Order Confirmation, a proper copyright notice will read substantially as follows: "Used with permission of [Rightsholder's name], from [Work's title, author, volume, edition number and year of copyright]; permission conveyed through Copyright Clearance Center, Inc." Such notice must be provided in a reasonably legible font size and must be placed either on a cover page or in another location that any person, upon gaining access to the material which is the subject of a permission, shall see, or in the case of republication Licenses, immediately adjacent to the Work as used (for example, as part of a by-line or footnote) or in the place where substantially all other credits or notices for the new work containing the republished Work are located. Failure to include the required notice results in loss to the Rightsholder and CCC, and the User shall be liable to pay liquidated damages for each such failure equal to twice the use fee specified in the Order Confirmation, in addition to the use fee itself and any other fees and charges specified.

10) Indemnity. User hereby indemnifies and agrees to defend the Rightsholder and CCC, and their respective employees and directors, against all claims, liability, damages, costs, and expenses, including legal fees and expenses, arising out of any use of a Work beyond the scope of the rights granted herein and in the Order Confirmation, or any use of a Work which has been altered in any unauthorized way by User, including claims of defamation or infringement of rights of copyright, publicity, privacy, or other tangible or intangible property.

11) Limitation of Liability. UNDER NO CIRCUMSTANCES WILL CCC OR THE RIGHTSHOLDER BE LIABLE FOR ANY DIRECT, INDIRECT, CONSEQUENTIAL, OR INCIDENTAL DAMAGES (INCLUDING WITHOUT LIMITATION DAMAGES FOR LOSS OF BUSINESS PROFITS OR INFORMATION, OR FOR BUSINESS INTERRUPTION) ARISING OUT OF THE USE OR INABILITY TO USE A WORK, EVEN IF ONE OR BOTH OF THEM HAS BEEN ADVISED OF THE POSSIBILITY OF SUCH DAMAGES. In any event, the total liability of the Rightsholder and CCC (including their respective employees and directors) shall not exceed the total amount actually paid by User for the relevant License. User assumes full liability for the actions and omissions of its principals, employees, agents, affiliates, successors, and assigns.

12) Limited Warranties. THE WORK(S) AND RIGHT(S) ARE PROVIDED "AS IS." CCC HAS THE RIGHT TO GRANT TO USER THE RIGHTS GRANTED IN THE ORDER CONFIRMATION DOCUMENT. CCC AND THE RIGHTSHOLDER DISCLAIM ALL OTHER WARRANTIES RELATING TO THE WORK(S) AND RIGHT(S), EITHER EXPRESS OR IMPLIED, INCLUDING WITHOUT LIMITATION IMPLIED WARRANTIES OF MERCHANTABILITY OR FITNESS FOR A PARTICULAR PURPOSE. ADDITIONAL RIGHTS MAY BE REQUIRED TO USE ILLUSTRATIONS, GRAPHS, PHOTOGRAPHS, ABSTRACTS, INSERTS, OR OTHER PORTIONS OF THE WORK (AS OPPOSED TO THE ENTIRE WORK) IN A MANNER CONTEMPLATED BY USER; USER UNDERSTANDS AND AGREES THAT NEITHER CCC NOR THE RIGHTSHOLDER MAY HAVE SUCH ADDITIONAL RIGHTS TO GRANT.

13) Effect of Breach. Any failure by User to pay any amount when due, or any use by User of a Work beyond the scope of the License set forth in the Order Confirmation and/or the Terms, shall be a material breach of such License. Any breach not cured within 10 days of written notice thereof shall result in immediate termination of such License without further notice. Any unauthorized (but licensable) use of a Work that is terminated immediately upon notice thereof may be liquidated by payment of the Rightsholder's ordinary license price therefor; any unauthorized (and unlicensable) use that is not terminated immediately for any reason (including, for example, because materials containing the Work cannot

reasonably be recalled) will be subject to all remedies available at law or in equity, but in no event to a payment of less than three times the Rightsholder's ordinary license price for the most closely analogous licensable use plus Rightsholder's and/or CCC's costs and expenses incurred in collecting such payment.

14) Additional Terms for Specific Products and Services. If a User is making one of the uses described in this Section 14, the additional terms and conditions apply:

a) *Print Uses of Academic Course Content and Materials (photocopies for academic coursepacks or classroom handouts).* For photocopies for academic coursepacks or classroom handouts the following additional terms apply:

i) The copies and anthologies created under this License may be made and assembled by faculty members individually or at their request by on-campus bookstores or copy centers, or by off-campus copy shops and other similar entities.

ii) No License granted shall in any way: (i) include any right by User to create a substantively non-identical copy of the Work or to edit or in any other way modify the Work (except by means of deleting material immediately preceding or following the entire portion of the Work copied) (ii) permit "publishing ventures" where any particular anthology would be systematically marketed at multiple institutions.

iii) Subject to any Publisher Terms (and notwithstanding any apparent contradiction in the Order Confirmation arising from data provided by User), any use authorized under the academic pay-per-use service is limited as follows:

A) any License granted shall apply to only one class (bearing a unique identifier as assigned by the institution, and thereby including all sections or other subparts of the class) at one institution;

B) use is limited to not more than 25% of the text of a book or of the items in a published collection of essays, poems or articles;

C) use is limited to no more than the greater of (a) 25% of the text of an issue of a journal or other periodical or (b) two articles from such an issue;

D) no User may sell or distribute any particular anthology, whether photocopied or electronic, at more than one institution of learning;

E) in the case of a photocopy permission, no materials may be entered into electronic memory by User except in order to produce an identical copy of a Work before or during the academic term (or analogous period) as to which any particular permission is granted. In the event that User shall choose to retain materials that are the subject of a photocopy permission in electronic memory for purposes of producing identical copies more than one day after such retention (but still within the scope of any permission granted), User must notify CCC of such fact in the applicable permission request and such retention shall constitute one copy actually sold for purposes of calculating permission fees due; and

F) any permission granted shall expire at the end of the class. No permission granted shall in any way include any right by User to create a substantively non-identical copy of the Work or to edit or in any other way modify the Work (except by means of deleting material immediately preceding or following the entire portion of the Work copied).

iv) Books and Records; Right to Audit. As to each permission granted under the academic pay-per-use Service, User shall maintain for at least four full calendar years books and records sufficient for CCC to determine the numbers of copies made by User under such permission. CCC and any representatives it may designate shall have the right to audit such books and records at any time during User's ordinary business hours, upon two days' prior notice. If any such audit shall determine that User shall have underpaid for, or underreported, any photocopies sold or by three percent (3%) or more, then User shall bear all the costs of any such audit; otherwise, CCC shall bear the costs of any such audit. Any amount determined by such audit to have been underpaid by User shall immediately be paid to CCC by User, together with interest thereon at the rate of 10% per annum from the date such amount was originally due. The provisions of this paragraph shall survive the termination of this License for any reason.

b) *Digital Pay-Per-Uses of Academic Course Content and Materials (e-coursepacks, electronic reserves, learning management systems, academic institution intranets).* For uses in e-coursepacks, posts in electronic reserves, posts in learning management systems, or posts on academic institution intranets, the following additional terms apply:

i) The pay-per-uses subject to this Section 14(b) include:

A) Posting e-reserves, course management systems, e-coursepacks for text-based content, which grants authorizations to import requested material in electronic format, and allows electronic access to this material to members of a designated college or university class, under the direction of an instructor designated by the college or university, accessible only under appropriate electronic controls (e.g., password);

B) Posting e-reserves, course management systems, e-coursepacks for material consisting of photographs or

other still images not embedded in text, which grants not only the authorizations described in Section 14(b)(i)(A) above, but also the following authorization: to include the requested material in course materials for use consistent with Section 14(b)(i)(A) above, including any necessary resizing, reformatting or modification of the resolution of such requested material (provided that such modification does not alter the underlying editorial content or meaning of the requested material, and provided that the resulting modified content is used solely within the scope of, and in a manner consistent with, the particular authorization described in the Order Confirmation and the Terms), but not including any other form of manipulation, alteration or editing of the requested material;

C) Posting e-reserves, course management systems, e-coursepacks or other academic distribution for audiovisual content, which grants not only the authorizations described in Section 14(b)(i)(A) above, but also the following authorizations: (i) to include the requested material in course materials for use consistent with Section 14(b)(i)(A) above; (ii) to display and perform the requested material to such members of such class in the physical classroom or remotely by means of streaming media or other video formats; and (iii) to "clip" or reformat the requested material for purposes of time or content management or ease of delivery, provided that such “clipping” or reformatting does not alter the underlying editorial content or meaning of the requested material and that the resulting material is used solely within the scope of, and in a manner consistent with, the particular authorization described in the Order Confirmation and the Terms. Unless expressly set forth in the relevant Order Conformation, the License does not authorize any other form of manipulation, alteration or editing of the requested material.

ii) Unless expressly set forth in the relevant Order Confirmation, no License granted shall in any way: (i) include any right by User to create a substantively non-identical copy of the Work or to edit or in any other way modify the Work (except by means of deleting material immediately preceding or following the entire portion of the Work copied or, in the case of Works subject to Sections 14(b)(1)(B) or (C) above, as described in such Sections) (ii) permit "publishing ventures" where any particular course materials would be systematically marketed at multiple institutions.

iii) Subject to any further limitations determined in the Rightsholder Terms (and notwithstanding any apparent contradiction in the Order Confirmation arising from data provided by User), any use authorized under the electronic course content pay-per-use service is limited as follows:

A) any License granted shall apply to only one class (bearing a unique identifier as assigned by the institution, and thereby including all sections or other subparts of the class) at one institution;

B) use is limited to not more than 25% of the text of a book or of the items in a published collection of essays, poems or articles;

C) use is limited to not more than the greater of (a) 25% of the text of an issue of a journal or other periodical or (b) two articles from such an issue;

D) no User may sell or distribute any particular materials, whether photocopied or electronic, at more than one institution of learning;

E) electronic access to material which is the subject of an electronic-use permission must be limited by means of electronic password, student identification or other control permitting access solely to students and instructors in the class;

F) User must ensure (through use of an electronic cover page or other appropriate means) that any person, upon gaining electronic access to the material, which is the subject of a permission, shall see:

- a proper copyright notice, identifying the Rightsholder in whose name CCC has granted permission,
- a statement to the effect that such copy was made pursuant to permission,
- a statement identifying the class to which the material applies and notifying the reader that the material has been made available electronically solely for use in the class, and
- a statement to the effect that the material may not be further distributed to any person outside the class, whether by copying or by transmission and whether electronically or in paper form, and User must also ensure that such cover page or other means will print out in the event that the person accessing the material chooses to print out the material or any part thereof.

G) any permission granted shall expire at the end of the class and, absent some other form of authorization, User is thereupon required to delete the applicable material from any electronic storage or to block electronic access to the applicable material.

iv) Uses of separate portions of a Work, even if they are to be included in the same course material or the same

university or college class, require separate permissions under the electronic course content pay-per-use Service. Unless otherwise provided in the Order Confirmation, any grant of rights to User is limited to use completed no later than the end of the academic term (or analogous period) as to which any particular permission is granted.

v) Books and Records; Right to Audit. As to each permission granted under the electronic course content Service, User shall maintain for at least four full calendar years books and records sufficient for CCC to determine the numbers of copies made by User under such permission. CCC and any representatives it may designate shall have the right to audit such books and records at any time during User's ordinary business hours, upon two days' prior notice. If any such audit shall determine that User shall have underpaid for, or underreported, any electronic copies used by three percent (3%) or more, then User shall bear all the costs of any such audit; otherwise, CCC shall bear the costs of any such audit. Any amount determined by such audit to have been underpaid by User shall immediately be paid to CCC by User, together with interest thereon at the rate of 10% per annum from the date such amount was originally due. The provisions of this paragraph shall survive the termination of this license for any reason.

c) *Pay-Per-Use Permissions for Certain Reproductions (Academic photocopies for library reserves and interlibrary loan reporting) (Non-academic internal/external business uses and commercial document delivery).* The License expressly excludes the uses listed in Section (c)(i)-(v) below (which must be subject to separate license from the applicable Rightsholder) for: academic photocopies for library reserves and interlibrary loan reporting; and non-academic internal/external business uses and commercial document delivery.

i) electronic storage of any reproduction (whether in plain-text, PDF, or any other format) other than on a transitory basis;

ii) the input of Works or reproductions thereof into any computerized database;

iii) reproduction of an entire Work (cover-to-cover copying) except where the Work is a single article;

iv) reproduction for resale to anyone other than a specific customer of User;

v) republication in any different form. Please obtain authorizations for these uses through other CCC services or directly from the rightsholder.

Any license granted is further limited as set forth in any restrictions included in the Order Confirmation and/or in these Terms.

d) *Electronic Reproductions in Online Environments (Non-Academic-email, intranet, internet and extranet).* For "electronic reproductions", which generally includes e-mail use (including instant messaging or other electronic transmission to a defined group of recipients) or posting on an intranet, extranet or Intranet site (including any display or performance incidental thereto), the following additional terms apply:

i) Unless otherwise set forth in the Order Confirmation, the License is limited to use completed within 30 days for any use on the Internet, 60 days for any use on an intranet or extranet and one year for any other use, all as measured from the "republication date" as identified in the Order Confirmation, if any, and otherwise from the date of the Order Confirmation.

ii) User may not make or permit any alterations to the Work, unless expressly set forth in the Order Confirmation (after request by User and approval by Rightsholder); provided, however, that a Work consisting of photographs or other still images not embedded in text may, if necessary, be resized, reformatted or have its resolution modified without additional express permission, and a Work consisting of audiovisual content may, if necessary, be "clipped" or reformatted for purposes of time or content management or ease of delivery (provided that any such resizing, reformatting, resolution modification or “clipping” does not alter the underlying editorial content or meaning of the Work used, and that the resulting material is used solely within the scope of, and in a manner consistent with, the particular License described in the Order Confirmation and the Terms.

15) Miscellaneous.

a) User acknowledges that CCC may, from time to time, make changes or additions to the Service or to the Terms, and that Rightsholder may make changes or additions to the Rightsholder Terms. Such updated Terms will replace the prior terms and conditions in the order workflow and shall be effective as to any subsequent Licenses but shall not apply to Licenses already granted and paid for under a prior set of terms.

b) Use of User-related information collected through the Service is governed by CCC's privacy policy, available online at www.copyright.com/about/privacy-policy/.

c) The License is personal to User. Therefore, User may not assign or transfer to any other person (whether a natural person or an organization of any kind) the License or any rights granted thereunder; provided, however, that, where applicable, User may assign such License in its entirety on written notice to CCC in the event of a transfer of all or substantially all of User's rights in any new material which includes the Work(s) licensed under this Service.

d) No amendment or waiver of any Terms is binding unless set forth in writing and signed by the appropriate parties, including, where applicable, the Rightsholder. The Rightsholder and CCC hereby object to any terms contained in any writing prepared by or on behalf of the User or its principals, employees, agents or affiliates and purporting to govern or otherwise relate to the License described in the Order Confirmation, which terms are in any way inconsistent with any Terms set forth in the Order Confirmation, and/or in CCC's standard operating procedures, whether such writing is prepared prior to, simultaneously with or subsequent to the Order Confirmation, and whether such writing appears on a copy of the Order Confirmation or in a separate instrument.

e) The License described in the Order Confirmation shall be governed by and construed under the law of the State of New York, USA, without regard to the principles thereof of conflicts of law. Any case, controversy, suit, action, or proceeding arising out of, in connection with, or related to such License shall be brought, at CCC's sole discretion, in any federal or state court located in the County of New York, State of New York, USA, or in any federal or state court whose geographical jurisdiction covers the location of the Rightsholder set forth in the Order Confirmation. The parties expressly submit to the personal jurisdiction and venue of each such federal or state court.

Last updated October 2022

Order Date	25-Sep-2022	Type of Use	Republish in a thesis/dissertation
Order License ID	1230384-7		
ISSN	0148-7191	Publisher	SOCIETY OF AUTOMOTIVE ENGINEERS,
		Portion	Chapter/article

LICENSED CONTENT

Publication Title	SAE technical paper series	Language	English
Article Title	Optical Investigations of an Oxygenated Alternative Fuel in a Single Cylinder DISI Light Vehicle Gasoline Engine	Country	United States of America
		Rightsholder	SAE International
		Publication Type	Monographic Series
Author/Editor	SOCIETY OF AUTOMOTIVE ENGINEERS.		
Date	01/01/1970		

REQUEST DETAILS

Portion Type	Chapter/article	Rights Requested	Main product
Page range(s)	1-17	Distribution	Worldwide
Total number of pages	17	Translation	Original language of publication
Format (select all that apply)	Print, Electronic	Copies for the disabled?	No
Who will republish the content?	Author of requested content	Minor editing privileges?	No
Duration of Use	Life of current edition	Incidental promotional use?	No
Lifetime Unit Quantity	More than 2,000,000	Currency	EUR

NEW WORK DETAILS

Title	Potentialbewertung von synthetischen, sauerstoffhaltigen C1-Kraftstoffen im direkteinspritzenden Ottomotor	Institution name	Technical University of Munich
		Expected presentation date	2023-02-01
Instructor name	Prof. Georg Wachtmeister		

ADDITIONAL DETAILS

Order reference number	N/A	The requesting person / organization to appear on the license	Sebastian Blochum / Technical University of Munich

REQUESTED CONTENT DETAILS

Title, description or numeric reference of the portion(s)	Optical Investigations of an Oxygenated Alternative Fuel in a Single Cylinder DISI Light Vehicle Gasoline Engine	Title of the article/chapter the portion is from	Optical Investigations of an Oxygenated Alternative Fuel in a Single Cylinder DISI Light Vehicle Gasoline Engine
Editor of portion(s)	Mühlthaler, Markus; Blochum, Sebastian; Stadler, Andreas; Härtl, Martin; Wachtmeister, Georg; MIYAMOTO, Akiyasu; Sauerland, Henning	Author of portion(s)	Mühlthaler, Markus; Blochum, Sebastian; Stadler, Andreas; Härtl, Martin; Wachtmeister, Georg; MIYAMOTO, Akiyasu; Sauerland, Henning
Volume of serial or monograph	N/A	Issue, if republishing an article from a serial	N/A
Page or page range of portion	1-17	Publication date of portion	2021-04-06

Marketplace Permissions General Terms and Conditions

The following terms and conditions ("General Terms"), together with any applicable Publisher Terms and Conditions, govern User's use of Works pursuant to the Licenses granted by Copyright Clearance Center, Inc. ("CCC") on behalf of the applicable Rightsholders of such Works through CCC's applicable Marketplace transactional licensing services (each, a "Service").

1) Definitions. For purposes of these General Terms, the following definitions apply:

"License" is the licensed use the User obtains via the Marketplace platform in a particular licensing transaction, as set forth in the Order Confirmation.

"Order Confirmation" is the confirmation CCC provides to the User at the conclusion of each Marketplace transaction. "Order Confirmation Terms" are additional terms set forth on specific Order Confirmations not set forth in the General Terms that can include terms applicable to a particular CCC transactional licensing service and/or any Rightsholder-specific terms.

"Rightsholder(s)" are the holders of copyright rights in the Works for which a User obtains licenses via the Marketplace platform, which are displayed on specific Order Confirmations.

"Terms" means the terms and conditions set forth in these General Terms and any additional Order Confirmation Terms collectively.

"User" or "you" is the person or entity making the use granted under the relevant License. Where the person accepting the Terms on behalf of a User is a freelancer or other third party who the User authorized to accept the General Terms on the User's behalf, such person shall be deemed jointly a User for purposes of such Terms.

"Work(s)" are the copyright protected works described in relevant Order Confirmations.

2) Description of Service. CCC's Marketplace enables Users to obtain Licenses to use one or more Works in accordance with all relevant Terms. CCC grants Licenses as an agent on behalf of the copyright rightsholder identified in the relevant Order Confirmation.

3) Applicability of Terms. The Terms govern User's use of Works in connection with the relevant License. In the event of any conflict between General Terms and Order Confirmation Terms, the latter shall govern. User acknowledges that Rightsholders have complete discretion whether to grant any permission, and whether to place any limitations on any grant, and that CCC has no right to supersede or to modify any such discretionary act by a Rightsholder.

4) Representations; Acceptance. By using the Service, User represents and warrants that User has been duly authorized by the User to accept, and hereby does accept, all Terms.

5) Scope of License; Limitations and Obligations. All Works and all rights therein, including copyright rights, remain the sole and exclusive property of the Rightsholder. The License provides only those rights expressly set forth in the terms and conveys no other rights in any Works

6) General Payment Terms. User may pay at time of checkout by credit card or choose to be invoiced. If the User chooses to be invoiced, the User shall: (i) remit payments in the manner identified on specific invoices, (ii) unless otherwise specifically stated in an Order Confirmation or separate written agreement, Users shall remit payments upon receipt of the relevant invoice from CCC, either by delivery or notification of availability of the invoice via the Marketplace platform,

and (iii) if the User does not pay the invoice within 30 days of receipt, the User may incur a service charge of 1.5% per month or the maximum rate allowed by applicable law, whichever is less. While User may exercise the rights in the License immediately upon receiving the Order Confirmation, the License is automatically revoked and is null and void, as if it had never been issued, if CCC does not receive complete payment on a timely basis.

7) General Limits on Use. Unless otherwise provided in the Order Confirmation, any grant of rights to User (i) involves only the rights set forth in the Terms and does not include subsequent or additional uses, (ii) is non-exclusive and non-transferable, and (iii) is subject to any and all limitations and restrictions (such as, but not limited to, limitations on duration of use or circulation) included in the Terms. Upon completion of the licensed use as set forth in the Order Confirmation, User shall either secure a new permission for further use of the Work(s) or immediately cease any new use of the Work(s) and shall render inaccessible (such as by deleting or by removing or severing links or other locators) any further copies of the Work. User may only make alterations to the Work if and as expressly set forth in the Order Confirmation. No Work may be used in any way that is unlawful, including without limitation if such use would violate applicable sanctions laws or regulations, would be defamatory, violate the rights of third parties (including such third parties' rights of copyright, privacy, publicity, or other tangible or intangible property), or is otherwise illegal, sexually explicit, or obscene. In addition, User may not conjoin a Work with any other material that may result in damage to the reputation of the Rightsholder. Any unlawful use will render any licenses hereunder null and void. User agrees to inform CCC if it becomes aware of any infringement of any rights in a Work and to cooperate with any reasonable request of CCC or the Rightsholder in connection therewith.

8) Third Party Materials. In the event that the material for which a License is sought includes third party materials (such as photographs, illustrations, graphs, inserts and similar materials) that are identified in such material as having been used by permission (or a similar indicator), User is responsible for identifying, and seeking separate licenses (under this Service, if available, or otherwise) for any of such third party materials; without a separate license, User may not use such third party materials via the License.

9) Copyright Notice. Use of proper copyright notice for a Work is required as a condition of any License granted under the Service. Unless otherwise provided in the Order Confirmation, a proper copyright notice will read substantially as follows: "Used with permission of [Rightsholder's name], from [Work's title, author, volume, edition number and year of copyright]; permission conveyed through Copyright Clearance Center, Inc." Such notice must be provided in a reasonably legible font size and must be placed either on a cover page or in another location that any person, upon gaining access to the material which is the subject of a permission, shall see, or in the case of republication Licenses, immediately adjacent to the Work as used (for example, as part of a by-line or footnote) or in the place where substantially all other credits or notices for the new work containing the republished Work are located. Failure to include the required notice results in loss to the Rightsholder and CCC, and the User shall be liable to pay liquidated damages for each such failure equal to twice the use fee specified in the Order Confirmation, in addition to the use fee itself and any other fees and charges specified.

10) Indemnity. User hereby indemnifies and agrees to defend the Rightsholder and CCC, and their respective employees and directors, against all claims, liability, damages, costs, and expenses, including legal fees and expenses, arising out of any use of a Work beyond the scope of the rights granted herein and in the Order Confirmation, or any use of a Work which has been altered in any unauthorized way by User, including claims of defamation or infringement of rights of copyright, publicity, privacy, or other tangible or intangible property.

11) Limitation of Liability. UNDER NO CIRCUMSTANCES WILL CCC OR THE RIGHTSHOLDER BE LIABLE FOR ANY DIRECT, INDIRECT, CONSEQUENTIAL, OR INCIDENTAL DAMAGES (INCLUDING WITHOUT LIMITATION DAMAGES FOR LOSS OF BUSINESS PROFITS OR INFORMATION, OR FOR BUSINESS INTERRUPTION) ARISING OUT OF THE USE OR INABILITY TO USE A WORK, EVEN IF ONE OR BOTH OF THEM HAS BEEN ADVISED OF THE POSSIBILITY OF SUCH DAMAGES. In any event, the total liability of the Rightsholder and CCC (including their respective employees and directors) shall not exceed the total amount actually paid by User for the relevant License. User assumes full liability for the actions and omissions of its principals, employees, agents, affiliates, successors, and assigns.

12) Limited Warranties. THE WORK(S) AND RIGHT(S) ARE PROVIDED "AS IS." CCC HAS THE RIGHT TO GRANT TO USER THE RIGHTS GRANTED IN THE ORDER CONFIRMATION DOCUMENT. CCC AND THE RIGHTSHOLDER DISCLAIM ALL OTHER WARRANTIES RELATING TO THE WORK(S) AND RIGHT(S), EITHER EXPRESS OR IMPLIED, INCLUDING WITHOUT LIMITATION IMPLIED WARRANTIES OF MERCHANTABILITY OR FITNESS FOR A PARTICULAR PURPOSE. ADDITIONAL RIGHTS MAY BE REQUIRED TO USE ILLUSTRATIONS, GRAPHS, PHOTOGRAPHS, ABSTRACTS, INSERTS, OR OTHER PORTIONS OF THE WORK (AS OPPOSED TO THE ENTIRE WORK) IN A MANNER CONTEMPLATED BY USER; USER UNDERSTANDS AND AGREES THAT NEITHER CCC NOR THE RIGHTSHOLDER MAY HAVE SUCH ADDITIONAL RIGHTS TO GRANT.

13) Effect of Breach. Any failure by User to pay any amount when due, or any use by User of a Work beyond the scope of the License set forth in the Order Confirmation and/or the Terms, shall be a material breach of such License. Any breach not cured within 10 days of written notice thereof shall result in immediate termination of such License without further notice. Any unauthorized (but licensable) use of a Work that is terminated immediately upon notice thereof may be liquidated by payment of the Rightsholder's ordinary license price therefor; any unauthorized (and unlicensable) use that is not terminated immediately for any reason (including, for example, because materials containing the Work cannot reasonably be recalled) will be subject to all remedies available at law or in equity, but in no event to a payment of less than three times the Rightsholder's ordinary license price for the most closely analogous licensable use plus Rightsholder's

and/or CCC's costs and expenses incurred in collecting such payment.

14) Additional Terms for Specific Products and Services. If a User is making one of the uses described in this Section 14, the additional terms and conditions apply:

a) *Print Uses of Academic Course Content and Materials (photocopies for academic coursepacks or classroom handouts).* For photocopies for academic coursepacks or classroom handouts the following additional terms apply:

i) The copies and anthologies created under this License may be made and assembled by faculty members individually or at their request by on-campus bookstores or copy centers, or by off-campus copy shops and other similar entities.

ii) No License granted shall in any way: (i) include any right by User to create a substantively non-identical copy of the Work or to edit or in any other way modify the Work (except by means of deleting material immediately preceding or following the entire portion of the Work copied) (ii) permit "publishing ventures" where any particular anthology would be systematically marketed at multiple institutions.

iii) Subject to any Publisher Terms (and notwithstanding any apparent contradiction in the Order Confirmation arising from data provided by User), any use authorized under the academic pay-per-use service is limited as follows:

A) any License granted shall apply to only one class (bearing a unique identifier as assigned by the institution, and thereby including all sections or other subparts of the class) at one institution;

B) use is limited to not more than 25% of the text of a book or of the items in a published collection of essays, poems or articles;

C) use is limited to no more than the greater of (a) 25% of the text of an issue of a journal or other periodical or (b) two articles from such an issue;

D) no User may sell or distribute any particular anthology, whether photocopied or electronic, at more than one institution of learning;

E) in the case of a photocopy permission, no materials may be entered into electronic memory by User except in order to produce an identical copy of a Work before or during the academic term (or analogous period) as to which any particular permission is granted. In the event that User shall choose to retain materials that are the subject of a photocopy permission in electronic memory for purposes of producing identical copies more than one day after such retention (but still within the scope of any permission granted), User must notify CCC of such fact in the applicable permission request and such retention shall constitute one copy actually sold for purposes of calculating permission fees due; and

F) any permission granted shall expire at the end of the class. No permission granted shall in any way include any right by User to create a substantively non-identical copy of the Work or to edit or in any other way modify the Work (except by means of deleting material immediately preceding or following the entire portion of the Work copied).

iv) Books and Records; Right to Audit. As to each permission granted under the academic pay-per-use Service, User shall maintain for at least four full calendar years books and records sufficient for CCC to determine the numbers of copies made by User under such permission. CCC and any representatives it may designate shall have the right to audit such books and records at any time during User's ordinary business hours, upon two days' prior notice. If any such audit shall determine that User shall have underpaid for, or underreported, any photocopies sold or by three percent (3%) or more, then User shall bear all the costs of any such audit; otherwise, CCC shall bear the costs of any such audit. Any amount determined by such audit to have been underpaid by User shall immediately be paid to CCC by User, together with interest thereon at the rate of 10% per annum from the date such amount was originally due. The provisions of this paragraph shall survive the termination of this License for any reason.

b) *Digital Pay-Per-Uses of Academic Course Content and Materials (e-coursepacks, electronic reserves, learning management systems, academic institution intranets).* For uses in e-coursepacks, posts in electronic reserves, posts in learning management systems, or posts on academic institution intranets, the following additional terms apply:

i) The pay-per-uses subject to this Section 14(b) include:

A) Posting e-reserves, course management systems, e-coursepacks for text-based content, which grants authorizations to import requested material in electronic format, and allows electronic access to this material to members of a designated college or university class, under the direction of an instructor designated by the college or university, accessible only under appropriate electronic controls (e.g., password);

B) Posting e-reserves, course management systems, e-coursepacks for material consisting of photographs or other still images not embedded in text, which grants not only the authorizations described in Section 14(b)(i)(A) above, but also the following authorization: to include the requested material in course materials for

use consistent with Section 14(b)(i)(A) above, including any necessary resizing, reformatting or modification of the resolution of such requested material (provided that such modification does not alter the underlying editorial content or meaning of the requested material, and provided that the resulting modified content is used solely within the scope of, and in a manner consistent with, the particular authorization described in the Order Confirmation and the Terms), but not including any other form of manipulation, alteration or editing of the requested material;

C) Posting e-reserves, course management systems, e-coursepacks or other academic distribution for audiovisual content, which grants not only the authorizations described in Section 14(b)(i)(A) above, but also the following authorizations: (i) to include the requested material in course materials for use consistent with Section 14(b)(i)(A) above; (ii) to display and perform the requested material to such members of such class in the physical classroom or remotely by means of streaming media or other video formats; and (iii) to "clip" or reformat the requested material for purposes of time or content management or ease of delivery, provided that such “clipping” or reformatting does not alter the underlying editorial content or meaning of the requested material and that the resulting material is used solely within the scope of, and in a manner consistent with, the particular authorization described in the Order Confirmation and the Terms. Unless expressly set forth in the relevant Order Conformation, the License does not authorize any other form of manipulation, alteration or editing of the requested material.

ii) Unless expressly set forth in the relevant Order Confirmation, no License granted shall in any way: (i) include any right by User to create a substantively non-identical copy of the Work or to edit or in any other way modify the Work (except by means of deleting material immediately preceding or following the entire portion of the Work copied or, in the case of Works subject to Sections 14(b)(1)(B) or (C) above, as described in such Sections) (ii) permit "publishing ventures" where any particular course materials would be systematically marketed at multiple institutions.

iii) Subject to any further limitations determined in the Rightsholder Terms (and notwithstanding any apparent contradiction in the Order Confirmation arising from data provided by User), any use authorized under the electronic course content pay-per-use service is limited as follows:

A) any License granted shall apply to only one class (bearing a unique identifier as assigned by the institution, and thereby including all sections or other subparts of the class) at one institution;

B) use is limited to not more than 25% of the text of a book or of the items in a published collection of essays, poems or articles;

C) use is limited to not more than the greater of (a) 25% of the text of an issue of a journal or other periodical or (b) two articles from such an issue;

D) no User may sell or distribute any particular materials, whether photocopied or electronic, at more than one institution of learning;

E) electronic access to material which is the subject of an electronic-use permission must be limited by means of electronic password, student identification or other control permitting access solely to students and instructors in the class;

F) User must ensure (through use of an electronic cover page or other appropriate means) that any person, upon gaining electronic access to the material, which is the subject of a permission, shall see:

- a proper copyright notice, identifying the Rightsholder in whose name CCC has granted permission,
- a statement to the effect that such copy was made pursuant to permission,
- a statement identifying the class to which the material applies and notifying the reader that the material has been made available electronically solely for use in the class, and
- a statement to the effect that the material may not be further distributed to any person outside the class, whether by copying or by transmission and whether electronically or in paper form, and User must also ensure that such cover page or other means will print out in the event that the person accessing the material chooses to print out the material or any part thereof.

G) any permission granted shall expire at the end of the class and, absent some other form of authorization, User is thereupon required to delete the applicable material from any electronic storage or to block electronic access to the applicable material.

iv) Uses of separate portions of a Work, even if they are to be included in the same course material or the same university or college class, require separate permissions under the electronic course content pay-per-use Service. Unless otherwise provided in the Order Confirmation, any grant of rights to User is limited to use completed no

later than the end of the academic term (or analogous period) as to which any particular permission is granted.

v) Books and Records; Right to Audit. As to each permission granted under the electronic course content Service, User shall maintain for at least four full calendar years books and records sufficient for CCC to determine the numbers of copies made by User under such permission. CCC and any representatives it may designate shall have the right to audit such books and records at any time during User's ordinary business hours, upon two days' prior notice. If any such audit shall determine that User shall have underpaid for, or underreported, any electronic copies used by three percent (3%) or more, then User shall bear all the costs of any such audit; otherwise, CCC shall bear the costs of any such audit. Any amount determined by such audit to have been underpaid by User shall immediately be paid to CCC by User, together with interest thereon at the rate of 10% per annum from the date such amount was originally due. The provisions of this paragraph shall survive the termination of this license for any reason.

c) *Pay-Per-Use Permissions for Certain Reproductions (Academic photocopies for library reserves and interlibrary loan reporting) (Non-academic internal/external business uses and commercial document delivery).* The License expressly excludes the uses listed in Section (c)(i)-(v) below (which must be subject to separate license from the applicable Rightsholder) for: academic photocopies for library reserves and interlibrary loan reporting; and non-academic internal/external business uses and commercial document delivery.

i) electronic storage of any reproduction (whether in plain-text, PDF, or any other format) other than on a transitory basis;

ii) the input of Works or reproductions thereof into any computerized database;

iii) reproduction of an entire Work (cover-to-cover copying) except where the Work is a single article;

iv) reproduction for resale to anyone other than a specific customer of User;

v) republication in any different form. Please obtain authorizations for these uses through other CCC services or directly from the rightsholder.

Any license granted is further limited as set forth in any restrictions included in the Order Confirmation and/or in these Terms.

d) *Electronic Reproductions in Online Environments (Non-Academic-email, intranet, internet and extranet).* For "electronic reproductions", which generally includes e-mail use (including instant messaging or other electronic transmission to a defined group of recipients) or posting on an intranet, extranet or Intranet site (including any display or performance incidental thereto), the following additional terms apply:

i) Unless otherwise set forth in the Order Confirmation, the License is limited to use completed within 30 days for any use on the Internet, 60 days for any use on an intranet or extranet and one year for any other use, all as measured from the "republication date" as identified in the Order Confirmation, if any, and otherwise from the date of the Order Confirmation.

ii) User may not make or permit any alterations to the Work, unless expressly set forth in the Order Confirmation (after request by User and approval by Rightsholder); provided, however, that a Work consisting of photographs or other still images not embedded in text may, if necessary, be resized, reformatted or have its resolution modified without additional express permission, and a Work consisting of audiovisual content may, if necessary, be "clipped" or reformatted for purposes of time or content management or ease of delivery (provided that any such resizing, reformatting, resolution modification or “clipping” does not alter the underlying editorial content or meaning of the Work used, and that the resulting material is used solely within the scope of, and in a manner consistent with, the particular License described in the Order Confirmation and the Terms.

15) Miscellaneous.

a) User acknowledges that CCC may, from time to time, make changes or additions to the Service or to the Terms, and that Rightsholder may make changes or additions to the Rightsholder Terms. Such updated Terms will replace the prior terms and conditions in the order workflow and shall be effective as to any subsequent Licenses but shall not apply to Licenses already granted and paid for under a prior set of terms.

b) Use of User-related information collected through the Service is governed by CCC's privacy policy, available online at www.copyright.com/about/privacy-policy/.

c) The License is personal to User. Therefore, User may not assign or transfer to any other person (whether a natural person or an organization of any kind) the License or any rights granted thereunder; provided, however, that, where applicable, User may assign such License in its entirety on written notice to CCC in the event of a transfer of all or substantially all of User's rights in any new material which includes the Work(s) licensed under this Service.

d) No amendment or waiver of any Terms is binding unless set forth in writing and signed by the appropriate parties,

including, where applicable, the Rightsholder. The Rightsholder and CCC hereby object to any terms contained in any writing prepared by or on behalf of the User or its principals, employees, agents or affiliates and purporting to govern or otherwise relate to the License described in the Order Confirmation, which terms are in any way inconsistent with any Terms set forth in the Order Confirmation, and/or in CCC's standard operating procedures, whether such writing is prepared prior to, simultaneously with or subsequent to the Order Confirmation, and whether such writing appears on a copy of the Order Confirmation or in a separate instrument.

e) The License described in the Order Confirmation shall be governed by and construed under the law of the State of New York, USA, without regard to the principles thereof of conflicts of law. Any case, controversy, suit, action, or proceeding arising out of, in connection with, or related to such License shall be brought, at CCC's sole discretion, in any federal or state court located in the County of New York, State of New York, USA, or in any federal or state court whose geographical jurisdiction covers the location of the Rightsholder set forth in the Order Confirmation. The parties expressly submit to the personal jurisdiction and venue of each such federal or state court.

Last updated October 2022

Order Date	25-Sep-2022	Type of Use	Republish in a thesis/dissertation
Order License ID	1230384-4		
ISSN	0148-7191	Publisher	SOCIETY OF AUTOMOTIVE ENGINEERS,
		Portion	Chapter/article

LICENSED CONTENT

Publication Title	SAE technical paper series	Language	English
Article Title	Comparison of Promising Sustainable C1-Fuels Methanol, Dimethyl Carbonate, and Methyl Formate in a DISI Single-Cylinder Light Vehicle Gasoline Engine	Country	United States of America
		Rightsholder	SAE International
		Publication Type	Monographic Series
Author/Editor	SOCIETY OF AUTOMOTIVE ENGINEERS.		
Date	01/01/1970		

REQUEST DETAILS

Portion Type	Chapter/article	Rights Requested	Main product
Page range(s)	1-22	Distribution	Worldwide
Total number of pages	22	Translation	Original language of publication
Format (select all that apply)	Print, Electronic	Copies for the disabled?	No
Who will republish the content?	Author of requested content	Minor editing privileges?	No
		Incidental promotional use?	No
Duration of Use	Life of current edition		
Lifetime Unit Quantity	More than 2,000,000	Currency	EUR

NEW WORK DETAILS

Title	Potentialbewertung von synthetischen, sauerstoffhaltigen C1-Kraftstoffen im direkteinspritzenden Ottomotor	Institution name	Technical University of Munich
		Expected presentation date	2023-02-01
Instructor name	Prof. Georg Wachtmeister		

ADDITIONAL DETAILS

Order reference number	N/A	The requesting person / organization to appear on the license	Sebastian Blochum / Technical University of Munich

REQUESTED CONTENT DETAILS

Title, description or numeric reference of the portion(s)	Comparison of Promising Sustainable C1-Fuels Methanol, Dimethyl Carbonate, and Methyl Formate in a DISI Single-Cylinder Light Vehicle Gasoline Engine	Title of the article/chapter the portion is from	Comparison of Promising Sustainable C1-Fuels Methanol, Dimethyl Carbonate, and Methyl Formate in a DISI Single-Cylinder Light Vehicle Gasoline Engine
Editor of portion(s)	Blochum, Sebastian; Fellner, Felix; Mühlthaler, Markus; Härtl, Martin; Wachtmeister, Georg; Yoneya, Naoki; Sauerland, Henning	Author of portion(s)	Blochum, Sebastian; Fellner, Felix; Mühlthaler, Markus; Härtl, Martin; Wachtmeister, Georg; Yoneya, Naoki; Sauerland, Henning
Volume of serial or monograph	N/A	Issue, if republishing an article from a serial	N/A
Page or page range of portion	1-22	Publication date of portion	2021-09-21

Marketplace Permissions General Terms and Conditions

The following terms and conditions ("General Terms"), together with any applicable Publisher Terms and Conditions, govern User's use of Works pursuant to the Licenses granted by Copyright Clearance Center, Inc. ("CCC") on behalf of the applicable Rightsholders of such Works through CCC's applicable Marketplace transactional licensing services (each, a "Service").

1) Definitions. For purposes of these General Terms, the following definitions apply:

"License" is the licensed use the User obtains via the Marketplace platform in a particular licensing transaction, as set forth in the Order Confirmation.

"Order Confirmation" is the confirmation CCC provides to the User at the conclusion of each Marketplace transaction. "Order Confirmation Terms" are additional terms set forth on specific Order Confirmations not set forth in the General Terms that can include terms applicable to a particular CCC transactional licensing service and/or any Rightsholder-specific terms.

"Rightsholder(s)" are the holders of copyright rights in the Works for which a User obtains licenses via the Marketplace platform, which are displayed on specific Order Confirmations.

"Terms" means the terms and conditions set forth in these General Terms and any additional Order Confirmation Terms collectively.

"User" or "you" is the person or entity making the use granted under the relevant License. Where the person accepting the Terms on behalf of a User is a freelancer or other third party who the User authorized to accept the General Terms on the User's behalf, such person shall be deemed jointly a User for purposes of such Terms.

"Work(s)" are the copyright protected works described in relevant Order Confirmations.

2) Description of Service. CCC's Marketplace enables Users to obtain Licenses to use one or more Works in accordance with all relevant Terms. CCC grants Licenses as an agent on behalf of the copyright rightsholder identified in the relevant Order Confirmation.

3) Applicability of Terms. The Terms govern User's use of Works in connection with the relevant License. In the event of any conflict between General Terms and Order Confirmation Terms, the latter shall govern. User acknowledges that Rightsholders have complete discretion whether to grant any permission, and whether to place any limitations on any grant, and that CCC has no right to supersede or to modify any such discretionary act by a Rightsholder.

4) Representations; Acceptance. By using the Service, User represents and warrants that User has been duly authorized by the User to accept, and hereby does accept, all Terms.

5) Scope of License; Limitations and Obligations. All Works and all rights therein, including copyright rights, remain the sole and exclusive property of the Rightsholder. The License provides only those rights expressly set forth in the terms and conveys no other rights in any Works

6) General Payment Terms. User may pay at time of checkout by credit card or choose to be invoiced. If the User chooses

to be invoiced, the User shall: (i) remit payments in the manner identified on specific invoices, (ii) unless otherwise specifically stated in an Order Confirmation or separate written agreement, Users shall remit payments upon receipt of the relevant invoice from CCC, either by delivery or notification of availability of the invoice via the Marketplace platform, and (iii) if the User does not pay the invoice within 30 days of receipt, the User may incur a service charge of 1.5% per month or the maximum rate allowed by applicable law, whichever is less. While User may exercise the rights in the License immediately upon receiving the Order Confirmation, the License is automatically revoked and is null and void, as if it had never been issued, if CCC does not receive complete payment on a timely basis.

7) General Limits on Use. Unless otherwise provided in the Order Confirmation, any grant of rights to User (i) involves only the rights set forth in the Terms and does not include subsequent or additional uses, (ii) is non-exclusive and non-transferable, and (iii) is subject to any and all limitations and restrictions (such as, but not limited to, limitations on duration of use or circulation) included in the Terms. Upon completion of the licensed use as set forth in the Order Confirmation, User shall either secure a new permission for further use of the Work(s) or immediately cease any new use of the Work(s) and shall render inaccessible (such as by deleting or by removing or severing links or other locators) any further copies of the Work. User may only make alterations to the Work if and as expressly set forth in the Order Confirmation. No Work may be used in any way that is unlawful, including without limitation if such use would violate applicable sanctions laws or regulations, would be defamatory, violate the rights of third parties (including such third parties' rights of copyright, privacy, publicity, or other tangible or intangible property), or is otherwise illegal, sexually explicit, or obscene. In addition, User may not conjoin a Work with any other material that may result in damage to the reputation of the Rightsholder. Any unlawful use will render any licenses hereunder null and void. User agrees to inform CCC if it becomes aware of any infringement of any rights in a Work and to cooperate with any reasonable request of CCC or the Rightsholder in connection therewith.

8) Third Party Materials. In the event that the material for which a License is sought includes third party materials (such as photographs, illustrations, graphs, inserts and similar materials) that are identified in such material as having been used by permission (or a similar indicator), User is responsible for identifying, and seeking separate licenses (under this Service, if available, or otherwise) for any of such third party materials; without a separate license, User may not use such third party materials via the License.

9) Copyright Notice. Use of proper copyright notice for a Work is required as a condition of any License granted under the Service. Unless otherwise provided in the Order Confirmation, a proper copyright notice will read substantially as follows: "Used with permission of [Rightsholder's name], from [Work's title, author, volume, edition number and year of copyright]; permission conveyed through Copyright Clearance Center, Inc." Such notice must be provided in a reasonably legible font size and must be placed either on a cover page or in another location that any person, upon gaining access to the material which is the subject of a permission, shall see, or in the case of republication Licenses, immediately adjacent to the Work as used (for example, as part of a by-line or footnote) or in the place where substantially all other credits or notices for the new work containing the republished Work are located. Failure to include the required notice results in loss to the Rightsholder and CCC, and the User shall be liable to pay liquidated damages for each such failure equal to twice the use fee specified in the Order Confirmation, in addition to the use fee itself and any other fees and charges specified.

10) Indemnity. User hereby indemnifies and agrees to defend the Rightsholder and CCC, and their respective employees and directors, against all claims, liability, damages, costs, and expenses, including legal fees and expenses, arising out of any use of a Work beyond the scope of the rights granted herein and in the Order Confirmation, or any use of a Work which has been altered in any unauthorized way by User, including claims of defamation or infringement of rights of copyright, publicity, privacy, or other tangible or intangible property.

11) Limitation of Liability. UNDER NO CIRCUMSTANCES WILL CCC OR THE RIGHTSHOLDER BE LIABLE FOR ANY DIRECT, INDIRECT, CONSEQUENTIAL, OR INCIDENTAL DAMAGES (INCLUDING WITHOUT LIMITATION DAMAGES FOR LOSS OF BUSINESS PROFITS OR INFORMATION, OR FOR BUSINESS INTERRUPTION) ARISING OUT OF THE USE OR INABILITY TO USE A WORK, EVEN IF ONE OR BOTH OF THEM HAS BEEN ADVISED OF THE POSSIBILITY OF SUCH DAMAGES. In any event, the total liability of the Rightsholder and CCC (including their respective employees and directors) shall not exceed the total amount actually paid by User for the relevant License. User assumes full liability for the actions and omissions of its principals, employees, agents, affiliates, successors, and assigns.

12) Limited Warranties. THE WORK(S) AND RIGHT(S) ARE PROVIDED "AS IS." CCC HAS THE RIGHT TO GRANT TO USER THE RIGHTS GRANTED IN THE ORDER CONFIRMATION DOCUMENT. CCC AND THE RIGHTSHOLDER DISCLAIM ALL OTHER WARRANTIES RELATING TO THE WORK(S) AND RIGHT(S), EITHER EXPRESS OR IMPLIED, INCLUDING WITHOUT LIMITATION IMPLIED WARRANTIES OF MERCHANTABILITY OR FITNESS FOR A PARTICULAR PURPOSE. ADDITIONAL RIGHTS MAY BE REQUIRED TO USE ILLUSTRATIONS, GRAPHS, PHOTOGRAPHS, ABSTRACTS, INSERTS, OR OTHER PORTIONS OF THE WORK (AS OPPOSED TO THE ENTIRE WORK) IN A MANNER CONTEMPLATED BY USER; USER UNDERSTANDS AND AGREES THAT NEITHER CCC NOR THE RIGHTSHOLDER MAY HAVE SUCH ADDITIONAL RIGHTS TO GRANT.

13) Effect of Breach. Any failure by User to pay any amount when due, or any use by User of a Work beyond the scope of the License set forth in the Order Confirmation and/or the Terms, shall be a material breach of such License. Any breach not cured within 10 days of written notice thereof shall result in immediate termination of such License without further notice. Any unauthorized (but licensable) use of a Work that is terminated immediately upon notice thereof may be liquidated by payment of the Rightsholder's ordinary license price therefor; any unauthorized (and unlicensable) use that

is not terminated immediately for any reason (including, for example, because materials containing the Work cannot reasonably be recalled) will be subject to all remedies available at law or in equity, but in no event to a payment of less than three times the Rightsholder's ordinary license price for the most closely analogous licensable use plus Rightsholder's and/or CCC's costs and expenses incurred in collecting such payment.

14) Additional Terms for Specific Products and Services. If a User is making one of the uses described in this Section 14, the additional terms and conditions apply:

a) *Print Uses of Academic Course Content and Materials (photocopies for academic coursepacks or classroom handouts).* For photocopies for academic coursepacks or classroom handouts the following additional terms apply:

i) The copies and anthologies created under this License may be made and assembled by faculty members individually or at their request by on-campus bookstores or copy centers, or by off-campus copy shops and other similar entities.

ii) No License granted shall in any way: (i) include any right by User to create a substantively non-identical copy of the Work or to edit or in any other way modify the Work (except by means of deleting material immediately preceding or following the entire portion of the Work copied) (ii) permit "publishing ventures" where any particular anthology would be systematically marketed at multiple institutions.

iii) Subject to any Publisher Terms (and notwithstanding any apparent contradiction in the Order Confirmation arising from data provided by User), any use authorized under the academic pay-per-use service is limited as follows:

A) any License granted shall apply to only one class (bearing a unique identifier as assigned by the institution, and thereby including all sections or other subparts of the class) at one institution;

B) use is limited to not more than 25% of the text of a book or of the items in a published collection of essays, poems or articles;

C) use is limited to no more than the greater of (a) 25% of the text of an issue of a journal or other periodical or (b) two articles from such an issue;

D) no User may sell or distribute any particular anthology, whether photocopied or electronic, at more than one institution of learning;

E) in the case of a photocopy permission, no materials may be entered into electronic memory by User except in order to produce an identical copy of a Work before or during the academic term (or analogous period) as to which any particular permission is granted. In the event that User shall choose to retain materials that are the subject of a photocopy permission in electronic memory for purposes of producing identical copies more than one day after such retention (but still within the scope of any permission granted), User must notify CCC of such fact in the applicable permission request and such retention shall constitute one copy actually sold for purposes of calculating permission fees due; and

F) any permission granted shall expire at the end of the class. No permission granted shall in any way include any right by User to create a substantively non-identical copy of the Work or to edit or in any other way modify the Work (except by means of deleting material immediately preceding or following the entire portion of the Work copied).

iv) Books and Records; Right to Audit. As to each permission granted under the academic pay-per-use Service, User shall maintain for at least four full calendar years books and records sufficient for CCC to determine the numbers of copies made by User under such permission. CCC and any representatives it may designate shall have the right to audit such books and records at any time during User's ordinary business hours, upon two days' prior notice. If any such audit shall determine that User shall have underpaid for, or underreported, any photocopies sold or by three percent (3%) or more, then User shall bear all the costs of any such audit; otherwise, CCC shall bear the costs of any such audit. Any amount determined by such audit to have been underpaid by User shall immediately be paid to CCC by User, together with interest thereon at the rate of 10% per annum from the date such amount was originally due. The provisions of this paragraph shall survive the termination of this License for any reason.

b) *Digital Pay-Per-Uses of Academic Course Content and Materials (e-coursepacks, electronic reserves, learning management systems, academic institution intranets).* For uses in e-coursepacks, posts in electronic reserves, posts in learning management systems, or posts on academic institution intranets, the following additional terms apply:

i) The pay-per-uses subject to this Section 14(b) include:

A) Posting e-reserves, course management systems, e-coursepacks for text-based content, which grants authorizations to import requested material in electronic format, and allows electronic access to this material to members of a designated college or university class, under the direction of an instructor designated by the college or university, accessible only under appropriate electronic controls (e.g., password);

B) Posting e-reserves, course management systems, e-coursepacks for material consisting of photographs or other still images not embedded in text, which grants not only the authorizations described in Section 14(b)(i)(A) above, but also the following authorization: to include the requested material in course materials for use consistent with Section 14(b)(i)(A) above, including any necessary resizing, reformatting or modification of the resolution of such requested material (provided that such modification does not alter the underlying editorial content or meaning of the requested material, and provided that the resulting modified content is used solely within the scope of, and in a manner consistent with, the particular authorization described in the Order Confirmation and the Terms), but not including any other form of manipulation, alteration or editing of the requested material;

C) Posting e-reserves, course management systems, e-coursepacks or other academic distribution for audiovisual content, which grants not only the authorizations described in Section 14(b)(i)(A) above, but also the following authorizations: (i) to include the requested material in course materials for use consistent with Section 14(b)(i)(A) above; (ii) to display and perform the requested material to such members of such class in the physical classroom or remotely by means of streaming media or other video formats; and (iii) to "clip" or reformat the requested material for purposes of time or content management or ease of delivery, provided that such “clipping” or reformatting does not alter the underlying editorial content or meaning of the requested material and that the resulting material is used solely within the scope of, and in a manner consistent with, the particular authorization described in the Order Confirmation and the Terms. Unless expressly set forth in the relevant Order Conformation, the License does not authorize any other form of manipulation, alteration or editing of the requested material.

ii) Unless expressly set forth in the relevant Order Confirmation, no License granted shall in any way: (i) include any right by User to create a substantively non-identical copy of the Work or to edit or in any other way modify the Work (except by means of deleting material immediately preceding or following the entire portion of the Work copied or, in the case of Works subject to Sections 14(b)(1)(B) or (C) above, as described in such Sections) (ii) permit "publishing ventures" where any particular course materials would be systematically marketed at multiple institutions.

iii) Subject to any further limitations determined in the Rightsholder Terms (and notwithstanding any apparent contradiction in the Order Confirmation arising from data provided by User), any use authorized under the electronic course content pay-per-use service is limited as follows:

A) any License granted shall apply to only one class (bearing a unique identifier as assigned by the institution, and thereby including all sections or other subparts of the class) at one institution;

B) use is limited to not more than 25% of the text of a book or of the items in a published collection of essays, poems or articles;

C) use is limited to not more than the greater of (a) 25% of the text of an issue of a journal or other periodical or (b) two articles from such an issue;

D) no User may sell or distribute any particular materials, whether photocopied or electronic, at more than one institution of learning;

E) electronic access to material which is the subject of an electronic-use permission must be limited by means of electronic password, student identification or other control permitting access solely to students and instructors in the class;

F) User must ensure (through use of an electronic cover page or other appropriate means) that any person, upon gaining electronic access to the material, which is the subject of a permission, shall see:

- a proper copyright notice, identifying the Rightsholder in whose name CCC has granted permission,
- a statement to the effect that such copy was made pursuant to permission,
- a statement identifying the class to which the material applies and notifying the reader that the material has been made available electronically solely for use in the class, and
- a statement to the effect that the material may not be further distributed to any person outside the class, whether by copying or by transmission and whether electronically or in paper form, and User must also ensure that such cover page or other means will print out in the event that the person accessing the material chooses to print out the material or any part thereof.

G) any permission granted shall expire at the end of the class and, absent some other form of authorization, User is thereupon required to delete the applicable material from any electronic storage or to block electronic access to the applicable material.

iv) Uses of separate portions of a Work, even if they are to be included in the same course material or the same university or college class, require separate permissions under the electronic course content pay-per-use Service. Unless otherwise provided in the Order Confirmation, any grant of rights to User is limited to use completed no later than the end of the academic term (or analogous period) as to which any particular permission is granted.

v) Books and Records; Right to Audit. As to each permission granted under the electronic course content Service, User shall maintain for at least four full calendar years books and records sufficient for CCC to determine the numbers of copies made by User under such permission. CCC and any representatives it may designate shall have the right to audit such books and records at any time during User's ordinary business hours, upon two days' prior notice. If any such audit shall determine that User shall have underpaid for, or underreported, any electronic copies used by three percent (3%) or more, then User shall bear all the costs of any such audit; otherwise, CCC shall bear the costs of any such audit. Any amount determined by such audit to have been underpaid by User shall immediately be paid to CCC by User, together with interest thereon at the rate of 10% per annum from the date such amount was originally due. The provisions of this paragraph shall survive the termination of this license for any reason.

c) *Pay-Per-Use Permissions for Certain Reproductions (Academic photocopies for library reserves and interlibrary loan reporting) (Non-academic internal/external business uses and commercial document delivery).* The License expressly excludes the uses listed in Section (c)(i)-(v) below (which must be subject to separate license from the applicable Rightsholder) for: academic photocopies for library reserves and interlibrary loan reporting; and non-academic internal/external business uses and commercial document delivery.

i) electronic storage of any reproduction (whether in plain-text, PDF, or any other format) other than on a transitory basis;

ii) the input of Works or reproductions thereof into any computerized database;

iii) reproduction of an entire Work (cover-to-cover copying) except where the Work is a single article;

iv) reproduction for resale to anyone other than a specific customer of User;

v) republication in any different form. Please obtain authorizations for these uses through other CCC services or directly from the rightsholder.

Any license granted is further limited as set forth in any restrictions included in the Order Confirmation and/or in these Terms.

d) *Electronic Reproductions in Online Environments (Non-Academic-email, intranet, internet and extranet).* For "electronic reproductions", which generally includes e-mail use (including instant messaging or other electronic transmission to a defined group of recipients) or posting on an intranet, extranet or Intranet site (including any display or performance incidental thereto), the following additional terms apply:

i) Unless otherwise set forth in the Order Confirmation, the License is limited to use completed within 30 days for any use on the Internet, 60 days for any use on an intranet or extranet and one year for any other use, all as measured from the "republication date" as identified in the Order Confirmation, if any, and otherwise from the date of the Order Confirmation.

ii) User may not make or permit any alterations to the Work, unless expressly set forth in the Order Confirmation (after request by User and approval by Rightsholder); provided, however, that a Work consisting of photographs or other still images not embedded in text may, if necessary, be resized, reformatted or have its resolution modified without additional express permission, and a Work consisting of audiovisual content may, if necessary, be "clipped" or reformatted for purposes of time or content management or ease of delivery (provided that any such resizing, reformatting, resolution modification or “clipping” does not alter the underlying editorial content or meaning of the Work used, and that the resulting material is used solely within the scope of, and in a manner consistent with, the particular License described in the Order Confirmation and the Terms.

15) Miscellaneous.

a) User acknowledges that CCC may, from time to time, make changes or additions to the Service or to the Terms, and that Rightsholder may make changes or additions to the Rightsholder Terms. Such updated Terms will replace the prior terms and conditions in the order workflow and shall be effective as to any subsequent Licenses but shall not apply to Licenses already granted and paid for under a prior set of terms.

b) Use of User-related information collected through the Service is governed by CCC's privacy policy, available online at www.copyright.com/about/privacy-policy/.

c) The License is personal to User. Therefore, User may not assign or transfer to any other person (whether a natural person or an organization of any kind) the License or any rights granted thereunder; provided, however, that, where applicable, User may assign such License in its entirety on written notice to CCC in the event of a transfer of all or

substantially all of User's rights in any new material which includes the Work(s) licensed under this Service.

d) No amendment or waiver of any Terms is binding unless set forth in writing and signed by the appropriate parties, including, where applicable, the Rightsholder. The Rightsholder and CCC hereby object to any terms contained in any writing prepared by or on behalf of the User or its principals, employees, agents or affiliates and purporting to govern or otherwise relate to the License described in the Order Confirmation, which terms are in any way inconsistent with any Terms set forth in the Order Confirmation, and/or in CCC's standard operating procedures, whether such writing is prepared prior to, simultaneously with or subsequent to the Order Confirmation, and whether such writing appears on a copy of the Order Confirmation or in a separate instrument.

e) The License described in the Order Confirmation shall be governed by and construed under the law of the State of New York, USA, without regard to the principles thereof of conflicts of law. Any case, controversy, suit, action, or proceeding arising out of, in connection with, or related to such License shall be brought, at CCC's sole discretion, in any federal or state court located in the County of New York, State of New York, USA, or in any federal or state court whose geographical jurisdiction covers the location of the Rightsholder set forth in the Order Confirmation. The parties expressly submit to the personal jurisdiction and venue of each such federal or state court.

Last updated October 2022

Order Date	25-Sep-2022	Type of Use	Republish in a thesis/dissertation
Order License ID	1230384-5		
ISSN	0148-7191	Publisher	SOCIETY OF AUTOMOTIVE ENGINEERS,
		Portion	Chapter/article

LICENSED CONTENT

Publication Title	SAE technical paper series	Rightsholder	SAE International
Article Title	Identification of In-Cylinder Aerosol Flow Induced Emissions due to Piston Ring Design in a DISI Single Cylinder LV Engine Using Oxygenated Synthetic Fuels	Publication Type	Monographic Series
		Start Page	2395
		End Page	2409
		Issue	5
		Volume	3
Author/Editor	SOCIETY OF AUTOMOTIVE ENGINEERS.		
Date	01/01/1970		
Language	English		
Country	United States of America		

REQUEST DETAILS

Portion Type	Chapter/article	Rights Requested	Main product
Page range(s)	1-15	Distribution	Worldwide
Total number of pages	15	Translation	Original language of publication
Format (select all that apply)	Print, Electronic	Copies for the disabled?	No
Who will republish the content?	Author of requested content	Minor editing privileges?	No
		Incidental promotional use?	No
Duration of Use	Life of current edition		
Lifetime Unit Quantity	More than 2,000,000	Currency	EUR

NEW WORK DETAILS

Title	Potentialbewertung von synthetischen, sauerstoffhaltigen C1-Kraftstoffen im direkteinspritzenden Ottomotor	Institution name	Technical University of Munich
		Expected presentation date	2023-02-01
Instructor name	Prof. Georg Wachtmeister		

ADDITIONAL DETAILS

Order reference number	N/A

The requesting person / organization to appear on the license	Sebastian Blochum / Technical University of Munich

REQUESTED CONTENT DETAILS

Title, description or numeric reference of the portion(s)	Identification of In-Cylinder Aerosol Flow Induced Emissions due to Piston Ring Design in a DISI Single Cylinder LV Engine Using Oxygenated Synthetic Fuels	Title of the article/chapter the portion is from	Identification of In-Cylinder Aerosol Flow Induced Emissions due to Piston Ring Design in a DISI Single Cylinder LV Engine Using Oxygenated Synthetic Fuels
Editor of portion(s)	Blochum, Sebastian; Ruch, Fabian H.; Bastuck, Thomas; Härtl, Martin; Mittler, Richard; Wachtmeister, Georg	Author of portion(s)	Blochum, Sebastian; Ruch, Fabian H.; Bastuck, Thomas; Härtl, Martin; Mittler, Richard; Wachtmeister, Georg
Volume of serial or monograph	3	Issue, if republishing an article from a serial	5
Page or page range of portion	2395-2409	Publication date of portion	2021-04-06

Marketplace Permissions General Terms and Conditions

The following terms and conditions ("General Terms"), together with any applicable Publisher Terms and Conditions, govern User's use of Works pursuant to the Licenses granted by Copyright Clearance Center, Inc. ("CCC") on behalf of the applicable Rightsholders of such Works through CCC's applicable Marketplace transactional licensing services (each, a "Service").

1) Definitions. For purposes of these General Terms, the following definitions apply:

"License" is the licensed use the User obtains via the Marketplace platform in a particular licensing transaction, as set forth in the Order Confirmation.

"Order Confirmation" is the confirmation CCC provides to the User at the conclusion of each Marketplace transaction. "Order Confirmation Terms" are additional terms set forth on specific Order Confirmations not set forth in the General Terms that can include terms applicable to a particular CCC transactional licensing service and/or any Rightsholder-specific terms.

"Rightsholder(s)" are the holders of copyright rights in the Works for which a User obtains licenses via the Marketplace platform, which are displayed on specific Order Confirmations.

"Terms" means the terms and conditions set forth in these General Terms and any additional Order Confirmation Terms collectively.

"User" or "you" is the person or entity making the use granted under the relevant License. Where the person accepting the Terms on behalf of a User is a freelancer or other third party who the User authorized to accept the General Terms on the User's behalf, such person shall be deemed jointly a User for purposes of such Terms.

"Work(s)" are the copyright protected works described in relevant Order Confirmations.

2) Description of Service. CCC's Marketplace enables Users to obtain Licenses to use one or more Works in accordance with all relevant Terms. CCC grants Licenses as an agent on behalf of the copyright rightsholder identified in the relevant Order Confirmation.

3) Applicability of Terms. The Terms govern User's use of Works in connection with the relevant License. In the event of any conflict between General Terms and Order Confirmation Terms, the latter shall govern. User acknowledges that Rightsholders have complete discretion whether to grant any permission, and whether to place any limitations on any grant, and that CCC has no right to supersede or to modify any such discretionary act by a Rightsholder.

4) Representations; Acceptance. By using the Service, User represents and warrants that User has been duly authorized by the User to accept, and hereby does accept, all Terms.

5) Scope of License; Limitations and Obligations. All Works and all rights therein, including copyright rights, remain the

sole and exclusive property of the Rightsholder. The License provides only those rights expressly set forth in the terms and conveys no other rights in any Works

6) General Payment Terms. User may pay at time of checkout by credit card or choose to be invoiced. If the User chooses to be invoiced, the User shall: (i) remit payments in the manner identified on specific invoices, (ii) unless otherwise specifically stated in an Order Confirmation or separate written agreement, Users shall remit payments upon receipt of the relevant invoice from CCC, either by delivery or notification of availability of the invoice via the Marketplace platform, and (iii) if the User does not pay the invoice within 30 days of receipt, the User may incur a service charge of 1.5% per month or the maximum rate allowed by applicable law, whichever is less. While User may exercise the rights in the License immediately upon receiving the Order Confirmation, the License is automatically revoked and is null and void, as if it had never been issued, if CCC does not receive complete payment on a timely basis.

7) General Limits on Use. Unless otherwise provided in the Order Confirmation, any grant of rights to User (i) involves only the rights set forth in the Terms and does not include subsequent or additional uses, (ii) is non-exclusive and non-transferable, and (iii) is subject to any and all limitations and restrictions (such as, but not limited to, limitations on duration of use or circulation) included in the Terms. Upon completion of the licensed use as set forth in the Order Confirmation, User shall either secure a new permission for further use of the Work(s) or immediately cease any new use of the Work(s) and shall render inaccessible (such as by deleting or by removing or severing links or other locators) any further copies of the Work. User may only make alterations to the Work if and as expressly set forth in the Order Confirmation. No Work may be used in any way that is unlawful, including without limitation if such use would violate applicable sanctions laws or regulations, would be defamatory, violate the rights of third parties (including such third parties' rights of copyright, privacy, publicity, or other tangible or intangible property), or is otherwise illegal, sexually explicit, or obscene. In addition, User may not conjoin a Work with any other material that may result in damage to the reputation of the Rightsholder. Any unlawful use will render any licenses hereunder null and void. User agrees to inform CCC if it becomes aware of any infringement of any rights in a Work and to cooperate with any reasonable request of CCC or the Rightsholder in connection therewith.

8) Third Party Materials. In the event that the material for which a License is sought includes third party materials (such as photographs, illustrations, graphs, inserts and similar materials) that are identified in such material as having been used by permission (or a similar indicator), User is responsible for identifying, and seeking separate licenses (under this Service, if available, or otherwise) for any of such third party materials; without a separate license, User may not use such third party materials via the License.

9) Copyright Notice. Use of proper copyright notice for a Work is required as a condition of any License granted under the Service. Unless otherwise provided in the Order Confirmation, a proper copyright notice will read substantially as follows: "Used with permission of [Rightsholder's name], from [Work's title, author, volume, edition number and year of copyright]; permission conveyed through Copyright Clearance Center, Inc." Such notice must be provided in a reasonably legible font size and must be placed either on a cover page or in another location that any person, upon gaining access to the material which is the subject of a permission, shall see, or in the case of republication Licenses, immediately adjacent to the Work as used (for example, as part of a by-line or footnote) or in the place where substantially all other credits or notices for the new work containing the republished Work are located. Failure to include the required notice results in loss to the Rightsholder and CCC, and the User shall be liable to pay liquidated damages for each such failure equal to twice the use fee specified in the Order Confirmation, in addition to the use fee itself and any other fees and charges specified.

10) Indemnity. User hereby indemnifies and agrees to defend the Rightsholder and CCC, and their respective employees and directors, against all claims, liability, damages, costs, and expenses, including legal fees and expenses, arising out of any use of a Work beyond the scope of the rights granted herein and in the Order Confirmation, or any use of a Work which has been altered in any unauthorized way by User, including claims of defamation or infringement of rights of copyright, publicity, privacy, or other tangible or intangible property.

11) Limitation of Liability. UNDER NO CIRCUMSTANCES WILL CCC OR THE RIGHTSHOLDER BE LIABLE FOR ANY DIRECT, INDIRECT, CONSEQUENTIAL, OR INCIDENTAL DAMAGES (INCLUDING WITHOUT LIMITATION DAMAGES FOR LOSS OF BUSINESS PROFITS OR INFORMATION, OR FOR BUSINESS INTERRUPTION) ARISING OUT OF THE USE OR INABILITY TO USE A WORK, EVEN IF ONE OR BOTH OF THEM HAS BEEN ADVISED OF THE POSSIBILITY OF SUCH DAMAGES. In any event, the total liability of the Rightsholder and CCC (including their respective employees and directors) shall not exceed the total amount actually paid by User for the relevant License. User assumes full liability for the actions and omissions of its principals, employees, agents, affiliates, successors, and assigns.

12) Limited Warranties. THE WORK(S) AND RIGHT(S) ARE PROVIDED "AS IS." CCC HAS THE RIGHT TO GRANT TO USER THE RIGHTS GRANTED IN THE ORDER CONFIRMATION DOCUMENT. CCC AND THE RIGHTSHOLDER DISCLAIM ALL OTHER WARRANTIES RELATING TO THE WORK(S) AND RIGHT(S), EITHER EXPRESS OR IMPLIED, INCLUDING WITHOUT LIMITATION IMPLIED WARRANTIES OF MERCHANTABILITY OR FITNESS FOR A PARTICULAR PURPOSE. ADDITIONAL RIGHTS MAY BE REQUIRED TO USE ILLUSTRATIONS, GRAPHS, PHOTOGRAPHS, ABSTRACTS, INSERTS, OR OTHER PORTIONS OF THE WORK (AS OPPOSED TO THE ENTIRE WORK) IN A MANNER CONTEMPLATED BY USER; USER UNDERSTANDS AND AGREES THAT NEITHER CCC NOR THE RIGHTSHOLDER MAY HAVE SUCH ADDITIONAL RIGHTS TO GRANT.

13) Effect of Breach. Any failure by User to pay any amount when due, or any use by User of a Work beyond the scope of

the License set forth in the Order Confirmation and/or the Terms, shall be a material breach of such License. Any breach not cured within 10 days of written notice thereof shall result in immediate termination of such License without further notice. Any unauthorized (but licensable) use of a Work that is terminated immediately upon notice thereof may be liquidated by payment of the Rightsholder's ordinary license price therefor; any unauthorized (and unlicensable) use that is not terminated immediately for any reason (including, for example, because materials containing the Work cannot reasonably be recalled) will be subject to all remedies available at law or in equity, but in no event to a payment of less than three times the Rightsholder's ordinary license price for the most closely analogous licensable use plus Rightsholder's and/or CCC's costs and expenses incurred in collecting such payment.

14) Additional Terms for Specific Products and Services. If a User is making one of the uses described in this Section 14, the additional terms and conditions apply:

a) *Print Uses of Academic Course Content and Materials (photocopies for academic coursepacks or classroom handouts).* For photocopies for academic coursepacks or classroom handouts the following additional terms apply:

i) The copies and anthologies created under this License may be made and assembled by faculty members individually or at their request by on-campus bookstores or copy centers, or by off-campus copy shops and other similar entities.

ii) No License granted shall in any way: (i) include any right by User to create a substantively non-identical copy of the Work or to edit or in any other way modify the Work (except by means of deleting material immediately preceding or following the entire portion of the Work copied) (ii) permit "publishing ventures" where any particular anthology would be systematically marketed at multiple institutions.

iii) Subject to any Publisher Terms (and notwithstanding any apparent contradiction in the Order Confirmation arising from data provided by User), any use authorized under the academic pay-per-use service is limited as follows:

A) any License granted shall apply to only one class (bearing a unique identifier as assigned by the institution, and thereby including all sections or other subparts of the class) at one institution;

B) use is limited to not more than 25% of the text of a book or of the items in a published collection of essays, poems or articles;

C) use is limited to no more than the greater of (a) 25% of the text of an issue of a journal or other periodical or (b) two articles from such an issue;

D) no User may sell or distribute any particular anthology, whether photocopied or electronic, at more than one institution of learning;

E) in the case of a photocopy permission, no materials may be entered into electronic memory by User except in order to produce an identical copy of a Work before or during the academic term (or analogous period) as to which any particular permission is granted. In the event that User shall choose to retain materials that are the subject of a photocopy permission in electronic memory for purposes of producing identical copies more than one day after such retention (but still within the scope of any permission granted), User must notify CCC of such fact in the applicable permission request and such retention shall constitute one copy actually sold for purposes of calculating permission fees due; and

F) any permission granted shall expire at the end of the class. No permission granted shall in any way include any right by User to create a substantively non-identical copy of the Work or to edit or in any other way modify the Work (except by means of deleting material immediately preceding or following the entire portion of the Work copied).

iv) Books and Records; Right to Audit. As to each permission granted under the academic pay-per-use Service, User shall maintain for at least four full calendar years books and records sufficient for CCC to determine the numbers of copies made by User under such permission. CCC and any representatives it may designate shall have the right to audit such books and records at any time during User's ordinary business hours, upon two days' prior notice. If any such audit shall determine that User shall have underpaid for, or underreported, any photocopies sold or by three percent (3%) or more, then User shall bear all the costs of any such audit; otherwise, CCC shall bear the costs of any such audit. Any amount determined by such audit to have been underpaid by User shall immediately be paid to CCC by User, together with interest thereon at the rate of 10% per annum from the date such amount was originally due. The provisions of this paragraph shall survive the termination of this License for any reason.

b) *Digital Pay-Per-Uses of Academic Course Content and Materials (e-coursepacks, electronic reserves, learning management systems, academic institution intranets).* For uses in e-coursepacks, posts in electronic reserves, posts in learning management systems, or posts on academic institution intranets, the following additional terms apply:

i) The pay-per-uses subject to this Section 14(b) include:

A) Posting e-reserves, course management systems, e-coursepacks for text-based content, which grants authorizations to import requested material in electronic format, and allows electronic access to this material to members of a designated college or university class, under the direction of an instructor designated by the college or university, accessible only under appropriate electronic controls (e.g., password);

B) Posting e-reserves, course management systems, e-coursepacks for material consisting of photographs or other still images not embedded in text, which grants not only the authorizations described in Section 14(b)(i)(A) above, but also the following authorization: to include the requested material in course materials for use consistent with Section 14(b)(i)(A) above, including any necessary resizing, reformatting or modification of the resolution of such requested material (provided that such modification does not alter the underlying editorial content or meaning of the requested material, and provided that the resulting modified content is used solely within the scope of, and in a manner consistent with, the particular authorization described in the Order Confirmation and the Terms), but not including any other form of manipulation, alteration or editing of the requested material;

C) Posting e-reserves, course management systems, e-coursepacks or other academic distribution for audiovisual content, which grants not only the authorizations described in Section 14(b)(i)(A) above, but also the following authorizations: (i) to include the requested material in course materials for use consistent with Section 14(b)(i)(A) above; (ii) to display and perform the requested material to such members of such class in the physical classroom or remotely by means of streaming media or other video formats; and (iii) to "clip" or reformat the requested material for purposes of time or content management or ease of delivery, provided that such “clipping” or reformatting does not alter the underlying editorial content or meaning of the requested material and that the resulting material is used solely within the scope of, and in a manner consistent with, the particular authorization described in the Order Confirmation and the Terms. Unless expressly set forth in the relevant Order Conformation, the License does not authorize any other form of manipulation, alteration or editing of the requested material.

ii) Unless expressly set forth in the relevant Order Confirmation, no License granted shall in any way: (i) include any right by User to create a substantively non-identical copy of the Work or to edit or in any other way modify the Work (except by means of deleting material immediately preceding or following the entire portion of the Work copied or, in the case of Works subject to Sections 14(b)(1)(B) or (C) above, as described in such Sections) (ii) permit "publishing ventures" where any particular course materials would be systematically marketed at multiple institutions.

iii) Subject to any further limitations determined in the Rightsholder Terms (and notwithstanding any apparent contradiction in the Order Confirmation arising from data provided by User), any use authorized under the electronic course content pay-per-use service is limited as follows:

A) any License granted shall apply to only one class (bearing a unique identifier as assigned by the institution, and thereby including all sections or other subparts of the class) at one institution;

B) use is limited to not more than 25% of the text of a book or of the items in a published collection of essays, poems or articles;

C) use is limited to not more than the greater of (a) 25% of the text of an issue of a journal or other periodical or (b) two articles from such an issue;

D) no User may sell or distribute any particular materials, whether photocopied or electronic, at more than one institution of learning;

E) electronic access to material which is the subject of an electronic-use permission must be limited by means of electronic password, student identification or other control permitting access solely to students and instructors in the class;

F) User must ensure (through use of an electronic cover page or other appropriate means) that any person, upon gaining electronic access to the material, which is the subject of a permission, shall see:

- a proper copyright notice, identifying the Rightsholder in whose name CCC has granted permission,
- a statement to the effect that such copy was made pursuant to permission,
- a statement identifying the class to which the material applies and notifying the reader that the material has been made available electronically solely for use in the class, and
- a statement to the effect that the material may not be further distributed to any person outside the class, whether by copying or by transmission and whether electronically or in paper form, and User must also ensure that such cover page or other means will print out in the event that the person accessing the material chooses to print out the material or any part thereof.

G) any permission granted shall expire at the end of the class and, absent some other form of authorization, User is thereupon required to delete the applicable material from any electronic storage or to block electronic access to the applicable material.

iv) Uses of separate portions of a Work, even if they are to be included in the same course material or the same university or college class, require separate permissions under the electronic course content pay-per-use Service. Unless otherwise provided in the Order Confirmation, any grant of rights to User is limited to use completed no later than the end of the academic term (or analogous period) as to which any particular permission is granted.

v) Books and Records; Right to Audit. As to each permission granted under the electronic course content Service, User shall maintain for at least four full calendar years books and records sufficient for CCC to determine the numbers of copies made by User under such permission. CCC and any representatives it may designate shall have the right to audit such books and records at any time during User's ordinary business hours, upon two days' prior notice. If any such audit shall determine that User shall have underpaid for, or underreported, any electronic copies used by three percent (3%) or more, then User shall bear all the costs of any such audit; otherwise, CCC shall bear the costs of any such audit. Any amount determined by such audit to have been underpaid by User shall immediately be paid to CCC by User, together with interest thereon at the rate of 10% per annum from the date such amount was originally due. The provisions of this paragraph shall survive the termination of this license for any reason.

c) *Pay-Per-Use Permissions for Certain Reproductions (Academic photocopies for library reserves and interlibrary loan reporting) (Non-academic internal/external business uses and commercial document delivery).* The License expressly excludes the uses listed in Section (c)(i)-(v) below (which must be subject to separate license from the applicable Rightsholder) for: academic photocopies for library reserves and interlibrary loan reporting; and non-academic internal/external business uses and commercial document delivery.

i) electronic storage of any reproduction (whether in plain-text, PDF, or any other format) other than on a transitory basis;

ii) the input of Works or reproductions thereof into any computerized database;

iii) reproduction of an entire Work (cover-to-cover copying) except where the Work is a single article;

iv) reproduction for resale to anyone other than a specific customer of User;

v) republication in any different form. Please obtain authorizations for these uses through other CCC services or directly from the rightsholder.

Any license granted is further limited as set forth in any restrictions included in the Order Confirmation and/or in these Terms.

d) *Electronic Reproductions in Online Environments (Non-Academic-email, intranet, internet and extranet).* For "electronic reproductions", which generally includes e-mail use (including instant messaging or other electronic transmission to a defined group of recipients) or posting on an intranet, extranet or Intranet site (including any display or performance incidental thereto), the following additional terms apply:

i) Unless otherwise set forth in the Order Confirmation, the License is limited to use completed within 30 days for any use on the Internet, 60 days for any use on an intranet or extranet and one year for any other use, all as measured from the "republication date" as identified in the Order Confirmation, if any, and otherwise from the date of the Order Confirmation.

ii) User may not make or permit any alterations to the Work, unless expressly set forth in the Order Confirmation (after request by User and approval by Rightsholder); provided, however, that a Work consisting of photographs or other still images not embedded in text may, if necessary, be resized, reformatted or have its resolution modified without additional express permission, and a Work consisting of audiovisual content may, if necessary, be "clipped" or reformatted for purposes of time or content management or ease of delivery (provided that any such resizing, reformatting, resolution modification or “clipping” does not alter the underlying editorial content or meaning of the Work used, and that the resulting material is used solely within the scope of, and in a manner consistent with, the particular License described in the Order Confirmation and the Terms.

15) Miscellaneous.

a) User acknowledges that CCC may, from time to time, make changes or additions to the Service or to the Terms, and that Rightsholder may make changes or additions to the Rightsholder Terms. Such updated Terms will replace the prior terms and conditions in the order workflow and shall be effective as to any subsequent Licenses but shall not apply to Licenses already granted and paid for under a prior set of terms.

b) Use of User-related information collected through the Service is governed by CCC's privacy policy, available online at www.copyright.com/about/privacy-policy/.

c) The License is personal to User. Therefore, User may not assign or transfer to any other person (whether a natural person or an organization of any kind) the License or any rights granted thereunder; provided, however, that, where applicable, User may assign such License in its entirety on written notice to CCC in the event of a transfer of all or substantially all of User's rights in any new material which includes the Work(s) licensed under this Service.

d) No amendment or waiver of any Terms is binding unless set forth in writing and signed by the appropriate parties, including, where applicable, the Rightsholder. The Rightsholder and CCC hereby object to any terms contained in any writing prepared by or on behalf of the User or its principals, employees, agents or affiliates and purporting to govern or otherwise relate to the License described in the Order Confirmation, which terms are in any way inconsistent with any Terms set forth in the Order Confirmation, and/or in CCC's standard operating procedures, whether such writing is prepared prior to, simultaneously with or subsequent to the Order Confirmation, and whether such writing appears on a copy of the Order Confirmation or in a separate instrument.

e) The License described in the Order Confirmation shall be governed by and construed under the law of the State of New York, USA, without regard to the principles thereof of conflicts of law. Any case, controversy, suit, action, or proceeding arising out of, in connection with, or related to such License shall be brought, at CCC's sole discretion, in any federal or state court located in the County of New York, State of New York, USA, or in any federal or state court whose geographical jurisdiction covers the location of the Rightsholder set forth in the Order Confirmation. The parties expressly submit to the personal jurisdiction and venue of each such federal or state court.

Last updated October 2022